



Institute of Physical Chemistry  
Polish Academy of Sciences  
Kasprzaka 44/52  
01-224 Warsaw, Poland

# **Nanoengineering of Thin Layers Of Semiconductor Photocatalysts In A Microreactor Environment For Lignin- Based Model Compounds Valorization**

A thesis submitted in conformity with the requirements for the degree of

Doctor of Philosophy

in the field of

Chemical Sciences

prepared within the International Doctoral Studies in Chemistry of the Institute of Physical  
Chemistry (IPC), Polish Academy of Sciences (PAS),  
Warsaw, Poland

by

**Swaraj Rashmi Pradhan**

Supervised by

dr hab. inż. Juan Carlos Colmenares (Assoc. Prof. IPC, PAS)

Warsaw, July 2023


## Declaration of originality

I, Swaraj rashmi Pradhan, declare that the research included within the present thesis was conducted by myself or in collaboration with and supported by others, as described in the acknowledgments section.

I attest that I have exercised reasonable care to ensure that the work is original, and does not, to the best of my knowledge, violate any Polish or International law, infringe any third party's copyright or other Intellectual Property Right, or contains any confidential material.

I accept that the Polish Academy of Sciences has the right to use plagiarism detection software to check the electronic version of the thesis. I confirm that no part of my thesis has been or will be submitted for obtaining a degree or diploma by the Institute of Physical Chemistry, Polish Academy of Science, or any other educational institution.

The copyright of this thesis rests with the author, and no quotation from it or information derived from it may be published without the author's prior written consent.



Signature

Warsaw, 17 July 2023

Signature

# Acknowledgments

This Ph.D. would not have been possible without the support of my supervisor, Prof. Dr. Juan Carlos Colmenares. I thank him for extending his unconditional support, encouragement, freedom, and guidance during my Ph.D. study. I have learned a lot from his feedback and very forward-looking suggestions. I am thankful for all our fruitful discussions and his valuable comments on my manuscript, which kept me motivated to explore many aspects of photocatalysis and microflow chemistry.

I would like to thank:

Dr. Dariusz Łomot for supporting and transferring his exceptional technical expertise in the specialized laboratory instruments and for helping me with experimental setups.

Dr. Dmytro Lisovytskiy for XRD and XRF measurements, Dr. Wojciech Lisowski for XPS measurement, Prof. Rafał Szmigielski and Dr. Klara Nestorowicz for the analysis and interpretation of GC-MS data, and Dr. K. Sobczak (CNBCh University of Warsaw) for HR-TEM measurements.

The administrative staff of the Institute of Physical Chemistry, especially Ms. Edyta Słojewska, Dr. Agnieszka Pietrzyk-Le, Ms. Joanna Wiszniewska, and Ms. Simona Popławska, for their help and cooperation.

Prof. Dr. Ramón Fernando Colmenares-Quintero from the Engineering Research Institute (In<sup>3</sup>), Universidad Cooperativa de Colombia, Medellín 50031, Colombia, for supporting my research as an external advisor.

I would like to extend my gratitude to all my teachers who helped me face the challenges and reach this step in life.

I have been lucky to be surrounded by great colleagues who supported me whenever I sought help for work and my personal life. I would like to thank Hermes Llain Jimenez, Dr. Vaishakh Nair, Abdul Qayyum, Laura Wrońska, Karolina Kawka, Agnieszka Dżugan, Dr. Rafael de Lima Oliveira, Behdokht Hashemi Hosseini, and Dr. Marta Paszkiewicz-Gawron. Special thanks to Dr. Ayesha Khan, Dr. Jovana Prekodravac, and Dr. Dimitrios Giannakoudakis for letting me be crazy in the lab.

I would like to thank Alcina, Jyoti, Neha, Rashmi, Tanvi, and Viki for being my home away from home. You have made this journey much more enjoyable. Thanks for being the family I can count on anytime I need. Life would not have been the same without you all!

I would also like to thank Abhishek, Anupama, Ankita, Devika, Debjita, Karthik, Karthika, Ganesh, Luca, Mattia, Mounika, Niriqsha, Praveen, Princy, Ranju, Sangami, Sakthi, Sarath, Sahir, Shakeel for providing the much-needed distraction from my Ph.D.

I always cherish the support and warm friendship from Amisha, Amit, Nishith, Dev bhai, and Maru di for standing with me virtually from different corners of the world. Time zone never stopped you from being in touch, kept me smiling, and helped me in every possible way.

A heartfelt thanks to Hari, Nelam, Vineeta di, and Arvind bhaiya for coming into my life during the end days of this journey and standing beside me for every tear and laugh. Thanks for listening to all my problems and just fading them away through your positivity. Your love is my biggest strength, and I am so thankful for being a part of your lives.

My sincere gratitude to my strength and solace, my parents, who were always there for me. I know how much they want me to stay near them, and I thank them for still supporting my every decision and being proud of me. Special thanks to Sibbu, Didi, Jiju, Tia, and Tej for being my constant source of motivation.

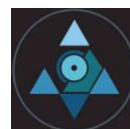
Special thanks to Dr. Nikhil for his love, and for supporting me during difficult times during Ph. D. and encouraging me to keep working towards my goal.

Lastly, I'd like to thank my inner self for enthusing me to achieve what I have always wanted.

Unfortunately, I cannot mention everyone here, but I extend my gratitude to every single person who supported me, from the beginning of this journey until this very moment in life.



I would like to acknowledge and thank the support from National Science Centre in Poland for providing the framework and financial support for my Ph.D. within the SonataBis 5 Project No. 2015/18/E/ST5/00306.



# List of Publications

Thesis is based on:

- P 1. Pradhan, S. R.;** Colmenares-Quintero, R. F.; Quintero, J. C. C. Designing Microflowreactors for Photocatalysis Using Sonochemistry: A Systematic Review Article. *Molecules* 2019, 24 (18). <https://doi.org/10.3390/molecules24183315>
- P 2. Pradhan, S. R.;** Nair, V.; Giannakoudakis, D. A.; Lisovytskiy, D.; Colmenares, J. C. Design and Development of TiO<sub>2</sub> Coated Microflow Reactor for Photocatalytic Partial Oxidation of Benzyl Alcohol. *Mol. Catal.* 2020, 486 (February), 110884. <https://doi.org/10.1016/j.mcat.2020.110884>
- P 3. Pradhan, S. R.;** Lisovytskiy, D.; Colmenares, J. C. Flow Photomicroreactor Coated with Monometal Containing TiO<sub>2</sub> Using Sonication: A Versatile Tool for Visible Light Oxidation. *Catal. Commun.* 2022, 162, 106375. <https://doi.org/10.1016/j.catcom.2021.106375>
- P 4. Pradhan, S. R.;** Paszkiewicz-Gawron, M.; Łomot, D.; Lisovytskiy, D.; Colmenares, J. C. Bimetallic TiO<sub>2</sub> Nanoparticles for Lignin-Based Model Compounds Valorization by Integrating Optocatalytic Flow-Microreactor. *Molecules* 2022, 27(24), 8731. <https://doi.org/10.3390/molecules27248731>.

Other publications (not included in this thesis):

1. Giannakoudakis, D. A.; Qayyum, A.; Nair, V.; Khan, A.; **Pradhan, S. R.;** Prekodravac, J.; Rekos, K.; LaGrow, A. P.; Bondarchuk, O.; Łomot, D.; et al. Ultrasound-Assisted Decoration of CuO<sub>x</sub> Nanoclusters on TiO<sub>2</sub> Nanoparticles for Additives Free Photocatalytic Hydrogen Production and Biomass Valorization by Selective Oxidation. *Mol. Catal.* 2021, 514. <https://doi.org/10.1016/j.mcat.2021.111664>

Patent application

1. Dariusz Łomot, **Swaraj Rashmi Pradhan**, Juan Carlos Colmenares Quintero. Patent application P.430411 (30.06.2019): "A flow microreactor system and the way of conducting photocatalytic processes using it".

# Active participation at scientific conferences

## Oral presentations:

1. **Swaraj Rashmi Pradhan**, Karolina Kawkab, Juan Carlos Colmenares, 5th International Conference on FOSSIL & RENEWABLE ENERGY, March 01-03, 2021, Houston, TX, USA.
2. **Swaraj Rashmi Pradhan**, Juan Carlos Colmenares, 5th International Conference on New Photocatalytic Materials for Environment, Energy and Sustainability (NPM -5) and The 6th International Conference on Photocatalytic and Advanced Oxidation Technologies for the Treatment of Water, Air, Soil and Surfaces (PAOT-6), January 28, 2022, Virtual.
3. **Swaraj Rashmi Pradhan**, Dmytro Lisovytskiy, Juan Carlos Colmenares, The 54th National Catalytic Colloquium, June, 2022, Krakow, Poland.

## Poster presentations:

1. **Swaraj Rashmi Pradhan**, Vaishakh Nair, Juan Carlos Colmenares, 17th International Conference on Chemistry and the Environment (ICCE 2019), Thessaloniki, Greece.
2. **Swaraj Rashmi Pradhan**, Dimitrios A. Giannakoudakis, Agnieszka Dżugan, Juan Carlos Colmenares, 5th EUGSC, Sept 2021, Virtual.
3. **Swaraj Rashmi Pradhan**, Dmytro Lisovytskiy, Juan Carlos Colmenares, The 11th European Conference on Solar Chemistry and Photocatalysis: Environmental Applications (SPEA11), June 2022, Turin, Italy.
4. **Swaraj Rashmi Pradhan**, Dmytro Lisovytskiy, Juan Carlos Colmenares, The 9th IUPAC International Conference on Green Chemistry (9th ICGC), September 2022, Athens, Greece.

# Abstract

This thesis aims to synthesize novel thin layers of materials assisted by ultrasound techniques with photocatalytic properties on the internal wall of fluoropolymer microtube reactor for selective oxidation of lignin-based model compounds. The materials were further modified with metals like Fe, Cu, and Co for advanced studies. It was expected that such materials will exhibit high surface areas and interesting properties. The critical step was to deposit sol-gel synthesized semiconductor metal oxides ( $\text{TiO}_2$ ,  $\text{ZnO}$ ) layer on the internal wall of polymeric (copolymers of tetrafluoroethylene and perfluoroethers - perfluoroalkoxy alkane) PFA microtube by a method assisted by ultrasounds. Oxidation reactions conducted in microspaces can allow precise control of parameters like reaction time, temperature, mixing, reproducibility and safety. Continuous flow reactions may also prevent or reduce side reactions and decomposition caused by over irradiation. Irradiation can be easily controlled by controlling of the flow rate of the pumping system. These above kind of controls are expected to increase selectivity, conversion, and yield.

The research plan includes the synthesis of nanoparticles modified with metals via the sol-gel method. Various characterizations like  $\text{N}_2$  physisorption, X-ray diffraction analysis, UV-Vis diffuse reflectance spectroscopy, etc., is part of the initial step. Doping of titania with metals for the application in heterogeneous photocatalysis improve the visible light response of the  $\text{TiO}_2$ . The synthesized catalysts were deposited onto the wall of microreactor and the characterization of microtubes was done through scanning electron microscope, optical microscope, to visualize immobilized catalyst layer. Microflow photocatalytic oxidation tests proved that the Fe- $\text{TiO}_2$  material has the highest photocatalytic conversion (28 %) of benzyl alcohol compared with the other  $\text{TiO}_2$  samples under visible light irradiation. The next goal was to investigate the photocatalytic performance of all the synthesized nanoparticles for the selective oxidation of different lignin-based model compounds such as benzyl alcohol, coniferyl alcohol, cinnamyl alcohol, and vanillyl alcohol in liquid phase under different light sources (UV and Visible). The alcohols containing hydroxy and methoxy groups (coniferyl and vanillin alcohol) showed high conversion (93 % and 52 %, respectively) with 8 % and 17 % selectivity towards their respective aldehydes, with the formation of other side products. The findings offer an insight into the ligand-to-metal charge transfer (LMCT) complex

formation, which was identified to be the main reason for the activity of synthesized catalysts under visible light.

## Abstrakt

Celem pracy jest synteza, wspomagana technikami ultradźwiękowymi, nowych cienkich warstw o właściwościach optokatalitycznych na wewnętrznej ścianie reaktora mikrorurowego z fluoropolimeru w celu selektywnego utleniania związków modelowych na bazie ligniny. Materiały te były następnie modyfikowane metalami takimi jak Fe, Cu i Co w celu przeprowadzenia zaawansowanych badań. Spodziewano się, że będą cechować się dużą powierzchnią właściwą i reaktywnością. Krytycznym etapem było osadzenie zsyntezowanych metodą zol-żel półprzewodnikowych tlenków metali ( $\text{TiO}_2$ ,  $\text{ZnO}$ ) na wewnętrznej ścianie polimerowej (kopolimery tetrafluoroetyleny i perfluoroeterów - perfluoroalkoxy alkane) mikrorurki PFA metodą wspomaganą ultradźwiękami. Reakcje utleniania prowadzone w mikro przestrzeniach mogą ułatwić precyzyjną kontrolę parametrów takich jak czas reakcji, temperatura, mieszanie, powtarzalność i bezpieczeństwo. Reakcje w ciągłym przepływie mogą również zapobiegać lub ograniczać reakcje uboczne i rozkład spowodowany nadmiernym napromieniowaniem świetlnym, które może być łatwo kontrolowane w systemie pompowym. Oczekuje się, że powyższe poczynania zwiększą selektywność, konwersję i wydajność.

Plan badań obejmuje syntezę nanocząstek modyfikowanych metalami metodą zol-żel. Różne metody charakteryzacji, takie jak fizySORPCJA  $\text{N}_2$ , analiza dyfrakcji rentgenowskiej, spektroskopia rozproszonego odbicia UV-Vis, itp. są częścią wstępnego etapu. Domieszkowanie tytanu metalami w heterogenicznej fotokatalizie poprawia czułość  $\text{TiO}_2$  na światło widzialne. Zsyntetyzowane katalizatory osadzono na ścianie mikroreaktora, a charakterystykę mikrorurek przeprowadzono za pomocą skaningowego mikroskopu elektronowego oraz mikroskopu optycznego, w celu uwidocznienia unieruchomionej warstwy katalizatora. Badania fotokatalitycznego utleniania w mikroreaktorze dowiodły, że materiał Fe- $\text{TiO}_2$  wykazuje najwyższą konwersję fotokatalityczną (28 %) alkoholu benzyłowego w porównaniu z innymi próbkami  $\text{TiO}_2$  pod wpływem promieniowania światła widzialnego. Kolejnym celem było zbadanie wydajności fotokatalitycznej wszystkich zsyntetyzowanych nanocząstek dla selektywnego utleniania różnych związków modelowych opartych na ligninie, takich jak alkohol benzyłowy, alkohol koniferyłowy, alkohol cynamyłowy i alkohol wanilinowy w fazie ciekłej pod różnymi źródłami światła (UV i widzialne). Alkohole zawierające grupy hydroksylowe i metoksyłowe (alkohol koniferyłowy

i wanilinowy) wykazywały wysoką konwersję (odpowiednio 93 % i 52 %) z 8 % i 17 % selektywnością w kierunku odpowiednich aldehydów, z tworzeniem innych produktów ubocznych. Wyniki dają wgląd w tworzenie kompleksu z przeniesieniem ładunku z ligandu na metal (LMCT), który okazał się być główną przyczyną aktywności zsyntetyzowanych katalizatorów w świetle widzialnym.

# Table of Contents

Declaration of originality .....	ii
Acknowledgments .....	iii
List of Publications .....	vi
Active participation at scientific conferences .....	vii
Abstract .....	viii
Abstrakt .....	x
Acronyms and Abbreviations .....	xiii
Chapter 1.....	16
1.    Introduction .....	16
1.1    Valorization of lignin .....	16
1.1.1    Need for a paradigm shift from existing methods .....	16
1.1.2    Role of sonication in surface modification .....	18
1.1.3    Semiconductor to achieve targeted goal .....	19
1.2    Research hypothesis and objectives .....	20
1.3    Organization of thesis .....	22
1.4    Final comments on this work .....	26
1.5    Challenges and future perspectives .....	30
References .....	31
Chapter 2 : Designing Microflow reactors for Photocatalysis Using Sonochemistry: A Systematic Review Article .....	32
Chapter 3 : Design and Development of TiO <sub>2</sub> coated microflow reactor for photocatalytic partial oxidation of benzyl alcohol .....	55
Chapter 4 : Flow photomicroreactor coated with monometal containing TiO <sub>2</sub> using sonication: a versatile tool for visible light oxidation .....	74
Chapter 5 : Bimetallic TiO <sub>2</sub> Nanoparticles for Lignin-Based Model Compounds Valorization by Integrating Optocatalytic Flow-Microreactor .....	84
Contributions of Authors .....	114
Curriculum Vitae .....	123



# Acronyms and Abbreviations

## A

AcN	Acetonitrile
AQY	Apparent quantum yield

## B

BET	Brunauer-Emmet-Teller
BJH	Barrett, Joyner, Halenda
BnAld	Benzaldehyde
BnOH	Benzyl alcohol

## C

CinOH	Cinnamyl alcohol
CinAld	Cinnamyl aldehyde
ConOH	Coniferyl alcohol
ConAld	Coniferyl aldehyde
CoT	0.25 at% of Co-TiO <sub>2</sub>
CuT	0.5 at% Cu-TiO <sub>2</sub>

## D

DMSO	Dimethylsulfoxide
------	-------------------

## E

EDXRF	Energy dispersive X-ray Fluorescence
EtOH	Ethanol

## F

FeT	0.5 at% of Fe-TiO <sub>2</sub>
FTIR	Fourier-Transform Infrared Spectroscopy

## **G**

GC-MS Gas Chromatography-Mass Spectrometry

## **H**

HAADF High Angle Annual Dark Field

HPLC High-Performance Liquid Chromatography

HR-SEM High Resolution Scanning Electron Microscopy

## **L**

LED Light-Emitting Diode

LMCT Ligand-to-Metal Charge Transfer

LSPR Localized Surface Plasmon Resonance

## **P**

PDMS Polydimethylsiloxane

PFA Perfluoroalkoxy Alkane

P-PFA Pretreated PFA

PT-PFA Pre-treated and deposited with P25 (commercially available TiO<sub>2</sub>) microreactor

## **S**

S-PFA Sol-gel synthesized TiO<sub>2</sub> deposited microtube

## **T**

TEM Transmission Electron Microscopy

TiO<sub>2</sub>-SG Sol-gel synthesized TiO<sub>2</sub>

T-PFA P25 coated tubes

TTIP Titanium (IV) Isopropoxide

## **U**

US Ultrasound

UV Ultraviolet

UV-vis DRS UV-visible Diffuse Reflectance Spectra

## **V**

VanOH

Vanillyl alcohol

VanAld

Vanillyl aldehyde

## **X**

XPS

X-ray photoelectron spectroscopy

XRD

X-ray diffraction

## **Z**

ZnO-SG

Sol-gel synthesized ZnO

# Chapter 1

## 1. Introduction

### 1.1 Valorization of lignin

The rise in consumption and production (manufacturing) to support the rapidly growing global population has adversely impacted the environment.<sup>1</sup> The sustainable disposal or reuse of industrial by-products is an active area of research in green chemistry. Lignin is a waste generated by paper and pulp mills that has been linked to severe aquatic and environmental problems. These industries produce tons of extracted lignin per year as a byproduct.<sup>2</sup> These have been classified as toxic substances, and in recent years, a promising treatment based on the total oxidation of hazardous organic compounds has been reported.<sup>3,4</sup>

Recently, researchers widely studied UV active heterogeneous photocatalysis because of their environmental friendly characteristics to photosensitize the complete mineralization of a wide range of organic substrates like phenols and pesticides, without the production of any harmful by-products.<sup>3</sup> These systems have limitations such as photo corrosion of catalyst, and it requires a unique experimental setup. This thesis will delve into these processes in greater detail in the following chapters.

#### 1.1.1 Need for a paradigm shift from existing methods

The concurrence of chemical engineering and organic chemistry gave rise to “Flow Chemistry” – the term used by the scientific community to describe the chemistry occurring during a continuous flow process in contrast to conventional batch chemistry.<sup>5,6</sup> The conventional batch suspension-based system gives rise to a large gradient in temperature, reaction time, and concentration over spatial position because of vigorous stirring.<sup>7</sup> Moreover, the nanoparticles should be filtered after the photocatalytic reaction, which requires time and energy. On the other hand, we can overcome these problems by shifting to photocatalytic materials immobilized on the internal wall of the microreactor, as the solution is subject to flow inside the microreactor.

In a typical microfluidic-based photocatalyst system, a solution stream containing the target organic compounds flows through the microchannel, with the catalyst immobilized on the inner wall of the reactor. Photocatalysts react to decompose the organic pollutants, and a strong oxidant (such as a hydroxyl radical) is generated when illuminated by UV light.<sup>8</sup>

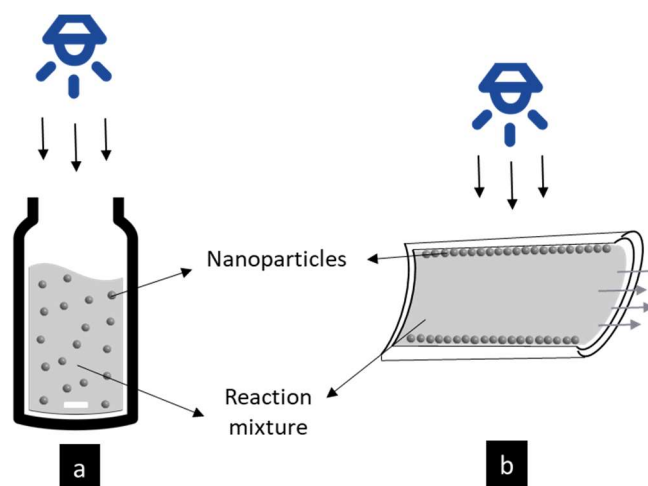


**Figure 1.** Conventional batch suspension-based system (a) and wall-coated microflow system (b).

Compared to the batch system, the microflow system has several advantages, such as (1) The short diffusion distance can help to increase the contact of photocatalytic materials with the compounds more efficiently. (2) By altering the microreactor geometry, the surface area of the photocatalytic materials can be increased. (3) The reuse of photocatalytic materials in a microfluidic-based system (Figure 1) is possible without any additional recovery process.<sup>9</sup> (4) Scaling up is reliable in a microflow system. (5) Selectivity and reproducibility can be improved for a reaction (6) The fast mixing and heat exchange can be achieved in the flow system.<sup>10</sup>

A microflow reactor can provide a small diffusion length and uniform light irradiation, thus enabling highly efficient photocatalysis and green chemistry processing.<sup>11</sup> In this work, we focus on a commercially available fluoropolymer-based microtube (PFA - perfluoroalkoxyalkane, a type of polymeric fluorocarbons) that demonstrates up to 96% for visible light and up to 91% for UV light transparency as well as admirable chemical stability.<sup>12</sup> Also, to maximize the photon utilization, PFA tubing can be easily bent into different shapes (highly flexible). Though the uses of these tubing have been demonstrated for continuous-

flow homogeneously catalyzed photochemical reactions<sup>13</sup>, they have been rarely employed with heterogeneous catalysts. The reason behind this is the solid suspension may cause a clogging problem that requires laborious separation. These problems can be minimized by immobilizing the photocatalysts onto the walls of the microreactor. However, the chemical inertness of fluoropolymer makes immobilization challenging. Researchers have made efforts by using methods like thermal processing (near a melting point of PFA of 285 °C)<sup>14</sup> and wet chemical processing<sup>15</sup> to facilitate the adhesion of photocatalysts to the fluoropolymer. However, because of the hydrophobic and chemically inert nature, the agent for a fluoropolymer is quite limited.<sup>16</sup>

The successful use of catalyst-coated microreactors for various use would largely depend on incorporation of catalyst on the wall of the microreactor. To obtain the wall-coated microreactor with a high number of exposed active sites, the control over stability and size of the preferred metal phase of photocatalysts are crucial. With this, the accessibility towards reacting molecules increases leading to better performances from both the reactor system and chemistry point of view. Recently, ultrasonic and microfluidics are introduced to revisit existing knowledge toolboxes to produce a technology push hoping to commercialize modern inventions.

### 1.1.2 Role of sonication in surface modification

Sonochemistry (acoustic cavitation) begins the growth and collapse of micrometer-sized bubbles in a liquid. When a bubble collapses in the presence of a significantly larger surface, it undergoes a noticeably uneven collapse, which gives rise to the crash of a high-speed jet of liquid into the surface. This can cause ultrasonic cleaning, localized erosion, and enhancement of surface chemistry. Integrating ultrasound with microflow reactors has proven to be one of the promising methods to address above discussed clogging and mixing issues that exist in conventional batch reactors (Figure 1).<sup>17,18</sup>

These small-scale microreactors offer a solution to non-uniformly generated acoustic field issues since the size range of ultrasonic effects is within the size range of that of the channels.<sup>19</sup> The work on the functionalization of microreactors is sparse in the literature. One of the main aims of this work is to provide a sonication-based method to modify the surface of a PFA

polymer tube using relatively mild reagents in a micro-space aqueous-based system. Recently, Sadowski et al.,<sup>20</sup> a group from Jagiellonian University, Krakow, has demonstrated that after surface modification of a polymer, increasing the number of available OH, it is possible to functionalize it with TiO<sub>2</sub>.

### 1.1.3 Semiconductor to achieve targeted goal

The low-cost, highly efficient photocatalysis process provides an alternative solution to remove the contaminants from the wastewater by producing less byproduct. In some typical photocatalytic wastewater treatments, the organic dyes are eliminated by employing semiconductor materials (TiO<sub>2</sub> and ZnO) under UV irradiation.<sup>21</sup> The semiconductor thin layer attained by conventional sol-gel processing is typically amorphous and exhibits a higher specific surface area. Conversion from the amorphous to the crystalline phase generally needs an annealing step (temperatures higher than 300 °C), which in most cases lead to a collapse of the pore system, and an increase of the particle size of the metal supported on the semiconductor with reduced specific surface area. Additionally, the use of microtubes in this work (made of perfluoroalkoxyalkane PFA, melting point 315 °C, max. operating temperature approx. 260 °C) restricts operations to lower temperatures. In recent years, low-temperature synthetic protocols towards nanoscale, crystalline, porous, and high surface area semiconductors have been developed and the research on semiconductor-based thin layers preparation is still a point of contention.<sup>22</sup> Taking into account the case of TiO<sub>2</sub>, the crystallinity is often poor from the synthesis process, and it is challenging to control the formation of the polymorphs. Regardless of all the research efforts, many of the synthesis procedures are still very difficult to predict the final properties of the product based on the present knowledge.

In the last decade, the advancement of metallic catalysts has been one of the most dynamic research topics in nanoscience.<sup>23</sup> Because of the synergetic effect between the two metals, the properties of bimetallic catalysts significantly differ from their monometallic analogs. As far as photocatalysis is concerned, the addition of second metal improved the physicochemical and photocatalytic properties of the materials.

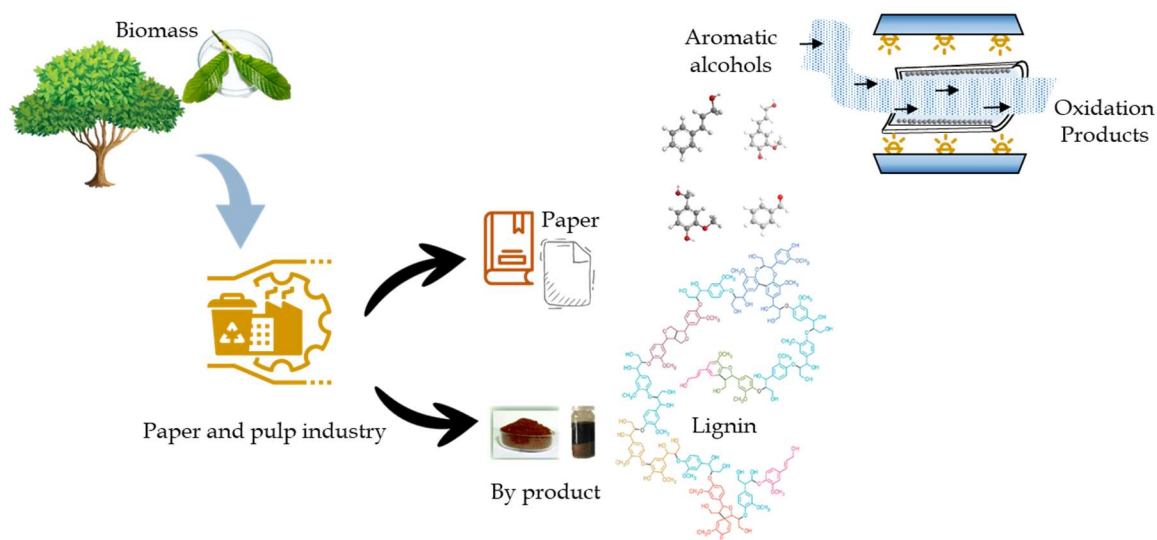


**Figure 2.** Lignin-based model compound valorization in wall-coated microreactor system.

## 1.2 Research hypothesis and objectives

This work proposes a novel methodology for the preparation of thin-layer nanocatalysts, which has strong potential to reduce Europe's reliance on imported rare earth/precious (toxic) metals by reducing their use (even replacing them) with those abundant transition metals (e.g., Fe, Cu, Co). We explored the use of noble metals (such as Au) as effective co-catalysts for the above metals by reducing the overpotential for surface photochemical reactions. The intensity of light upon the catalyst varies on the location of the batch reactor whereas in the microflow system, the intensity on the whole system is homogenous.

In this doctoral research, I aim to valorize lignin-based model compounds by exploiting catalyst-coated microflow system. In the scope of this work, it is believed that ultrasound will help in deposition of catalysts inside PFA tubes without the use of any binder. I further explored the effectiveness of the microflow system in achieving the necessary environment for our targeted application (compared to the conventional batch system).

The research hypotheses formulated for this Ph.D. thesis are outlined as follows:

*Hypothesis 1:* The activity of the catalyst can be improved for lignin-based model compounds (benzyl alcohol, BnOH) oxidation in microflow over the batch system with better yield of product.



Objective:

1. Evaluate the photocatalytic activity of in batch as well as in microflow system, with an aim to study the partial oxidation of benzyl alcohol.
2. Investigate the difference in the structure of the catalyst before and after deposition onto the wall of the microreactor by X-ray diffraction (XRD), N<sub>2</sub> physisorption, scanning electron microscopy (SEM), optical microscope, and UV-vis diffuse reflectance spectroscopy (DRS).

*Hypothesis 2:* The use of ultrasound for surface modification can further help in better deposition of catalyst onto the wall of PFA tube.

Objective:

1. Understand the effect of ultrasound on PFA tube surface by analyzing it by SEM and optical microscope.
2. Correlate the photocatalytic activity of the wall-coated microtube prepared with and without the presence of ultrasound under UV light.

*Hypothesis 3:* Introduction of transition metal (metal-containing; e.g., Cu, Fe, Co) and co-catalytic amount of noble metal (bimetal containing; e.g., Cu, Fe with Au) can improve the photocatalytic activity of the synthesized catalysts.

Objective:

1. Develop a low-temperature (80 °C) sol-gel synthesis method for the synthesis of TiO<sub>2</sub> and metal-doped TiO<sub>2</sub>.
2. Understand the effect of metal-doped TiO<sub>2</sub> by characterizing them through a wide range of techniques, e.g. XRD, N<sub>2</sub> physisorption, SEM, and UV-vis DRS.

*Hypothesis 4:* Alcohol can be chemisorbed over TiO<sub>2</sub> and form a visible light-active ligand-to-metal charge transfer (LMCT)-complex involving the methoxy (OCH<sub>3</sub>) and hydroxy (OH) group of alcohols with TiO<sub>2</sub>.

Objective:

1. Understand the LMCT-complex formation between the OH, OCH<sub>3</sub> group of alcohol and TiO<sub>2</sub>, through various characterization techniques (FT-IR spectroscopy, UV-Visible DRS spectroscopy).
2. Evaluate the role of surface hydroxy (OH) groups of TiO<sub>2</sub> in LMCT-mediated visible light activation of TiO<sub>2</sub> through heat treatment (to remove the surface OH groups).

### 1.3 Organization of thesis

This Ph.D. is done as a part of the SonataBis 5 (Project No. 2015/18/E/ST5/00306). The thesis takes the form of a cumulative doctoral thesis, with the core chapters presented as publications published in reputable international scientific peer-reviewed journals. Chapter 1 introduces the background to this research topic, with a specific focus on the research objectives and hypothesis that will be addressed during this doctoral work. Publication **P 1** builds a comprehensive literature review of microflow reactors and ultrasound approaches. The current state of art methods adopted for TiO<sub>2</sub> immobilization onto the surface of the microreactor is discussed elaborately in Chapter 2 (**P 1**).

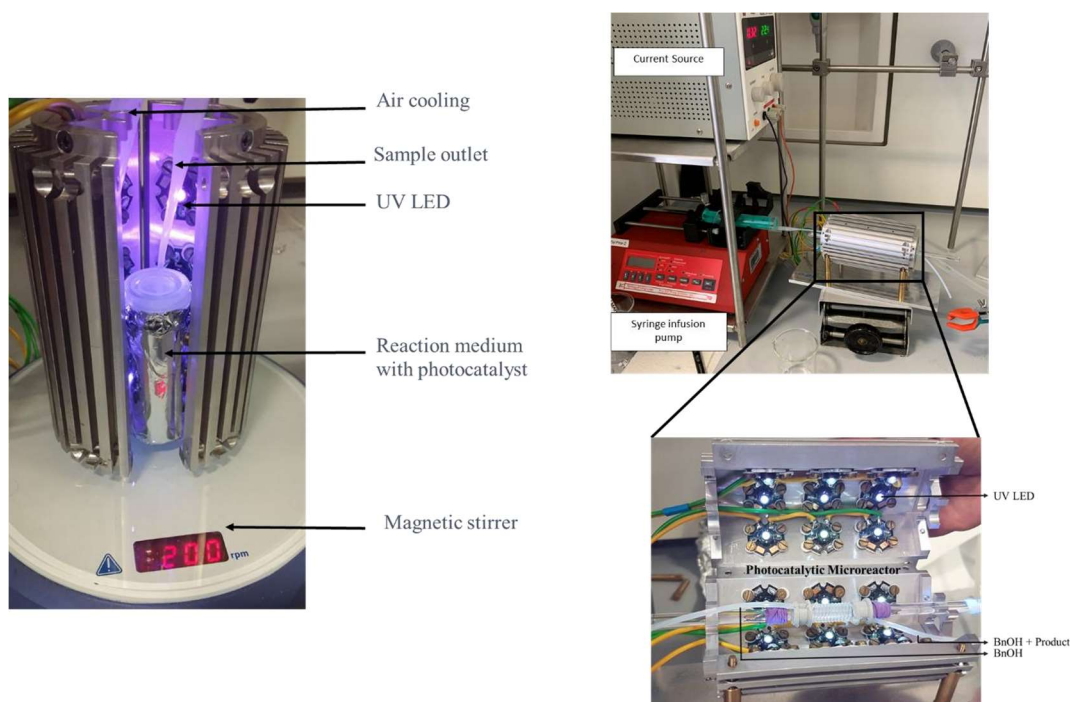


*Figure 3. Experimental setup for batch (left) and microflow (right) experiment.*

In the next section, I described the evolution of my research starting from the inception of the concept of combining ultrasound (for catalyst deposition) and microreactors for photocatalytic selective oxidation. Utilizing a continuous microreactor has already been proven to enhance irradiation throughout the reaction mixture, resulting in significantly reduced reaction times compared to batch reactors. The initial focus was to develop the appropriate experimental setup for both batch and microflow reactions. The experimental setup used for the photocatalytic experiment is shown in Figure 3. With the continuous flow of air (fan), the temperature inside the cylinder was maintained at room temperature. The intensity of the LEDs (Figure 3) was measured to be  $18 \times 9 \text{ W/m}^2$ , determined via light meter (Delta OHM HD 2302.0) with LP 471 RAD probe having 400-1050 nm spectral range. The photocatalytic oxidation reactions of alcohols were also carried out under UV and visible light using a UV LED lamp ( $\lambda = 375$  and  $515$  nm, respectively) measured by a Delta OHM HD 2302.0 light meter (with a LP 471 UVA probe with a spectral range of 315-400 nm and with LP 471 RAD probe having 400-1050 nm spectral range, respectively). The distance between the photoreactor wall and the irradiation source was maintained to be  $\sim 2$  cm. At given illumination time intervals, 0.15 mL aliquots were collected, and subsequently filtered via nylon filter (CHROMAFIL,  $0.2 \mu\text{m}$  pore size, 15 mm diameter) to remove the photocatalyst. The same experiments were performed with all photocatalysts.

Commercial P25  $\text{TiO}_2$  was used in a 25 mL batch reactor, and for photocatalytic reaction, 10 mg of catalyst and 20 mL (optimized concentration 0.5 g/L) of 1mM BnOH solution were used. Experiments were carried out and samples were collected at different interval time. Dark adsorption studies were carried out for 10 mg of catalyst in 20 mL of solution at room temperature. I optimized the parameters like catalyst concentration, solvent, and mixing speed for the batch photocatalytic system. Detailed discussion is provided in **P 2**.

To evaluate the efficacy of ultrasonic waves on a PFA (perfluoroalkoxy) tube immersed in a bath at various heights from the bottom, two sets of foil tests<sup>24</sup> were conducted. The first set involved placing aluminum foil horizontally with respect to the bottom of the ultrasound source, positioned at different depths. The results demonstrated that altering the height from the bottom had a diminishing effect on the interaction between the ultrasound (US) and the

foil (Figure 4 (a)). For both 70% and 100% power settings, a height of 2 cm from the bottom yielded the most favorable outcomes in terms of the ultrasound's impact.

The second set of tests aimed to investigate the influence of ultrasound on a spirally bound PFA tube enveloping a glass rod. Similarly, aluminum foil was wrapped around the glass rod, and the experiment was carried out. The findings from this study also support the conclusion that a height of 2 cm from the bottom of the ultrasound bath is effective for the coiled system (Figure 4 (b, c, d)).

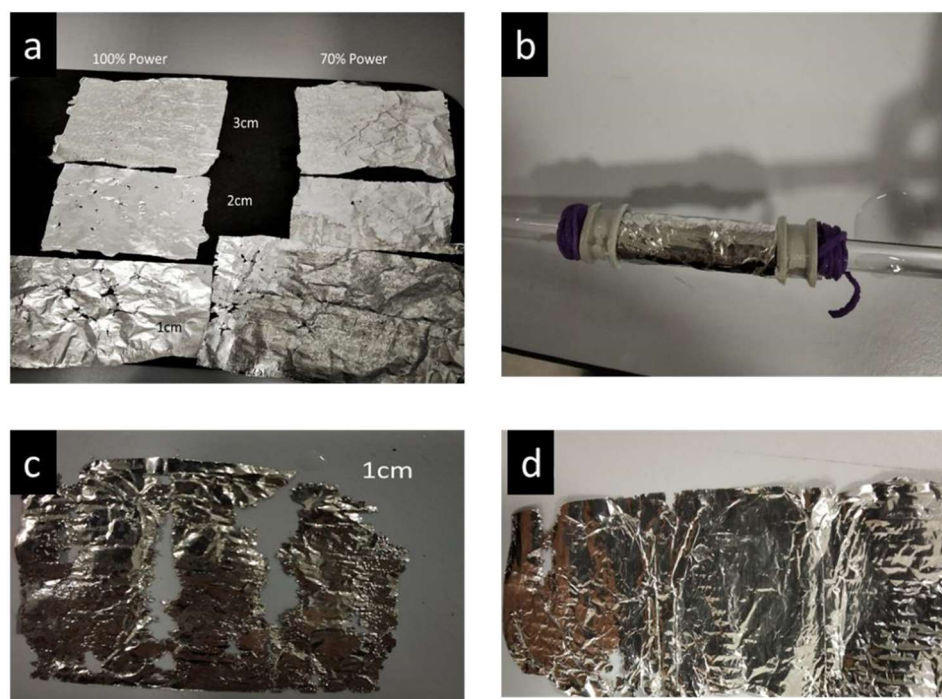


**Figure 4.** Two different methods were used to observe the effect of ultrasound: aluminum foil inside the Ultrasonic bath (a), and aluminum foil wrapped around glass rod (b, c and d).

Based on the aforementioned investigations, it can be deduced that, for our study, the optimal height from the bottom of the ultrasound bath ranges from 1 to 2 cm. Within this height range, the effect of ultrasound has been determined to be particularly advantageous for surface modification of the PFA tube. The observed outcomes highlight the significance of ultrasound treatment in this specific region, indicating its potential utility in altering the surface characteristics of the PFA tube. More pictures of this setup are available in publication P 2 (Chapter 3). This chapter proposes a new “green chemistry” oriented approach to prepare a thin layer microreactor system towards additive-free selective photocatalytic partial oxidation

of a lignin-based model compound, benzyl alcohol. The results show that the microreactor system displays better photo-reactivity with regard to both benzyl alcohol conversion and benzyl aldehyde selectivity. The utilization of ultrasonication (US) during the coating process leads to an enhanced mass deposition, and as a result, better photoreactivity compared to deposition without US.

The subsequent phase of my research involved the integration of metal with TiO<sub>2</sub>. To achieve this, I employed a pre-existing sol-gel method for synthesizing monometallic TiO<sub>2</sub> and optimized the atomic percentage of the metal on TiO<sub>2</sub>. I conducted thorough catalyst characterization and performed photocatalytic tests to elucidate the catalyst's activity (reported in **P 3**). To enhance the activity of TiO<sub>2</sub> nanoparticles, I decided to augment the monometal TiO<sub>2</sub> with a noble material, specifically gold (Au), as detailed in publication **P 4**. I successfully synthesized and characterized TiO<sub>2</sub> nanoparticles modified with bimetallic compositions. Our studies reveal that the LMCT complex formation of TiO<sub>2</sub> with the methoxy and hydroxy groups (directly connected with the aromatic ring) exists in the structure of coniferyl alcohol (ConOH) and vanillyl alcohol (VanOH), which was crucial to activate the TiO<sub>2</sub> catalyst under visible light. A detailed explanation is given in **P 4**.

## 1.4 Final comments on this work

Waste generated from large-scale manufacturing processes is an ever-growing source of environmental hazard, and reducing the production of these harmful chemicals has been a dominant area of research in green and sustainable chemistry. The goal of my thesis was to use recent advancements in the field of photocatalyst, microfluidics, and ultrasound to develop a system for lignin-based model compound valorization by adopting a greener approach. This compilation of three works and one review—contains a full picture of my research.

- In **P 1**, I have presented a comprehensive review of state of art methods for preparing wall-coated microflow reactors which are used for photocatalytic oxidation reactions. I further identified the scope of developments in polymer-based microtubes by using low energy-based ultrasound for deposition of catalyst in the wall of microreactor. This chapter was published as a review article in *Molecules* journal.

- Following the research gaps identified above, in **P 2**, I synthesized TiO<sub>2</sub> by following a simple sol-gel method and deposited it inside perfluoroalkoxy alkane (PFA) tube using an ultrasonic bath. I optimized the key parameters like power of ultrasound, time of deposition and length of tube for catalyst deposition. I performed a comparison study of commercial P25 with my synthesized TiO<sub>2</sub> both in batch and microflow systems for selective oxidation of benzyl alcohol (BnOH, model compound for lignin). The findings showed a greener approach to coat the inner walls of a microtube with a thin layer of photoactive TiO<sub>2</sub> to utilize the obtained microreactors towards the selective photocatalytic partial oxidation of benzyl alcohol, without the use of any addition reagent (like oxidant). This work has already been cited 24 times by researchers working in this domain.
- I further modified the photocatalyst (TiO<sub>2</sub>) by doping metals Fe, Cu and Co to it. In **P 3**, I optimized the atomic percentage of metal in TiO<sub>2</sub> and did a comparative photocatalytic activity study of the three metals. I also performed the required characterizations to explain the experimental results. I showed that, among all the metal TiO<sub>2</sub> samples, the 0.5 at % Fe-TiO<sub>2</sub> (cheap and abundant metal) photocatalyst exhibited comparatively better BnOH conversion under visible light (515 nm) in a microflow system.
- In **P 4**, to make our catalyst active under visible light, which is the dominant part of solar radiation, I tried to modify monometallic TiO<sub>2</sub> with Au. Though there was no remarkable activity under visible light (515 nm), the addition of this second metal in a co-catalytic amount to TiO<sub>2</sub> helped to increase the selectivity of the catalyst towards benzaldehyde (~ 100%) under UV light (375 nm). Furthermore, I extended my study to other lignin-based model compounds like coniferyl, cinnamyl, and vanillin alcohols. The methyl and hydroxy group of vanillin and coniferyl alcohol form a complex with TiO<sub>2</sub>, which makes the system active under visible light.

The powerful new approaches discussed above could address the key hypothesis formulated at the beginning of the thesis.

*Hypothesis 1:* Photocatalytic activity of the catalyst can be improved for lignin-based model compounds (benzyl alcohol, BnOH) oxidation in microflow over the batch system with better product yield.

Utilization of microreactors as an eco-friendly, in terms of simplicity, safety, time, energy, material cost, and environmental impact approach for the selective upgrade of biomass-derived compounds were performed by our research group to enhance the capability of the photoreactors and to determine which factors and features of the catalyst play the most crucial role. In **P 2**, I showcased that the photocatalytic conversion of benzyl alcohol in the microflow system increased compared to the batch reactor. Upon deposition on the microreactor's walls, the synthesized material revealed a better photo-reactivity regarding benzyl alcohol conversion and benzyl aldehyde selectivity, a trend in absolute contrast with the batch experiments case. For monometallic catalysts, in Chapter 4, among all the metal TiO<sub>2</sub> samples, the 0.5 at% Fe-TiO<sub>2</sub> (cheap and abundant metal) photocatalyst exhibited the highest BnOH conversion (28%, detailed discussion is given in **P 3**) under visible light (515 nm) in microflow system.

*Hypothesis 2:* Using ultrasound for surface modification can further help in better deposition of catalyst onto the wall of the PFA tube.

In this thesis, I considered the optimization of parameters like length of tube, ultrasonic power, and time of deposition for coating of catalyst and studied the photocatalytic activity with all the microtubes prepared with combinations from Design Expert. In **P 2**, I observed that ultrasonication during the coating process plays a vital role, leading to an enhanced mass deposition and as a result, better photoreactivity compared to deposition without ultrasound. The higher availability of the active sites in this wall-coated microreactor helped in better conversion.

*Hypothesis 3:* Introduction of transition metal (metal-containing; e.g., Cu, Fe, Co) and co-catalytic amount of noble metal (bimetal containing; e.g., Cu, Fe with Au) to improve the photocatalytic activity of the synthesized catalysts.

**P 3** of this thesis shows the benefits of using metal TiO<sub>2</sub> (e.g., Cu, Fe, Co). The metal-containing TiO<sub>2</sub> showed higher photocatalytic activity under UV irradiation than the synthesized TiO<sub>2</sub> in the batch system. Among the three metals, although Cu and Fe showed almost similar activity in the batch system under UV light, in the microflow system (after deposition of catalyst in the wall of PFA), Fe-TiO<sub>2</sub> showed better activity under UV and Vis light. Though adding a second metal (Au) to this monometal TiO<sub>2</sub> enhanced the benzaldehyde selectivity to 100%, it did not improve the activity of the catalyst under visible light as we hypothesized.

*Hypothesis 4:* Alcohol can be chemisorbed over TiO<sub>2</sub> and form a visible light-active ligand-to-metal charge transfer (LMCT)-complex involving the methoxy (OCH<sub>3</sub>) and hydroxy (OH) group of alcohols with TiO<sub>2</sub>.

In **P 4**, I showcased that the LMCT complex formation of TiO<sub>2</sub> with the methoxy (OCH<sub>3</sub>) and OH groups (directly connected with the aromatic ring) exists in the structure of coniferyl alcohol (ConOH) and vanillyl alcohol (VanOH), is crucial to activate the catalyst under visible light. This has further been corroborated by UV-Vis and FTIR studies. Removing the OH group from TiO<sub>2</sub> with high temperature, I observed the deactivation of the catalyst under visible light confirming that the OH groups are crucial for LMCT complex formation and visible light activity of the catalyst.

In summary, I presented herein a “green chemistry” oriented approach to coat the inner walls of a microtube with a thin layer of photoactive TiO<sub>2</sub> to use the obtained microreactors towards the selective photocatalytic partial oxidation of lignin-based model compounds. Additionally, the whole process was developed to be environment-friendly as the catalyst synthesis process did not include any high-temperature calcination step, unlike commercial P25 TiO<sub>2</sub>, and the photocatalytic selective oxidation route was additive-free (no additional oxidants). TiO<sub>2</sub>-based heterogeneous photocatalysis carried out under mild experimental conditions such as ambient pressure and temperature, utilizing oxygen (present in the reaction medium) as an oxidizing agent, and UV and visible light as irradiation sources is a green and economical approach for the valorization of biomass-based platform chemicals. In a broader context, we believe that the presented work demonstrates the potential of an ultrasonic-assisted bimetallic TiO<sub>2</sub> wall-coated microreactor for selective oxidation of lignin-based model compounds using



solar energy and will serve as a conceptual blueprint for further developments. On the other hand, even though modifications were done to sol-gel synthesized ZnO with metals (considering the optimized parameters from experiments with TiO<sub>2</sub>), commercially available ZnO showed better activity compared to our synthesized ZnO and metal-modified ZnO.

## 1.5 Challenges and future perspectives

In this part of my dissertation, challenges and possible directions for future studies are given.

During this doctoral research, I explored many innovative strategies to push the boundaries toward the valorization of lignin compounds. However, there still exist many challenges that could be hurdles to widespread adoption; while simultaneously opening up possible research directions for future works. They are:

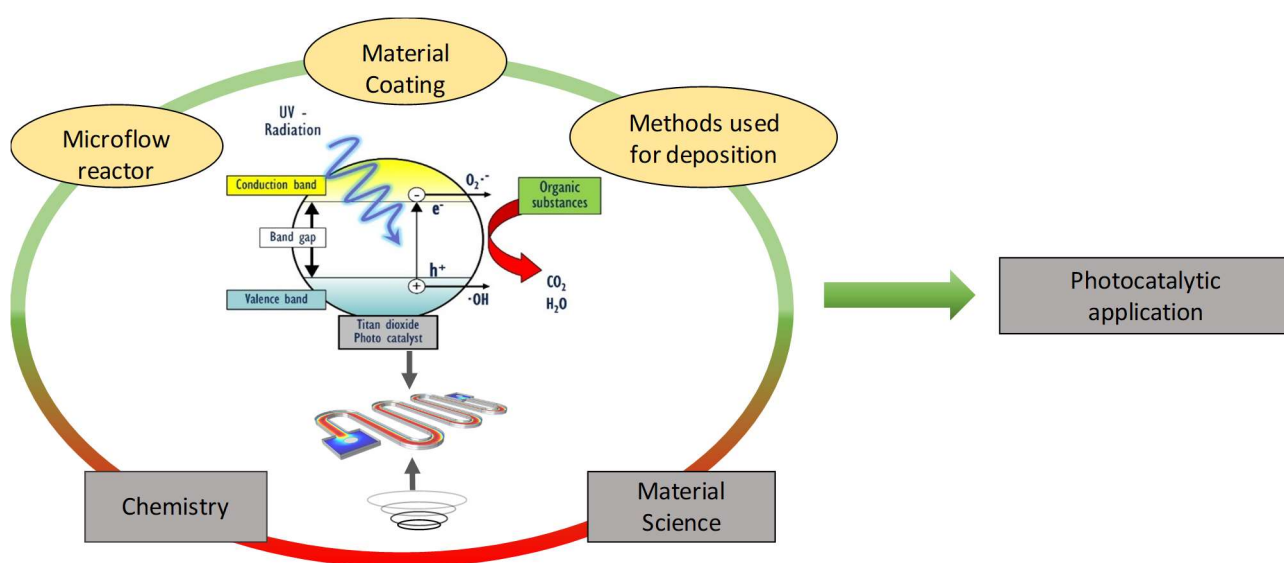
- According to our initial plan, we aimed to use ultrasound for the synthesis of our catalyst. We also used it for the synthesis of TiO<sub>2</sub>. Whereas, the addition of metal to the process made the gel thicker by making the mixing process difficult. Hence, we shifted to mechanical mixing (magnetic stirrer). Maybe the use of high-power ultrasound for this sol-gel synthesis can improve the crystallinity of the catalyst, which might will improve the activity of the catalyst.
- As the catalyst depositions occur at micro-scale, it was difficult to characterize or study the catalysts inside the microflow system deeply. This still is an active challenge to overcome.
- The current work uses irradiation light for photocatalysis using LED light sources. Going forward, this source should be replaced with naturally available solar irradiation. To start with, we can use solar light simulators.
- We can improve the catalysts by changing the synthetic route - 80 °C which might activate the rutile phase (or overall crystallinity) and activate the catalyst under visible light. Also, we can shift towards greener solvents, like water, for photocatalytic experiments.
- In the future, we can work on numbering up the system in order to work on an industrial scale.

## REFERENCES

- 1 S. E. Vollset, E. Goren, C. W. Yuan, J. Cao, A. E. Smith, T. Hsiao, C. Bisignano, G. S. Azhar, E. Castro, J. Chalek, A. J. Dolgert, T. Frank, K. Fukutaki, S. I. Hay, R. Lozano, A. H. Mokdad, V. Nandakumar, M. Pierce, M. Pletcher, T. Robalik, K. M. Steuben, H. Y. Wunrow, B. S. Zlavog and C. J. L. Murray, *Lancet*, 2020, **396**, 1285–1306.
- 2 J. Zakzeski, P. C. A. Bruijninx, A. L. Jongerius and B. M. Weckhuysen, *Chem. Rev.*, 2010, **110**, 3552–3599.
- 3 S. R. Kadam, V. R. Mate, R. P. Panmand, L. K. Nikam, M. V. Kulkarni, R. S. Sonawane and B. B. Kale, *RSC Adv.*, 2014, **4**, 60626–60635.
- 4 S. Rana, N. Gupta and R. S. Rana, *Mater. Today Proc.*, 2018, **5**, 4218–4224.
- 5 T. Noël, Y. Cao and G. Laudadio, *Acc. Chem. Res.*, 2019, **52**, 2858–2869.
- 6 N. Kockmann, R. Hartman and A. Kulkarni, *J. Flow Chem.*, 2021, **11**, 211–212.
- 7 X. Zhang, Y. Wang, F. Hou, H. Li, Y. Yang, X. Zhang, Y. Yang and Y. Wang, *Appl. Surf. Sci.*, 2017, **391**, 476–483.
- 8 K. M. Lee, C. W. Lai, K. S. Ngai and J. C. Juan, *Water Res.*, 2016, **88**, 428–448.
- 9 Z. Gao, C. Pan, C. Choi and C. Chang, *Symmetry (Basel)*, 2021, **13**, 1325.
- 10 S. R. Pradhan, R. F. Colmenares-Quintero and J. C. C. Quintero, *Molecules*, , DOI:10.3390/molecules24183315.
- 11 N. Wang, X. Zhang, Y. Wang, W. Yu and H. L. W. Chan, *Lab Chip*, 2014, **14**, 1074–1082.
- 12 Y. Su, N. J. W. Straathof, V. Hessel and T. Noël, *Chem. - A Eur. J.*, 2014, **20**, 10562–10589.
- 13 S. Vidyacharan, B. T. Ramanjaneyulu, S. Jang and D. P. Kim, *ChemSusChem*, 2019, **12**, 2581–2586.
- 14 B. Ramos, S. Ookawara, Y. Matsushita and S. Yoshikawa, *J. Environ. Chem. Eng.*, 2014, **2**, 1487–1494.
- 15 J. J. Richardson, M. Björnmalm and F. Caruso, *Science (80-. )*, , DOI:10.1126/science.aaa2491.
- 16 C. Khositanon, S. Deepracha, S. Assabumrungrat, M. Ogawa and N. Weeranoppanant, *Ind. Eng. Chem. Res.*, 2022, **61**, 1322–1331.
- 17 D. Fernandez Rivas and S. Kuhn, *Top. Curr. Chem.*, 2016, 374.
- 18 M. Schoenitz, L. Grundemann, W. Augustin and S. Scholl, *Chem. Commun.*, 2015, **51**,

- 8213–8228.
- 19 A. P. U. S. Kuhn, Z. Dong, C. Delacour, K. Carogher, *Mater. Sci. Eng.*, 2020, **13**, 344.
  - 20 R. Sadowski, A. Wach, M. Buchalska, P. Kuśtrowski and W. Macyk, *Appl. Surf. Sci.*, 2019, **475**, 710–719.
  - 21 Y. Jiang, Y. Sun, H. Liu, F. Zhu and H. Yin, *Dye. Pigment.*, 2008, **78**, 77–83.
  - 22 G. Varshney, S. R. Kanel, D. M. Kempisty, V. Varshney, A. Agrawal, E. Sahle-Demessie, R. S. Varma and M. N. Nadagouda, *Coord. Chem. Rev.*, 2016, **306**, 43–64.
  - 23 M. Sankar, N. Dimitratos, P. J. Miedziak, P. P. Wells, J. Kiely and G. J. Hutchings, *Chem Soc Rev*, 2012, **41**, 8099–8139.

# Chapter 2 : Designing Microflow reactors for Photocatalysis Using Sonochemistry: A Systematic Review Article



*The present chapter discusses the research work described in a published manuscript (P 1), authored by Swaraj rashmi Pradhan, Ramón Fernando Colmenares-Quintero and Juan Carlos Colmenares. (Molecules 24 (2019) 3315; doi:10.3390/molecules24183315)*

Review

# Designing Microflowreactors for Photocatalysis Using Sonochemistry: A Systematic Review Article

Swaraj Rashmi Pradhan <sup>1,\*</sup>, Ramón Fernando Colmenares-Quintero <sup>2</sup> and Juan Carlos Colmenares Quintero <sup>1,\*</sup>

<sup>1</sup> Institute of Physical Chemistry, Polish Academy of Sciences, Kasprzaka 44/52, 01-224 Warsaw, Poland

<sup>2</sup> Universidad Cooperativa de Colombia, Calle 50A No. 41–34 Medellín, Colombia; ramon.colmenaresq@campusucc.edu.co

\* Correspondence: srpradhan@ichf.edu.pl (S.R.P.); jcarloscolmenares@ichf.edu.pl (J.C.C.Q.); Tel.: +48-22-343-3215 (J.C.C.Q.)

Academic Editor: Gregory Chatel

Received: 31 July 2019; Accepted: 8 September 2019; Published: 12 September 2019



**Abstract:** Use of sonication for designing and fabricating reactors, especially the deposition of catalysts inside a microreactor, is a modern approach. There are many reports that prove that a microreactor is a better setup compared with batch reactors for carrying out catalytic reactions. Microreactors have better energy efficiency, reaction rate, safety, a much finer degree of process control, better molecular diffusion, and heat-transfer properties compared with the conventional batch reactor. The use of microreactors for photocatalytic reactions is also being considered to be the appropriate reactor configuration because of its improved irradiation profile, better light penetration through the entire reactor depth, and higher spatial illumination homogeneity. Ultrasound has been used efficiently for the synthesis of materials, degradation of organic compounds, and fuel production, among other applications. The recent increase in energy demands, as well as the stringent environmental stress due to pollution, have resulted in the need to develop green chemistry-based processes to generate and remove contaminants in a more environmentally friendly and cost-effective manner. It is possible to carry out the synthesis and deposition of catalysts inside the reactor using the ultrasound-promoted method in the microfluidic system. In addition, the synergistic effect generated by photocatalysis and sonochemistry in a microreactor can be used for the production of different chemicals, which have high value in the pharmaceutical and chemical industries. The current review highlights the use of both photocatalysis and sonochemistry for developing microreactors and their applications.

**Keywords:** ultrasound; flow microreactor; photocatalysis; water/air detoxification; organic synthesis; semiconductor

## 1. Introduction

With the continuous and prosperous development of modern civilizations, environmental contamination has spread far and wide. Faced with this issue, humankind reached a consensus on the need for environmental treatment and remediation. Green chemistry is the implementation of twelve principles [1] (Figure 1) that lowers the use or generation of hazardous substances in the design, manufacture, and application of chemical products [2]. Our society is increasingly demanding the innovation of newer approaches to be sustainable in order to preserve the environment. It is crucial for these approaches to be less dependent on self-depleting sources or sources that effuse green-house gases in use.

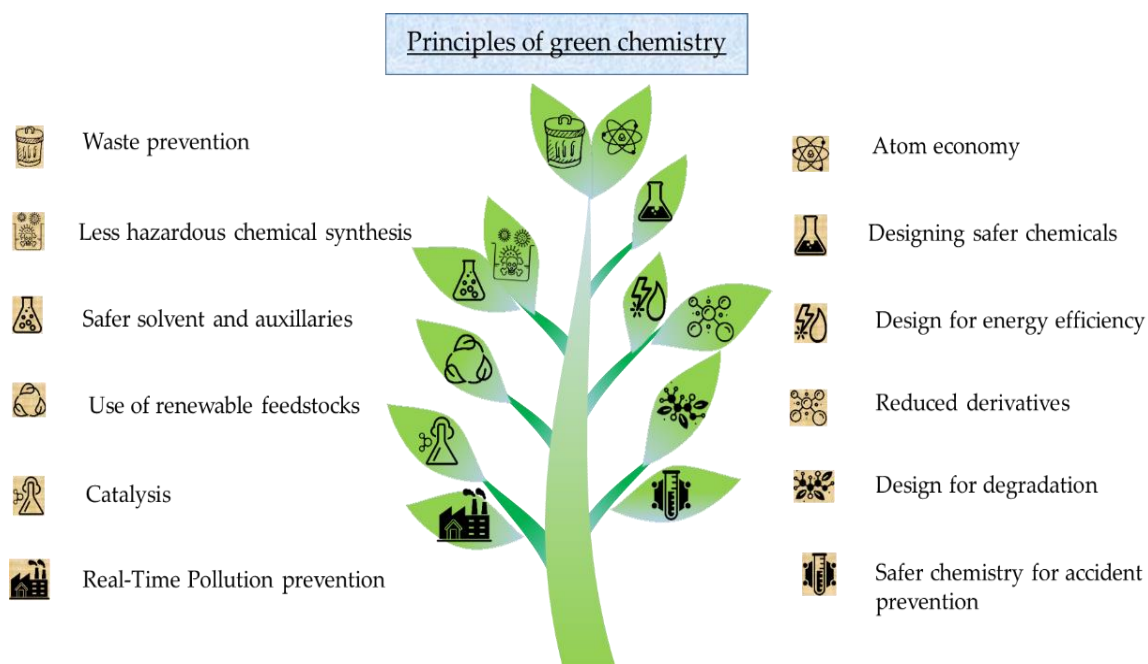


**Figure 1.** The twelve principles of green chemistry.

Photocatalysis occupies an essential place in the ecological equilibrium and is a good example of green chemistry [3]. Photocatalysis activates reactions depending on the light (clean and superabundantly available from the Sun) as an energy source. Therefore, research on the utilization of solar energy has continued to be an important topic [2,4]. Photocatalysis in microreactors is attracting the attention of many researchers because of its greener aspect. Because of reduced reagent requirements, shorter reaction time, lessening of by-products, and minimized energy consumption, microreactors are regarded as a green synthetic approach [5]. Nowadays, many groups are working on synthesizing catalysts inside a microreactor. Among the catalysts, titania-based catalysts are well-known photocatalysts under UV (Ultraviolet) light and have been identified as a form of technology playing an important role in solving many of the problems in water purification [6].

In this review article, after a brief introduction, theoretical backgrounds of the flow microreactor, ultrasound, and their combined studies are discussed. Ultrasound irradiation is accepted as an environmentally benign technique to carry out chemical reactions [7]. The application of ultrasound waves has been considered as an agreeable technique in chemistry. Early works on catalyst synthesis in a microreactor using ultrasound and their comparison with conventional batch experiments and future challenges are reviewed in this article.

As illustrated in Figure 2, the scientific community is trying to make our planet green by combining chemical engineering (e.g., manufacturing microchannels by ultrasound) with material chemistry (e.g., photocatalysts). The major purpose of this review article is to highlight the challenges ahead of the design and development of (photo)catalytic microfluidic reactors using ultrasound. To the best of our knowledge, this is the first technical review in the field of microflow reactors for photocatalysis using sonochemistry, which is promising for the upcoming studies in this branch of science.

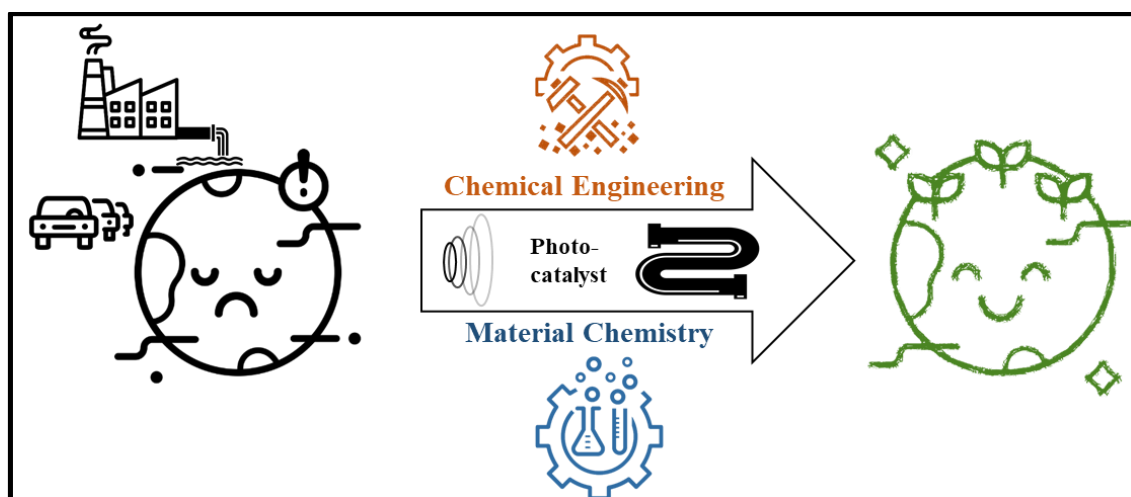


Figure 2. Two branches, trying to produce greener chemistry.

## 2. Theoretical Background

There are two main types of flow-reactor system that people use for synthetic photochemistry—micro and macro flow [8]. For various applications, people use the micro-synthesis technique in disciplines of both engineering and sciences. Definition of a microfluidic segment in a microreactor is described as a minimum unit having properties that can be used to improve various operations and reactions [5]. Microreactors offer new possibilities of reactions. Microreactors have been proven to be highly effective for catalytic reactions because of their indispensable advantages, such as uniform illumination without light attenuation, large surface-to-volume ratio and, consequently, attaining of a high heat and mass transfer rate, and the resultant satisfactory catalytic effect [9,10]. Also, one can easily control the contact time, shape, and size of the interface between fluids in these systems [11,12]. The aforementioned attributes make microreactors ideal for highly exothermic and fast reactions.

Recently, much attention has been paid to the development of microreactor technology for various applications, such as the synthesis of chemical compounds, environmental protection, biomedical and pharmaceutical studies, and healthcare, among others [9,13]. In a review article, Moraveji et al. discussed on two disadvantages of flow reactors—pressure drop and type of photocatalytic microreactor to be considered [14]. Yue et al. tried to overcome these issues by incorporation of a photocatalyst thin layer [10]. The potential development of more complicated flow reactions on progressively complex targets became viable because of the small volume of microreactors. Hence, the quantities of materials needed to optimize reaction conditions are greatly minimized, leading to reduce waste [15].

In the past decade, continuous flow microreactors have received considerable attention for performing organic transformations in safer and efficient ways. Even if microfluidic systems have a wide range of users in several fields, their commercialization is still limited [13]. It is now possible to reach the maximum selectivity of exothermic or endothermic, complex, extremely fast, and multiphase chemical reactions using a photocatalytic microreactor [16]. Very efficient degradation and different organic molecule synthesis, along with selective cleavage of peptides and proteins, have been done using micro-photoreactors immobilized with  $\text{TiO}_2$  catalyst, which can be very favorable for the synthesis of chemicals, pharmaceuticals, and proteomics [17]. Figure 3 shows a typical example of a photocatalytic microreactor used for wastewater treatment.

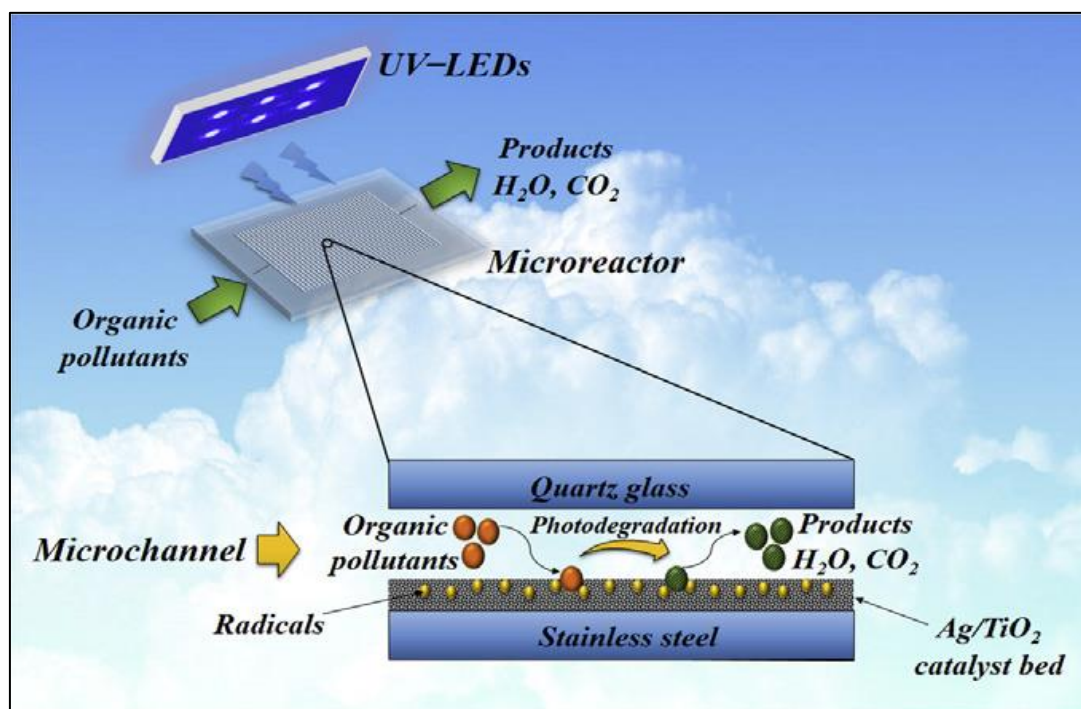


**Figure 3.** UV-LEDs-assisted preparation of silver-deposited TiO<sub>2</sub> catalyst bed inside microchannels as a high-efficiency micro-photoreactor for cleaning polluted water. Reprinted from [18] with permission of Elsevier.

Ultrasound has been applied in several research fields. These include, but are not limited to, structural modification of materials, and their transmissions, imaging, medical treatment, materials processing, acoustic microscopy, and more recently, wireless communications [19]. Use of ultrasound in a liquid facilitates the breaking of chemical bonds through sonolysis process, resulting in the formation of free radicals. Acoustic cavitation, bubble formation in a liquid exposed to pressure fields, causes several chemical and physical effects [20]. These processes are useful for the synthesis of nanomaterials, incrementation of catalytic chemical reactions, destruction of pharmaceutical waste, wastewater treatment, degradation of organic pollutants, and are representative of a method of production of fuels [21]. In conventional systems, ultrasound is also used to intensify liquid-liquid processes because of its efficient agitation effects and non-invasive nature [19,22]. It accelerates chemical reactions by intensifying mass transfer.

Currently, ultrasonics and microfluidics are introduced to revisit existing knowledge toolboxes to produce a technology-push hoping to commercialize modern inventions. Upon irradiation of an ultrasound wave, acoustic cavitation forms, such as cavitation microstreaming, shock wave, and jetting [23]. In this year (2019) until the time of submission, only five articles had been indexed by Scopus, which are retrievable by the combined keywords “microreactor” and “ultrasound.” The number of research articles published in the last decade is represented in Figure 4.



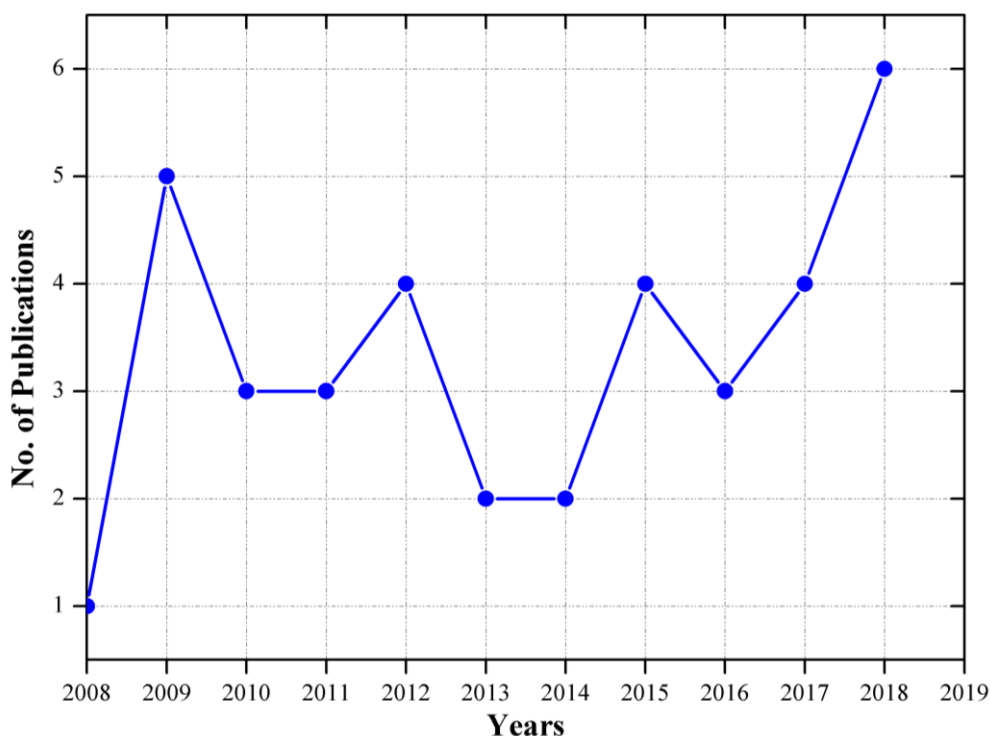


**Figure 4.** Work done with microreactors together with ultrasound in respective years (source: Scopus, access on 30 July 2019).

### 3. Side-by-Side Comparative Evaluation of Flow System to Batch

Microfluidics has many advantages compared with bulk chemistry, the first being slow diffusion. Therefore, to make the reaction faster, the distance required for interaction has to be smaller. The smaller channel dimensions also help to minimize the amount of sample required for analysis with reducing the by-products [13]. Recent advancement in this field has signified that miniaturization of reactors can be profitable in terms of kinetics, safety, and cost [24]. Because of its advantages, the synthesis of nanoparticles in microfluidics has become prominent in the past years [5]. The use of continuous microreactor led to the improvement of irradiation over the reaction mixture and offers a considerably reduced reaction time and better yields of products compared to batch reactors [25]. Batch reactors have a major disadvantage in the linear decrease in the intensity of the electromagnetic radiation with the square of the distance of the light source used [26,27]. The photocatalytic microreactors avoid this disadvantage by having a homogeneous illumination over the whole surface of the microchannel exposed to the light source [28]. Otherwise, the molecules undergoing photodegradation, under the control of the injection flow, constantly leave the reaction environment, avoiding the presence of by-products in the reaction mixture. The application of these devices to synthetic photochemistry started to spread from the 21st century [8].

There are several techniques for the prototyping of microfluidic systems [29], and different methods for the preparation of  $\text{TiO}_2$  films in photocatalytic microreactors [30]. These techniques should be fast and cost-effective from the design stage to the final system test. To fulfill the requirements, the production must be based on a simple technique and utilize low-cost instrumental resources [28]. Nanoparticle synthesis using continuous flow methods can produce a narrow size distribution of nanoparticles, which cannot be possible in a batch reactor. It has been proven that total reaction rate and photocatalyst mass transfer can be tuned with specific control, especially on size and shape, but also control over porosity, crystallinity, and thickness [14].

Noël et al. stated two important reasons for photochemistry achieving a remarkable increase in attention from researchers in academia and industry. The first reason is the exposure of visible light photo redox catalysis for organic synthetic chemistry. The second is the use of continuous-flow

reactors [31]. In one of their publications, they compared their results in flow to those obtained in batch experiments [32]. They reported a negligible loss in activity when the reaction was performed in flow. In fact, in the flow reaction, they observed higher activity at very short residence times. This result concluded with the major advantages of flow chemistry. It stated that increased mass- and heat-transfer allows the flow reactor to have very fast and efficient heating. These properties make it ideal for fast reactions.

The same authors have also suggested a list of nine good reasons to utilize photo flow [31]. The reasons are as follows:

1. Improved irradiation of the reaction mixture;
2. Reliable scale-up;
3. Improved reaction selectivity and increased reproducibility;
4. Fast mixing;
5. Fast heat exchange;
6. Multiphase chemistry;
7. Multistep reaction sequences;
8. Immobilized catalysts;
9. Increased safety of operation.

Noël et al. developed a completely automated microfluidic system that can handle solids efficiently at high concentrations through acoustic irradiation [32]. They experimented with the amination reaction of aryl triflates, aryl bromides, and aryl chlorides. Working with the flow system assisted in carrying out the reactions at a very short time and in figuring out the conversions and yields accurately. They concluded that their system is ideal for multistep syntheses, which requires a heterogeneous reaction. Furthermore, microflow photocatalytic reactors have shown to be a competent setup compared to batch [33], as can be seen in the selective organic synthesis in heterogeneous photocatalysis in a microflow, which is still in an underdeveloped stage as compared to traditional batch systems.

#### 4. Ultrasound: The Useful Tool for Chemists

Ultrasonic irradiation increases turbulence in the liquid phase, decreasing mass transfer limitations, and increasing the catalytically active surface area via the de-agglomeration and fragmentation of the particles [34]. Different effects of ultrasonic waves are shown in Figure 5. Nucleation, cavitation, bubble dynamics/interactions, thermodynamics, and chemical processes are the mechanisms of sonolysis.

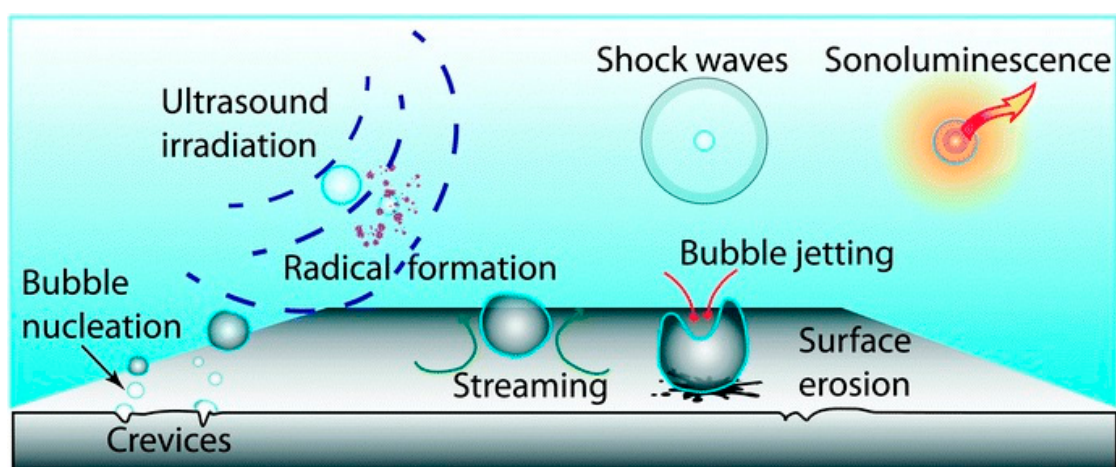
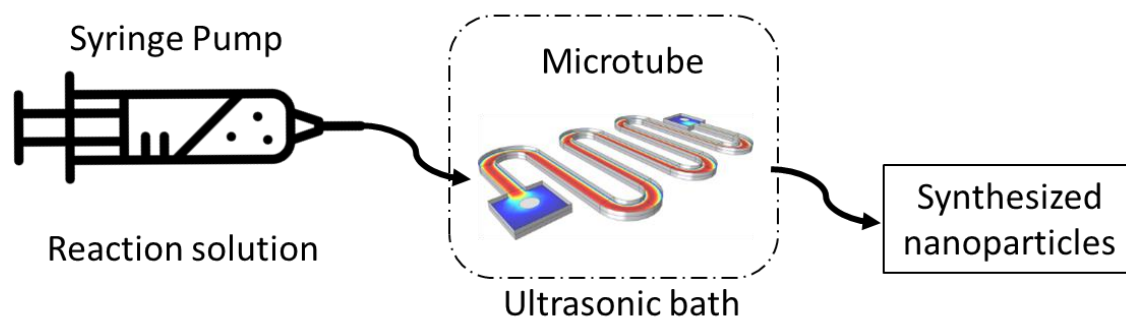


Figure 5. Effect of sonication. Reprinted from [20] with permission of the Royal Society of Chemistry.

Bridging and constriction are important mechanisms that lead to clogging in microfluidic devices, which can be eliminated via acoustic irradiation and fluid velocity, respectively [35]. Rivas et al., in their article, discussed the ultrasound approaches to control the particle formation inside the microchannel [33].

#### 4.1. Synthesis of Materials

There has been a large amount of research in synthetic fields under ultrasonic environments, such as the synthesis of nano inorganic materials. There are comparatively fewer studies on the effect of solids on sonochemical activity [20]. Countless articles exist up until today on the use of ultrasound for material synthesis. This process deals with the formation, gradual growth, and bursting bubbles (Figure 5). Application of ultrasound to the solution, for nanomaterial synthesis, produces shock waves, leading to an increase in temperature and pressure necessary for chemical reactions [13] (a diagram has been given to demonstrate the synthesis of nanoparticles using microtube and ultrasonic bath, Figure 6). A simple, ultrasound-assisted wet impregnation method was applied to synthesize materials by Colmenares et al. [36].



**Figure 6.** Diagram showing the use of ultrasound in a flow reactor for the synthesis of nanoparticles.

#### 4.2. For Immobilization of Catalyst

Deposition of metal particles on a substrate by ultrasound is a process in which both the reduction of the oxidized metal precursor and the deposition of the resulting metallic particles are driven by ultrasonic irradiation. This technique has been employed to coat metallic particles on various substrates. Earlier investigations indicated that the technique could yield well-dispersed metal nanoparticles tightly adhered to the surface of a substrate [37,38]. It can be stated that ultrasound plays a vital role in developing thin-film of well-dispersed nanoparticles. Many researchers have taken advantage of ultrasound to immobilize nanoparticles. Recently, Liu et al. worked on the deposition of metallic platinum nanoparticles on CdS for photocatalytic hydrogen evolution using ultrasound [39]. However, the development of a more adaptable system that is more synthetically feasible is needed [32].

#### 4.3. For Photocatalytic Experiments

In a review article, Qui et al. discussed heterogeneous sonocatalysts for treatment of organic pollutants in aqueous phase [40]. They discussed briefly the development of sonocatalysts from the past to the present in accordance with the different types of catalytic mechanisms. Teh et al., in another review article, discussed the development and modification of titania-based photocatalysts for pollutant-degradation using ultrasound technology [41]. They also stated the key operating parameters of ultrasound, followed by its application in the synthesis of the photocatalyst. Colmenares et al. synthesized magnetically separable materials by following the improved wet impregnation method assisted by ultrasonic irradiation. They developed a simple method for the preparation of magnetically separable  $\text{TiO}_2$ /maghemite-silica photo-active nanocomposites. The resulting nanomaterials were further tested for their photocatalytic activities in the liquid phase of selective oxidation of benzyl alcohol in both aqueous and organic phase [36]. The unusual reaction conditions (extremely high temperatures and pressures forming quickly in liquids because of acoustic cavitation phenomena)

of the ultrasonic irradiation technique were key factors in achieving homogeneously impregnated materials with nano-sized particles, and in the formation of heterojunctions. The catalysts were found to be highly photocatalytically active. Yu et al. also worked on photocatalyst synthesis [42]. They synthesized three-dimensional and thermally stable mesoporous  $\text{TiO}_2$  with high photocatalytic activity by high-intensity ultrasound-induced agglomeration.

## 5. Early Works on Microreactors

Microfluidic technology can be used profitably for the synthesis of nanomaterials and their catalytic studies. Efficient heat and mass transport in the miniaturized reaction chambers of microfluidic chips impart greater control at the molecular level. The microfluidic pathway offers an edge over the normal batch processes in terms of laminar flow, short molecular diffusion distance, and effective mixing [13,14,31]. Previously, many groups concentrated their work on exploring microfluidic photocatalytic microreactors for environmental application. Das et al. wrote a review article focusing on the fabrication techniques and operating parameters for this type of microreactor [43].

Based on the method used to incorporate catalysts on the inner wall of the microreactor, it can be divided into three classes: (i) packed-bed, (ii) monolithic, and (iii) inner wall-functionalized [9] (Figure 7). The packed-bed reactor can be explained as the immobilization of a catalyst on insoluble support and is haphazardly assembled in the reactor, whereas in a monolithic reactor, the catalyst is made in the shape of structured material. In an inner wall-functionalized reactor, the catalyst is covalently attached to the interior wall of the reactor. To ensure a smooth flow of reagents, minimization in the mass transfer resistance was provided. Because of the complexity of the synthesis, their application is still limited [31]. Tao et al. proposed a synthesis procedure based on microfluidics for the production of  $\text{Ag@Cu}_2\text{O}$  core-shell nanoparticles [44]. Sachdev et al. presented a microfluidic method for the synthesis of hollow Au shells and  $\text{Fe}_3\text{O}_4\text{@Au}$  core-shell nanoparticles within an emulsion droplet [45] ('@' stands for core-shell by the respective authors).

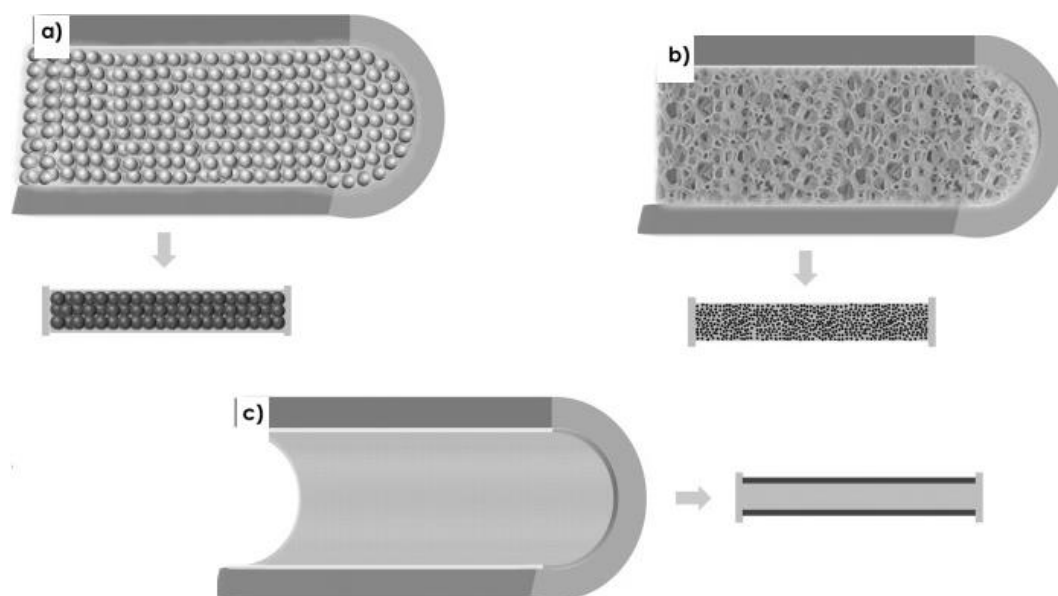


**Figure 7.** Schematic representation of the cross-section of a microchannel in (a) packed-bed, (b) monolithic, and (c) wall-coated microreactors. Reprinted from [9] with permission of Wiley.

Flow chemistry has started to make an extensive impact on the way many chemists carry out synthesis over the last 15 years [8]. Microfluidics has significant applications in various fields [46,47]. In the year 2015, Yao et al. published a review article related to various applications of microreactors [5]. This review article was mainly based on structures and applications of microreactors in the synthesis of nanoparticles, and also on bio-substances, organics, and polymers. The whole article focused on

multiphase microreactors. Knowles et al. used dual-channel microreactors for transformations, which are synthetically useful [8]. The same reactor was also applied for the synthesis of the antimalarial artemisinin, and the conversion of  $\alpha$ -terpinene to ascaridole successfully. An additional application of microflow photochemistry includes the synthesis of vitamin D3 [7].

Nanoparticle synthesis in microreactor types for on-chip photocatalyst synthesis has been reviewed, along with challenges in handling the nanoparticles in microsystems [14]. The most important design parameter of photocatalytic reactors is the illuminated specific surface area of the photocatalyst. Matsushita et al. have developed a photocatalytic microreactor system, which has a considerably large surface area per unit volume [26]. Research over the past decade focused on enabling multi-step processes by developing complex microchemical systems. The prime example of such multistep microchemical synthesis is multi-step Heck synthesis carried out in continuous flow [19]. Microfluidic systems provide a platform for a broad range of syntheses. These allow automated optimization [48] and rapid experimentation (e.g., reaction conditions, catalysts) [49]. Moreover, microfluidic systems allow safe synthesis and increase the feasible reaction space (performing synthesis in supercritical solvents). Additionally, the residence time of species and the reactor temperature can be precisely controlled. All these studies focused on the use of microreactors for chemical synthesis in flows [19].

In a review article, the importance of continuous-flow photo-microreactors in water treatment, organic synthetic chemistry, and materials science was described [31]. Some recent examples pointed to complex applications, such as the synthesis of complex biologically active molecules [50]. Automated and self-optimizing flow processes have been developed to reduce manual labor [31]. In a recent article, Cambié et al. stated that a multidisciplinary approach would be the best strategy to overcome the remaining hurdles in chemistry. Intense collaborations between academia and industry are the most important part. To address the challenges of the future, industrial income has become more vital because of the drop in funding opportunities [31]. Considerable research in this field has been done in the last decade, and making further progress will be challenging.

In another article, Shchukin et al. [51] stated the advantages of microflow photocatalytic process as (i) possibility of providing definite characteristics to the microreactor by removing additional functionalities; (ii) high active area for reaction with increased yield of photoreactions; (iii) less volume (micron and submicron), allowing one to perform photochemical synthesis in the highly organized solvent; (iv) reduced concentration and heating effects on adding reagents in the reaction; (v) possibility of modelling and mimicking photo-induced processes in nature on the micron and submicron level. So far, many articles have reported on several microns and submicron-confined environments for performing photocatalytic processes. However, there are only a few examples of spatially confined individual reactors for the semiconductor-catalyzed photodegradation reactions to date [49]. The study of reaction kinetics and mechanisms, influence of different parameters (e.g., size of the microreactor), adsorption of the reactants and intermediates, and solvent structure in the interior, among others, on the photosynthetic technique, along with a comparison of reaction products with those obtained by catalytic photolysis in non-confined media (e.g., in the slurry of dispersed photocatalyst) is scarce in the literature. These details can help in understanding the chemical and physicochemical processes occurring in the environment, as well as the development of spatially confined photosynthetic approaches. The results of conventional heterogeneous photocatalysis can be improved by exploiting the physical processes that occur in confined geometries with controlled diffusion of the reagents [51].

Various photocatalytic reactors have been reviewed for different applications [52,53]. Most of them can be classified into microreactors and slurry reactors. Some can be handled with suspended photocatalysts immobilized in the latter by considering the specific surface area of the catalyst and uniform light penetration in the reactor volume by various approaches [54]. The slurry reactors provide several active sites per unit volume. These microreactors were often used for air treatment [55]. Because of the limited designs available, photocatalytic reactors are still not commonly implemented in industrial processes. In the case of a three-phase microreactor with dispersing catalyst nano-powder,



the higher adsorption rate was found in wastewater treatment. It has been seen that the photocatalytic activity decreases with particle size [56]. The mean particle size also can be easily adjusted by the pH of the solution and choice of solvent [57]. The accumulated particles inside a micro path make the recycling process difficult after the photocatalytic step [43].

The typical flow systems found in the catalytic layer immobilized channel are slug flow or annular flow (Figure 8), depending on the operating conditions [58]. The important leverage of a microreactor with the immobilized thin-film catalyst is that it does not require a discrete step to separate the photocatalyst after the reaction. The high surface area of the catalyst also helps in increment of mass transfer in bulk and inter-phase. For example, oxygen that accepts electrons and, resultantly, does not allow recombination of electron-hole pair in the photocatalysis, leads to high reaction efficiency [59]. The lower interfacial catalyst surface area per mass is the main disadvantage of the inner surface-immobilized photocatalytic thin film of microreactors [60]. The combined effects of mass transfer with photocatalytic reaction have been studied in Charles et al.'s and Corbel et al.'s works [61,62].

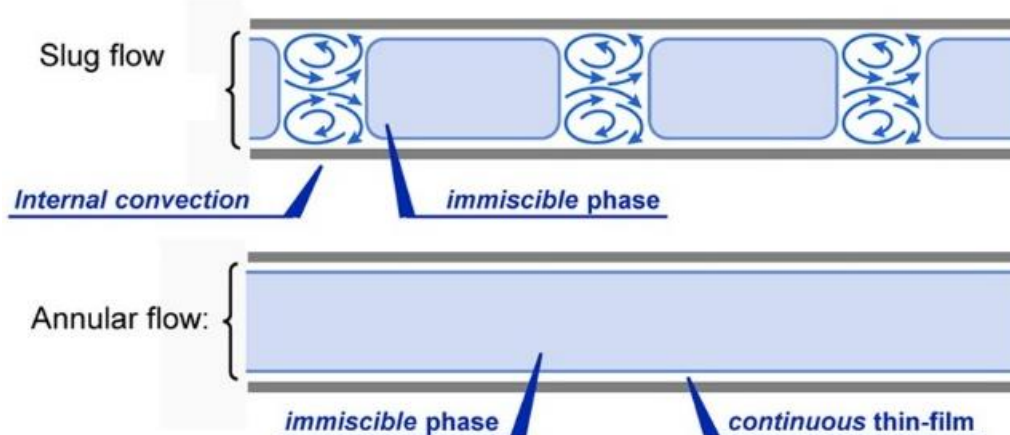


**Figure 8.** Particle formation in a single-channel microreactor. Reprinted from [31] with permission of American Chemical Society.

Different microreactors have been developed to upsurge the reaction efficiency [63], such as micro-capillary reactors [64], single-microchannel reactors [18,65], and planar reactors, although it's photocatalytic, as well as energy efficiency, still needs to be improved [66]. In a review article, Heggio et al. discussed the work of different researchers to attain high throughput. Some researchers tried to achieve this by increasing the length or number of microchannels, whereas others tried to enlarge the dimension by keeping one dimension in the microscale.

In a review article, Woolley et al. discussed the materials (silicon, glass, and ceramics) and polymers (elastomers, thermoplastics, and paper) that scientists are using in microreactors for different purposes (microreactor's fabrication). Hybrid devices have shown promising ability to gain the benefits of each material's strengths [13]. Professor George Whitesides used polydimethylsiloxane (PDMS) to create inexpensive microfluidic devices, and Yoshida's microreactor initiatives in Japan built up considerable interest in the microreactor area [5]. Das and Srivastava inspected various techniques to construct microstructures, such as mechanical micro-cutting, lithography, and etching technology. On the basis of the material of the devices, they divided the micro-photoreactors into four groups: ceramic microreactors, polymeric microreactors, metallic microreactors, and glass microreactors [43].

Signs of progress done in the modification and design of the structure of microreactors over the last ten year has been reported, and it has also introduced the improvement in organic reactions and synthesis of inorganic materials. Exemplary reviews have been published on the reaction process, the impact on downstream processing, and the product properties [67,68]. Multiphase microfluidic devices have also been discussed to synthesize inorganic and metal nanoparticles [5].

Some polymers, on the other hand, are presented as a good alternative for use in photochemistry and have been applied for the intensification of photochemical processes [69]. This paper focused on multichannel microreactors, which can be used for a wide range of liquid-phase organic synthesis reactions. The reactor system showed better potential because of the presence of several microchannels and the simplicity of parallelly arranging a number of these devices [69]. In a study, Ramos et al. investigated the possibility of employing UV-transparent polymer microtubes as supports for TiO<sub>2</sub> (titanium dioxide) photocatalysts, and their applicability in the oxidation of organic pollutants [64].

Because of the advancement in syntheses such as increased mass and heat transfer, operational safety, the potential for purifying continuously, control over residence time, and scalability by parallel operation of several devices, the usage of microfluidic devices has attracted consideration from the pharmaceutical industry [70]. Despite these advantages, one of the biggest hurdles in the development of flow chemistry methods is the handling of solids, such as precipitates during the reaction, leading to clogging of the microchannels. Among all the approaches, the use of ultrasound is an effective way to avoid clogging. In order to prevent the particles from interacting with the reactor walls, segmented liquid-liquid flow can be used [71]. Though this is an efficient way to handle solids, the efficiency of the reaction can be reduced by using an additional solvent. Recently, Buchwald et al. presented a biphasic system of an organic solvent and water, which could solubilize both the organic and inorganic components of a reaction [72,73].

Microfluidic reactors have been developed to implement miniaturized laboratories for (i) synthesis of organic and inorganic compounds, and (ii) analytical tests and biomedical applications [28]. In these situations, the process parameters (P, T, V, and concentration) must be highly controlled in well-defined time units, in order to reduce raw material costs, analysis time, and risks in reagent handling, or potentially dangerous flammable, explosive, corrosive, and carcinogenic products, and bacteriological agents. From the advantages of the method, it can be stated that high temperature and long-time are not required. It is noteworthy that the diameter of the core-shell can be controlled by the concentration of the inner particle in the organic phase, and the diameter of hollow shells can be adjusted by varying the flow rate [14]. Y. Matsushita et al. examined the feasibility of the micro-reaction system on organic photoreactions, finding that the photocatalysis of TiO<sub>2</sub> can be categorized into two types: homogeneous photocatalytic reaction and heterogeneous photocatalytic reaction systems. Among the different types of catalyst-based photochemical reactions, homogeneous-based photocatalysis has been broadly studied in microfluidic-based flow systems for selective organic synthesis [33].

## 6. Immobilization of Nanoparticles Inside the Microtube

Most research on photocatalytic reactions has been carried out using dispersed powders in conventional batch reactors. However, systems with the immobilized catalyst can avoid the separation of dispersed powders (preventing light penetration) after the reaction, as they have low interfacial surface areas. Thus, Matsushita et al. have developed photocatalytic microreactors with an immobilized TiO<sub>2</sub> layer [74]. The thermal oxidation [75], physical vapor deposition (PVD) [76], chemical vapor deposition (CVD) [77,78], dip-coating [79], spin-coating [80], electrospun [81], sputtering [82], sol-gel [83], and electrodeposit [84] methods are techniques for the film formation step needed in the design of immobilized photoreactors. Figure 9 represents a sol-gel-based deposition of TiO<sub>2</sub> inside a glass microtube.

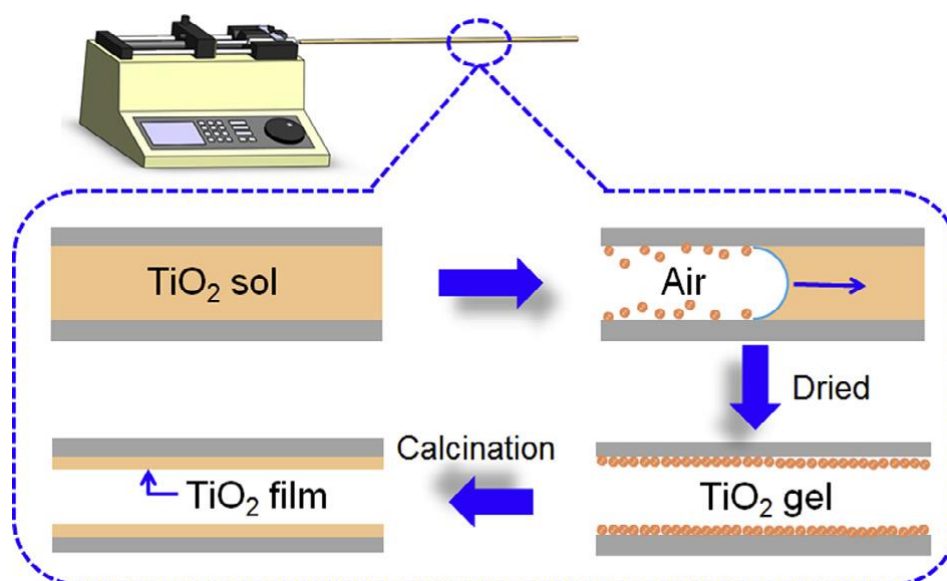


**Figure 9.** TiO<sub>2</sub> thin film inside a microtube using the sol-gel method. Reprinted from [57] with permission of Elsevier.

Recently, Sohrabi et al. [14], in their review article, discussed the challenges as well as opportunities of microfluidic reactors. They stated that the main challenges in microfluidic nanoparticle synthesis and application are the crystallization of the photocatalyst, the poly-dispersity of particles and channel clogging, and the carryover of suspended photocatalysts. It would be worthwhile to devote much effort in the wall-coated microreactor by selecting suitable surfactants and manipulating polymerization conditions [85]. Lopez-Orozco et al. claimed that the high surface reactivity would enable the attachment of functional groups to synthesized microreactors inside nanocomposites or the microchannel. The evolution of the research on composite-based microreactors has been quite encouraging [86]. In the simplest case, the intrinsic activity of the wall of the reactor is sufficient to catalyze the reaction.

In most cases, a sufficient number of active sites cannot be provided by the surface of the microreactor or improve the existing surface area—some surface modification is required. Moreover, a surface pre-treatment can help to improve the adhesion of coatings to attain maximum potential for immobilization of the catalyst. Plasma oxidative treatment, thermal or chemical oxidation, UV radiation, anodic oxidation, and chemical modification are some methods that have been used for pre-treatment [87].

A microreactor with the photocatalytic thin film deposited on its inner spaces is a substitute for the slurry photocatalytic reactors [88]. H. Nakamura et al., in their article, discussed the modification of the inner wall of a microreactor and coating it for photocatalytic and enzymatic reaction studies. They used self-arrangement of colloidal particles to modify the microreactor inner wall. They observed an increase in conversion rate as well as yield [89]. Yue demonstrated the process of synthesis in microflow by improving heat and mass transfer rates. He explained some applications of catalytic processes in microfluidic reactors, for instance, selective hydrogenation, aerobic oxidation of alcohols, and direct hydrogen peroxide synthesis. He also discussed the multiphase flow in wall-coated microreactors and gas-liquid flow patterns in packed-bed microreactors [10]. The study on the amine N-alkylation processes in a microreactor with immobilized TiO<sub>2</sub> has also been discussed earlier [26]. More examples of immobilized titania inside various types of microreactors are presented in the following Table 1.

On another note, many interesting novel contributions come from three-dimensional (3D) printed microchannels, which can be fabricated from plastic, metals, or glass. These types of microchannels can be made efficiently and quickly and are capable of manufacturing structures from microns to several centimeters. Different types of 3D printers are shown in the following Figure 10.



**Table 1.** Immobilization of a catalyst inside different types of microreactors.

Reference	Type of Microreactor	Method of TiO <sub>2</sub> Immobilization	Outcomes from TiO <sub>2</sub> Characterization
[17]	metal-titanium foil	Anodization and hydrothermal treatment	Good mechanical properties of titania nanotube film, nanotubes of TiO <sub>2</sub> (TEM, SEM)
[57]	glass capillaries	Sol-gel	Homogenous dispersion, narrow particle size distribution (SEM, TEM)
[18]	stainless steel microreactor	Sol-gel	Uniform distribution of catalyst on surface, crystalline size is 32 nm, the reflectance spectrum of pure TiO <sub>2</sub> is 393 nm (HRTEM, XRD, DRS)
[74]	self-adhesive fluorine resin (EFEP) channel and switched between two glass plates	Sputtering	Growth of anatase peaks (XRD)
[90]	Silica capillary	Wash coating and calcination	The thickness of the deposited layer 88 nm (Field Emission Gun-Scanning Electron Microscopy(FEG-SEM))
[91]	Dual-film optofluidic microreactor	Hydrothermally prepared nanorod growth on fluorine-doped tin oxide (FTO) glass	2.4 μm thick film of TiO <sub>2</sub> nanorods inside glass tube (SEM)
[92]	coil-type photoelectrocatalytic microreactor	Anodization	25 nm thickness and 12 to 15 μm length of titania nanotubes (FESEM)
[93,94]	fluorinated ethylene propylene (FEP) microtube	Ultrasound-based deposition	Structural transformation of polymer tube with ultrasound, thickness of catalyst layer was 3–6 μm (confocal microscopy, SEM)

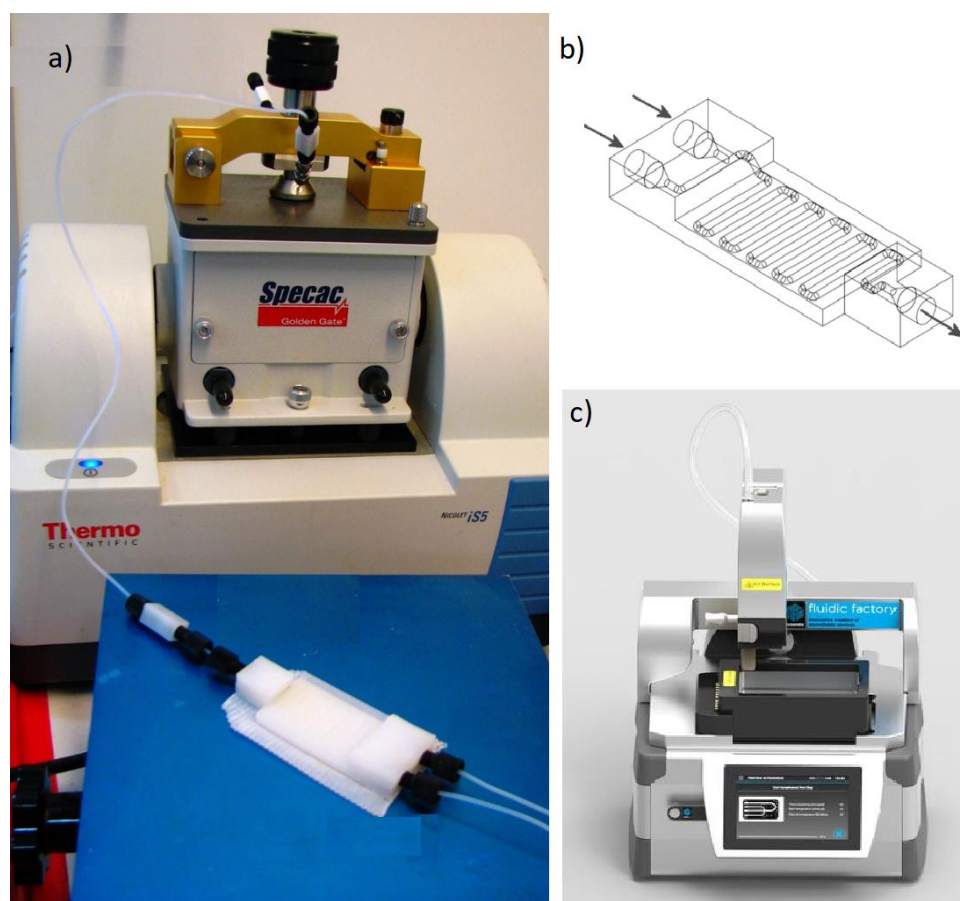


**Figure 10.** (a) Flow system setup and ATR-IR flow cell with connections. (b) Schematic representation of the three-dimensional (3D)-printed reactionware devices showing the internal channels ('a' and 'b' are reprinted from [95] with permission of American Chemical Society). (c) Picture of the Fluidic Factory 3D microdevice printer made by Dolomite Microfluidics.

In a microfluidic device that was produced by rapid prototyping and was economically feasible and simple, a coating of TiO<sub>2</sub> nanoparticles was applied, forming a photocatalytic microfluidic reactor destined to the degradation of organic dyes. It is important to point out that rapid prototyping of microfluidic devices is also relevant for the testing of small quantities of photocatalytic nanomaterials that are being developed in the research laboratories and that still lack the characterization of their photocatalytic efficiency. This new methodology will allow us to quickly test synthesized materials in reduced quantities, in addition to generating less waste. This more sustainable approach respects green chemistry requirements [96]. The possibility of varying the geometry of the microreactor, creating larger contact areas and a stronger bond between the photocatalytic coating and the surfaces of the microreactor, can further improve the photo-degradation efficiency of the microfluidic device, allowing for the increase of the flow velocity and, from this, the increasing of the volume of the treated solution. Different designs of the geometry of the device, implementation of a dye solution reflux system, photocatalyst chemical functionalization, and a light-emitting diode-based UV light system are being tested to improve the performance of the photocatalytic microreactor for potential applications in selective oxidation of functional groups of organic compounds [28].

Ultrasonic waves were used to break up agglomerations of particles [32,97]. The use of light transparent fluorinated ethylene propylene (FEP) microtubes (excellent visible light transmission, UV transmission: ~80%, temperature: -270 to 205 °C) with TiO<sub>2</sub> leads to maximum usage of light for activating the photocatalyst for higher phenol degradation [93]. The design of a highly effective photoreactor is decisive to get the highest reaction rates with the immobilized form of a catalyst. Use of sonication for designing reactors, especially the deposition of a catalyst inside a microreactor, is a novel approach.

## 7. Photocatalytic Experiment

The amount of light absorption of a photocatalyst at a given wavelength can be determined by the light intensity [98]. The photocatalyst activation step, the formation rate of electron-hole, is strongly dependent on the light intensity, and light distribution within the reactor undoubtedly determines the overall efficiency of the photocatalytic process. A light source of minimal space and lower photon cost is suitable for the microreactor system to take advantage of the miniaturized reaction vessel. Thus, Matsushita et al. employed UV-LEDs for the excitation light source of a photocatalyst [26]. Furthermore, it limited the depth of light penetration because of the absorption and scattering [99], as expressed by the Bouguer-Lambert-Beer law [100]. It should be noted that safety issues should be paid attention to, even in photochemical reactors for bio-applications [101], and with toxic or hazardous compounds [102]. Saien and Soleymani [54] explained the slurry photocatalytic microreactor as a favorable technique in dispersing TiO<sub>2</sub> particles. Some experiments for the degradation of phenol used a high energy 125 W UV mercury lamp [52]. The manufacture of a microfluidic device with the nanostructured TiO<sub>2</sub> coating has been described as being integrated on the inner surface of the microchannels in the work of Pandoli et al. Subsequently, efficiency was evaluated for the degradation of aqueous solutions of organic dyes in continuous flow under the action of UV light [28].

Currently, photochemistry using microspace is a major attraction of the scientific community for green chemistry application (Figure 11).

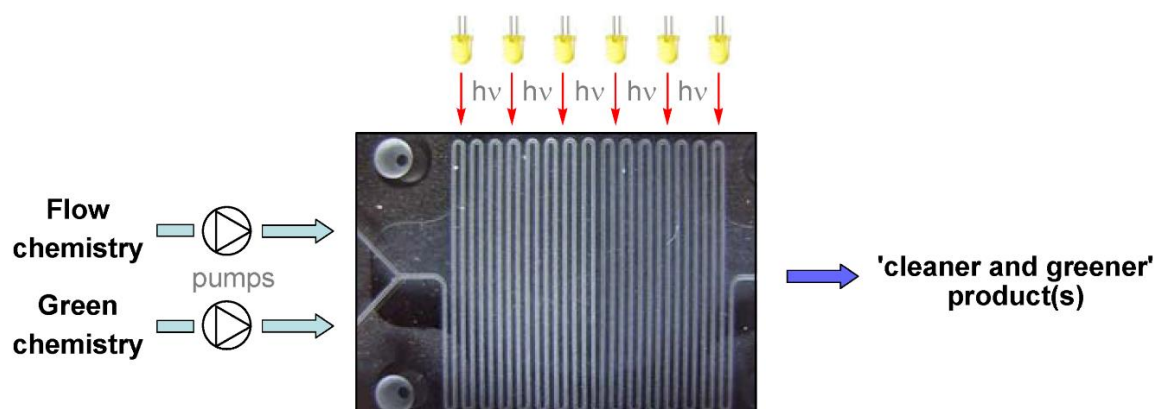
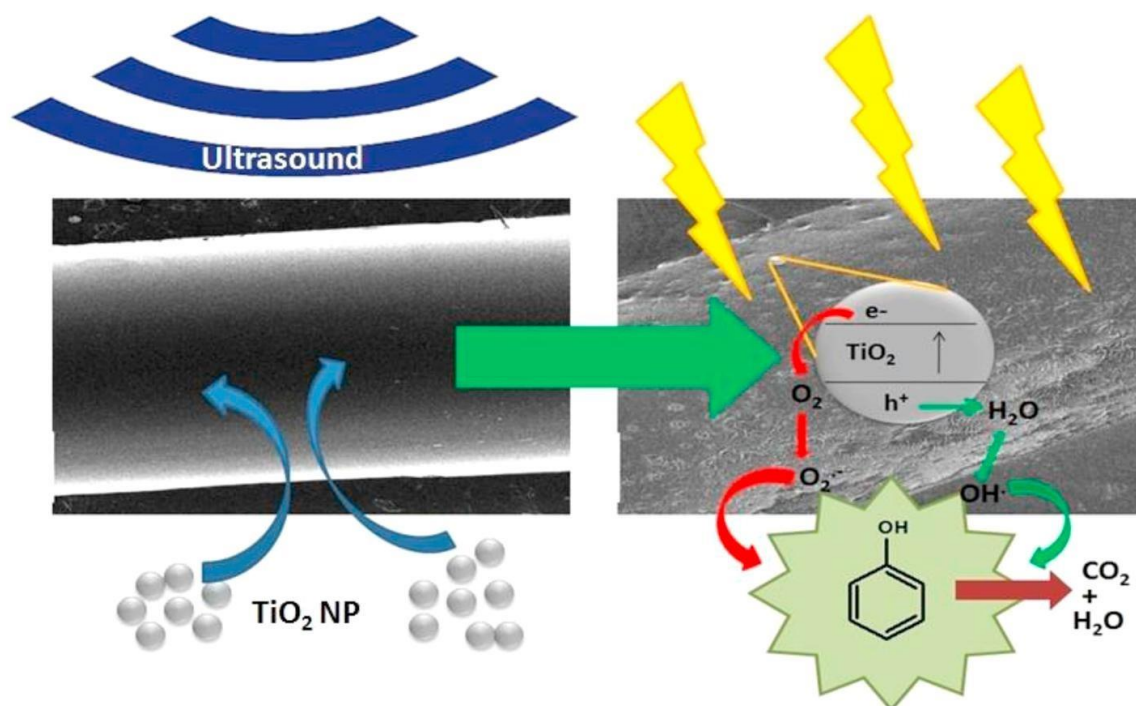


Figure 11. Concept of microflow photochemistry. Reprinted from [63] with permission of MDPI.

### 8. Microreactor with Ultrasound for Photocatalysis: A New Way Forward

Sonochemical processes are highly efficient in terms of selectivity, reaction time, and operational simplicity [93,103–106] while being used for the synthesis of various semiconductor-based nanoparticles in batch reactions. Combination of the ultrasound transducer and the microfluidic reactor [107] has gained the attention of many researchers. Such designed systems can then be applied to microfluidic liquid-liquid extraction [108], degradation of contaminants [103,109,110], and particle synthesis [111,112]. These types of reactors are broadly used in laboratories and industrial applications, but the analysis and comparison of results obtained with them are extremely difficult, which has limited the scaling-up of sonochemical reactors in the industry [113].

Many studies have been performed, and thus it is well verified that the advantages of ultrasound technique includes short reaction times, improved conversion, enhanced yields, and mild conditions [114]. A capillary microreactor, together with ultrasound, was designed and presented by Aljbour et al. to carry out some chemical reactions. They investigated the hydrolysis of benzyl chloride in a two-phase slug flow system. The increase in the rate of the hydrolysis reaction has been noticed with an increase in temperature, along with the effect of ultrasound. They noticed that the impact of ultrasound slowed down with an increase in the temperature. They also noted that the flow rate inside capillaries escalated the mass transfer between phases. The ultrasound helped in increment of the intensity of the internal circulations by splitting the large slugs into smaller sized slugs [7]. Sonication has been initially applied to homogeneous reactions; however, this approach has now been employed to heterogeneous reactions [115]. Ultrasound has some disadvantages, such as inefficient energy transfer via impedance and secondary effects such as streaming, sound field attenuation, heating, bulk mixing, emitter erosion, and sound emission. The parameters that influence sonochemical reactions and consider how they may be implemented to achieve systematic optimization has been discussed earlier [21]. Recently, Colmenares and co-workers were able to demonstrate for the first time an ultrasound-aided deposition of commercial TiO<sub>2</sub> nanoparticles in an FEP-based microtube (Figure 12) using a probe-type ultrasonic system [93,94]. From AT-IR spectra, CH stretching peak in the modified tube, which was absent in the unmodified FEP microtube, confirmed that ultrasound brings some chemical changes in the inner walls of the FEP microtube.



**Figure 12.** Photocatalytic phenol degradation in ultrasound ( $\text{TiO}_2$ )-deposited FEP microtube. Reprinted from [93] with permission of Elsevier.

Current progress in photocatalysis on microreactor systems using ultrasound has been reviewed by Matsushita et al. They stated that the relative effect of ultrasound is more pronounced at a lower temperature compared to silent conditions. According to them, the reason is that the ultrasonic waves enhanced contact between reactants by damaging the phase boundary. In the silent condition, the contact between phases showed more mass transfer limitation. Increment of the vapor pressure of the liquid medium, as a result of elevated temperature, lead to easier effective cavitation [116]. This trend is more detectable at higher flow rates because of the lower exposure time to the ultrasonic irradiation. Rivas et al. focused on the control of cavitation as a means to improve the energy efficiency of sonochemical reactors, as well as in the solid handling with ultrasound. They discussed some examples of microfluidic clogging prevention, numbering-up, and scaling-up strategies. In their work, they tried to reduce the clogging of the microreactor and lengthen the operational time of the reactor [19]. Ultrasound-assisted capillary microreactors have also been proposed and tested as a potential reactor for the multiphase aqueous-organic system. The effect of ultrasound irradiation under different temperatures, capillary lengths, and flow velocity was also examined [7].

Sonochemistry could play a key role in overcoming limitations caused by solid formations by introducing ultrasound in conventional flow systems and microreactors [117,118]. Mass transfer limitation in microreactors can now be partially overcome by the help of ultrasound. The well-defined configuration of microreactors makes this easy and provides an ideal platform to investigate and control the acoustic cavitation process [118]. Colmenares et al. established a novel low energy ( $<80^\circ\text{C}$ ) ultrasound-based deposition method using a probe-type ultrasonic system for coating of commercial  $\text{TiO}_2$  nanoparticles in the inner walls of FEP microtubes, knowing its importance in catalysis and photocatalysis fields [93,94]. The method is simple to implement and is environmentally friendly with low heat generation and has been filed for a patent [94]. The FEP microtube was pretreated with water using the ultrasound process, which resulted in physical changes of the inner surface of the FEP microtube, creating rough spots and an etched surface—facilitating the stable immobilization, under sonication, of  $\text{TiO}_2$  nanoparticles on FEP internal walls. It has been demonstrated that the change in the surface characteristics (functionalization by pretreatment and  $\text{TiO}_2$  nanoparticle deposition) of the inner walls of the fluoropolymer is due to the physical effect of ultrasound (a promising device



for phenol degradation in water). Another work of Colmenares et al. reported, for the first time, the selective oxidation of benzyl alcohol to benzaldehyde in a photocatalytic microreactor under UV-LED as the light source [33]. In this work, they used an ultrasonic bath (with a temperature close to ambient) for immobilization of ZnO inside a microtube.

## 9. Future Challenges and Conclusions

Since its introduction three decades ago, the field of microfluidics has witnessed significant growth in scientific research done across multiple disciplines, especially towards biological and medical applications. The advantages provided by the unique physical and chemical interactions of particles that take place inside the microscale channels, along with the coupling of multiple functionalities, has continued to drive the scientific advances of microfluidics. Outstanding research has been done in terms of materials and functions, their integration, and applications of microfluidics. In microfluidics, glass and silicon have been traditionally used most frequently, but recently polymeric materials have gained considerable attention, especially in the area of low-cost, and disposable devices. Still, there is a need to develop better material with improved properties, as the current generation of the material comes with its inherent advantages and disadvantages. The further improvement of the current method (e.g., different microreactor lengths, the application of different nanoparticles, physical and chemical effect optimization of ultrasound) will provide new ways, not only for environmental applications but also for new green organic synthesis protocols [93]. Even with this state of research, microfluidics has not been accepted outside of academia. However, acceptance of new technologies outside of academic research has always been slow, and more work should be done to promote wider and practical applicability of microfluidics. Heterogeneous photocatalysis in a microflow system for generation of value-added chemicals is a novel green chemistry approach requiring the understanding of photocatalysis, microfluidics, and reactor design. Research on the development of low energy and environmentally friendly-based photo-microreactor systems for photocatalysis is yet to be explored. In the areas of environmental and spatial analysis, effort should focus on creating robust and portable devices that can operate unattended for long periods. There are also some challenges related to 3D microreactors to be overcome, including chemical compatibility and operation at high pressures and temperatures [119].

The interesting use of ultrasound irradiation in catalyst synthesis is gaining more and more value from both the fundamental and application point of view. Sonication is giving us a great opportunity as a real green and cost-effective methodology and is foreseen to hold great potential in the near future [103]. Using low energy-based ultrasound for photocatalyst synthesis inside polymer-based microtubes (that does not deteriorate with age) will pave a new path towards the greener approach.

**Author Contributions:** J.C.C.Q. and S.R.P. planned the conceptual ideas and conceived proof outline. S.R.P. drafted the manuscript. R.F.C.-Q. did conceptualization, review, and editing. J.C.C.Q. and R.F.C.-Q. revised the manuscript critically for essential intellectual content. All authors discussed and contributed to the final manuscript.

**Funding:** J.C. Colmenares and Miss Swaraj Rashmi Pradhan gratefully acknowledge the support from the National Science Centre in Poland within Sonata Bis Project No. 2015/18/E/ST5/00306. (More info at <https://photo-catalysis.org/>).

**Conflicts of Interest:** The authors declare no conflict of interest.

## References

1. Anastas, P.T.; Warner, J.C. *Green Chemistry: Theory and Practice*; Oxford University Press: New York, NY, USA, 1998.
2. Meng, X.; Zhang, Z.; Li, X. Synergetic photoelectrocatalytic reactors for environmental remediation: A review. *J. Photochem. Photobiol. C Photochem. Rev.* **2015**, *24*, 83–101. [[CrossRef](#)]
3. Colmenares, J.C.; Lisowski, P.; Łomot, D. A novel biomass-based support (Starbon) for TiO<sub>2</sub> hybrid photocatalysts: A versatile green tool for water purification. *RSC Adv.* **2013**, *3*, 20186–20192. [[CrossRef](#)]

4. Yang, Z.; Liu, M.; Lin, C. Photocatalytic activity and scale-up effect in liquid-solid mini-fluidized bed reactor. *Chem. Eng. J.* **2016**, *291*, 254–268. [[CrossRef](#)]
5. Yao, X.; Zhang, Y.; Du, L.; Liu, J.; Yao, J. Review of the applications of microreactors. *Renew. Sustain. Energy Rev.* **2015**, *47*, 519–539. [[CrossRef](#)]
6. Colmenares, J.C.; Varma, R.S.; Nair, V. Selective photocatalysis of lignin-inspired chemicals by integrating hybrid nanocatalysis in microfluidic reactors. *Chem. Soc. Rev.* **2017**, *46*, 6675–6686. [[CrossRef](#)] [[PubMed](#)]
7. Aljbour, S.; Tagawa, T.; Yamada, H. Ultrasound-assisted capillary microreactor for aqueous-organic multiphase reactions. *J. Ind. Eng. Chem.* **2009**, *15*, 829–834. [[CrossRef](#)]
8. Knowles, J.P.; Elliott, L.D.; Booker-Milburn, K.I. Flow photochemistry: Old light through new windows. *Beilstein J. Org. Chem.* **2012**, *8*, 2025–2052. [[CrossRef](#)]
9. Munirathinam, R.; Huskens, J.; Verboom, W. Supported catalysis in continuous-flow microreactors. *Adv. Synth. Catal.* **2015**, *357*, 1093–1123. [[CrossRef](#)]
10. Yue, J. Multiphase flow processing in microreactors combined with heterogeneous catalysis for efficient and sustainable chemical synthesis. *Catal. Today* **2018**, *308*, 3–19. [[CrossRef](#)]
11. Dimov, S.; Gasenko, O. Catalytic combustion and steam reforming of hydrocarbons in microreactor. *MATEC Web Conf.* **2017**, *115*, 03011. [[CrossRef](#)]
12. Licklider, L.; Kuhr, W.G. Optimization of on-line peptide mapping by capillary zone electrophoresis. *Anal. Chem.* **1994**, *66*, 4400–4407. [[CrossRef](#)]
13. Nge, P.N.; Rogers, C.I.; Woolley, A.T. Advances in microfluidic materials, functions, integration, and applications. *Chem. Rev.* **2013**, *113*, 2550–2583. [[CrossRef](#)] [[PubMed](#)]
14. Sohrabi, S.; Keshavarz Moraveji, M.; Iranshahi, D. A review on the design and development of photocatalyst synthesis and application in microfluidic reactors: Challenges and opportunities. *Rev. Chem. Eng.* **2019**, *0*, 1–36. [[CrossRef](#)]
15. Aran, H.C.; Salamon, D.; Rijnaarts, T.; Mul, G.; Wessling, M.; Lammertink, R.G.H. Porous photocatalytic membrane microreactor (P2M2): A new reactor concept for photochemistry. *J. Photochem. Photobiol. A Chem.* **2011**, *225*, 36–41. [[CrossRef](#)]
16. Worz, O.; Jackel, K.P.; Richter, T.; Wolf, A. Microreactors—A new efficient tool for reactor development. *Chem. Eng. Technol.* **2001**, *24*, 138–142. [[CrossRef](#)]
17. Krivec, M.; Žagar, K.; Suhadolnik, L.; Čeh, M.; Dražić, G. Highly efficient TiO<sub>2</sub>-based microreactor for photocatalytic applications. *ACS Appl. Mater. Interfaces* **2013**, *5*, 9088–9094. [[CrossRef](#)] [[PubMed](#)]
18. Eskandarloo, H.; Badiel, A.; Behnajady, M.A.; Ziarani, G.M. UV-LEDs assisted preparation of silver deposited TiO<sub>2</sub> catalyst bed inside microchannels as a high efficiency microphotoreactor for cleaning polluted water. *Chem. Eng. J.* **2015**, *270*, 158–167. [[CrossRef](#)]
19. Fernandez Rivas, D.; Kuhn, S. Synergy of microfluidics and ultrasound: Process intensification challenges and opportunities. *Top. Curr. Chem.* **2016**, *374*, 70. [[CrossRef](#)]
20. Fernandez Rivas, D.; Cintas, P.; Gardeniers, H.J.G.E. Merging microfluidics and sonochemistry: Towards greener and more efficient micro-sono-reactors. *Chem. Commun.* **2012**, *48*, 10935–10947. [[CrossRef](#)]
21. Wood, R.J.; Lee, J.; Bussemaker, M.J. A parametric review of sonochemistry: Control and augmentation of sonochemical activity in aqueous solutions. *Ultrason. Sonochem.* **2017**, *38*, 351–370. [[CrossRef](#)]
22. Cintas, P. Ultrasound and green chemistry—Further comments. *Ultrason. Sonochem.* **2016**, *28*, 257–258. [[CrossRef](#)] [[PubMed](#)]
23. Dong, Z.; Zhao, S.; Zhang, Y.; Yao, C.; Chen, G.; Yuan, Q. Mixing and residence time distribution in ultrasonic microreactors. *AIChE J.* **2017**, *63*, 1404–1418. [[CrossRef](#)]
24. Wang, H.; Nakamura, H.; Uehara, M.; Miyazaki, M.; Maeda, H. Preparation of titania particles utilizing the insoluble phase interface in a microchannel reactor. *Chem. Commun.* **2002**, *2*, 1462–1463. [[CrossRef](#)] [[PubMed](#)]
25. Chandrasekhar, D.; Borra, S.; Kapure, J.S.; Shivaji, G.S.; Srinivasulu, G.; Maurya, R.A. Visible-light photoredox catalysis: Direct synthesis of fused  $\beta$ -carboline through an oxidation/[3 + 2] cycloaddition/oxidative aromatization reaction cascade in batch and flow microreactors. *Org. Chem. Front.* **2015**, *2*, 1308–1312. [[CrossRef](#)]
26. Matsushita, Y.; Ichimura, T.; Ohba, N.; Kumada, S.; Sakeda, K.; Suzuki, T.; Tanibata, H.; Murata, T. Recent progress on photoreactions in microreactors. *Pure Appl. Chem.* **2007**, *79*, 1959–1968. [[CrossRef](#)]

27. Oelgemoeller, M. Highlights of photochemical reactions in microflow reactors. *Chem. Eng. Technol.* **2012**, *35*, 1144–1152. [[CrossRef](#)]
28. Pandoli, O.; del Rosso, T.; Santos, V.M.; Rezende, R.D.S.; Marinkovic, B.A. Prototyping of photocatalytic microrreactors and photodegradation tests of organic colors prototyping of photocatalytic microreactor and testing of photodegradation of organic. *Quim. Nova* **2015**, *38*, 859–863.
29. Ren, K.; Zhou, J.; Wu, H. Materials for microfluidic chip fabrication. *Acc. Chem. Res.* **2013**, *46*, 2396–2406. [[CrossRef](#)]
30. Wang, N.; Lei, L.; Zhang, X.M.; Tsang, Y.H.; Chen, Y.; Chan, H.L.W. A comparative study of preparation methods of nanoporous TiO<sub>2</sub> films for microfluidic photocatalysis. *Microelectron. Eng.* **2011**, *88*, 2797–2799. [[CrossRef](#)]
31. Cambié, D.; Bottecchia, C.; Straathof, N.J.W.; Hessel, V.; Noël, T. Applications of continuous-flow photochemistry in organic synthesis, material science, and water treatment. *Chem. Rev.* **2016**, *116*, 10276–10341. [[CrossRef](#)]
32. Noël, T.; Naber, J.R.; Hartman, R.L.; McMullen, J.P.; Jensen, K.F.; Buchwald, S.L. Palladium-catalyzed amination reactions in flow: Overcoming the challenges of clogging via acoustic irradiation. *Chem. Sci.* **2011**, *2*, 287–290. [[CrossRef](#)]
33. Nair, V.; Colmenares, J.C.; Lisovytskiy, D. Ultrasound assisted ZnO coating in a microflow based photoreactor for selective oxidation of benzyl alcohol to benzaldehyde. *Green Chem.* **2019**, *21*, 1241–1246. [[CrossRef](#)]
34. Aljbour, S.; Yamada, H.; Tagawa, T. Ultrasound-assisted phase transfer catalysis in a capillary microreactor. *Chem. Eng. Process. Process Intensif.* **2009**, *48*, 1167–1172. [[CrossRef](#)]
35. Hartman, R.L.; Naber, J.R.; Zaborenko, N.; Buchwald, S.L.; Jensen, K.F. Overcoming the challenges of solid bridging and constriction during Pd-catalyzed C-N bond formation in microreactors abstract: We investigate the mechanisms that govern plugging in microreactors. *Org. Process Res. Dev.* **2010**, *14*, 1347–1357. [[CrossRef](#)]
36. Colmenares, J.C.; Ouyang, W.; Ojeda, M.; Kuna, E.; Chernyayeva, O.; Lisovytskiy, D.; De, S.; Luque, R.; Balu, A.M. Mild ultrasound-assisted synthesis of TiO<sub>2</sub> supported on magnetic nanocomposites for selective photo-oxidation of benzyl alcohol. *Appl. Catal. B Environ.* **2016**, *183*, 107–112. [[CrossRef](#)]
37. Pol, V.G.; Grisaru, H.; Gedanken, A. Coating noble metal nanocrystals (Ag, Au, Pd, and Pt) on polystyrene spheres via ultrasound irradiation. *Langmuir* **2005**, *21*, 3635–3640. [[CrossRef](#)]
38. Zhong, Z.; Mastai, Y.; Koltypin, Y.; Zhao, Y.; Gedanken, A. Sonochemical coating of nanosized nickel on alumina submicrospheres and the interaction between the nickel and nickel oxide with the substrate. *Chem. Mater.* **1999**, *11*, 2350–2359. [[CrossRef](#)]
39. Liu, S.; Guo, Z.; Qian, X.; Zhang, J.; Liu, J.; Lin, J. Sonochemical deposition of ultrafine metallic Pt nanoparticles on CdS for efficient photocatalytic hydrogen evolution. *Sustain. Energy Fuels* **2019**, *3*, 1048–1054. [[CrossRef](#)]
40. Qiu, P.; Park, B.; Choi, J.; Thokchom, B.; Pandit, A.B. A review on heterogeneous sonocatalyst for treatment of organic pollutants in aqueous phase based on catalytic mechanism. *Ultrason. Sonochem.* **2018**, *45*, 29–49. [[CrossRef](#)]
41. Yang, C.; Yeong, T.; Ching, J. An application of ultrasound technology in synthesis of titania-based photocatalyst for degrading pollutant. *Chem. Eng. J.* **2017**, *317*, 586–612.
42. Yu, J.C.; Zhang, L.; Yu, J. Rapid synthesis of mesoporous TiO<sub>2</sub> with high photocatalytic activity by ultrasound-induced agglomeration. *New J. Chem.* **2002**, *26*, 416–420. [[CrossRef](#)]
43. Das, S.; Srivastava, V.C. Microfluidic-based photocatalytic microreactor for environmental application: A review of fabrication substrates and techniques, and operating parameters. *Photochem. Photobiol. Sci.* **2016**, *15*, 714–730. [[CrossRef](#)]
44. Tao, S.; Yang, M.; Chen, H.; Ren, M.; Chen, G. Microfluidic synthesis of Ag @ Cu<sub>2</sub>O core-shell nanoparticles with enhanced photocatalytic activity. *J. Colloid Interface Sci.* **2017**, *486*, 16–26. [[CrossRef](#)]
45. Sachdev, S.; Maugi, R.; Kirk, C.; Zhou, Z.; Christie, S.D.R.; Platt, M. Synthesis and assembly of gold and iron oxide particles within an emulsion droplet; Facile production of core @ shell particles. *Colloid Interface Sci. Commun.* **2017**, *16*, 14–18. [[CrossRef](#)]
46. Jas, G.; Kirschning, A. Continuous flow techniques in organic synthesis. *Chem. Eur. J.* **2003**, *9*, 5708–5723. [[CrossRef](#)]
47. Baxendale, I.R.; Schou, S.C.; Sedelmeier, J.; Ley, S.V. Multi-step synthesis by using modular flow reactors: The preparation of yne-ones and their use in heterocycle synthesis. *Communication* **2010**, *16*, 89–94. [[CrossRef](#)]

48. McMullen, J.P.; Jensen, K.F. Rapid determination of reaction kinetics with an automated microfluidic system. *Org. Process Res. Dev.* **2011**, *15*, 398–407. [[CrossRef](#)]
49. Kreutz, J.E.; Shukhaev, A.; Du, W.; Druskin, S.; Daugulis, O.; Ismagilov, R.F. Evolution of catalysts directed by genetic algorithms in a plug-based microfluidic device tested with oxidation of methane by oxygen. *J. Am. Chem. Soc.* **2010**, *132*, 128–3132. [[CrossRef](#)]
50. Pastre, J.C.; Browne, D.L.; Ley, S.V. Flow chemistry syntheses of natural products. *Chem. Soc. Rev.* **2013**, *42*, 8849–8869. [[CrossRef](#)]
51. Shchukin, D.G.; Sviridov, D.V. Photocatalytic processes in spatially confined micro- and nanoreactors. *J. Photochem. Photobiol. C Photochem. Rev.* **2006**, *7*, 23–39. [[CrossRef](#)]
52. Meng, X.; Zhang, Z.; Li, X. *Ce Pt T*; Elsevier Ireland Ltd.: Shannon, Ireland, 2015; ISBN 2227404701.
53. Lakerveld, R.; Sturm, G.S.J.; Stankiewicz, A.I.; Stefanidis, G.D. Integrated design of microwave and photocatalytic reactors. Where are we now? *Curr. Opin. Chem. Eng.* **2014**, *5*, 37–41. [[CrossRef](#)]
54. Saien, J.; Soleymani, A.R. Feasibility of using a slurry falling film photo-reactor for individual and hybridized AOPs. *J. Ind. Eng. Chem.* **2012**, *18*, 1683–1688. [[CrossRef](#)]
55. Leblebici, M.E.; Stefanidis, G.D.; Van Gerven, T. Comparison of photocatalytic space-time yields of 12 reactor designs for wastewater treatment. *Chem. Eng. Process. Process Intensif.* **2015**, *97*, 106–111. [[CrossRef](#)]
56. Heggo, D.; Ookawara, S. Multiphase photocatalytic microreactors. *Chem. Eng. Sci.* **2017**, *169*, 67–77. [[CrossRef](#)]
57. Shen, C.; Wang, Y.J.; Xu, J.H.; Luo, G.S. Glass capillaries with TiO<sub>2</sub> supported on inner wall as microchannel reactors. *Chem. Eng. J.* **2015**, *277*, 48–55. [[CrossRef](#)]
58. Liu, M.; Zhu, X.; Chen, R.; Liao, Q.; Feng, H.; Li, L. Catalytic membrane microreactor with Pd/ $\gamma$ -Al<sub>2</sub>O<sub>3</sub> coated PDMS film modified by dopamine for hydrogenation of nitrobenzene. *Chem. Eng. J.* **2016**, *301*, 35–41. [[CrossRef](#)]
59. Stephan, B.; Ludovic, L.; Dominique, W. Modelling of a falling thin film deposited photocatalytic step reactor for water purification: Pesticide treatment. *Chem. Eng. J.* **2011**, *169*, 216–225. [[CrossRef](#)]
60. Chen, Y.; Dionysiou, D.D. Effect of calcination temperature on the photocatalytic activity and adhesion of TiO<sub>2</sub> films prepared by the P-25 powder-modified sol-gel method. *J. Mol. Catal. A Chem.* **2006**, *244*, 73–82. [[CrossRef](#)]
61. Charles, G.; Roques-Carmes, T.; Becheikh, N.; Falk, L.; Commenge, J.; Corbel, S. Determination of kinetic constants of a photocatalytic reaction in micro-channel reactors in the presence of mass-transfer limitation and axial dispersion. *J. Photochem. Photobiol. A Chem.* **2011**, *223*, 202–211. [[CrossRef](#)]
62. Corbel, S.; Becheikh, N.; Roques-Carmes, T.; Zahraa, O. Mass transfer measurements and modeling in a microchannel photocatalytic reactor. *Chem. Eng. Res. Des.* **2013**, *92*, 657–662. [[CrossRef](#)]
63. Oelgemöller, M.; Shvydkiv, O. Recent advances in microflow photochemistry. *Molecules* **2011**, *16*, 7522–7550. [[CrossRef](#)]
64. Ramos, B.; Ookawara, S.; Matsushita, Y.; Yoshikawa, S. Low-cost polymeric photocatalytic microreactors: Catalyst deposition and performance for phenol degradation. *J. Environ. Chem. Eng.* **2014**, *2*, 1487–1494. [[CrossRef](#)]
65. Padoin, N.; Andrade, L.; Angelo, J.; Mendes, A.; Moreira, R.D.F.P.M.; Soares, C. Intensification of photocatalytic pollutant abatement in microchannel reactor using TiO<sub>2</sub> and TiO<sub>2</sub>-graphene. *AIChE J.* **2016**, *62*, 2794–2802. [[CrossRef](#)]
66. Liao, W.; Wang, N.; Wang, T.; Xu, J.; Han, X. Biomimetic microchannels of planar reactors for optimized photocatalytic efficiency of water purification. *Biomicrofluidics* **2016**, *10*, 014123. [[CrossRef](#)]
67. Wilms, D.; Klos, J.; Frey, H. Trends in polymer science microstructured reactors for polymer synthesis: A renaissance of continuous flow processes for tailor-made macromolecules? *Macromol. Chem. Phys.* **2008**, *209*, 343–356. [[CrossRef](#)]
68. Kumar, M.; Rao, N.; Khandekar, S.; Kunzru, D. Distributed hydrogen production from ethanol in a microfuel processor: Issues and challenges. *Renew. Sustain. Energy Rev.* **2011**, *15*, 524–533.
69. Hornung, C.H.; Hallmark, B.; Baumann, M.; Baxendale, I.R.; Ley, S.V.; Hester, P.; Clayton, P.; MacKley, M.R. Multiple microcapillary reactor for organic synthesis. *Ind. Eng. Chem. Res.* **2010**, *49*, 4576–4582. [[CrossRef](#)]
70. Davis, G. Microfluidics: Its impact on drug discovery. *Innov. Pharm. Technol.* **2008**, *25*, 24–27.
71. Microfluidics, D.; Song, H.; Chen, D.L.; Ismagilov, R.F. Reactions in droplets in microfluidic channels. *Angew. Chem. Int. Ed.* **2006**, *45*, 7336–7356.

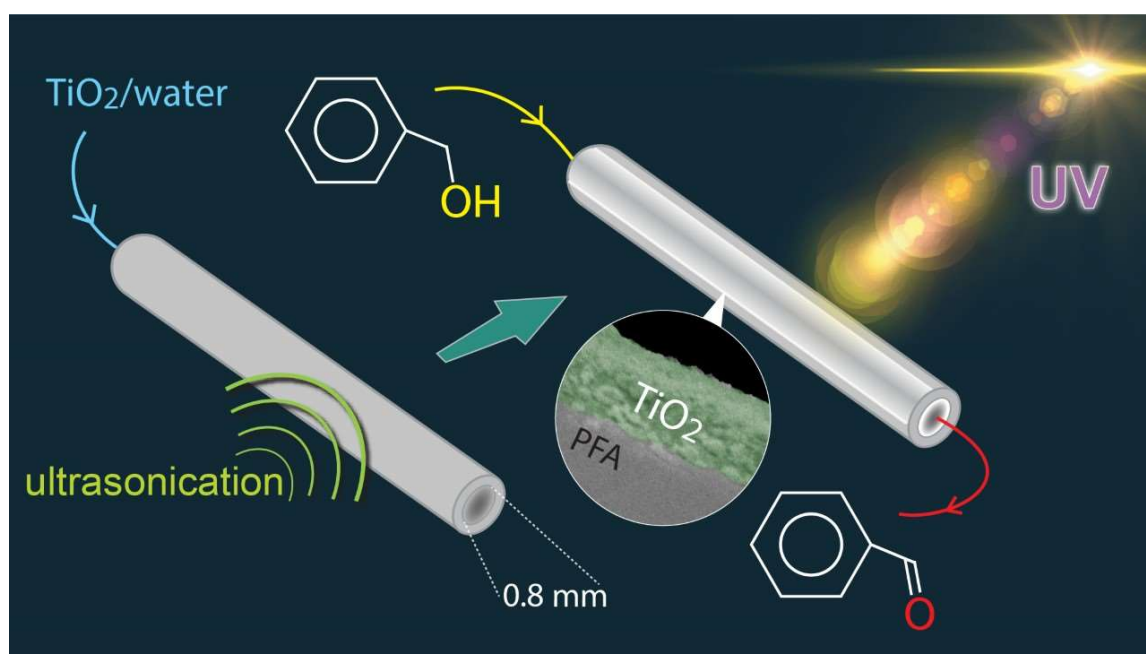


72. McMullen, J.P.; Stone, M.T.; Buchwald, S.L.; Jensen, K.F. An integrated microreactor system for self-optimization of a heck reaction: From micro- to mesoscale flow systems. *Angew. Chem. Int. Ed.* **2010**, *49*, 7076–7080. [[CrossRef](#)]
73. Naber, J.R.; Buchwald, S.L. Packed-bed reactors for continuous-flow C-N cross-coupling. *Angew. Chem. Int. Ed.* **2010**, *49*, 9469–9474. [[CrossRef](#)]
74. Okawa, A.; Yoshida, R.; Isozaki, T.; Shigesato, Y.; Matsushita, Y.; Suzuki, T. Photocatalytic oxidation of benzene in a microreactor with immobilized TiO<sub>2</sub> thin films deposited by sputtering. *Catal. Commun.* **2017**, *100*, 1–4. [[CrossRef](#)]
75. Hawkins, A.R.; Schmidt, H. *Handbook of Optofluidics*; Taylor and Francis Group: Boca Raton, FL, USA, 2010.
76. Ohering, M. *Materials Science of Thin Films, Deposition and Structure*; Academic Press: San Diego, CA, USA, 2002.
77. Visan, A.; Rafieian, D.; Ogieglo, W.; Lammertink, R.G.H. Modeling intrinsic kinetics in immobilized photocatalytic microreactors. *Appl. Catal. B Environ.* **2014**, *150*, 93–100. [[CrossRef](#)]
78. Pierson, H.O. *Handbook of Chemical Vapor Deposition: Technology, and Applications*; Noyes Publications: Norwich, NY, USA, 2001.
79. Grosso, D.; Marie, P. How to exploit the full potential of the dip-coating process to better control film formation. *J. Mater. Chem.* **2011**, *21*, 17033–17038. [[CrossRef](#)]
80. Taylor, P.; Edler, K.J.; Roser, S.J. Growth and characterization of mesoporous silica films. *Int. Rev. Phys. Chem.* **2001**, *20*, 387–466.
81. Meng, Z.; Zhang, X.; Qin, J. A high efficiency microfluidic-based photocatalytic microreactor using electrospun nanofibrous TiO<sub>2</sub> as a photocatalyst. *Nanoscale* **2013**, 4687–4690. [[CrossRef](#)]
82. Ra, D.; Driessen, R.T.; Ogieglo, W.; Lammertink, R.G.H. Intrinsic photocatalytic assessment of reactively sputtered TiO<sub>2</sub> films. *ACS Appl. Mater. Interfaces* **2015**, *7*, 8727–8732.
83. Piveteau, L.; Gasser, B.; Schlapbach, L. Evaluating mechanical adhesion of sol-gel titanium dioxide coatings containing calcium phosphate for metal implant application. *Biomaterials* **2000**, *21*, 2193–2201. [[CrossRef](#)]
84. Manivannan, A.; Spataru, N.; Arihara, K.; Fujishima, A. Electrochemical deposition of titanium oxide on boron-doped diamond electrodes. *Electrochem. Solid Lett.* **2005**, *8*, 138–140. [[CrossRef](#)]
85. Chein, R.; Chen, L.; Chen, Y.; Chung, J.N. Heat transfer effects on the methanol-steam reforming with partially filled catalyst layers. *Int. J. Hydrog. Energy* **2009**, *34*, 5398–5408. [[CrossRef](#)]
86. Lopez-Orozco, S.; Inayat, A.; Schwab, A.; Selvam, T.; Schwieger, W. Zeolitic materials with hierarchical porous structures. *Adv. Mater.* **2011**, *23*, 2602–2615. [[CrossRef](#)]
87. Tanimu, A.; Jaenicke, S.; Alhooshani, K. Heterogeneous catalysis in continuous flow microreactors: A review of methods and applications. *Chem. Eng. J.* **2017**, *327*, 792–821. [[CrossRef](#)]
88. Abramovic, B.F.; Šojic, D.V.; Krstic, J.B.; Finc, N.L.; Banic, N.D.; Boc, I.P. Efficiency of neonicotinoids photocatalytic degradation by using annular slurry reactor. *Chem. Eng. J.* **2016**, *286*, 184–190.
89. Nakamura, H.; Li, X.; Wang, H.; Uehara, M.; Miyazaki, M.; Shimizu, H.; Maeda, H. A simple method of self assembled nano-particles deposition on the micro-capillary inner walls and the reactor application for photo-catalytic and enzyme reactions. *Chem. Eng. J.* **2004**, *101*, 261–268. [[CrossRef](#)]
90. Rebrov, E.V.; Berenguer-Murcia, A.; Skelton, H.E.; Johnson, B.F.G.; Wheatley, A.E.H.; Schouten, J.C. Capillary microreactors wall-coated with mesoporous titania thin film catalyst supports. *Lab Chip* **2009**, *9*, 503–506. [[CrossRef](#)]
91. Li, L.; Tang, D.; Song, Y.; Jiang, B. Dual-film optofluidic microreactor with enhanced light-harvesting for photocatalytic applications. *Chem. Eng. J.* **2018**, *339*, 71–77. [[CrossRef](#)]
92. Suhadolnik, L.; Krivec, M.; Kristina, Ž.; Dra, G.; Ceh, M. A TiO<sub>2</sub>-nanotubes-based coil-type microreactor for highly efficient photoelectrocatalytic degradation of organic compounds. *J. Ind. Eng. Chem.* **2017**, *47*, 384–390. [[CrossRef](#)]
93. Colmenares, J.C.; Nair, V.; Kuna, E.; Lomot, D. Development of photocatalyst coated fluoropolymer based microreactor using ultrasound for water remediation. *Ultrason. Sonochem.* **2018**, *41*, 297–302. [[CrossRef](#)]
94. Colmenares, J.C.; Kuna, E.; Lomot, D. Method and the Device for Deposition of Nanoparticles on the Inner Walls of a Polymer Capillary, Using Ultrasonic Waves. Patent PL 231485, 7 November 2018.
95. Dragone, V.; Sans, V.; Rosnes, M.H.; Kitson, P.J.; Cronin, L. 3D-printed devices for continuous-flow organic chemistry. *Beilstein J. Org. Chem.* **2013**, *9*, 951–959. [[CrossRef](#)]

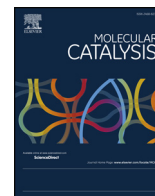
96. Corrêa, A.G.; Zuin, V.G.; Ferreira, V.F.; Vazquez, P.G. Green chemistry in Brazil. *Pure Appl. Chem.* **2013**, *85*, 1643–1653. [[CrossRef](#)]
97. Wu, K.; Kuhn, S. Strategies for solids handling in microreactors. *Chim. Oggi* **2014**, *32*, 62–67.
98. Cassano, A.E.; Alfano, O.M. Reaction engineering of suspended solid heterogeneous photocatalytic reactors. *Catal. Today* **2000**, *58*, 167–197. [[CrossRef](#)]
99. Kar, A.; Smith, Y.R. Improved photocatalytic degradation of textile dye using titanium dioxide nanotubes formed over titanium wires. *Environ. Sci. Technol.* **2009**, *43*, 3260–3265. [[CrossRef](#)]
100. Colina Marquez, J.; Machuca-Martinez, F.; Puma, G.L. Radiation absorption and optimization of solar photocatalytic reactors for environmental applications. *Environ. Sci. Technol.* **2010**, *44*, 5112–5120. [[CrossRef](#)]
101. Seeberger, P.H. Highly efficient continuous flow reactions using singlet oxygen as a “green” reagent. *Org. Lett.* **2011**, *13*, 5008–5011.
102. Wang, X.; Cuny, G.D.; Noel, T. A mild, one-pot Stadler–Ziegler synthesis of arylsulfides facilitated by photoredox catalysis in batch and continuous-flow. *Angew. Chem. Int. Ed.* **2013**, *52*, 7860–7864. [[CrossRef](#)]
103. Carlos, J. Sonication-induced pathways in the synthesis of light-active catalysts for photocatalytic oxidation of organic contaminants. *ChemSusChem* **2014**, *7*, 1512–1527.
104. Tang, Z.R.; Yin, X.; Zhang, Y.; Xu, Y.J. One-pot, high-yield synthesis of one-dimensional ZnO nanorods with well-defined morphology as a highly selective photocatalyst. *RSC Adv.* **2013**, *3*, 5956–5965. [[CrossRef](#)]
105. Chatel, G.; Valange, S.; Behling, R.; Carlos, J. A combined approach using sonochemistry and photocatalysis: How to apply sonophotocatalysis for biomass conversion? *ChemCatChem* **2017**, *9*, 2615–2621. [[CrossRef](#)]
106. Xu, H.; Zeiger, B.W.; Suslick, K.S. Sonochemical synthesis of nanomaterials. *Chem. Soc. Rev.* **2013**, 2555–2567. [[CrossRef](#)]
107. Bora, M.; Shusteff, M. Efficient coupling of acoustic modes in microfluidic channel devices. *Lab Chip* **2015**, *15*, 3192–3202. [[CrossRef](#)]
108. John, J.J.; Kuhn, S.; Braeken, L.; Van Gerven, T. Ultrasound assisted liquid-liquid extraction in microchannels—A direct contact method. *Chem. Eng. Process. Process Intensif.* **2016**, *102*, 37–46. [[CrossRef](#)]
109. Thangavadivel, K.; Konagaya, M.; Okitsu, K.; Ashokkumar, M. Ultrasound-assisted degradation of methyl orange in a micro reactor. *J. Environ. Chem. Eng.* **2014**, *2*, 1841–1845. [[CrossRef](#)]
110. Sathishkumar, P.; Viswanathan, R. Review on the recent improvements in sonochemical and combined sonochemical oxidation processes—A powerful tool for destruction of environmental contaminants. *Renew. Sustain. Energy Rev.* **2016**, *55*, 426–454. [[CrossRef](#)]
111. Rossi, D.; Jamshidi, R.; Sa, N.; Kuhn, S.; Gavriilidis, A.; Mazzei, L. Continuous-flow sonocrystallization in droplet-based micro fluidics. *Cryst. Growth Des.* **2015**, *15*, 5519–5529. [[CrossRef](#)]
112. Jiang, M.; Papageorgiou, C.D.; Waetzig, J.; Hardy, A.; Langston, M.; Braatz, R.D. Indirect ultrasonication in continuous slug-flow crystallization. *Cryst. Growth Des.* **2015**, *15*, 2486–2492. [[CrossRef](#)]
113. Rivas, D.F.; Castro-Hernández, E.; Villanueva Perales, A.L.; van der Meer, W. Evaluation method for process intensification alternatives. *Chem. Eng. Process. Process Intensif.* **2018**, *123*, 221–232. [[CrossRef](#)]
114. Wang, M.; Rajendran, V. Kinetics for dichlorocyclopropanation of 1,7-octadiene under the influence of ultrasound assisted phase-transfer catalysis conditions. *J. Mol. Catal. A Chem.* **2007**, *273*, 5–13. [[CrossRef](#)]
115. Hyun, S.; Hyang, J.; Cho, D. An analysis method for degradation kinetics of lowly concentrated PAH solutions under UV light and ultrasonication. *J. Ind. Eng. Chem.* **2009**, *15*, 157–162.
116. Thompson, L.H.; Doraiswamy, L.K. Sonochemistry: Science and engineering. *Ind. Eng. Chem. Res.* **1999**, *38*, 1215–1249. [[CrossRef](#)]
117. Laudadio, G.; Gemoets, H.P.L.; Hessel, V.; Noe, T. Flow synthesis of diaryliodonium triflates. *J. Org. Chem.* **2017**, *82*, 11735–11741. [[CrossRef](#)]
118. Joseph, J.; Kuhn, S.; Braeken, L.; Van Gerven, T. Ultrasound assisted liquid-liquid extraction with a novel interval-contact reactor. *Chem. Eng. Process. Process Intensif.* **2017**, *113*, 35–41.
119. Rizkin, B.A.; Popovic, F.G.; Hartman, R.L.; Rizkin, B.A.; Popovic, F.G.; Hartman, R.L. Spectroscopic microreactors for heterogeneous catalysis. *J. Vac. Sci. Technol. A Vac. Surf. Films* **2019**, *37*, 050801. [[CrossRef](#)]



## Chapter 3 : Design and Development of TiO<sub>2</sub> coated microflow reactor for photocatalytic partial oxidation of benzyl alcohol



*The present chapter discusses the research work described in a published manuscript (P 2), authored by Swaraj rashmi Pradhan, Vaishakh Nair, Dimitrios A. Giannakoudakis, Dmytro Lisovytskiy and Juan Carlos Colmenares. (Molecular Catalysis 486 (2020) 110884; doi:10.1016/j.mcat.2020.110884)*



## Design and development of TiO<sub>2</sub> coated microflow reactor for photocatalytic partial oxidation of benzyl alcohol



Swaraj R. Pradhan<sup>a,\*</sup>, Vaishakh Nair<sup>a,b</sup>, Dimitrios A. Giannakoudakis<sup>a</sup>, Dmytro Lisovtyskiy<sup>a</sup>, Juan C. Colmenares<sup>a,\*</sup>

<sup>a</sup> Institute of Physical Chemistry, Polish Academy of Sciences, Kasprzaka 44/52, 01-224 Warsaw, Poland

<sup>b</sup> Department of Chemical Engineering, National Institute of Technology Karnataka (NITK), Surathkal, Srinivasanagar P.O. Mangalore 575025, India

### ARTICLE INFO

#### Keywords:

Photocatalysis  
Ultrasound  
Fluoropolymer  
Selective photo-oxidation  
Microfluidic photoreactor  
Titanium dioxide deposition  
Wall-Coated microtube

### ABSTRACT

The synthesis of valuable organic compounds from naturally available and renewable biomass is an open field of research towards adaptation in real-life applications. Photocatalytic valorization is assumed as a potential candidate, although the lower efficiency of the traditional batch photocatalytic reactor sets some drawbacks. Recently, photocatalytic microreactors revealed as a prosperous candidate for various photocatalytic reactions, especially for selective oxidation. This area of research is challenging due to the development of the proper photocatalytic microreactor for the targeted application. Deposition of the catalyst on the internal surface of the microreactor, the sufficient utilization of the irradiation, optimization of the reaction parameters are among the most vital parameters that should be considered upon the design. Although, to obtain the most active material and tune its crucial features to maximize its catalytic performance inside the microreactors is the uppermost important part. This work introduces ultrasound-assisted TiO<sub>2</sub> deposition on the inner walls of a perfluoroalkoxyalkane microtube under mild conditions. The deposition experiments were carried out with commercial and sol-gel synthesized TiO<sub>2</sub>. The materials were characterized by XRD, UV-vis DRS, Scanning Electron Microscopy (SEM), and nitrogen sorption. The photocatalytic activities of the TiO<sub>2</sub> nano-engineered fluoropolymer based microreactors were evaluated for the oxidation of benzyl alcohol in flow.

### 1. Introduction

Lignin is a significant organic waste coming out from paper and pulp industries. With continuous modernization, environmental contamination has spread extensively. Faced with this issue, humankind reached a consensus on the need for environmental treatment and remediation, which requires planning and implementation using the concepts of both photocatalysis and chemical engineering. Recently, more attention has been paid to the development of microreactor technology for various applications, such as synthesis of chemical compounds, environmental protection, biomedical and pharmaceutical studies, healthcare, etc. [1,2]. Among the various photo-active candidates, titania-based materials, and especially the nano-scaled ones, are well-known and performing photocatalyst under UV light [3]. Due to its versatility, efficient photo activity, high stability, low cost, and safety to the environment and humans, titanium dioxide (TiO<sub>2</sub>) has been systematically used in many environmental and energy applications [4].

Microreactor based catalytic approaches are regarded as green synthetic methods due to decreased requirements in reagent, minimized

energy consumption, lessening of by-products, and shorter reaction time [5]. The photocatalytic reaction in a microreactor generally can be categorized into two types: homogeneous photocatalytic reaction and heterogeneous photocatalytic reaction systems [6]. There are various photocatalytic reactions have been carried out for selective oxidation of benzyl alcohol [7–14]. Among these catalyst based photochemical reactions, homogeneous photocatalysis has been extensively studied in microfluidic-based flow systems for selective organic synthesis [15], but the major drawback in the homogenous catalyst system is the separation of catalyst and, in general, the purification needed in order to obtain the desired compounds. Catalyst separation difficulties can be avoided upon the twist to heterogeneous catalytic approaches, for instance by immobilization of the photocatalyst on a fixed support. Also, it is a great challenge to design and develop continuous flow microreactors capable of utilizing the power of light successfully. Generally, the microreactor performance can be enhanced by decreasing its size. This principle can also be valid for heterogeneous photocatalytic microreactors since a higher transfer rate of reactants and uniform illumination without attenuation are easily possible.

\* Corresponding authors.

E-mail addresses: [srpradhan@ichf.edu.pl](mailto:srpradhan@ichf.edu.pl) (S.R. Pradhan), [jcarloscolmenares@ichf.edu.pl](mailto:jcarloscolmenares@ichf.edu.pl) (J.C. Colmenares).

<https://doi.org/10.1016/j.mcat.2020.110884>

Received 5 February 2020; Received in revised form 7 March 2020; Accepted 10 March 2020

2468-8231/© 2020 The Author(s). Published by Elsevier B.V. This is an open access article under the CC BY-NC-ND license (<http://creativecommons.org/licenses/by-nc-nd/4.0/>).

According to the method of incorporation of the catalyst, microreactors can be divided into three classes: (i) packed-bed; (ii) monolithic; and (iii) wall coated [1]. The packed and monolithic type of photo-microreactors have lower optical access due to complicated internal arrangement of the photocatalyst in the microreactor; more complex catalyst forms are better for potential applications such as catalyst filaments, wires, and membranes. On the other hand, wall-coated microreactors were introduced as a better approach for photocatalysis experiment as the penetration of light through the wall is simple compared to the other continuous-flow microreactors [16].

It is also well verified that the advantages of ultrasound-assisted technique are the increased conversion, improved yields, short reaction times under mild conditions [17,18]. However, this approach has now been also employed for heterogeneous reactions [19], or sophisticated materials synthesis [20,21]. Ultrasound is frequently used in conventional systems to intensify liquid-liquid processes due to its efficient agitation effects and non-invasive nature [22,23]. The ultrasonic irradiation increases turbulence in the liquid phase, decreasing mass transfer limitations, and increasing the catalytically active surface area via the de-agglomeration and fragmentation of the particles [24]. This technique has additionally been employed to coat metallic particles on various substrates [25,26]. Many researchers took advantage of ultrasound to immobilize the nanoparticles on metallic surface. To have immobilized thin film on the inner wall to avoid downstream catalyst recovery we could use microreactors [27].

Previously, we proposed a novel and prosperous approach to prepare wall coated microtube [28]. Herein, we reported a ultrasound-based approach for photocatalysis inside a wall coated (with synthesized as well as commercial  $\text{TiO}_2$ ) fluoropolymer based microcapillary for the oxidation of benzyl alcohol (BnOH) towards benzaldehyde (BnAld). The step-wise approach is shown in Fig. 1. Also, a thorough comparison of a commercial  $\text{TiO}_2$  (P25) with a sol-gel nanostructured synthesized catalyst has been explored.

## 2. Experimental section

### 2.1. Materials

Titanium (IV) Isopropoxide (TTIP, 98 %, Acros Organics),  $\text{TiO}_2$  nanoparticles (P25, Evonik), Benzyl alcohol (BnOH, 99.5 %, ChemPure), ethanol (EtOH, 99.8 %), methanol (HPLC grade), acetonitrile (AcN, HPLC grade), 0.1 % of  $\text{H}_3\text{PO}_4$ , Propan-2-ol (99.7%, POCH), a SunFire™ Chromatography column (C18 3.5  $\mu\text{m}$ , Waters) with 4.6  $\times$  150 mm of bed support, and Perfluoroalkoxy alkane (PFA, 0.8 mm ID) were used.

### 2.2. Synthesis and characterization of catalysts

The synthesis of  $\text{TiO}_2$  nanoparticles was carried out using Titanium (IV) isopropoxide (TTIP) based on the sol-gel based method. In a 25 ml vial, 4 ml of TTIP was dissolved in 15 ml of 2-propanol, followed by sonication for 60 min using an ultrasonic bath (100 % power, 37 kHz on continuous sweep mode; temperature  $\sim 26^\circ\text{C}$ ). Afterward, milli-Q water (5 mL) was added to the solution at a rate of  $0.167 \text{ ml min}^{-1}$  using a syringe infusion pump (Programmable Double Syringe Pump (WPI), NE-4000) under the influence of ultrasound at room temperature. After 60 min, the suspension was transferred to centrifugation vials, rinsing the reaction vial with 10 ml of Propan-2-ol. The solid product was separated and cleaned (with water and ethanol) during centrifugation. For the second and last cycle of centrifugation, 25 ml of Propan-2-ol and 20 ml of Milli-Q water were added to the tube. After this separations process, the remaining clean and white product was collected and kept in an oven for drying at  $80^\circ\text{C}$  for 12 h. The obtained white material was ground in an agate mortar and transferred to a sealed vial.

Both commercial  $\text{TiO}_2$  P25 (Evonik) and synthesized catalysts ( $\text{TiO}_2$ -SG) were characterized by UV-vis diffuse reflectance spectra (UV-vis DRS) and Powder X-ray diffraction (XRD). Additionally, surface morphology study was performed by high resolution scanning electron microscopy (HR-SEM), and the textural properties were determined by Nitrogen sorption. More details on characterization can be found in the supporting information.

### 2.3. Ultrasound-assisted deposition of catalyst inside the microtube

The optimization of catalyst deposition inside the PFA microtube was performed based on results obtained from a design experiment software (Design Expert 11) [29], considering the following parameters: length of the tube, power of ultrasound irradiation, and duration of deposition. The deposition carried out inside the ultrasonic bath (Sonorex-digital RC, 37 kHz, 120 W) at room temperature. Details can be found in supporting information.

### 2.4. Photocatalytic selective partial oxidation of benzyl alcohol

Photocatalysis studies in the batch system were carried out to optimize the key parameters like different solvents, mixing speed and loading of the catalyst. In the photocatalytic experiment, 1 mM BnOH solution was prepared with BnOH by adding solvents (acetonitrile (AcN), Milli-Q water, 10:90 v/v AcN/water and 90/10 v/v AcN/water). Different catalyst loadings (0.5, 1, 2 g /L of commercial  $\text{TiO}_2$ ) were

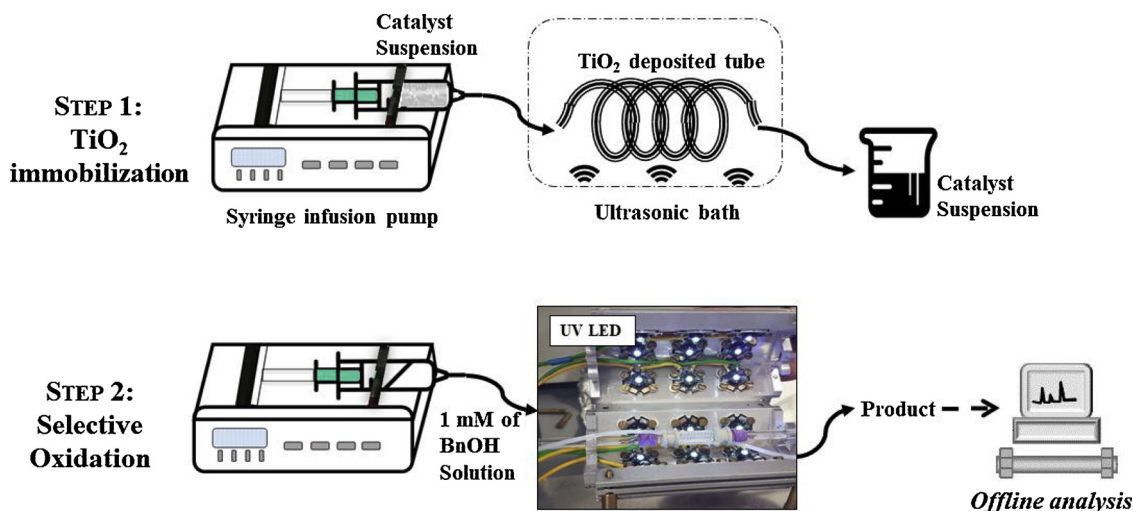


Fig. 1. Procedure for catalyst immobilization and photocatalysis experiment inside microreactor.



prepared by mixing catalysts with 1 mM of BnOH in AcN to optimize the catalyst concentration. The reaction mixture was stirred at different mixing speeds (200, 400, 600 rpm) at room temperature (Fig. S1, S2, S3). Prior to light experiments under UV irradiation (375 nm, power = 2.86 W /m<sup>2</sup>), dark adsorption studies were carried out in order to determine the adsorption/reactivity in the dark and the duration to reach adsorption equilibrium (30 min). To maintain the temperature inside the system constant (~ 25 °C), a home-made cooling system was designed and immersed inside the water bath.

After the ultrasound-assisted deposition, the P25 coated tubes (T-PFA) were kept inside an oven for drying at 80 °C for 12 h. The commercial catalyst was used as a benchmark and to optimize all the parameters for the photocatalytic experiments/deposition. The same procedure (after optimization) was followed for the deposition of sol-gel synthesized TiO<sub>2</sub> into the microtube, and the obtained microreactors are referred to as S-PFA. The microtubes after drying were used for the photocatalytic experiments under UV irradiation by LED (375 nm, intensity = 2.86 W /m<sup>2</sup>, by Radiometer).

From the batch experiments, the parameters like concentration of catalyst, solvent, time of light irradiation were taken into consideration for determining the experimental parameters for the continuous flow photocatalysis tests. The tube of 30 cm length (Deposition condition: 120 W ultrasonic power, 75 min of deposition) showed better selectivity and conversion (Table 1).

### 3. Results and discussion

#### 3.1. Deposition of catalyst inside PFA microtube

The first goal was to determine the optimum parameters to deposit the semiconductor catalyst phase inside the microtubes, considering two factors; the amount of the deposited catalyst and, more importantly, the best photocatalytic oxidation of benzyl alcohol (BnOH) to benzaldehyde (BnAld). At this step, we used the commercial TiO<sub>2</sub> P25 (Evonik) as catalyst and a low cost and low power (120 W (100 %) US power, 37 kHz in continuous sweep mode) ultrasonic bath.

Ultrasonication assistance was taken into consideration for having a positive effect either during the deposition of the active phase or for the pre-treatment of the inner walls of the tube before the deposition. Initially, we determined if the ultrasound irradiation (US) plays a crucial role during the deposition. Following similar process, tubes were prepared with or without US during the deposition. The results showed that the ultrasound-assisted deposition led to an ~50 % higher mass deposition as well as to a higher conversion of benzyl alcohol compared to the deposition in the absence of US. For that reason, we adapted the ultrasound-assisted deposition approach for all the following evaluations.

**Table 1**

Information of tubes selected for the catalyst deposition and photocatalytic studies (from design expert), and conversion and selectivity in microflow system after 30 min of illumination.

T-PFA Tube No.	Ultrasonic Power (W)	Length of tube(cm)	Time of deposition(min)	Weight of catalyst deposited (mg)	Conversion (%)	Selectivity (%)
A1	84	40	75	0.1	5	62
A2	48		30	0.2	6	83
A3	120		100	0.4	6	88
A4	48		120	0.2	7	54
A5	120		120	0.3	4	85
B1	48	30	75	0.2	5	84
B2	120		75	0.3	8	87
B3	84		30	0.2	9	74
B4	84	50	120	0.4	3	80
C1	48		75	0.3	6	86
C2	120		75	0.2	8	75
C3	84		30	0.2	10	63
C4	84		120	0.3	5	76

#### 3.2. Effect of pre-treatment before deposition of catalyst

Several chemical and physical effects are resulted from ultrasound are caused due to acoustic cavitation, corrosion, high temperature, the formation and collapse of bubbles in a liquid exposed to oscillating pressure fields [30]. So, the next target was to verify if the pre-treatment of the PFA tubes by ultrasound irradiation (US-pre-treatment) can influence the deposition and, as a result, the photocatalytic activity of the decorated with P25 microtubes. The microtubes were firstly pre-treated with US inside the ultrasonic bath, by passing 5 ml Milli-Q water (1 mL/min) through a clean tube under the influence of ultrasound, with the obtained tube referred to as P-PFA.

No weight loss was observed after the US-treatment, although, as can be seen from the SEM images (Fig. 2a, 2b), the surface of the inner walls became smoother. Two deposited tubes were obtained by ultrasound-assisted deposition of P25 phase to the clean PFA and US pre-treated one, referred to as T-PFA and PT-PFA, respectively. The deposition of titania nanoparticles takes place on the modified surface of the inner walls of the PFA microtube by physical interaction of nanoparticle suspension and the inner wall of the microtube. We believe, ultrasound potentially induces the increase of the surface free energy of PFA microtube, which is helping in the immobilization of catalyst nanoparticles inside the tube.

The cross-section SEM images revealed that in the case of T-PFA, the thickness of the coating layer could be more pronounced, reaching up to 7.3 μm in height (Fig. 2c). In the case of the latter, the maximum height of the P25 deposited layer was found 3.6 μm (Fig. 2d). We assign the higher in deposition thickness in the case of the US-pre-treated tube to the smoother surface compared to no US-pre-treatment microtubes. We have to point out that the catalyst deposition was not perfect in homogeneity (based on SEM analysis), and we gave more research effort towards this direction.

The maximum mass of catalyst loading was found to be equal (average of 0.01 mg /cm) in both cases, suggesting the same effect of US either during the deposition or US-pre-treatment prior the deposition.

#### 3.3. Effect of ultrasound during deposition of catalyst

The experiments were conducted for the optimized concentration of commercial TiO<sub>2</sub>, i.e., 0.5 g /L. Two microreactors were prepared to test the photocatalytic oxidation of BnOH in acetonitrile. For the first microreactor, the ultrasonic bath was used during the deposition of catalyst and the other was done in the absence. The photocatalytic activity was analyzed, and the results are shown in Fig. S5. There was an increment in selectivity and conversion after 10 min of irradiation time with US assisted deposition method. This increment in the activity might be because of the better immobilization or dispersion of catalysts in the presence of ultrasound.

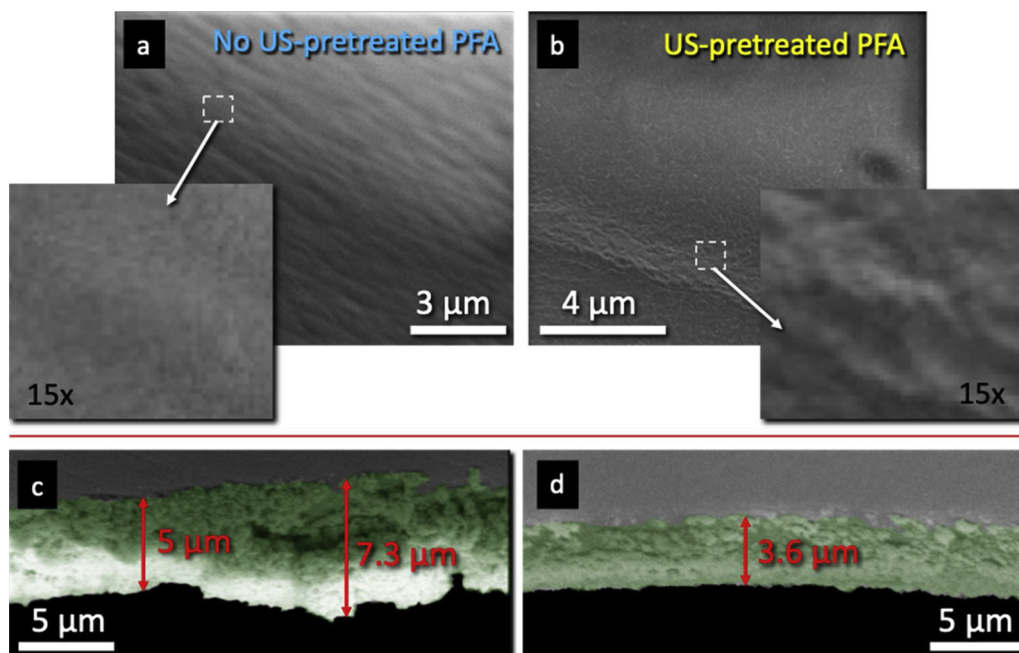


Fig. 2. SEM images of the inner walls of unmodified PFA microtube (a), ultrasonication pretreated PFA (P-PFA) microtube (b), and cross-section images of P25-TiO<sub>2</sub> deposited microtube (T-PFA) (c), sol-gel synthesized TiO<sub>2</sub> deposited microtube (S-PFA) (d).

### 3.4. Photocatalytic studies

The PT-PFA (pre-treated and deposited with P25) microreactor showed BnOH conversion and BnAld selectivity 6 and 65 %, respectively. In the case of T-PFA microreactor, the BnOH conversion was almost equal (5%), although the selectivity to BnAld was 17 % higher than that of PT-PFA. This can be linked to the different deposition extent, as observed from the SEM. In both cases, no leaching of TiO<sub>2</sub> occurred (Fig. S6). Based on the above-discussed results, we discarded the option of US-pre-treatment, and we focused on the utilization of US during the nano-engineering/deposition step of the preparation of the catalyst deposited microreactors, as both processes had an almost similar effect. By this approach, we could avoid the step of ultrasound pre-treatment and use the commercial microtubes after cleaning.

The following and predominant research goal in this study was to determine if the deposition of the synthesized TiO<sub>2</sub> phase can lead to improve the oxidative performances compared to benchmark P25. For this purpose, TiO<sub>2</sub> nanoparticles were synthesized based on a sol-gel synthetic route (TiO<sub>2</sub>-SG).

The optical features of the synthesized (TiO<sub>2</sub>-SG) and commercial TiO<sub>2</sub> (P25) in their powder form were evaluated based on the UV-vis diffuse reflectance spectra (Fig. S7) and the derived Tauc plots (Fig. 3a) after applying the Kubelka-Munk function [31,32]. The light absorption for P25 occurred for wavelength lower than 412 nm, while for TiO<sub>2</sub>-SG, lower than 388 nm. The extrapolation from the Tauc plots revealed that the estimated band gaps are ~ 3.2 and ~ 3.3 eV for P25 and TiO<sub>2</sub>-SG, respectively, values consistent with those reported in the literature for anatase phase [33].

The XRD patterns of the powders are collected in Fig. 3b. Both samples revealed the reflections at 25.3°, 37.9°, 47.8°, 54.5°, and 62.7°, characteristic for the (101), (004), (200), (105), and (204) diffraction peaks of the anatase crystal structure (JCPDS 02- 0406) [34–36]. Although, in the case of the synthesized material, all the peaks were found broader and of lower intensity, suggesting the smaller in size crystallinity compared to P25. The dimensions of the crystal phases were estimated by the Scherer equation (Table 2) [37–40]. The size of the anatase crystallinity was 3.7 nm for the synthesized material, while for the P25 was found 17.7 nm.

Although, both samples revealed to possess a dual-phase

crystallinity, anatase and rutile for P25, and anatase and brookite for TiO<sub>2</sub>-SG. The latter phase can be identified from the characteristic diffraction peak (121) at 30.3° and of rutile (110) at 27.4° [34,35].

The analysis of the phases composition by full profile analysis by using Rietveld method [41] showed that TiO<sub>2</sub>-SG consists of ~69 % anatase phase and ~31 % of brookite phase, while P25 ~87 % anatase and ~13 % rutile. The crystallinity of the titanium dioxide is a key feature in photochemical utilization. Palmisano et al., synthesized different phases of TiO<sub>2</sub> and did a comparative study for the photocatalytic selective oxidation with commercial P25 [42]. They concluded that commercial TiO<sub>2</sub> is less photocatalytically active compared to synthesized. Also, Kandiel et al., in a similar type of study, showed that pure brookite phase titania nanoparticles show higher photocatalytic efficiency for the oxidation of methanol, compared to pure anatase phase nanoparticles or P25 [43]. To have a thorough comparison, we synthesized amorphous phase TiO<sub>2</sub> by following the same procedure. As an additional step, we kept the suspension on a magnetic stirrer for 12 h before centrifugation. This amorphous catalyst was found to be photocatalytically inactive (Fig. S8).

Another crucial factor for the utilization of material as a photocatalyst is the textural features. The nitrogen adsorption/desorption isotherm of TiO<sub>2</sub>-SG (Fig. 3c) showed with a shape of Type I and Type IV combination; the former at the low range of relative pressure less than 0.1 and the latter for  $p/p_0 > 0.1$ . This is indicative of materials with a broad distribution in the size of pores from big microporous to narrow mesoporous (Fig. 3d). The hysteresis loop of H2 type suggests a complex pore structure, with the pore necks to have a wide distribution in size [44]. The pore size distribution revealed that the main volume of the pores for the TiO<sub>2</sub>-SG is in the range from 2.2 to 5 nm, while for P25 from 7.5 to 8 nm.

This synthesized catalyst revealed a significant high surface area for metal oxides 284 m<sup>2</sup> /g, more than five times higher compared to P25. The total pore volume of TiO<sub>2</sub>-SG was found 0.29 cm<sup>3</sup>/g, a value around 32 % greater than the one of P25. The smaller in size pores and the higher surface area as well as total pore volume for the synthesized material can be important assets since upon the entrance of the organic compound inside the pore, can be stay more, while the higher porosity can arise an elevated availability of the catalytic sites and better light utilization [45].

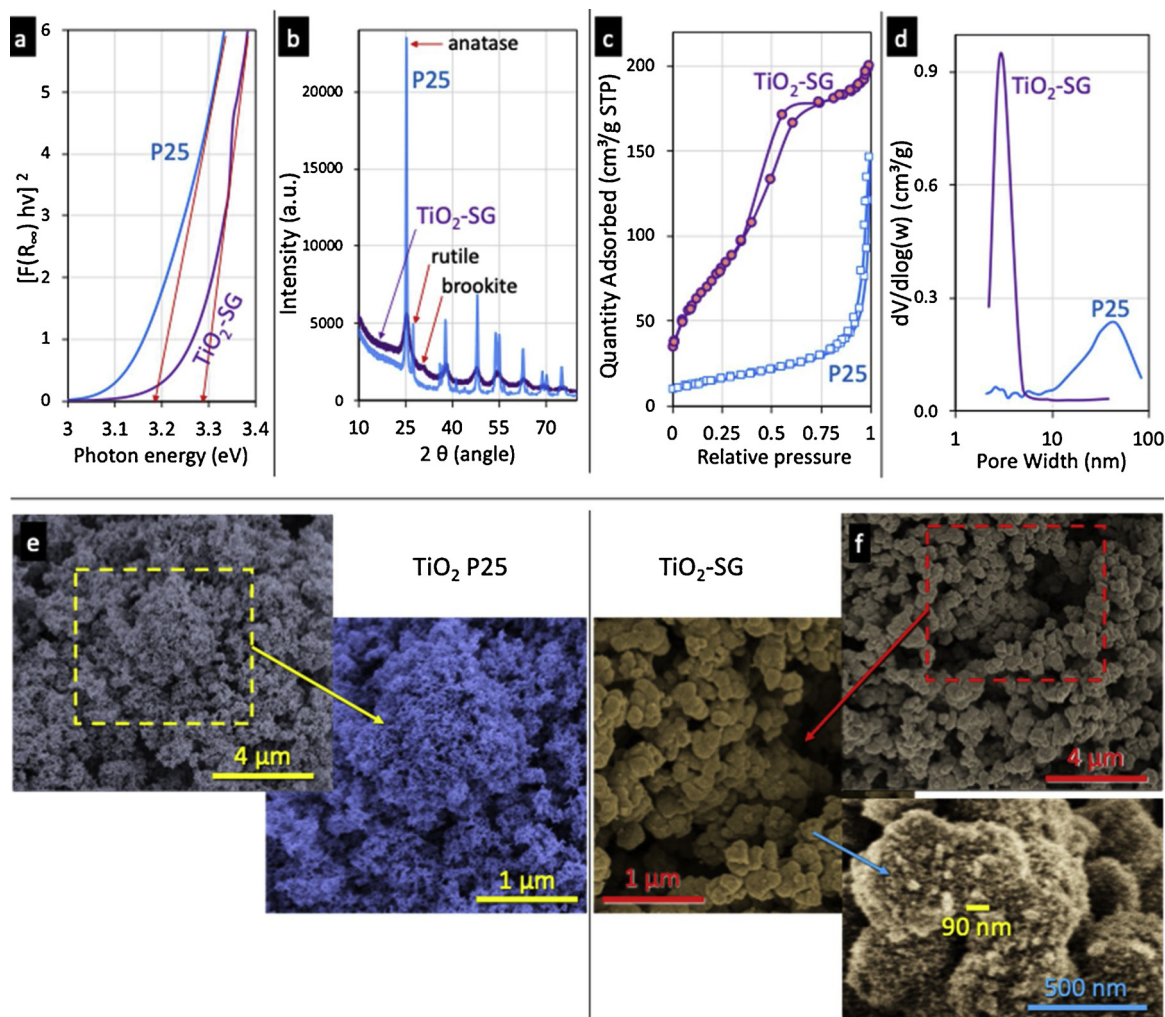


Fig. 3. Characterization plots of P25 and  $\text{TiO}_2$ -SG catalysts bandgap calculation (a), XRD patterns (b),  $\text{N}_2$  adsorption/desorption isotherm (c), pore size distribution (d) and SEM images of P25 (e) and  $\text{TiO}_2$ -SG (f) nanoparticles (Colored in order to have clear separation).

From the SEM analysis of the commercial P25 and synthesized  $\text{TiO}_2$  (Fig. 3e, 3f), it is clear that the synthesized catalyst forms agglomerates with sizes from 250 to 550 nm consisting of nanoparticles with size less than 35 nm. P25 showed a network of nanoparticles of size less than 35 nm, although no extended aggregation can be observed.

The ability of the material to absorb and scatter the incoming light irradiation also affects their photocatalytic activity, with the size of the particles to play a key role [46–48]. This can be further confirmed from the following photocatalytic evaluation of the materials. Prior to the photocatalysis experiments under UV irradiation, adsorption studies in the dark were carried out, and the adsorption equilibrium reached after 30 min, with no conversion. The oxidative photocatalytic activity of P25 and  $\text{TiO}_2$ -SG in their powder form was evaluated under the irradiation of UV light ( $2.86 \text{ W/m}^2$ ) in batch experiments.

After the optimization of various parameters (more details at the supplementary information), the optimal parameters were determined to be 0.5 g/L of catalyst, 1 mM of BnOH in acetonitrile, and stirring at 400 rpm at room temperature. Based on the evolutions of the BnOH

conversion and selectivity to BnAld up to 60 min (Fig. 4), it can be concluded that P25 outperformed the synthesized  $\text{TiO}_2$  from the conversion point of view. Regarding the selectivity, it was, reaching an almost stable value of 28 % for P25, while for  $\text{TiO}_2$ -SG, the selectivity was always above 80 %. Another important outcome is that the conversion of BnOH was continuously increasing for P25, while for  $\text{TiO}_2$ -SG was stable. Taking into consideration that BnAld was not decomposed between 30 and 60 min, it can be concluded that the surface of  $\text{TiO}_2$ -SG particles or the active catalytic sites were either blocked or they do not possess the ability for further oxidation or/and decomposition of BnAld. There were no other aromatic byproduct formed (like benzoic acid) or aliphatic ones during this photocatalysis test.

### 3.5. Characterization and photocatalytic reaction in S-PFA microtube

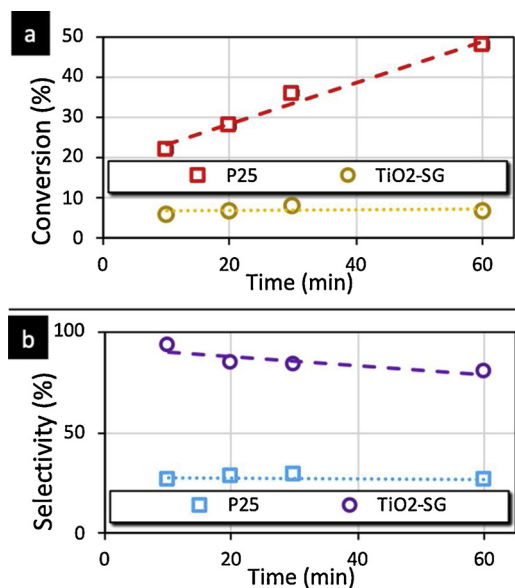
The morphology of the  $\text{TiO}_2$ -SG coated PFA microtube was analyzed by SEM. From the cross-section analysis of S-PFA (Fig. 5a) can be seen that the thickness of the deposited layer of the  $\text{TiO}_2$ -SG can reach

Table 2

Details of the crystallographic and textural features of the studied materials.

Sample	Anatase:Rutile:Brookite phases (%)	Anatase (nm)	Rutile (nm)	Brookite (nm)	Specific surface area ( $\text{m}^2/\text{g}$ )	Pore volume (BJH) ( $\text{cm}^3/\text{g}$ )	Pore size (nm)
P25	87:13:0	17.7	24.8	–	53	0.22	16.3
$\text{TiO}_2$ -SG	69:0:31	3.7	–	5.4	284	0.29	3.2





**Fig. 4.** Comparison between the conversion and selectivity of commercial P25 with synthesized TiO<sub>2</sub>-SG in batch photocatalysis system (0.5 g /L, 400 RPM, 1 mM BnOH in AcN, room temperature).

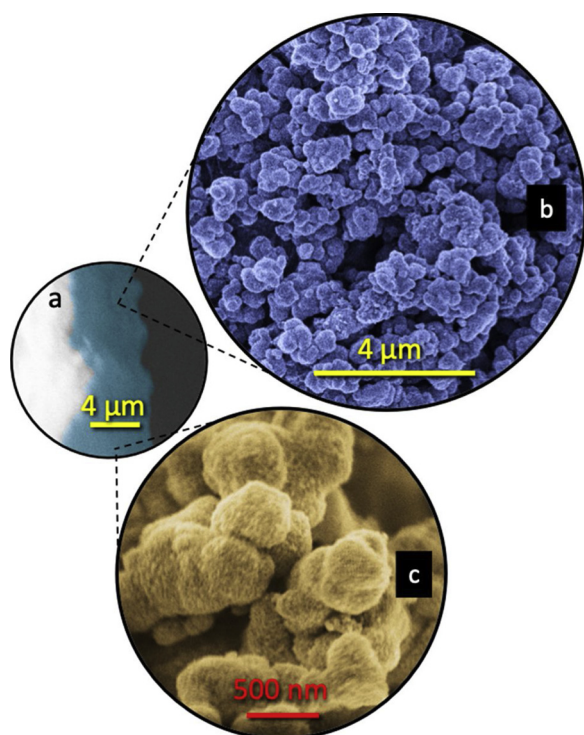


**Fig. 5.** SEM and HR-SEM micrographs of the inner walls deposited with the synthesized TiO<sub>2</sub> microreactor (S-PFA) at different magnifications.

up to 5 μm, which is similar to the thickness observed in the case of P25 decoration. The HR-SEM micrographs of S-PFA, from the top, (Fig. 5b,c) demonstrate that the deposition occurred without significant alterations of the morphological features of the TiO<sub>2</sub>-SG particles. The presence of larger in size aggregates maybe can lead to a positive impact on the reactivity by disturbing the flow of the solution inside the microtube and preventing the formation of a stable layer of the solvent above /around the upper surface of the deposited phase. The heterogeneous flow can lead to increase in mixing and elevated contact time of the liquid with the catalyst particles.

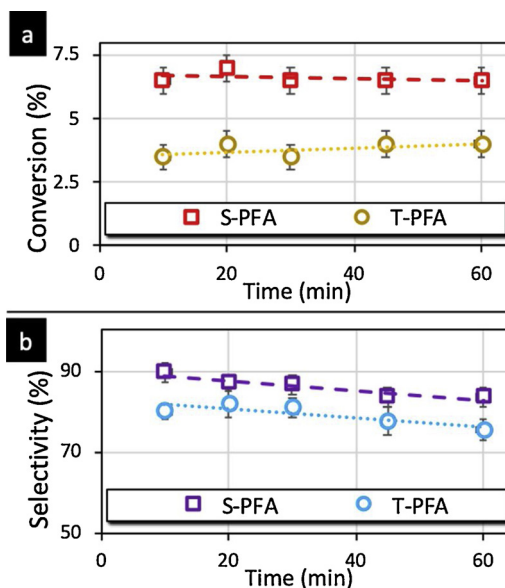


**Fig. 6.** Conversion of BnOH and BnAld selectivity of commercial P25 deposited (T-PFA) and synthesized TiO<sub>2</sub> deposited (S-PFA) microtube.

In order to compare the results from commercial P25 with the synthesized catalyst, the same experiment was carried out, and the result is shown in Fig. 6. The decrease in conversion from batch to flow system can be because of the size of the tube and the amount of catalyst inside the tube. The specific conversion rate was calculated using the given formula,

$$\text{Specific Conversion Rate} = (\mu\text{mol} / \text{m}^2 \text{ min}) = \frac{C_{\text{BnOH}_0} - C_{\text{BnOH}_t}}{A_c * \text{time}}$$

Where  $A_c$  is the active surface area (specific surface area multiplied with the concentration of catalyst) of the catalyst taking part in the photocatalytic BnOH conversion.

The synthesized catalyst deposited microtube shows the specific conversion rate of 6 μmol /m<sup>2</sup> min and 87 % of BnAld selectivity after 30 min of irradiation time. From the results, it is clear that the sol-gel synthesized catalyst shows comparatively better selectivity and conversion in one hour of irradiation time compared to commercial P25 TiO<sub>2</sub>.

The use of continuous flow microreactors led to improve irradiation over the reaction mixture and offer considerably shorter reaction time and better yields of products compared to batch reactors [49]. Before photocatalytic experiments, the photolysis test in microtube was performed for the same flow rate (0.134 ml /min) and it showed null conversion. The commercial P25 TiO<sub>2</sub> catalyst, after 30 min of irradiation time, showed 79 % BnAld selectivity in a micro photoreactor, which was 32 % in a batch reactor. This catalyst had a specific conversion rate of 13 μmol /m<sup>2</sup> min in the batch reactor whereas in the flow reactor, the specific conversion rate decreased to 5 μmol /m<sup>2</sup> min.

#### 4. Conclusions

In summary, we presented herein a “green chemistry” oriented approach to coat the inner walls of a microtube with a thin layer of photoactive TiO<sub>2</sub> in order to utilize the obtained microreactors towards the selective photocatalytic partial oxidation of a lignin-based model compound, benzyl alcohol, without the use of any addition reagent (like oxidant). The utilization of ultrasonication (US) during the coating process plays a vital role, leading to an enhanced mass deposition, and as a result, better photoreactivity compared to deposition without US. Going a step further, we synthesized nanostructured titanium dioxide (TiO<sub>2</sub>-SG) nanoparticles following a sol-gel synthetic pathway and

compared with the commercially available P25. The main difference between the commercial and the synthesized samples is that the latter apart from the anatase crystallinity also revealed brookite phase crystals, while P25 is a mixture of anatase and rutile. TiO<sub>2</sub>-SG also showed a very high specific surface area (284 m<sup>2</sup> /g) for a metal oxide-based material, almost five times higher than that of P25. After a detailed optimization of the photocatalytic parameters, it was found that in batch, the synthesized catalyst has a significantly lower oxidative conversion performance compared to P25. The most essential and exciting outcome was that upon deposition on the microreactor's walls, the synthesized material revealed a better photoreactivity on regards to both benzyl alcohol conversion and benzyl aldehyde selectivity, a trend in absolute contrast with the batch experiments case. We link this to the higher availability of the active sites upon the deposition on the tube's walls and the high surface area of the synthesized nanoparticles. The catalyst synthesis makes the whole approach environment-friendly as it does not include any calcination step unlike TiO<sub>2</sub> P25. Further exploration on the utilization of nano-engineered microreactors as an additive-free eco-friendly, in terms of simplicity, safety, time, energy, material cost, and environmental impact approach for the selective upgrade of biomass-derived compounds was performed by our research group to enhance the capability of the photoreactors and to determine which factors and features of the catalyst play the most crucial role.

#### CRediT authorship contribution statement

**Swaraj R. Pradhan:** Data curation, Writing - original draft. **Vaishakh Nair:** Supervision, Writing - review & editing. **Dimitrios A. Giannakoudakis:** Writing - review & editing. **Dmytro Lisovyskiy:** Methodology. **Juan C. Colmenares:** Conceptualization, Supervision, Funding acquisition, Writing - review & editing.

#### Declaration of Competing Interest

The authors declare that they have no known competing financial interests or personal relationships that could have appeared to influence the work reported in this paper.

#### Acknowledgments

This work is supported by the National Science Centre in Poland within Sonata Bis 5 Project No. 2015/18/E/ST5/00306.

#### Appendix A. Supplementary data

Supplementary material related to this article can be found, in the online version, at doi:<https://doi.org/10.1016/j.mcat.2020.110884>.

#### References

- [1] R. Munirathinam, J. Huskens, W. Verboom, *Adv. Synth. Catal.* 357 (2015) 1093–1123.
- [2] P.N. Nge, C.I. Rogers, A.T. Woolley, *Chem. Rev.* 113 (2013) 2550–2583.

- [3] D.A. Giannakoudakis, G. Chatel, J.C. Colmenares, *Top. Curr. Chem.* 378 (2020).
- [4] D. Angel, C. Juan, *Titan. Dioxide - Mater. Sustain. Environ.* 16 (2018) 305–329.
- [5] X. Yao, Y. Zhang, L. Du, J. Liu, J. Yao, *Renew. Sustain. Energy Rev.* 47 (2015) 519–539.
- [6] M. Oelgemöller, O. Shvydkiv, *Molecules* 16 (2011) 7522–7550.
- [7] N. Zhang, Y. Zhang, M.Q. Yang, Z.R. Tang, Y.J. Xu, *J. Catal.* 299 (2013) 210–221.
- [8] N. Zhang, Y. Zhang, X. Pan, M.Q. Yang, Y.J. Xu, *J. Phys. Chem. C* 116 (2012) 18023–18031.
- [9] M.Q. Yang, Y.J. Xu, *Phys. Chem. Chem. Phys.* 15 (2013) 19102–19118.
- [10] N. Zhang, M.Q. Yang, S. Liu, Y. Sun, Y.J. Xu, *Chem. Rev.* 115 (2015) 10307–10377.
- [11] C. Han, Z.R. Tang, J. Liu, S. Jin, Y.J. Xu, *Chem. Sci.* 10 (2019) 3514–3522.
- [12] C. Han, S.H. Li, Z.R. Tang, Y.J. Xu, *Chem. Sci.* 9 (2018) 8914–8922.
- [13] T. Chen, Z. Xu, L. Zhou, J. Qiu, M. Wang, J. Wang, *Mol. Catal.* 474 (2019) 110422.
- [14] F. Li, D. Hu, Y. Yuan, B. Luo, Y. Song, S. Xiao, G. Chen, Y. Fang, F. Lu, *Mol. Catal.* 452 (2018) 75–82.
- [15] V. Nair, J.C. Colmenares, D. Lisovyskiy, *Green Chem.* 21 (2019) 1241–1246.
- [16] J.C. Colmenares, R.S. Varma, V. Nair, *Chem. Soc. Rev.* 46 (2017) 6675–6686.
- [17] M. Wang, V. Rajendran, *J. Mol. Catal. A Chem.* 273 (2007) 5–13.
- [18] Y. Wang, P. Prinsen, F. Mangin, A. Yopez, A. Pineda, E. Rodríguez-Castellón, M.R. Hasan Shah Gilani, G. Xu, C. Len, R. Luque, *Mol. Catal.* 474 (2019) 110409.
- [19] S. Hyun, J. Hyang, D. Cho, *J. Ind. Eng. Chem.* 15 (2009) 157–162.
- [20] J.C. Colmenares, W. Ouyang, M. Ojeda, E. Kuna, O. Chernyayeva, D. Lisovyskiy, S. De, R. Luque, A.M. Balu, *Appl. Catal. B Environ.* 183 (2016) 107–112.
- [21] A.J. Sahani, A.S. Burange, S.D. Thakur, R.V. Jayaram, *Mol. Catal.* 476 (2019) 110534.
- [22] D. Fernandez Rivas, S. Kuhn, *Top. Curr. Chem.* 374 (2016).
- [23] P. Cintas, *Ultrason. Sonochem.* 28 (2016) 257–258.
- [24] S. Aljbour, H. Yamada, T. Tagawa, *Chem. Eng. Process. Process Intensif.* 48 (2009).
- [25] V.G. Pol, H. Grisaru, A. Gedanken, *Langmuir* 21 (2005) 3635–3640.
- [26] Z. Zhong, Y. Mastai, Y. Kolytyn, Y. Zhao, A. Gedanken, *Chem. Mater.* 11 (1999).
- [27] D. Heggo, S. Ookawara, *Chem. Eng. Sci.* 169 (2017) 67–77.
- [28] J.C. Colmenares, V. Nair, E. Kuna, D. Lomot, *Ultrason. Sonochem.* 41 (2018) 297–302.
- [29] S.A. Weissman, N.G. Anderson, *Org. Process Res. Dev.* 19 (2015) 1605–1633.
- [30] D. Fernandez Rivas, P. Cintas, H.J.G.E. Gardeniens, *Chem. Commun.* 48 (2012) 10935–10947.
- [31] J.F. Guayaquil-Sosa, B. Serrano-Rosales, P.J. Valadés-Pelayo, H. de Lasa, *Appl. Catal. B Environ.* 211 (2017) 337–348.
- [32] P. Kubelka, F. Munk, *Z. Tech. Phys.* 12 (1931) 593–601.
- [33] S.M. Gupta, M. Tripathi, *Chin. Sci. Bull.* 56 (2011) 1639–1657.
- [34] L.-L. Tan, W.-J. Ong, S.-P. Chai, A. Mohamed, *Nanoscale Res. Lett.* 8 (2013) 465.
- [35] N. Viriya-empikul, T. Charinpanitkul, N. Sano, A. Soottitantawat, T. Kikuchi, K. Faungnawakij, W. Tanthapanichakoon, *Mater. Chem. Phys.* 118 (2009) 254–258.
- [36] S. Ko, J. Pekarovic, P.D. Fleming, P. Ari-Gur, *Mater. Sci. Eng. B Solid-State Mater. Adv. Technol.* 166 (2010) 127–131.
- [37] P. Scherrer, *Göttinger Nachrichten Math. Phys.* 2 (1918) 98–100.
- [38] U. Holzwarth, N. Gibson, *Nat. Nanotechnol.* 6 (2011) 534.
- [39] H.S. Saroyan, S. Bele, D.A. Giannakoudakis, V.F. Samanidou, T.J. Bandosz, E.A. Deliyanni, *J. Colloid Interface Sci.* 539 (2019) 516–524.
- [40] J. Lombardi, L. Yang, F.A. Pearsall, N. Farahmand, Z. Gai, S.J.L. Billinge, S. O'Brien, *Chem. Mater.* 31 (2019) 1318–1335.
- [41] H.M. Rietveld, *J. Appl. Crystallogr.* 2 (1969) 65–71.
- [42] S. Yurdakal, B.S. Tek, O. Alagöz, V. Augugliaro, V. Loddo, G. Palmisano, L. Palmisano, *ACS Sustain. Chem. Eng.* 1 (2013) 456–461.
- [43] T.A. Kandiel, L. Robben, A. Alkaim, D. Bahnemann, *Photochem. Photobiol. Sci.* 12 (2013) 602–609.
- [44] K.S.W. Sing, R.T. Williams, *Adsorp. Sci. Technol.* 22 (2004) 773–782.
- [45] G. Srinivas, V. Krungleviciute, Z.X. Guo, T. Yildirim, *Energy Environ. Sci.* 7 (2014) 335–342.
- [46] Y. Park, W. Kim, D. Monllor-Satoca, T. Tachikawa, T. Majima, W. Choi, *J. Phys. Chem. Lett.* 4 (2013) 189–194.
- [47] Z. Pap, V. Danciu, Z. Cegléd, Á. Kukovecz, A. Oszkó, A. Dombi, K. Mogyorósi, *Appl. Catal. B Environ.* 101 (2011) 461–470.
- [48] D. Friedmann, C. Mendive, D. Bahnemann, *Appl. Catal. B Environ.* 99 (2010) 398–406.
- [49] D. Chandrasekhar, S. Borra, J.S. Kapure, G.S. Shivaji, G. Srinivasulu, R.A. Maurya, *Org. Chem. Front.* 2 (2015) 1308–1312.

## Supporting Information

### Design and Development of TiO<sub>2</sub> coated microflow reactor for photocatalytic partial oxidation of benzyl alcohol

Swaraj R. Pradhan <sup>a,\*</sup>, Vaishakh Nair <sup>a,b</sup>, Dimitrios A. Giannakoudakis <sup>a</sup>, Dmytro  
Lisovytskiy, Juan C. Colmenares <sup>a,\*</sup>

<sup>a</sup> *Institute of Physical Chemistry, Polish Academy of Sciences, Kasprzaka 44/52, 01-224 Warsaw, Poland.*

<sup>b</sup> *Department of Chemical Engineering, National Institute of Technology Karnataka (NITK), Surathkal,  
Srinivasanagar P.O. Mangalore 575025 India*

\* Correspondence: [jcarloscolmenares@ichf.edu.pl](mailto:jcarloscolmenares@ichf.edu.pl), [srpradhan@ichf.edu.pl](mailto:srpradhan@ichf.edu.pl); Tel.: +48 22 343 3215

#### Selective oxidation of Benzyl alcohol

Conversion and selectivity were calculated from the benzyl alcohol (BnOH) and benzaldehyde (BnAld) concentrations **determined by HPLC:**

$$\text{Conversion (\%)} = \frac{\text{Converted BnOH moles}}{\text{Initial BnOH moles}} \times 100\%$$

$$\text{Selectivity (\%)} = \frac{\text{Produced BnAld moles}}{\text{Converted BnOH moles}} \times 100\%$$

#### Characterization of catalysts and microtubes

**The optical properties of the synthesized powder samples were determined based on the diffuse reflectance UV-visible spectra (DRS UV-vis)** on U-3900 made by Hitachi (Hitachi Limited Company, Tokyo, Japan). Powder X-ray diffraction (XRD) measurements were

performed in a Bruker D8 DISCOVER A25 diffractometer (Bruker Corporation, Billerica, MA, USA) equipped with a vertical goniometer under theta-theta geometry using Ni filtered  $\text{CuK}$  ( $\lambda = 1.5418 \text{ \AA}$ ) radiation and operated at 40 KeV and 40 mA. Wide angle scanning patterns were collected from  $10^\circ$  to  $80^\circ$  with a step size of  $0.01^\circ$  and counting time of 500 s per step. The average crystallite size ( $D$  in nm) was determined according to the Scherrer equation:

$$D = k \lambda / \beta \cos \theta$$

where  $D$  is the average crystallite size of the catalyst (nm),  $\lambda$  is the wavelength of the  $\text{Cu } k\alpha$  X-ray radiation ( $\lambda = 0.154056 \text{ nm}$ ),  $k$  is a coefficient usually taken as 0.9,  $\beta$  is the full width at half maximum (FWHM) intensity of the peak observed at  $2\theta$  (radian), and  $\theta$  is the diffraction angle. The elemental maps of the samples were also obtained by scanning electron microscopy (SEM). The textural properties of  $\text{TiO}_2$  were determined by  $\text{N}_2$  physisorption experiments using a Micromeritics automated system (Micromeritics Instrument Corporation, ASAP 2020) based on the Brunauer-Emmet-Teller (BET) and the Barret-Joyner-Halenda (BJH) methods. Prior to adsorption measurements, samples were degassed under vacuum (0.1 Pa) for 6 h at  $80^\circ \text{C}$ . The powder form of the catalysts were used as received after drying, while selected pieces of the deposited microtubes were cut off and prepared for determination of coating thickness and surface morphology by high resolution scanning electron microscope (HR-SEM) by a FEI Nova NanoSEM 450.

Samples collected from the outlet the catalyst deposited PFA microtube during photocatalysis test, were examined using the energy dispersive X-ray fluorescence (EDXRF) spectrometer (Mini- Pal 4, PANalytical &Co.) with Rh tube and silicon drift detector to check the titania residual. The spectra were collected in air atmosphere, without using a filter, at a tube voltage of 30 kV.

To identify and quantify the BnOH, BnAlc and acid present, as well other possible aromatic or aliphatic products, the collected samples analyzed using high-pressure liquid

chromatography (HPLC), equipped with a dual absorbance detector (Waters 2487) and the SunFire™ column provided by Waters, using a mobile phase containing a mixture of organic solvents and a 0.05% H<sub>3</sub>PO<sub>4</sub> (5M) aqueous solution (CH<sub>3</sub>CN : CH<sub>3</sub>OH : H<sub>2</sub>O = 20 : 2.5 : 77.5 v/v).

## Experimental Section

### BATCH EXPERIMENTS

#### Optimization of catalysis concentration

In order to determine the optimum catalyst concentration, three different loadings were tested (0.5, 1, and 2 g /L). The batch experiments were performed with 1mM of BnOH in AcN as solvent at room temperature at 400 RPM under UV-LED (375nm) irradiation. The results after monitoring the BnOH conversion and BnAld selectivity are collected in Figure S1. Before illumination, we carried out in the dark adsorption experiment with batch system as well as in flow system and the values are given in Table S1. 0.5 g /L of commercial P25 catalyst showed the highest selectivity, while the conversion per mass of catalyst was also the highest even after 120 min compared to other two concentrations.

**Table S1**

Results for dark adsorption studies in batch and systems.

Time [min]	Batch	Flow
	Conversion (%)	
0	1.02	0.98
15	1.01	0.79
30	1.00	0.99
60	1.01	0.99
90	1.01	1.00

120	1.0	1.00
-----	-----	------

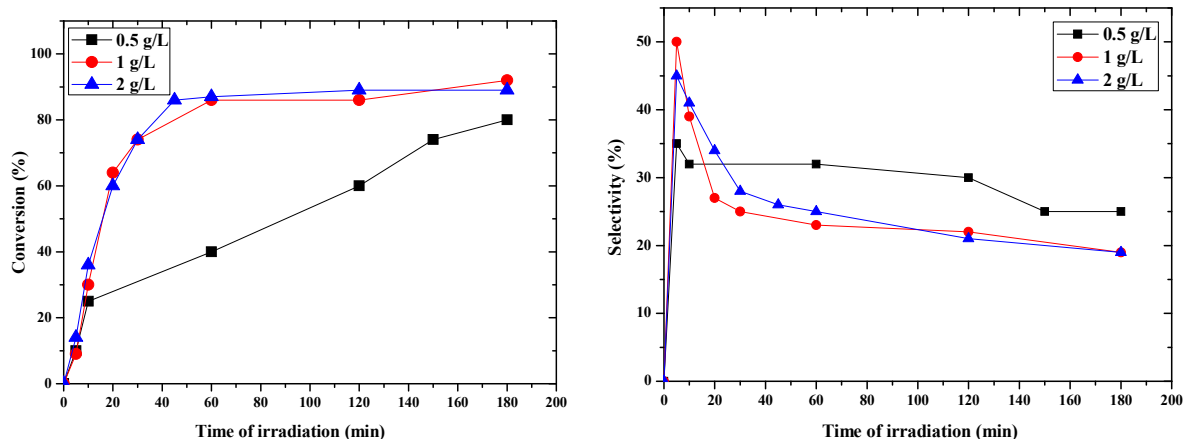


**Figure S1.** Conversion, and selectivity in batch photocatalysis system for different TiO<sub>2</sub> P25 concentrations (conditions: 400 rpm, room temperature, 1 mM initial BnOH concentration in AcN, UV-LED).

### Optimization of RPM

Other parameters like the effect of RPM and solvents were studied using 0.5 g /L of catalyst. The optimized result found from these above factors is, 0.5 g /L of catalyst in acetonitrile at reaction speed of 400 RPM gives better conversion and selectivity compared to other results in batch system. To study the effect of RPM on the photocatalytic activity, experiments were performed under different **mixing rate** (200, 400, and 600 RPM). From the result (Figure S2), it can be seen that the best selectivity (26%) was achieved at 400 RPM and also reached to a comparable conversion after 3hrs of light illumination with other two RPM conditions.

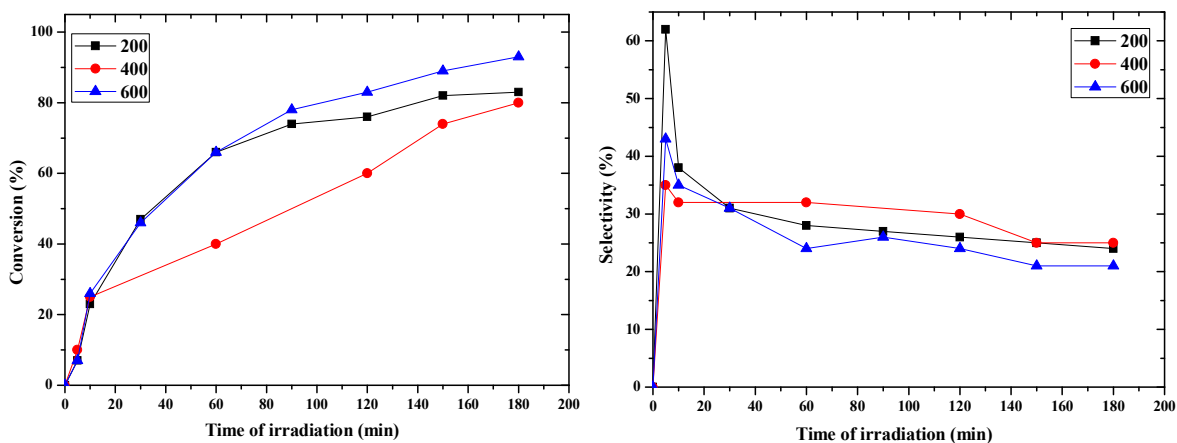


**Figure S2.** Conversion and selectivity in batch photocatalysis system for different RPM using TiO<sub>2</sub> P25 catalyst in AcN (room temperature, 1 mM initial BnOH concentration in AcN, UV-LED).

### Effect of the Solvent

In order to look upon the effect of solvent on the photocatalytic batch studies, these experiments were performed in the same condition (0.5 g /L at 400RPM) with different solvents (AcN, Water, 10/90 AcN/Water, 90/10 AcN/Water). From this result, it can be concluded that the mixture of solvents gave very good selectivity during the initial phase of the reaction, but later, there was a decrease (Figure S3). For water as a solvent, the selectivity was observed to be low.

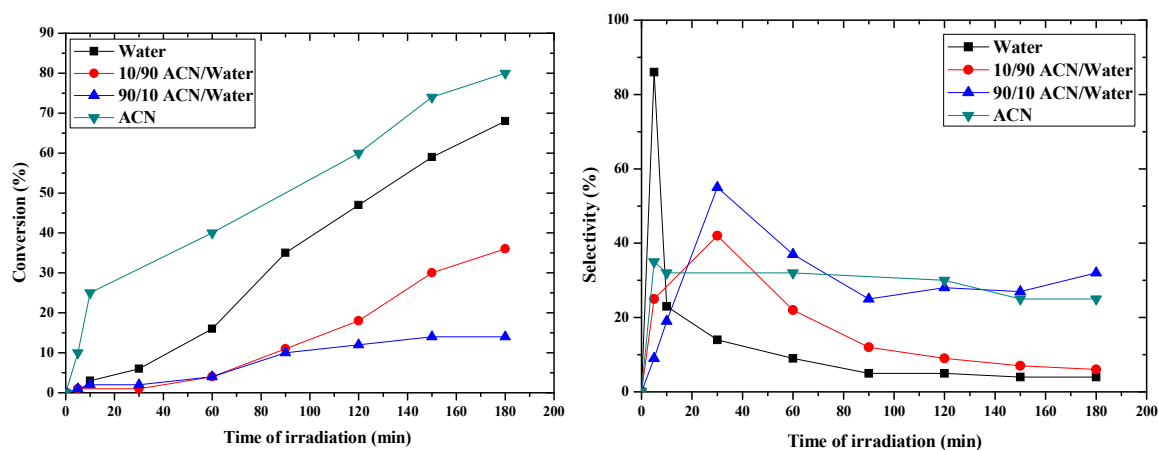


**Figure S3.** Conversion and, Selectivity in batch photocatalysis system for different solvents a) water, b) 10/90 AcN/Water, c)90/10 AcN/Water with P25 TiO<sub>2</sub> at 400RPM.

Hence it was concluded that AcN is the appropriate solvent for selective oxidation of BnOH using TiO<sub>2</sub> because of high conversion and comparable selectivity after 3hrs of illumination to other solvent conditions.

The photocatalytic experiments in the batch reactor with commercial P25 catalyst were repeated two times and the relative error was less than 8% (Figure S4). This shows that the results were reproducible.

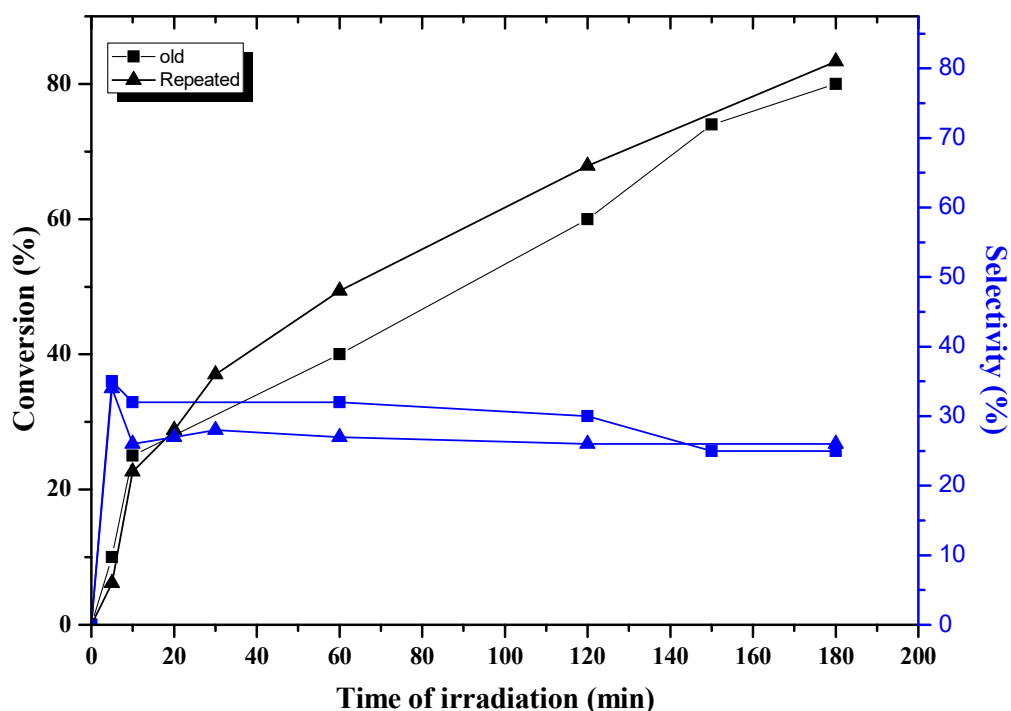


**Figure S4.** Comparison between repeated values of Conversion and, Selectivity for 0.5g/L of TiO<sub>2</sub> in 1mM AcN solution at 400 RPM in batch.

## MICROFLOW EXPERIMENTS

### Ultrasound assisted deposition

Initially, PFA tubes of a suitable length were washed with MilliQ water and ethanol (EtOH) with the help of the syringe pump and later were kept for drying inside an oven at 80 °C overnight. The deposition of commercial TiO<sub>2</sub> (P25, Evonik) in the dried PFA tubes were carried out by passing aqueous TiO<sub>2</sub> suspension, prepared in milliQ water. During the



deposition, the microtubes were kept inside an ultrasonic bath (Sonorex-digital RC, 37 kHz). Three factors provided as input i.e; time of deposition **under ultrasound exposure** (30-120min), ultrasound power during deposition (40-100%) and length of the tube (30-50cm). Based on these parameters, the **optimization of the experimental methodology was established using the Design** expert software (Table 1).

To determine the deposited mass of catalyst inside the tubes, all tubes were weighted before and after the deposition of catalyst using a high precision weighing balance from Mettler Toledo. Table 1 showcases the amount of TiO<sub>2</sub> deposited in microtubes at different conditions.

Using the optimized parameters achieved from the batch photocatalytic experiments (0.5 g /L catalyst in AcN), the photocatalysis experiments were carried out inside a PFA microchannel. Using a syringe infusion pump, BnOH solution **(20ml)** was injected through the tube at the rate of 0.133 ml min<sup>-1</sup> (Optimized data from batch experimental study). Adsorption experiment of BnOH in dark condition was carried out for 30 min and at different time intervals (calculated from rate of flow) samples were collected from the outlet and analyzed.

Table 1 **collects** the results after 30 min of photocatalytic test for each tube. From those results, it can be concluded that B2 test (Deposition condition: 30 cm tube length, 100 % amplitude = 120W US power, and 75 min of irradiation time) **revealed the best** selectivity and conversion (having 0.3mg catalyst deposited inside the microtube).

#### **Pretreatment of PFA microtube before deposition of catalyst**

By passing 5 mL milliQ water (1 mL/min) through a clean tube (cleaned with water and ethanol before using) under the influence of ultrasound (**100 % amplitude, 120W US power**, 37 kHz), Pretreated PFA (P-PFA) was prepared. After drying it in the oven at 80 °C for 1h, the tube was used for deposition of commercial P25 TiO<sub>2</sub> (PT-PFA) inside this microtube.

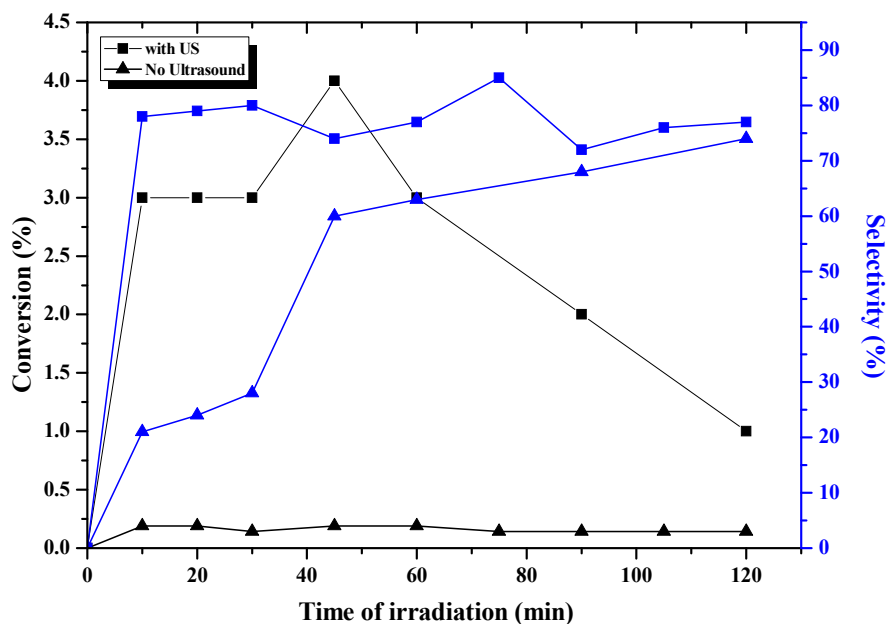
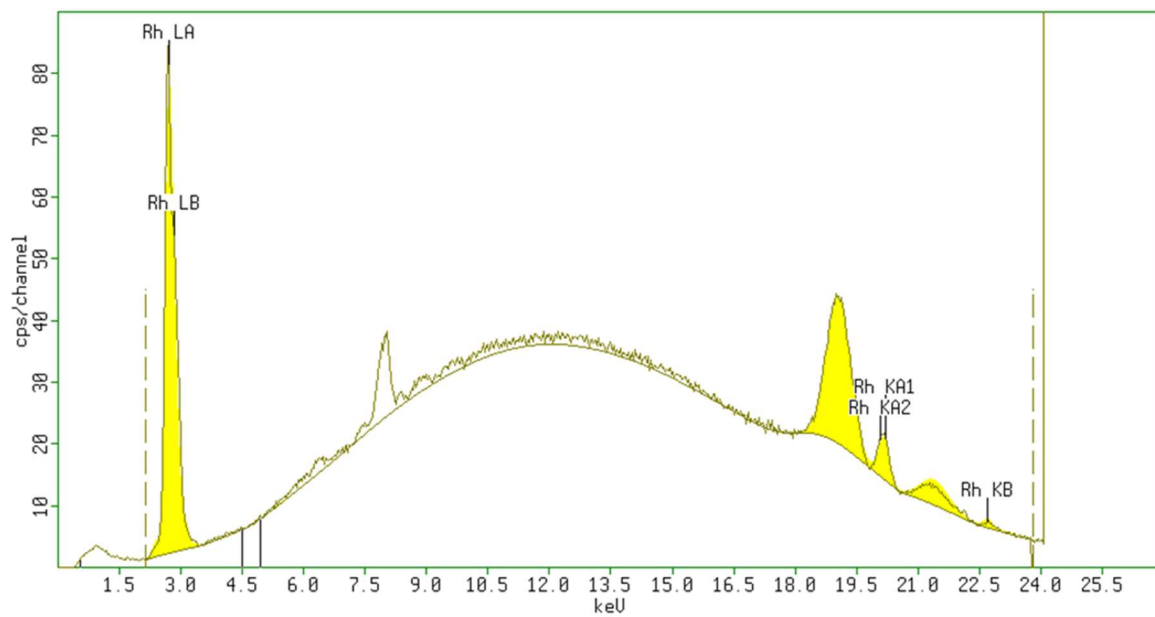


**Figure S5.** Photocatalytic activity of microtube deposited with P25 catalyst with and without the presence of ultrasound.

### Titanium dioxide leaching test

The EDXRF characterization carried out to determine possible **titanium** leaching in the sample collected after photocatalytic test from the outlet of microtube after 60 min. The results (Figures S6, S7) showed the absence of any titanium cation in the spectrum, confirming that no leaching of  $\text{Ti}^{4+}/\text{TiO}_2$  occurred during the reaction process as well as the strong and stable attachment of the nanocatalysts particles on the inner walls of the PFA tubes.

a)



b)

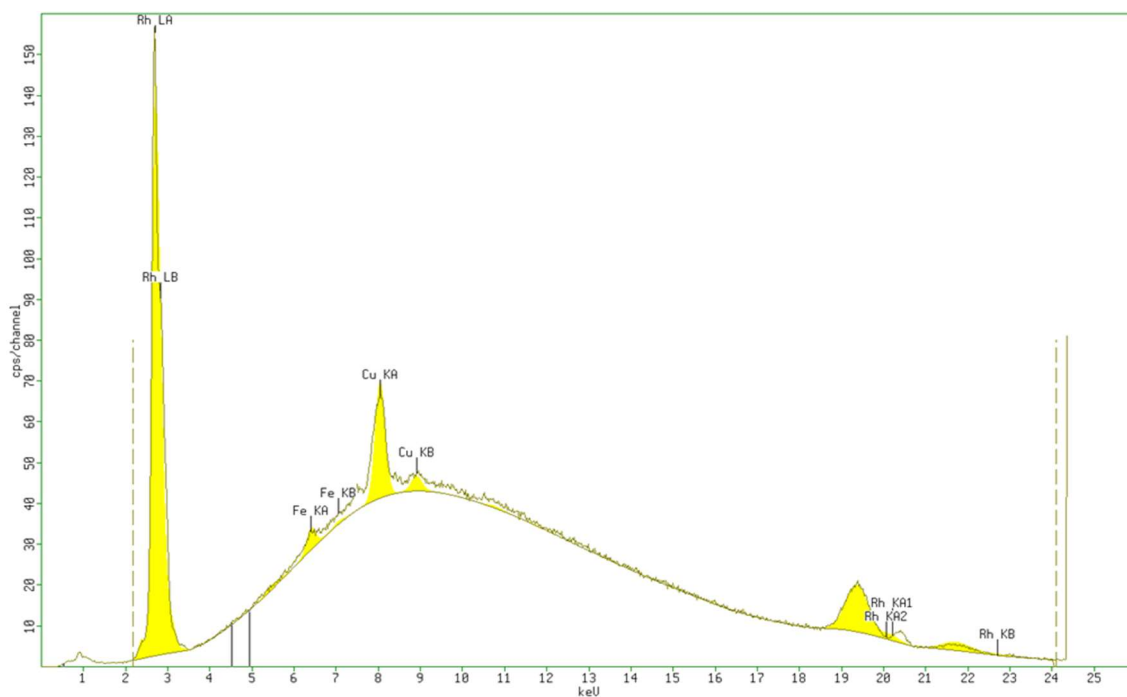


**Figure S6.** EDXRF measurement of the sample from the outlet of a) P25 TiO<sub>2</sub> and b) synthesized TiO<sub>2</sub> deposited PFA.

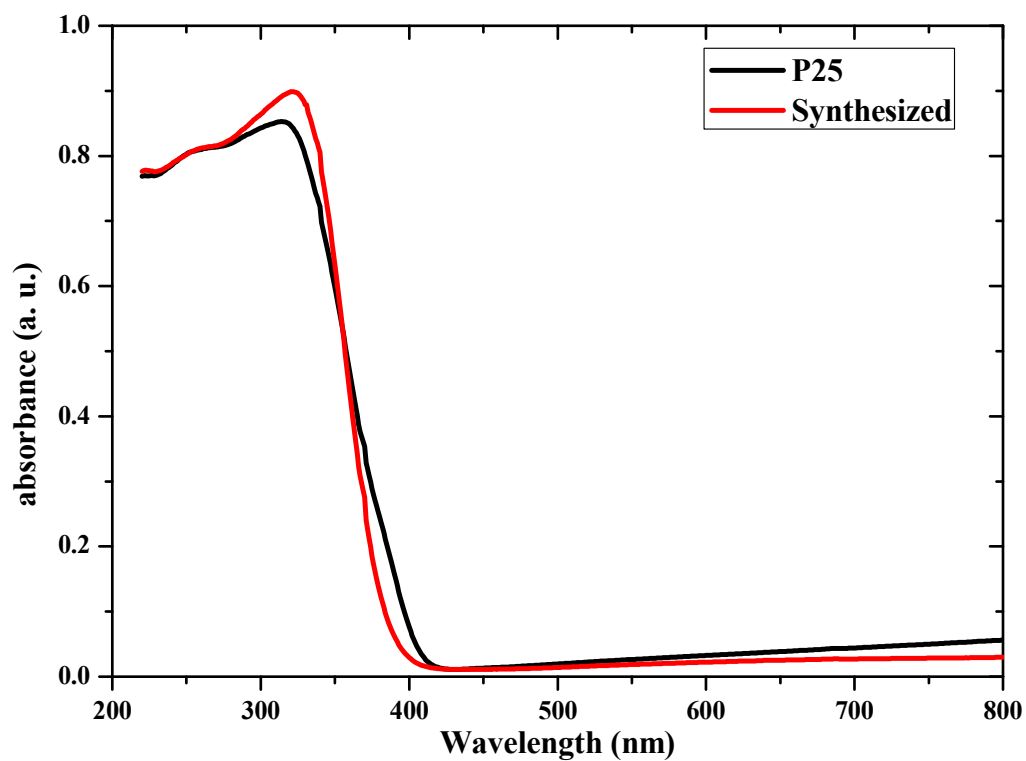


**Figure S7.** UV-Vis DRS of commercial P25 and synthesized TiO<sub>2</sub> nanoparticles.

To have an insight for the photocatalysis with amorphous phase of TiO<sub>2</sub>, similar experiments were carried using an amorphous in crystallinity TiO<sub>2</sub> material catalyst deposited on the microreactor's walls. The result (Figure S8) showed that the utilization of this sample did not led to a photoactive system.

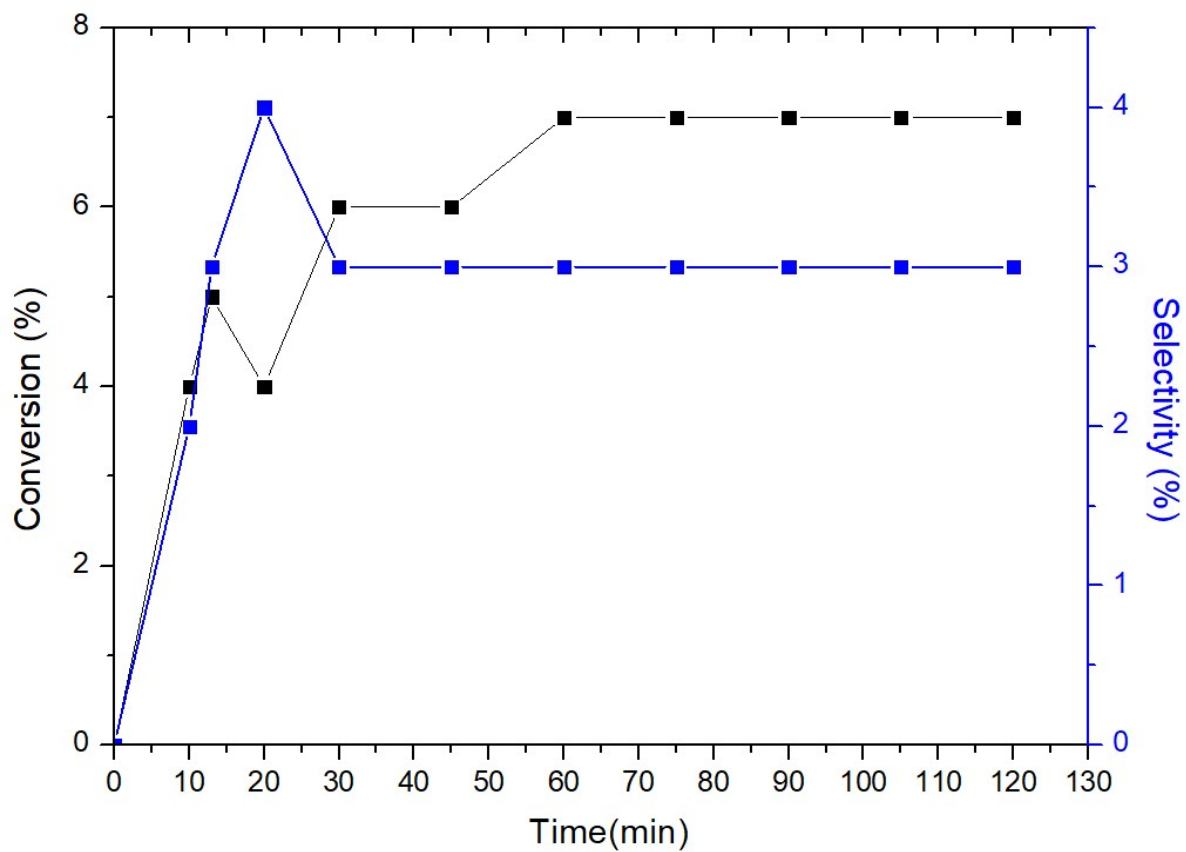
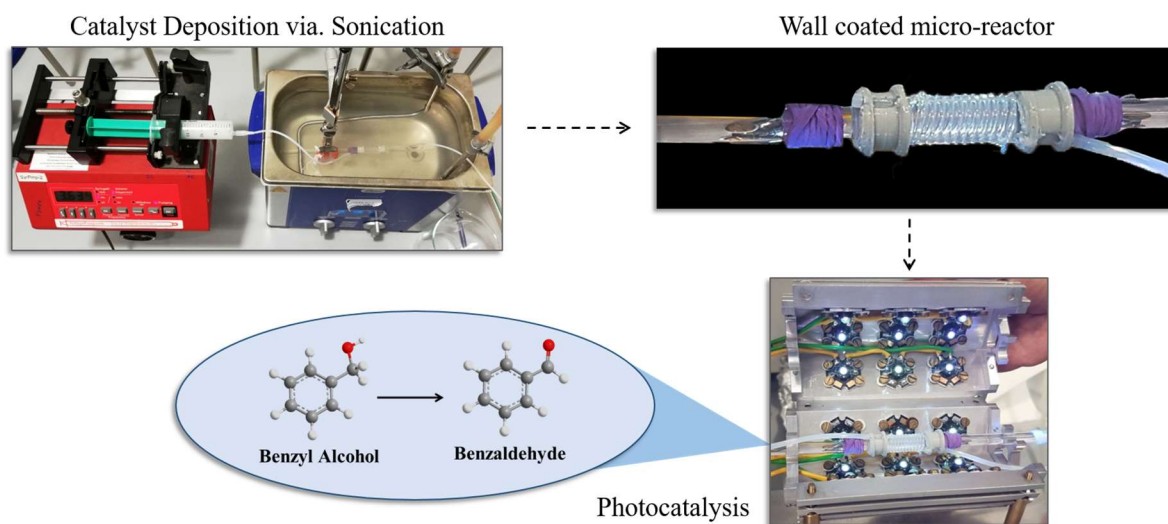
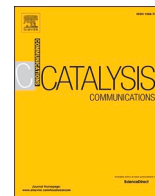


**Figure S8.** Photocatalytic results from amorphous catalyst deposited microtube.

## Chapter 4 : Flow photomicroreactor coated with monometal containing TiO<sub>2</sub> using sonication: a versatile tool for visible light oxidation



*The present chapter discusses the research work described in a published manuscript (P 3), authored by Swaraj rashmi Pradhan, Dmytro Lisovytskiy and Juan Carlos Colmenares. (Catalysis Communications 162 (2022) 106375; doi: 10.1016/j.catcom.2021.106375)*



Short communication

## Flow photomicroreactor coated with monometal containing TiO<sub>2</sub> using sonication: A versatile tool for visible light oxidation

Swaraj R. Pradhan<sup>\*</sup>, Dmytro Lisovytskiy, Juan C. Colmenares<sup>\*</sup>

Institute of Physical Chemistry, Polish Academy of Sciences, Kasprzaka 44/52, 01-224 Warsaw, Poland

## ARTICLE INFO

## Keywords:

Wall-coated microreactor  
 Monometallic titanium dioxide  
 Photocatalysis  
 Fluoropolymer  
 Selective photo-oxidation  
 Ultrasonic irradiation

## ABSTRACT

Ultrasonication was used for deposition of synthesized Metal-TiO<sub>2</sub> in the wall of a microtube. A detailed investigation of the photocatalytic activity was made by varying the atomic percentage of metals doped in TiO<sub>2</sub>. The sol-gel synthesized materials were analyzed by various techniques like X-ray diffraction (XRD), Scanning Electron Microscopy (SEM), etc. The photocatalytic activities of the monometallic TiO<sub>2</sub> fluoropolymer-based microreactors were evaluated for the oxidation of benzyl alcohol in flow. Microflow photocatalytic oxidation tests proved that the Fe-TiO<sub>2</sub> material has the highest photocatalytic conversion of benzyl alcohol compared with the other titania samples under UV and visible light irradiation.

### 1. Introduction

Lignin is the major by-product of the paper and pulp industries. The complex structure of lignin is a stumbling block that prevents its conversion to a value-added product, which can be helped by the depolymerization of lignin to model lignin compounds. Since benzyl alcohol is a key structural unit of most lignin model compounds, the scientific community is focused on studying its reactivity and transformation strategies [1–4]. The oxidation of aromatic alcohols (benzyl alcohol) to their corresponding carbonyl compounds (especially aldehydes) is one of the important organic transformations as carbonyl compounds are widely used in food, beverages, and pharmaceutical industries and also as precursors in chemical industries [5–7].

In recent years, the photo-assisted transformation of benzyl alcohol to benzaldehyde has attracted a great deal of attention as a potential alternative to replace the industrial synthesis route effectively. Photocatalysis is considered a sustainable, environment-friendly advanced technology because of its clean, energy-saving, and low-cost operation. Among various semiconductor photocatalysts used in the past three decades, TiO<sub>2</sub> received the most attention due to its biological and chemical inertness, cost-effectiveness, and the strong oxidizing power of the photo-generated holes [8]. However, one of the major drawbacks of using pure TiO<sub>2</sub> is that only ultraviolet light (UV) photons can displace the valence band electrons of TiO<sub>2</sub> due to its high bandgap energy (3.2 eV), which utilizes only 5% of the available solar radiation. Prior studies have demonstrated that doping TiO<sub>2</sub> with transition metal ions can

enhance its photocatalytic activity and have been well explored for alcohol oxidation [9–13].

The use of microfluidic reactor has enabled the safe use of molecular oxygen as a green oxidant and enabled readily obtaining a range of benzaldehydes within short reaction times [14]. The chemistry of solid catalyst immobilization on the internal walls of microreactors used in photocatalysis is nowadays well-known [15,16]. Recently, Pradhan et al. [17] have proposed a novel ultrasound based approach for deposition, which helped in better immobilization of catalyst on the wall of the microreactor. In this current work, we showcase the effect of metal (Fe, Cu, and Co) doped TiO<sub>2</sub> catalyst inside a fluoropolymer-based microcapillary for the oxidation of benzyl alcohol (BnOH) under UV and visible light irradiation.

### 2. Experimental section

#### 2.1. Materials

TiO<sub>2</sub> nanoparticles (P25, Evonik) were used as received and often used as a benchmark photocatalyst. Titanium (IV) Isopropoxide (TTIP, 98%, Acros Organics), Benzyl alcohol (BnOH, 99.5%, ChemPure), ethanol (EtOH, 99.8%), methanol (HPLC grade), acetonitrile (AcN, HPLC grade), 0.1% of H<sub>3</sub>PO<sub>4</sub> (aq.), propan-2-ol (99.7%, POCH) were used. Iron (III) nitrate (98%), cobalt (II) acetate tetrahydrate (98%), copper (II) acetate monohydrate (98%) were used as received for metal precursors. To prepare solutions, deionized water (Milli-Q) was used. A

<sup>\*</sup> Corresponding authors.

E-mail addresses: [srpradhan@ichf.edu.pl](mailto:srpradhan@ichf.edu.pl) (S.R. Pradhan), [jcarloscolmenares@ichf.edu.pl](mailto:jcarloscolmenares@ichf.edu.pl) (J.C. Colmenares).

<https://doi.org/10.1016/j.catcom.2021.106375>

Received 3 November 2021; Received in revised form 25 November 2021; Accepted 26 November 2021

Available online 27 November 2021

1566-7367/© 2021 Published by Elsevier B.V. This is an open access article under the CC BY-NC-ND license (<http://creativecommons.org/licenses/by-nc-nd/4.0/>).



SunFire™ Chromatography column (C18 3.5  $\mu\text{m}$ , Waters) with 4.6  $\times$  150 mm of bed support and Perfluoroalkoxy alkane (PFA, 0.8 mm ID, BOLA) were used.

## 2.2. Synthesis and deposition of catalysts

The photocatalysts were prepared using sol-gel synthesis method. All the chemicals were used as received without further purification. To synthesize different atomic percentages of metal-containing nanocomposites, metal precursors were dissolved in 2-propanol and followed the previously established sol-gel route [17]. For low-temperature synthesis, sol-gel is an ingenious approach; it is also easier to incorporate metal into  $\text{TiO}_2$  [5]. The metal precursors copper acetate, cobalt acetate, and iron nitrate were used to synthesize Cu-TiO<sub>2</sub>, Co-TiO<sub>2</sub>, and Fe-TiO<sub>2</sub>, respectively. After catalyst synthesis, ultrasonic-assisted depositions were performed using ultrasonic bath (Sonorex-digital RC, 37 kHz, 100% amplitude) in sweep mode. The tube was placed in the ultrasonic bath (Fig. S. 1). The catalyst suspension was passed through a cleaned PFA microtube under the influence of ultrasound using a syringe pump for 75 min. For detailed information, please refer to supporting information.

## 2.3. Characterization of catalysts and samples

The synthesized samples were characterized using a UV/VIS/NIR spectrophotometer Jasco V-570 equipped with an integrating sphere, and the bandgap was calculated from the Tauc plot derived from UV-vis diffuse reflectance spectra after applying the Kubelka-Munk function [18,19]. Powder X-ray diffraction (XRD) measurements were performed employing the Bragg-Brentano configuration. This type of arrangement was provided using PANalytical Empyrean diffraction platform, powered at 40 kV  $\times$  40 mA and equipped with a vertical goniometer, with theta-theta geometry using Ni filtered Cu K $\alpha$  radiation ( $\lambda = 1.5418 \text{ \AA}$ ). XRD patterns were collected from 10° to 80° with a step size of 0.008° and counting time up to 60 s per step. The average crystallite size (D, in nm) was determined according to the Scherrer equation:

$$D = k \lambda / \beta \cos \theta$$

where D is the average crystallite size of the catalyst (nm),  $\lambda$  is the wavelength of the Cu K $\alpha$  X-ray radiation ( $\lambda = 0.154056 \text{ nm}$ ), k is a coefficient usually taken as 0.9,  $\beta$  is the integral breadth (ratio of peak area to peak maximum, in radians) of the peak observed at  $2\theta$ , and  $\theta$  is the diffraction angle. The elemental maps of the samples were obtained by scanning electron microscopy (SEM) by using a FEI Nova NanoSEM 450. Textural properties of  $\text{TiO}_2$  were determined by  $\text{N}_2$  physisorption using a micromeritics automated system (Micromeritics Instrument Corporation, Norcross, GA, USA) with the Brunauer-Emmet-Teller (BET, for surface area measurement) and the Barret-Joyner-Halenda (BJH, for porosity measurement) methods. Before adsorption measurements, samples were degassed under vacuum (0.1 Pa) for 12 h at 80° C.

After photocatalytic experiments, samples were collected and examined using the energy dispersive X-ray fluorescence (EDXRF) spectrometer (Mini-Pal 4, PANalytical.Co.) with Rh tube with silicon drift detector to check the metals and titania residual. To identify and quantify alcohol, aldehyde, and acid present, the collected samples were analyzed using high-pressure liquid chromatography (HPLC, Waters) using a mobile phase containing a mixture of organic solvents and a 0.05%  $\text{H}_3\text{PO}_4$  (5 M) aqueous solution ( $\text{CH}_3\text{CN}:\text{CH}_3\text{OH}:\text{H}_2\text{O} = 20:2.5:77.5 \text{ v/v}$ ).

## 3. Results and discussion

### 3.1. Optimisation of metal loading in $\text{TiO}_2$ -based composite

Photocatalytic experiments in the batch reactor were carried out to

optimize the atomic percentage of metal in  $\text{TiO}_2$  before moving to microflow reactor system. Firstly, studies with different atomic percentages (0.25, 0.5, 1, and 1.5) of copper in Cu-TiO<sub>2</sub> were performed. A cylindrical UV - LED system (375 nm wavelength) was used as a light source whose intensity was 16.6  $\text{W/m}^2$  (measured by Delta OHM HD 2302.0 radiometer). Photocatalytic experiments in the batch reactor were performed with 0.5 g/L of catalyst concentration for 60 min under UV light, taken from our previous work [17]. Fig. 1 shows the photocatalytic selective oxidation of BnOH for each atomic percentage of Cu doped  $\text{TiO}_2$  catalyst and comparison with sol-gel synthesized  $\text{TiO}_2$  (SolT) after one hour of irradiation time. Parallely, similar batch photocatalytic experiments were performed with Co-TiO<sub>2</sub> and Fe-TiO<sub>2</sub> as well.

Compared to all atomic percentages of Cu within the composite material, BnAld selectivity for 0.5% Cu-TiO<sub>2</sub> (CuT) is increased compared to 1% Cu-TiO<sub>2</sub>. Increasing the atomic percentage of Cu further, though, there is a slight increase in the selectivity, but there is a decline in BnOH conversion. Also, CuT showed better BnOH conversion (33%) with 94% benzaldehyde (BnAld) selectivity compared to the synthesized  $\text{TiO}_2$  (SolT). On the other hand, by decreasing the atomic percentage of Co from 0.5 at.% to 0.25 at.% in the case of Co-TiO<sub>2</sub>, there was a considerable increment in the activity (Fig. S. 2). After one hour of photocatalytic experiment, the lesser atomic percentage of metal showed 32% BnOH conversion with 84% towards BnAld selectivity. 0.5 at.% of Fe in  $\text{TiO}_2$  showed different activity compared to the other two metal catalysts discussed above. The BnOH conversion for this catalyst was increased to 45%, but the selectivity lowered to 34% after one hour of irradiation time (Fig. S. 3). This might be because of the high porosity, and low surface area of the FeT catalyst.

From the above batch photocatalytic selective oxidation experiments, we selected the optimized atomic percentage of the metal in  $\text{TiO}_2$ -based composite (0.5 at.% of Cu-TiO<sub>2</sub> (CuT), 0.5 at.% of Fe-TiO<sub>2</sub> (FeT), and 0.25 at.% of Co-TiO<sub>2</sub> (CoT)) for deposition on the internal wall of the microreactor, and further experimentation.

### 3.2. Characterizations of the synthesized catalysts

The XRD patterns of the sol-gel synthesized catalysts were collected in Fig. 2. Both SolT and FeT samples revealed the reflections at 25.3°, 37.9°, 47.8°, 54.5°, and 62.7°, characteristic for the (011), (004), (020), (015), and (024) diffraction peaks of the anatase crystal structure (similar to JCPDS 02-0406 card). In addition to peaks from anatase, both the catalysts show the presence of peaks originating from the brookite phase, (211) at 30.3°. In the case of the FeT material, the peaks of anatase phase were found narrow and of higher intensity, suggesting a larger crystallite size (D) than SolT (Table 1). Also, from the XRD patterns of all metal-containing  $\text{TiO}_2$ , there are no visible peaks from metal-

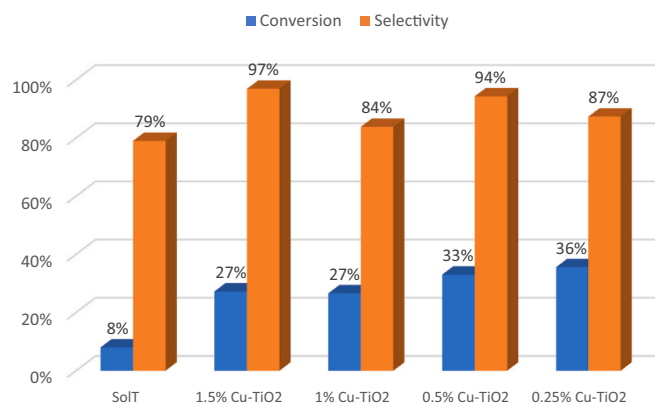
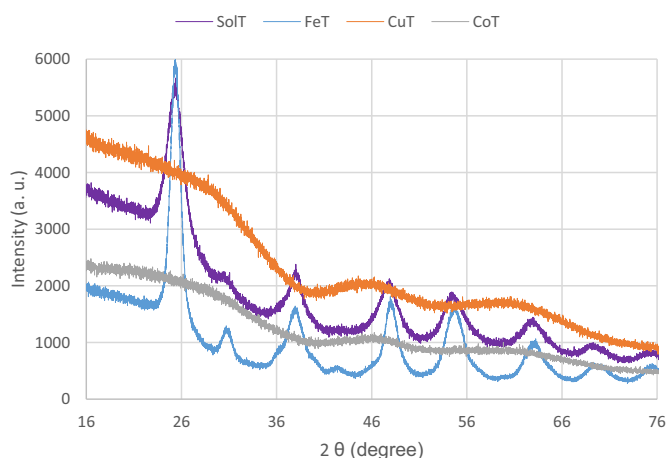


Fig. 1. Comparison of photocatalytic activity between synthesized  $\text{TiO}_2$  and different atomic percentages of Cu-TiO<sub>2</sub> (0.5 g/L) under UV light with 1 mM BnOH in batch photoreactor after 60 min of irradiation.



**Fig. 2.** XRD patterns of different monometallic synthesized TiO<sub>2</sub> catalysts **Key:** For used catalysts sol-gel synthesized TiO<sub>2</sub> (purple), 0.5 at.% Fe-TiO<sub>2</sub> (blue), 0.5 at.% Cu-TiO<sub>2</sub> (orange) and 0.25 at.% Co-TiO<sub>2</sub> (grey). (For interpretation of the references to colour in this figure legend, the reader is referred to the web version of this article.) (For interpretation of the references to colour in this figure legend, the reader is referred to the web version of this article.)

containing phases (or pure metal phases), but only from titanium oxides (most probably because of very low content of metals).

The average crystallite size (*D*) of the anatase was 3.7 nm for the SolT, while for the FeT was found 5.9 nm. In contrast, CuT material had no visible peaks of nano/polycrystalline TiO<sub>2</sub> phases and appeared amorphous. Cu heteroatoms were thought to intrude (mostly retarding the crystallization of the final metal oxide) on crystal nucleation and growth [20]. Also, CoT showed an amorphous structure. Fe ions can be substituted at Ti sites within TiO<sub>2</sub> due to similar ionic radius to Ti<sup>4+</sup> (0.64 Å) (Fe<sup>3+</sup> = 0.65 Å), whereas ionic radii of Cu<sup>2+</sup> (0.73 Å) and Co<sup>2+</sup> (0.74 Å) are bigger than 0.64 Å, hence their different effects on crystal nucleation and TiO<sub>2</sub> growth are possible. The synthesized catalysts were not treated at high temperatures (not calcination step) to keep our synthetic method green. Studies showed that the crystalline pure anatase phase of Co-TiO<sub>2</sub> would be visible upon treatment of sample at 450 °C, and after that the rutile phase starts to grow [21]. Also, another possible explanation is that doping of metal could inhibit the crystalline growth of TiO<sub>2</sub> particles [22].

The CuT and CoT catalysts showed type II adsorption isotherm, which is for very small pores or microporous adsorbents (Fig. 3). In this case, adsorption occurs by filling the micropores. The adsorbate adsorption rate depends on the available pore volume instead of the total interior surface area. A combination of type II and type IV adsorption isotherms was detected for FeT and SolT, which shows the

**Table 1**

Textural and structural properties of synthesized catalysts.

Photocatalyst	Anatase:Rutile:Brookite phases (%)	Specific surface area (m <sup>2</sup> /g)	Pore volume (BJH) (cm <sup>3</sup> /g)	Average Pore size (nm)	Bandgap (eV)	Average crystallite size D (nm)
SolT	69:0:31	284	0.29	3.2	3.3	3.7
CuT	–	577	0.12	3.2	3.4	–
FeT	66:0:34	161	0.31	4.2	3.1	5.9
CoT	–	566	0.22	3.2	3.4	–

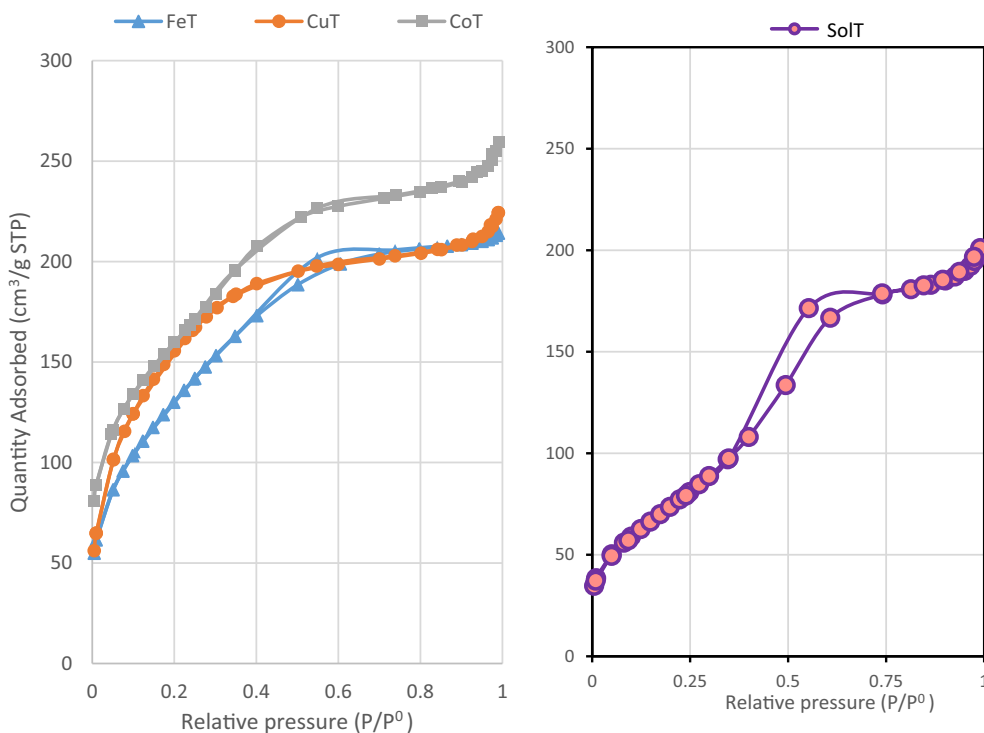


**Fig. 3.** Comparison of N<sub>2</sub> sorption isotherm of monometallic TiO<sub>2</sub> (0.5 at.% of Cu-TiO<sub>2</sub> (CuT), 0.5 at.% of Fe-TiO<sub>2</sub> (FeT) and 0.25 at.% of Co-TiO<sub>2</sub> (CoT) with sol-gel synthesized TiO<sub>2</sub> (SolT) catalyst. (For interpretation of the references to colour in this figure legend, the reader is referred to the web version of this article.)

pore size distribution from big microporous to narrow mesoporous [23]. H2 type hysteresis loop of FeT and SolT suggests a complex pore structure made up of interconnected networks of different sizes and shapes [24]. The average pore size distribution was calculated using BJH (Barrett-Joyner-Halenda) method. The pore size, pore-volume, bandgap, crystallite size, and specific surface area of all synthesized materials are presented in Table 1. Among all the synthesized photocatalysts, FeT catalysts showed low surface area ( $161 \text{ m}^2/\text{g}$ ) compared to others, and showed the better photocatalytic activity in a microflow reactor. The higher porosity of FeT can increase the availability of the catalytic sites and better light utilization [25].

For synthesized  $\text{TiO}_2$ , the bandgap was around 3.3 eV, CuT and CoT have a bandgap of 3.4 eV (Fig. 4. a). The bandgap was found lowered by  $\sim 0.2$  eV for FeT catalyst. All the above catalysts (SolT, FeT, CuT, and CoT) were immobilized inside the PFA microtube using a sonication-promoted technique described earlier in the manuscript. Optimized parameters from batch systems and design expert calculation (Design Expert 11) were considered for the microflow reactor [17]. The flow rate was set to reproduce enough space-time according to the reactor's dimensions. During the photolysis test for 30 min, benzyl alcohol (in flow microreactor) showed negligible conversion in the dark, hence, no reactivity was confirmed for all the catalysts.

By moving from batch to microflow, the specific conversion rate increased for all the catalysts. This trend might be due to the higher availability of catalyst active sites upon the deposition on the microreactor walls [26,27], and taking advantage of high surface to volume ratio very characteristic when working in microspace. Continuous flow microreactors offered considerably shorter reaction time and led to improved irradiation over the reaction mixture than batch reactors. Also, ultrasonic irradiation increases turbulence in the liquid phase, improving the catalyst active surface area via the de-agglomeration and fragmentation of the catalyst's nanoparticles [28]. The photocatalytic experiment under UV light showed that FeT has a better specific conversion rate,  $3518 \mu\text{mol}/\text{m}^2 \text{ hr}$ , than other catalysts (Fig. 5) which value is almost three times higher than that of SolT ( $1048 \mu\text{mol}/\text{m}^2 \text{ hr}$ ). The specific conversion rate was calculated using the given formula,

$$\text{Specific Conversion Rate} = (\mu\text{mol}/\text{m}^2 \text{ hr}) = \frac{C_{\text{BnOH}_0} - C_{\text{BnOH}_t}}{A_C * \text{time}}$$

Where  $A_C$  is the active surface area of the catalyst taking part in the photocatalytic BnOH conversion. In microflow photocatalysis, though the BnOH conversion was better compared to batch, there was negligible selectivity towards benzaldehyde. This is in contrast with the

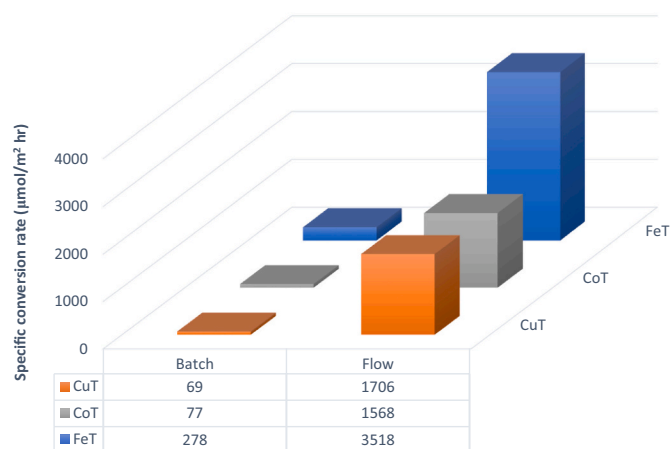


Fig. 5. Comparison between all synthesized monometallic  $\text{TiO}_2$  photocatalytic conversion under UV light with 1 mM BnOH in batch and microflow system (0.5 at.% of Cu- $\text{TiO}_2$  (CuT), 0.25% of Co- $\text{TiO}_2$  (CoT), and 0.5 at.% of Fe- $\text{TiO}_2$  (FeT)).

observations in the batch reaction, where the BnAlD selectivity was higher (35%, Fig. S. 3). One of the plausible reasons for such behavior might be that the spent time of the sample inside the microflow reactor is not sufficient for the desorption of the oxidized product from the monometallic catalytic reactor surface, and we are planning to focus on this issue in our further mechanistic studies. When similar experiments were carried out under visible light (515 nm) system, microtubes deposited with CuT and CoT did not show any activity. However, the FeT deposited PFA tube system showed 28% (specific conversion rate:  $9222 \mu\text{mol}/\text{m}^2 \text{ hr}$ ) BnOH conversion under visible light (Fig. 4.b). The enhanced photocatalytic activity was mainly attributed to the increment in crystallite size of anatase phase, high porosity, and low surface area of the FeT catalyst.

Catalyst deposited tubes were characterized by SEM and optical microscope for surface morphology studies. From the cross-section analysis of PFA tubes (Fig. 6) can be seen that the thickness of the deposited layer of the catalyst can vary between 2 and  $4 \mu\text{m}$ , which is similar to the thickness observed in the case of SolT deposition [17].

The SEM micrographs of CuT and CoT catalyst deposited PFA tube, from the top (Fig. 6) demonstrate that after the deposition, there are agglomerations of particles with the size of nearly  $1 \mu\text{m}$  inside the wall.

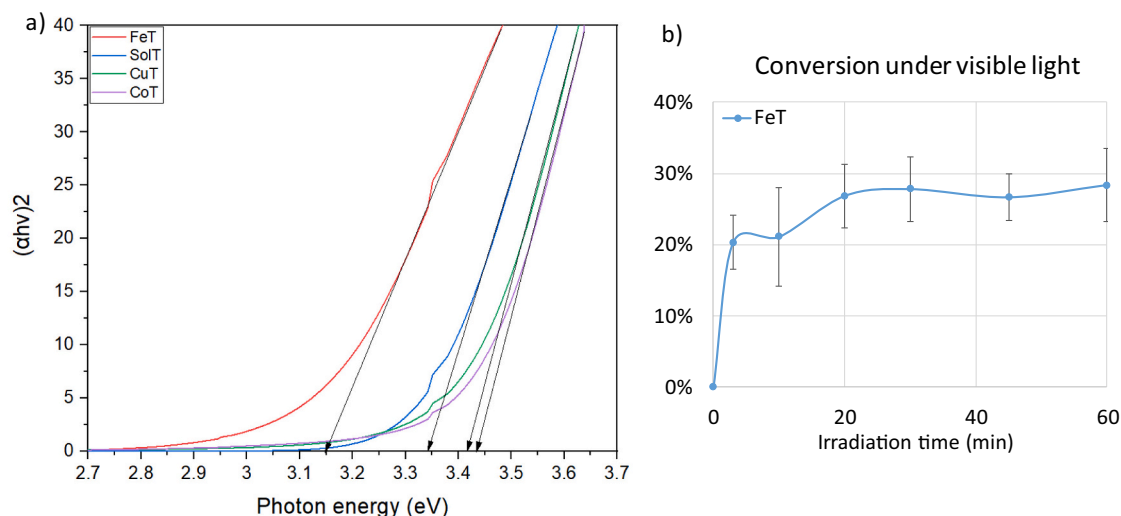
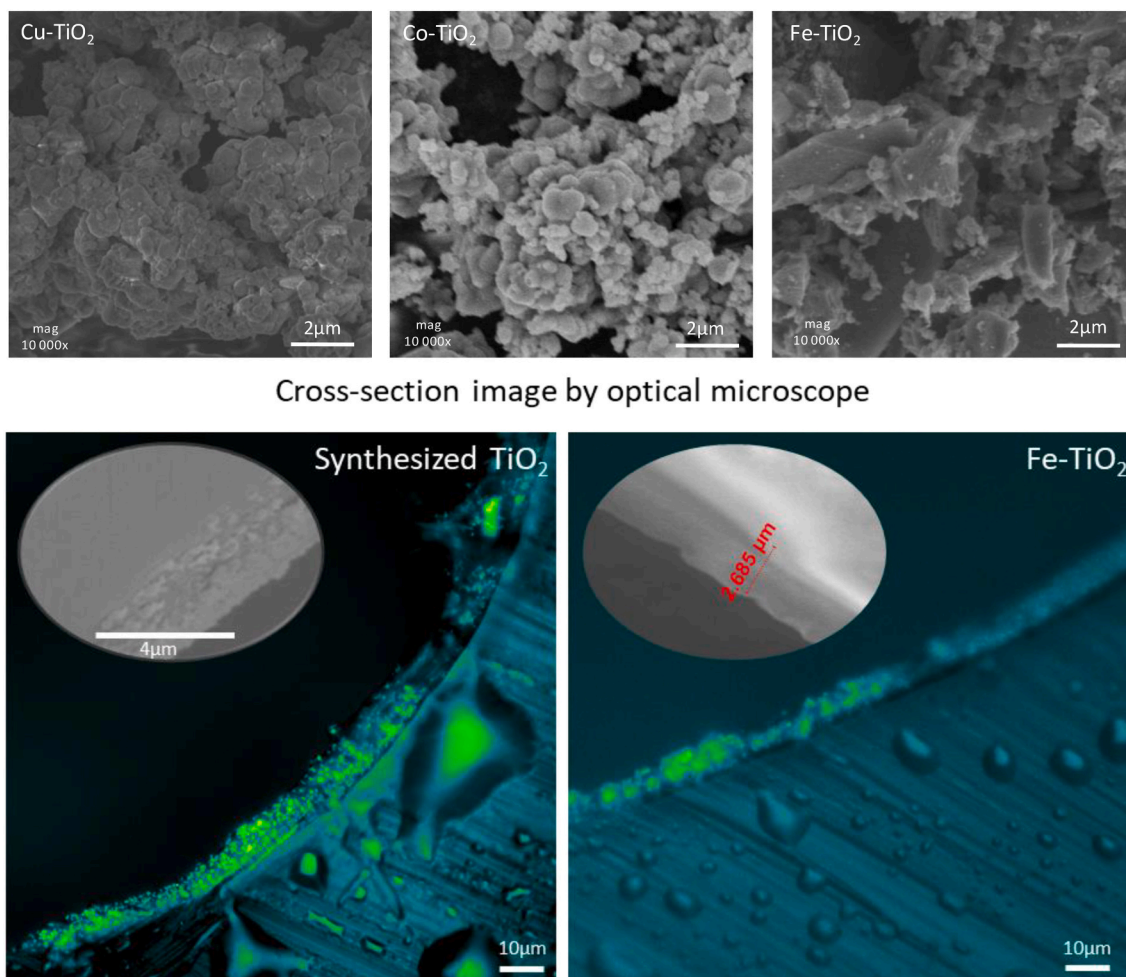


Fig. 4. (a) Bandgap calculation of sol-gel synthesized  $\text{TiO}_2$  (SolT) and monometallic  $\text{TiO}_2$  (0.5 at.% of Cu- $\text{TiO}_2$  (CuT), 0.5 at.% of Fe- $\text{TiO}_2$  (FeT) and 0.25% of Co- $\text{TiO}_2$  (CoT) catalysts (b) Photocatalytic activity of synthesized 0.5 at.% Fe- $\text{TiO}_2$  (FeT) under visible light with 1 mM BnOH in microflow system.



**Fig. 6.** SEM micrographs image of the inner walls of microtube deposited with 0.5 at.% of Cu-TiO<sub>2</sub> (CuT), 0.25% of Co-TiO<sub>2</sub> (CoT), and 0.5 at.% of Fe-TiO<sub>2</sub> (FeT) catalysts.

The presence of big aggregates leads to reduced activity by disturbing the flow of the solution inside the microtube. Because of the flake-like structure of FeT, the hindrance in continuous microflow is minimized compared to that of the highly agglomerated Co and Cu - TiO<sub>2</sub>. The morphology of this FeT flake catalyst provides more surface access to BnOH for photocatalytic conversion. The small agglomerations (200 - 300 nm) and much better dispersion in the case of FeT (Fig. 6) can lead to improved transfer of light and better interaction of the reagent with the surface of the catalyst. Moreover, no leaching from the catalyst deposited microtube after an hour of the experiment was confirmed with the ED-XRF analysis (Fig. S. 4).

#### 4. Conclusions

We synthesized TiO<sub>2</sub> photocatalyst doped with different metals (Cu, Co, and Fe) following the sol-gel method and successfully characterized the obtained composites by applying different techniques. The metal-containing TiO<sub>2</sub> showed higher photocatalytic activity under UV irradiation than the synthesized TiO<sub>2</sub> in the batch system. Compared to the batch reactor, the photocatalytic conversion of benzyl alcohol in the microflow reactor has been substantially improved. The use of sonication during catalyst deposition in a Teflon-based flow microreactor can lead to enhanced mass deposition and dispersion, which helps in better benzyl alcohol conversion. Among all the metal-containing TiO<sub>2</sub> samples, the 0.5 at.% Fe-TiO<sub>2</sub> (both, iron and titanium, as cheap, safe and abundant metals) photocatalyst exhibited the highest BnOH conversion under visible light (515 nm) in the microflow system. This could be

explained by the higher crystallite size observed in XRD analysis, high porosity, and flake-like morphology of the photocatalyst. We were able to set up an additive free (without adding an oxidative agent) visible light active system for oxidation of lignin-based model compound, benzyl alcohol, and inspire ourselves, and certainly the scientific community, to continue merging heterogeneous photocatalysis with flow microreactors as an excellent example of process intensification.

#### Author contributions

Swaraj rashmi Pradhan: Writing - Original draft preparation, Data analysis, Catalyst characterization, Conceptualization, Investigation, Visualization. Dmytro Lisovtyskiy: Investigation, data processing. Juan Carlos Colmenares, Writing – review & editing, Resources, Conceptualization, Supervision, Project administration. All authors discussed and contributed to the work.

#### Declaration of Competing Interest

The authors declare no conflict of interest.

#### Acknowledgments

The authors want to thank Ms. Agnieszka Dżugan (Warsaw University of Technology) for her help in experimentation. This work is supported by the National Science Centre in Poland within Sonata Bis 5 Project No. 2015/18/E/ST5/00306. For more info, please visit our



website: <https://photo-catalysis.org>

## Appendix A. Supplementary data

Supplementary data to this article can be found online at <https://doi.org/10.1016/j.catcom.2021.106375>.

## References

- [1] F. Li, D. Hu, Y. Yuan, B. Luo, Y. Song, S. Xiao, G. Chen, Y. Fang, F. Lu, Zeolite Y encapsulated Cu (II) and Zn (II)-imidazole-salen catalysts for benzyl alcohol oxidation, *Mol. Catal.* 452 (2018) 75–82, <https://doi.org/10.1016/j.mcat.2018.04.002>.
- [2] T. Chen, Z. Xu, L. Zhou, J. Qiu, M. Wang, J. Wang, Highly efficient polymer-based nanoreactors for selective oxidation of alcohols in water, *Mol. Catal.* 474 (2019), 110422, <https://doi.org/10.1016/j.mcat.2019.110422>.
- [3] C. Han, S.H. Li, Z.R. Tang, Y.J. Xu, Tunable plasmonic core-shell heterostructure design for broadband light driven catalysis, *Chem. Sci.* 9 (2018) 8914–8922, <https://doi.org/10.1039/c8sc04479a>.
- [4] C. Han, Z.R. Tang, J. Liu, S. Jin, Y.J. Xu, Efficient photoredox conversion of alcohol to aldehyde and H<sub>2</sub> by heterointerface engineering of bimetal-semiconductor hybrids, *Chem. Sci.* 10 (2019) 3514–3522, <https://doi.org/10.1039/c8sc05813j>.
- [5] X. Lang, W. Ma, C. Chen, H. Ji, J. Zhao, Selective aerobic oxidation mediated by TiO<sub>2</sub> photocatalysis, *Acc. Chem. Res.* 47 (2014) 355–363, <https://doi.org/10.1021/ar4001108>.
- [6] M. Qi, Y. Li, F. Zhang, Z. Tang, Y. Xiong, Y. Xu, Switching light for site-directed spatial loading of cocatalysts onto heterojunction photocatalysts with boosted redox catalysis, *ACS Catal.* 10 (2020) 3194–3202, <https://doi.org/10.1021/acscatal.9b05420>.
- [7] M. Qi, Y. Li, M. Anpo, Z. Tang, Y. Xu, Efficient photoredox-mediated C–C coupling organic synthesis and hydrogen production over engineered semiconductor quantum dots, *ACS Catal.* 10 (2020) 14327–14335.
- [8] Q. Xu, Y. Ma, J. Zhang, X. Wang, Z. Feng, C. Li, Enhancing hydrogen production activity and suppressing CO formation from photocatalytic biomass reforming on Pt/TiO<sub>2</sub> by optimizing anatase-rutile phase structure, *J. Catal.* 278 (2011) 329–335, <https://doi.org/10.1016/j.jcat.2011.01.001>.
- [9] S.R. Kadam, V.R. Mate, R.P. Panmand, L.K. Nikam, M.V. Kulkarni, R.S. Sonawane, B.B. Kale, A green process for efficient lignin (biomass) degradation and hydrogen production via water splitting using nanostructured C, N, S-doped ZnO under solar light, *RSC Adv.* 4 (2014) 60626–60635, <https://doi.org/10.1039/c4ra10760h>.
- [10] S. Yurdakal, G. Palmisano, V. Loddo, O. Alagöz, V. Augugliaro, L. Palmisano, Selective photocatalytic oxidation of 4-substituted aromatic alcohols in water with rutile TiO<sub>2</sub> prepared at room temperature, *Green Chem.* 11 (2009) 510–551, <https://doi.org/10.1039/b819862d>.
- [11] T. Lv, J. Zhao, M. Chen, K. Shen, D. Zhang, J. Zhang, G. Zhang, Q. Liu, Boosted visible-light photodegradation of methylene blue by V and co-doped TiO<sub>2</sub>, *Materials (Basel)* 11 (2018), <https://doi.org/10.3390/ma11101946>.
- [12] J. Chen, F. Qiu, W. Xu, S. Cao, H. Zhu, Recent progress in enhancing photocatalytic efficiency of TiO<sub>2</sub>-based materials, *Appl. Catal. A Gen.* 495 (2015) 131–140, <https://doi.org/10.1016/j.apcata.2015.02.013>.
- [13] S.P. Pitre, T.P. Yoon, J.C. Scaiano, Titanium dioxide visible light photocatalysis: surface association enables photocatalysis with visible light irradiation, *Chem. Commun.* 53 (2017) 4335–4338, <https://doi.org/10.1039/c7cc01952a>.
- [14] M. Roseau, N. Dhaouadi, C. Rolando, L. Chausset-Boissarie, M. Penhoat, Continuous photocatalyzed aerobic oxidation of benzylic organotrifluoroborates to benzaldehydes under Taylor flow conditions, *J. Flow Chem.* 10 (2020) 347–352, <https://doi.org/10.1007/s41981-019-00053-w>.
- [15] S. Sohrabi, M. Keshavarz Moraveji, D. Iranshahi, A review on the design and development of photocatalyst synthesis and application in microfluidic reactors: challenges and opportunities, *Rev. Chem. Eng.* 36 (2020) 687–722, <https://doi.org/10.1515/revce-2018-0013>.
- [16] D. Cambié, C. Bottecchia, N.J.W. Straathof, V. Hessel, T. Noël, Applications of continuous-flow photochemistry in organic synthesis, material science, and water treatment, *Chem. Rev.* 116 (2016) 10276–10341, <https://doi.org/10.1021/acs.chemrev.5b00707>.
- [17] S.R. Pradhan, V. Nair, D.A. Giannakoudakis, D. Lisovtyskiy, J.C. Colmenares, Design and development of TiO<sub>2</sub> coated microflow reactor for photocatalytic partial oxidation of benzyl alcohol, *Mol. Catal.* 486 (2020), 110884, <https://doi.org/10.1016/j.mcat.2020.110884>.
- [18] J.F. Guayaquil-Sosa, B. Serrano-Rosales, P.J. Valadés-Pelayo, H. de Lasa, Photocatalytic hydrogen production using mesoporous TiO<sub>2</sub>doped with Pt, *Appl. Catal. B Environ.* 211 (2017) 337–348, <https://doi.org/10.1016/j.apcatb.2017.04.029>.
- [19] P. Kubelka, F. Munk, Reflection characteristics of paints, *Z. Tech. Phys.* 12 (1931) 593–601.
- [20] C. Garlisi, G. Scandura, J. Szlachetko, S. Ahmadi, J. Sa, G. Palmisano, E-beam evaporated TiO<sub>2</sub> and cu-TiO<sub>2</sub> on glass: performance in the discoloration of methylene blue and 2-propanol oxidation, *Appl. Catal. A Gen.* 526 (2016) 191–199, <https://doi.org/10.1016/j.apcata.2016.08.022>.
- [21] F. Mostaghni, Y. Abed, Structural, optical and photocatalytic properties of co-TiO<sub>2</sub> prepared by sol-gel technique, *Mater. Res.* 19 (2016) 741–745, <https://doi.org/10.1590/1980-5373-MR-2016-0191>.
- [22] A. El Mragui, O. Zegaoui, I. Daou, J.C.G. Esteves da Silva, Preparation, characterization, and photocatalytic activity under UV and visible light of Co, Mn, and Ni mono-doped and (P,Mo) and (P,W) co-doped TiO<sub>2</sub> nanoparticles: a comparative study, *Environ. Sci. Pollut. Res.* 28 (2021) 25130–25145, <https://doi.org/10.1007/s11356-019-04754-6>.
- [23] B. Abebe, H.C.A. Murthy, E. Amare, Summary on Adsorption and Photocatalysis for Pollutant Remediation: Mini Review, 2018, pp. 225–255, <https://doi.org/10.4236/jeas.2018.84012>.
- [24] K.S.W. Sing, R.T. Williams, Physisorption hysteresis loops and the characterization of nanoporous materials, *Adsorpt. Sci. Technol.* 22 (2004) 773–782, <https://doi.org/10.1260/0263617053499032>.
- [25] G. Srinivas, V. Krungleviciute, Z.X. Guo, T. Yildirim, Exceptional CO<sub>2</sub> capture in a hierarchically porous carbon with simultaneous high surface area and pore volume, *Energy Environ. Sci.* 7 (2014) 335–342, <https://doi.org/10.1039/c3ee42918k>.
- [26] H. Maleki, V. Bertola, Recent advances and prospects of inkjet printing in heterogeneous catalysis, *Catal. Sci. Technol.* 10 (2020) 3140–3159, <https://doi.org/10.1039/d0cy00040j>.
- [27] P. Peter, Application of catalysts to metal microreactor systems, *Chem. Kinet.* (2012) 325–344, <http://www.intechopen.com/books/chemical-kinetics/application-of-catalysts-to-microreactor-systems>.
- [28] S. Aljbour, H. Yamada, T. Tagawa, Ultrasound-assisted phase transfer catalysis in a capillary microreactor, *Chem. Eng. Process. Process Intensif.* 48 (2009) 1167–1172, <https://doi.org/10.1016/j.cep.2009.04.004>.

# Flow photomicroreactor coated with monometal containing TiO<sub>2</sub> using sonication: a versatile tool for visible light oxidation

Swaraj R. Pradhan<sup>\*a</sup>, Dmytro Lisovytskiy<sup>a</sup>, Juan C. Colmenares<sup>\*a</sup>

<sup>a</sup> *Institute of Physical Chemistry, Polish Academy of Sciences, Kasprzaka 44/52, 01-224  
Warsaw, Poland.*

## Appendix A. Supplementary data

### *Ultrasound-assisted deposition of catalysts in PFA*

A 30 cm PFA microtube (microcapillary 0.8 mm ID), pure from the market, undergoes a cleaning process by passing through 5 ml of MilliQ water (analytical grade) and 5 ml of ethanol. Both solvents are introduced into the microtube at a constant flow rate of 1 mL/min using a syringe infusion pump (New Era Pump Systems, Inc.). The tube is placed in the oven for 1h at approx. 80 °C and used for further deposition. For the catalyst deposition, an ultrasonic bath (Sonorex-digital RC, 37 kHz, 100% amplitude) was used in sweep mode. The tube was placed in the ultrasonic bath (Figure S. 1). The catalyst suspension was passed through a cleaned PFA microtube under the influence of ultrasound (120W) using a syringe pump for 75 minutes (0.34 ml/min).

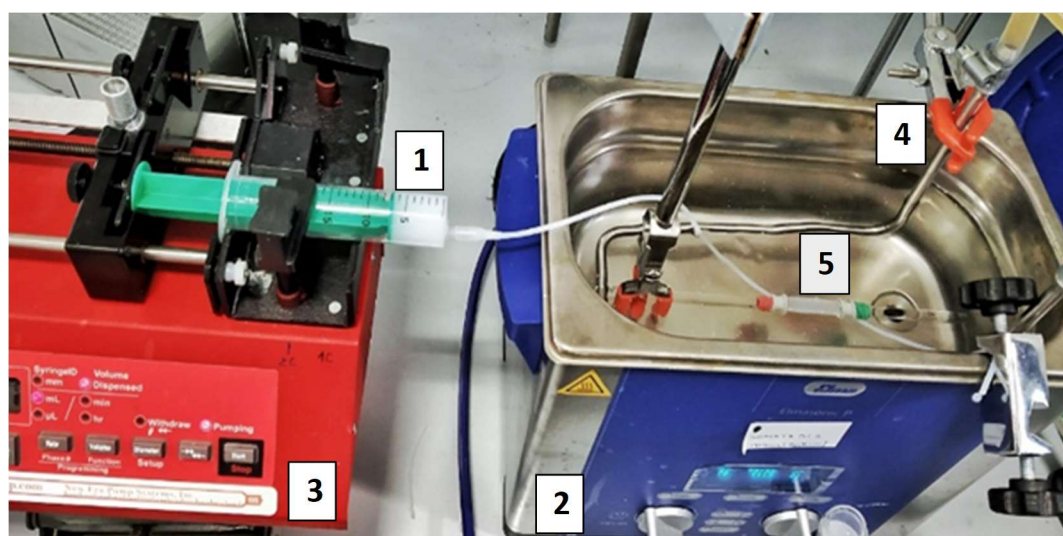


**Figure S. 1.** Catalyst deposition to the inner wall of the PFA microtube; (1) semiconductor oxide suspension, (2) ultrasonic bath, (3) Syringe infusion pump, (4) water cooling system, and (5) PFA microtube

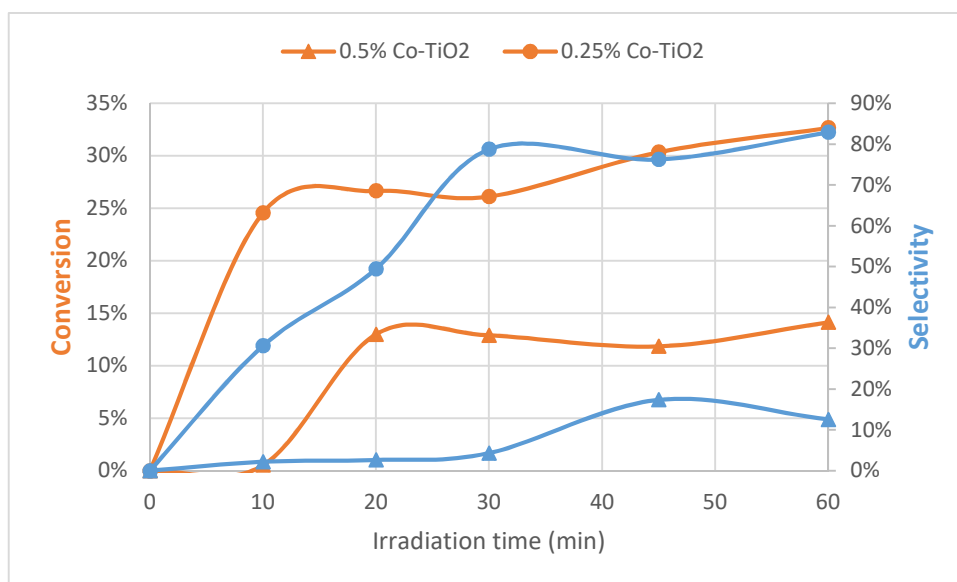


**Figure S. 2.** Optimization of at% of Co-TiO<sub>2</sub> (0.5g/L) under UV light with 1mM BnOH in batch system

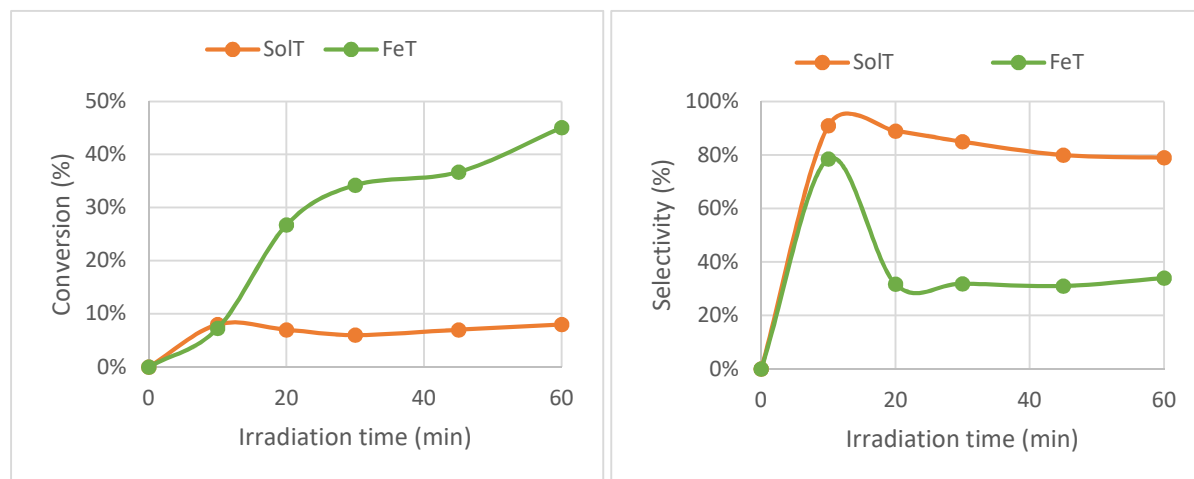


**Figure S. 3.** Photocatalytic activity of synthesized TiO<sub>2</sub> (SolT) and 0.5 at% Fe-TiO<sub>2</sub> (FeT) under UV light with 1mM BnOH in batch system



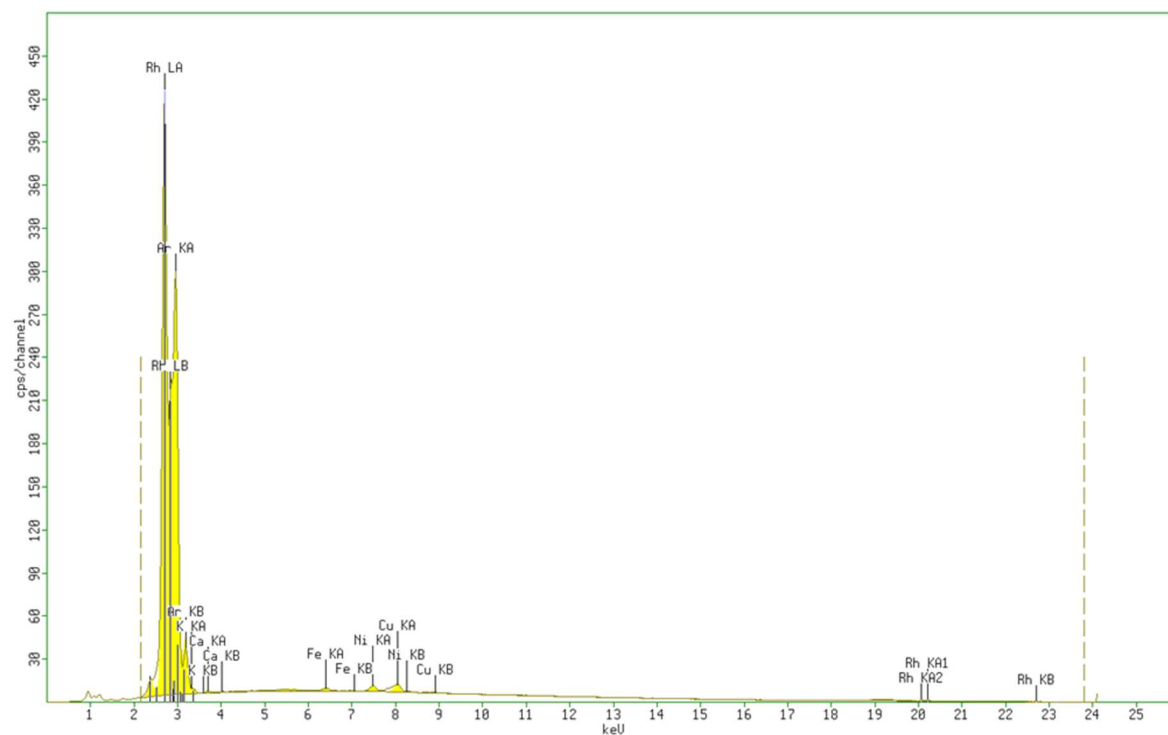
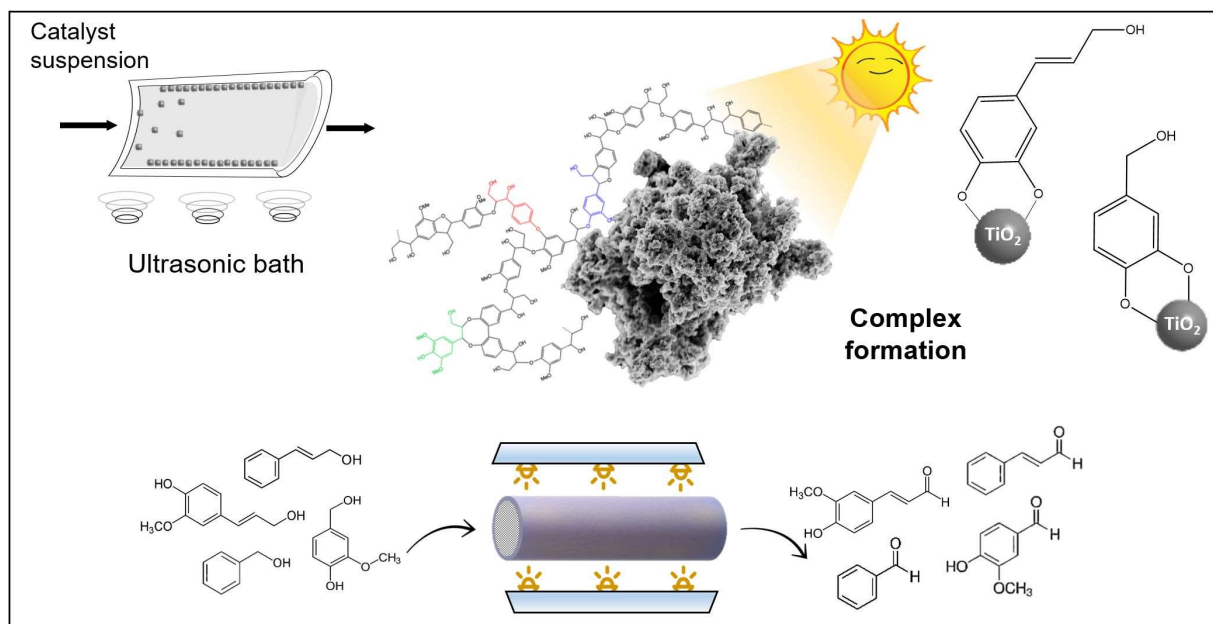


**Figure S. 4.** EDXRF measurement of the sample from the outlet of synthesized Fe-TiO<sub>2</sub> deposited PFA tube. (Rh-peak from Rh lamp, Fe and Cu peaks- are finger prints of the spectrometer)

EDXRF analysis confirmed (no traces of Ti presence) no leaching from the catalyst coated microtube after one hour of the experiment.

## Chapter 5 : Bimetallic TiO<sub>2</sub> Nanoparticles for Lignin-Based Model Compounds Valorization by Integrating Optocatalytic Flow-Microreactor



The present chapter discusses the research work described in a published manuscript (P 4), authored by Swaraj rashmi Pradhan, Marta PaszkiewiczGawron, Dariusz Łomot, Dmytro Lisovytskiy and Juan Carlos Colmenares. (*Molecules* 27 (2022) 8731; <https://doi.org/10.3390/molecules27248731>)

Article

# Bimetallic TiO<sub>2</sub> Nanoparticles for Lignin-Based Model Compounds Valorization by Integrating an Optocatalytic Flow-Microreactor

Swaraj Rashmi Pradhan \*<sup>1</sup>, Marta Paszkiewicz-Gawron, Dariusz Łomot, Dmytro Lisovtyskiy and Juan Carlos Colmenares \*<sup>2</sup>

Institute of Physical Chemistry, Polish Academy of Sciences, Kasprzaka 44/52, 01-224 Warsaw, Poland

\* Correspondence: srpradhan@ichf.edu.pl (S.R.P.); jcarloscolmenares@ichf.edu.pl (J.C.C.);

Tel.: +48-22-3433-3215 (J.C.C.)

**Abstract:** The challenge of improving the activity of TiO<sub>2</sub> by modifying it with metals and using it for targeted applications in microreactor environments is an active area of research. Recently, microreactors have emerged as successful candidates for many photocatalytic reactions, especially for the selective oxidation process. The current work introduces ultrasound-assisted catalyst deposition on the inner walls of a perfluoro-alkoxy alkane (PFA) microtube under mild conditions. We report Cu-Au/TiO<sub>2</sub> and Fe-Au/TiO<sub>2</sub> nanoparticles synthesized using the sol-gel method. The obtained photocatalysts were thoroughly characterized by UV-Vis diffuse-reflectance spectroscopy (DRS), high-resolution scanning electron microscopy (HR-SEM), high-resolution transmission electron microscopy (HR-TEM), X-ray diffraction analysis (XRD), Fourier transform infrared spectroscopy (FTIR), X-ray photoelectron spectroscopy (XPS), and N<sub>2</sub> physisorption. The photocatalytic activity under UV (375 nm) and visible light (515 nm) was estimated by the oxidation of lignin-based model aromatic alcohols in batch and fluoropolymer-based flow systems. The bimetallic catalyst exhibited improved photocatalytic selective oxidation. Herein, four aromatic alcohols were individually investigated and compared. In our experiments, the alcohols containing hydroxy and methoxy groups (coniferyl and vanillin alcohol) showed high conversion (93% and 52%, respectively) with 8% and 17% selectivity towards their respective aldehydes, with the formation of other side products. The results offer an insight into ligand-to-metal charge transfer (LMCT) complex formation, which was found to be the main reason for the activity of synthesized catalysts under visible light.

**Keywords:** bimetallic titanium dioxide; photocatalytic selective oxidation; fluoropolymer; wall-coated microreactor; aromatic alcohol; ultrasonic irradiation



**Citation:** Pradhan, S.R.; Paszkiewicz-Gawron, M.; Łomot, D.; Lisovtyskiy, D.; Colmenares, J.C. Bimetallic TiO<sub>2</sub> Nanoparticles for Lignin-Based Model Compounds Valorization by Integrating an Optocatalytic Flow-Microreactor. *Molecules* **2022**, *27*, 8731. <https://doi.org/10.3390/molecules27248731>

Academic Editors: Veljko R. Djokić and Zoran V. Šaponjić

Received: 4 November 2022

Accepted: 6 December 2022

Published: 9 December 2022

**Publisher's Note:** MDPI stays neutral with regard to jurisdictional claims in published maps and institutional affiliations.



**Copyright:** © 2022 by the authors. Licensee MDPI, Basel, Switzerland. This article is an open access article distributed under the terms and conditions of the Creative Commons Attribution (CC BY) license (<https://creativecommons.org/licenses/by/4.0/>).

## 1. Introduction

TiO<sub>2</sub> is used as a photocatalyst for the degradation of impurities, a component of self-cleaning coatings, cosmetics, and for the production of hydrogen in water decomposition reactions [1,2]. Despite the numerous application possibilities, however, its industrial use is very limited. TiO<sub>2</sub> due to wide band gap is capable of absorbing only UV radiation, which constitutes only 3 to 5% of solar radiation. The consequence of this is the fact that TiO<sub>2</sub> still does not have satisfactory photocatalytic efficiency under visible light irradiation [3,4]. The use of UV lamps as a radiation source, due to the high energy consumption, significantly increases the cost of the process, which is an important factor limiting the broader use of this method in removing pollutants on an industrial scale. Consequently, many studies focused on the visible response of TiO<sub>2</sub> photocatalysts by: (i) doping with metal or non-metal ions, (ii) hetero-junctions creation with other semiconductors [5,6], (iii) sensitization [7], (iv) the formation of a surface complex with energy transfer [8,9] or (v) surface modification with noble metals nanoparticles [10]. By doping TiO<sub>2</sub> with transition-metal ions (Fe, Cu, Co, Mn, and Ni) was reported to be effective for the enhancement of the photocatalytic activity by changing the

banding structure of TiO<sub>2</sub> due to the interstitial doping Ti<sup>3+</sup> states as well as the formation of surface oxygen vacancies, which, together, cause the red-shift absorption edge of TiO<sub>2</sub> [11–14]. Among the noble metals, gold pays more attention in selective photo-oxidation reactions under visible light irradiation [15]. In the past few decades, the rapid expansion of gold (Au) catalysis has developed many new approaches to the aerobic oxidation of alcohols [16,17]. However, bimetallic catalysts have been observed to outperform their monometallic counterparts in conventional heterogeneous catalysis [18,19]. The noble bimetallic nanoparticles have been extensively studied for application in photocatalysis [20].

Because of their high-value products for the fine chemical, agrochemical, and pharmaceutical sectors, alpha beta-unsaturated aldehydes are essential to a sustainable chemical economy [21]. For example, cinnamyl aldehyde (CinAld) serves as an insect repellent and also provides the flavor and aroma of cinnamon; CinAld is both a food and perfume additive. These aldehydes are usually derived by selective oxidation of their corresponding alcohols.

Catalyst testing in flow microreactors has many advantages over traditional batch reactors. These are, but not limited to, the followings: (i) operating parameters such as temperature, pressure, and feed concentrations can be easily varied in flow microreactors to obtain an insight into the reaction mechanism and kinetics [22]; (ii) the consumption of chemicals and waste production are significantly reduced; and (iii) easy testing of catalyst stability under different reaction conditions. Liquid phase catalytic oxidation chemistry in continuous-flow microreactors has recently been summarized from technological and chemical perspectives [23].

Considering the potential of metals containing TiO<sub>2</sub> catalytic materials and flow microreactors as a powerful tool for catalyst testing, studying the bimetallic catalysts in a flow microreactor for photocatalytic selective oxidation of a lignin-based model compound into a value-added product is an exciting field of research. In this work, the photocatalytic activity of synthesized bimetallic TiO<sub>2</sub> nanoparticles was evaluated under UV light and visible light irradiations both in batch and microflow systems, using benzyl alcohol (BnOH), vanillin alcohol (VanOH), cinnamyl alcohol (CinOH), and coniferyl alcohol (ConOH) as model compounds of organic-based waste, lignin. The structural properties of the synthesized catalysts were analyzed by X-ray diffraction (XRD) and Fourier transform infrared (FTIR) spectroscopy. The optical properties were investigated using UV–vis diffuse reflectance (DRS), a surface morphology study was performed by high-resolution scanning electron microscopy (HR-SEM) and high-resolution transmission electron microscopy (HR-TEM), and the textural properties were determined by nitrogen sorption. We demonstrated that the addition of a second metal-to-metal TiO<sub>2</sub> nanoparticle increased the selective oxidation of BnOH to 100% towards benzaldehyde (BnAld). In addition, the complex formation between TiO<sub>2</sub> and other aromatic alcohols (containing methoxy and hydroxyl groups) activated the sol–gel-synthesized catalyst under visible light. Under batch experiment conditions, ConOH and VanOH showed conversion of 93% and 52%, respectively, under visible light (515 nm).

## 2. Results and Discussion

Oxidation of benzyl alcohol (BnOH) was often used as a model reaction for the oxidation of aromatic alcohols. In order to verify the reactivity of the prepared Cu-Au/TiO<sub>2</sub> and Fe-Au/TiO<sub>2</sub> catalysts in the batch system and the performance in the microreactor system, oxidation of BnOH was initially carried out under UV light (375 nm). From the photocatalytic experiment, it was found that modification of TiO<sub>2</sub> with bimetallics increased the selective oxidation of BnOH to aldehydes under UV light. In a batch system, the synthesized Cu-Au/TiO<sub>2</sub> with copper acetate precursor (CuA-Au/TiO<sub>2</sub>) catalyst has a significantly higher conversion of BnOH (60%) compared to other bimetallic catalysts with 100% selectivity towards benzaldehyde (BnAld) (Figure 1a).

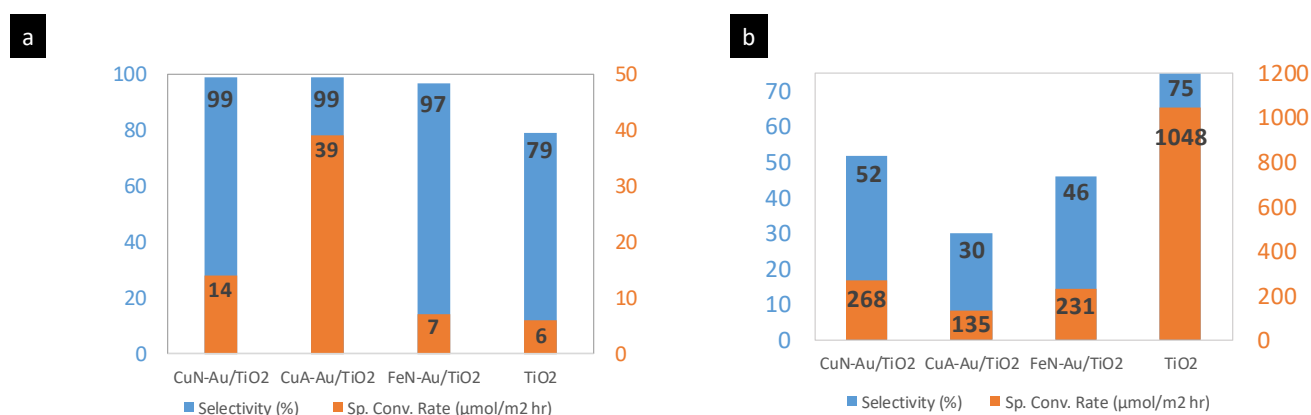


**Figure 1.** Photocatalytic activity of sol-gel-synthesized bimetallic TiO<sub>2</sub> in the batch system (a) and microflow system (b) after 60 min of the photocatalytic experiment with 1 mM BnOH under UV light.

Upon the deposition of catalysts on the walls of the microreactor, the synthesized bimetallic materials revealed better photo reactivity in regard to both BnOH specific conversion rates, an absolute contrast trend with the batch experiments (Figure 1a). After 3 h of light experiment, the specific conversion rate of Cu-Au/TiO<sub>2</sub> prepared using copper nitrate precursor (CuN-Au/TiO<sub>2</sub>) in the batch system was 14  $\mu\text{mol}/\text{m}^2 \cdot \text{h}$ , whereas, in the microflow system, it reached 268  $\mu\text{mol}/\text{m}^2 \text{ h}$ .

The specific surface areas determined from N<sub>2</sub> physisorption for the Cu-Au/TiO<sub>2</sub> and Fe-Au/TiO<sub>2</sub> varied from 251 to 547  $\text{g}/\text{m}^2$ , which was predominantly controlled by the type of precursor used for synthesis (Table 1). The use of nitrate precursor during the synthesis procedure caused a significant increase (about two-fold) in the specific surface area with reduced crystallinity (Figure 2a) compared to pure TiO<sub>2</sub>. Au phase is not a dominant phase for these catalysts; therefore a small peak of Au is observed. Amorphous phases dominate in CuN-Au/TiO<sub>2</sub> and FeN-Au/TiO<sub>2</sub> samples, such phases do not give peaks in the XRD pattern, and on the background of such phases, even a small peak from nanocrystalline gold is easily detectable. The crystallite size of Au for each catalyst are shown in Table 1.

**Table 1.** Crystallographic, structural, and textural features of the synthesized bimetallic catalysts.

Sample	Anatase: Brookite: Gold Crystalline Phases (%)	Specific Surface Area ( $\text{m}^2/\text{g}$ )	Average Pore Size (nm)	Pore Volume (BJH) ( $\text{cm}^3/\text{g}$ )	Average Crystallite Size (Dcr) [nm] (Au Phase) by XRD
TiO <sub>2</sub>	69:31:0	284	3.2	0.3	n/a
CuA-Au/TiO <sub>2</sub>	68:31:0.44	251	6.8	0.3	11
CuN-Au/TiO <sub>2</sub>		541	3.1	0.4	18
FeN-Au/TiO <sub>2</sub>		547	2.8	0.2	18

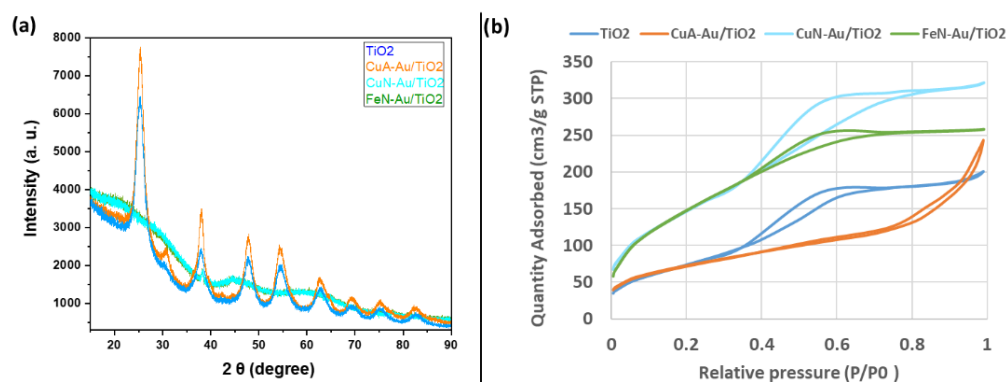


**Figure 2.** XRD patterns of different bimetallic synthesized catalysts (a) and N<sub>2</sub> sorption isotherm of bimetallic TiO<sub>2</sub> (b) compared to sol-gel-synthesized TiO<sub>2</sub> catalyst.

A combination of type II and IV adsorption isotherms was noticed for sol-gel-synthesized  $\text{TiO}_2$  and the bimetallic catalysts with nitrate precursors (Figure 2b) [24]. The H2-type hysteresis loop of these catalysts suggested a complex pore structure [25]. On the other hand, the bimetallic catalyst with acetate precursor ( $\text{CuA-Au/TiO}_2$ ) showed a type-IV adsorption isotherm [24], suggesting the presence of mesopores. The shape of the hysteresis loops was of type H3, which indicates the presence of aggregates of slit-shaped conical pores composed of primary particles, which can give rise to piled-up pores [26–28].

The Tauc plots (Figure S2) revealed that the bandgaps for all the synthesized catalysts were  $\sim 3.4$  eV. In addition, the BJH (Barrett–Joyner–Halenda) method was used to calculate the average pore size distribution, and the values are provided in Table 1.

The average pore size was lower for samples synthesized using nitrate precursors than for samples that were prepared with acetate precursors. This observation can be explained by a partial modification of the  $\text{TiO}_2$  surface by nitrate decomposition and evolving gaseous  $\text{NO}_x$  during the synthesis procedure. The photocatalytic activity in the microflow system (Figure 1b) of  $\text{CuN-Au/TiO}_2$  and  $\text{FeN-Au/TiO}_2$  accompanied by their larger specific area, as a consequence, may provide more active sites and shorten the bulk diffusion length of charge carriers, thus suppressing bulk recombination [29]. However, the pore volume was much higher for the sample  $\text{CuN-Au/TiO}_2$  ( $0.4 \text{ cm}^3/\text{g}$ ) than for  $\text{FeN-Au/TiO}_2$  ( $0.2 \text{ cm}^3/\text{g}$ ), even though nitrogen salts were used in both cases during the preparation. This dependency can be caused by steric hindrance during the growth of the  $\text{TiO}_2$  crystallites via Ostwald ripening [30]. The molecular structure of iron (III) nitrate nonahydrate is bigger than copper (II) nitrate trihydrate (computed by PubChem), which consequently causes more steric hindrance.

The synthesized bimetallic catalysts were investigated using transmission electron microscopy (TEM). The composition of the particles was studied using STEM (high-angle annular dark field, HAADF) and EDXS mapping. In the  $\text{CuA-Au/TiO}_2$  sample, the TEM analysis revealed that primary nanoparticles were clustered to form more oversized agglomerates during the formation stage itself (Figure 3). The results of the TEM analysis showed that Ti, O, and Cu are evenly distributed throughout the sample surface (Figure 3d,e).

The application of the HAADF method confirmed the presence of the expected elements, such as Ti, Cu, and Au (Figure 3c–e), and also, from XPS analysis of  $\text{CuA-Au/TiO}_2$ , we were able to confirm the presence of 0.1 at% Cu and 0.03 at% Au in the catalyst surface (Figure S4). Gold and copper nanoparticles were evenly distributed in the tested sample (Figure 3b–d) which is very important in terms of the influence on the photocatalytic activity. Based on TEM analysis (Figure 3), UV–Vis DRS spectra (Figure S3), and XPS analysis (Figure S4), it can be deduced that surface incorporation of Cu and Au atoms on the  $\text{TiO}_2$  has occurred. On the UV–Vis spectra, the red shift of absorption for  $\text{CuA-Au/TiO}_2$  in comparison to bare  $\text{TiO}_2$  and no obvious peak from copper nanoparticles (NPs) can be seen. The absence of the peak coming from Cu NPs could be due to the low amount of Cu NPs on the  $\text{TiO}_2$  surface. The same results regarding the slight red shift of absorption to 403 nm for copper nanospheres coupled with  $\text{TiO}_2$  were obtained by Monga et al. and also other research groups [31–33]. The distinct peak derived from Au nanoparticles occurred at 560 nm due to the charge transfer from the metal ion to  $\text{TiO}_2$  [32]. The abovementioned absorption in the range of visible irradiation may be due to the localized surface plasmon resonance (LSPR). It has been shown that in the mechanism using LSPR, metal can act as an electron trap and thus inhibit the recombination process of electron-hole pairs [34,35]. The characteristic LSPR band maximum at 555 nm [36] indicates the presence of Au nanoparticles in the  $\text{CuN-Au/TiO}_2$  sample, shown on the UV–Vis DRS spectra (Figure S3).

It can be clearly seen in the TEM pictures (Figure 3b) that the obtained gold nanoparticles have a spherical shape, and the particle size distribution of Au was in the range of 10–40 nm, with the highest contribution of the fraction from 15 to 25 nm and mean size equal to 22.1 nm (Figure 3a). The nanometric size and shape of the obtained Au particles are good enough to provoke LSPR [31,37]. This proves that the particles in nanoscale with a favorable spherical shape were successfully obtained during the synthesis procedure. Gołabiewska et al. [38] have shown that the spherical shape of gold nanoparticles was very beneficial for increasing



the photocatalytic activity in the range of visible irradiation. They compared the photoactivity of different shapes of Au particles deposited on TiO<sub>2</sub> microspheres and proved that visible light activity decreased in the following order: spheres > rods > stars [38]. It can also be added that in the case of the CuA-Au/TiO<sub>2</sub> sample, the inter-planar spacing for gold was 0.24 nm, which corresponds to the separation between the (111) lattice planes of Au (Figure 3b), which was consistent with the results obtained by XRD analysis (Table 1).

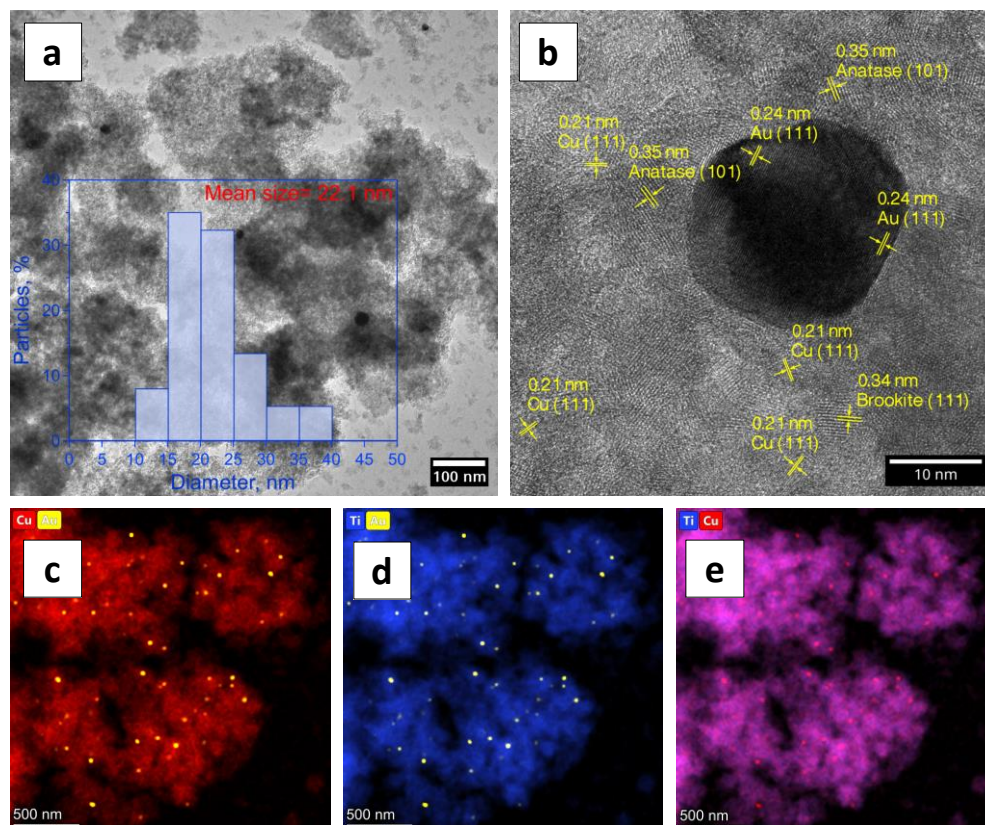


**Figure 3.** TEM images of the obtained CuA-Au/TiO<sub>2</sub> sample: SE mode with a particle size distribution (a), SE mode (b), EDS HAADF analysis of Cu (c) and Au, EDS HAADF analysis of Ti and Au (d), and EDS HAADF analysis of Ti and Cu (e).

Very similar to the CuA-Au/TiO<sub>2</sub> TEM analysis results were the results obtained for the CuN-Au/TiO<sub>2</sub> sample, where the gold particles have a nanometric size and spherical shape; in addition, they were evenly distributed over the entire sample (Figure 4a–e). The difference in the photocatalytic activity of these samples was probably due to the precursors used (nitrate and acetate). The average size of the Au particles ranges between 10–50 nm, also less than 5% in the range 60–70 nm, with a significant predominance of particles with sizes from 10 to 30 nm, where the mean size was 24.7 nm (Figure 4a). Moreover, the Au particle has planes (111) and (200), which correspond to 0.24 and 0.20 nm, respectively (Figure 4b).

The TEM micrographs of FeN-Au/TiO<sub>2</sub> shown in Figure 5 gave a bright observation of the sample in which the particles are much bigger than those obtained in the case of the samples containing copper (the mean sizes of the particles were 22.1 nm for CuN-Au/TiO<sub>2</sub> and 24.7 nm for CuA-Au/TiO<sub>2</sub>). The particle size was found in the range of up to 60 nm and also in the range from 80 to 140 nm, with the mean size equal to 60.6 nm. (Figure 5a). It should be emphasized that in the UV–Vis DRS spectrum (Figure S3), no characteristic peak from the LSPR of gold particles was detected. Similar results were obtained by Duan et al., where despite the presence of gold particles in the sample, confirmed by other analytical methods, the characteristic peak of approx. 550 nm was not observed [39]. Similar results were obtained for the FeN-Au/TiO<sub>2</sub> sample; there were big agglomerates which caused an



uneven distribution of Au particles on the  $\text{TiO}_2$  (Figure 5d,e), which could be the reason for the absence of the peak from Au NPs in the UV–Vis DRS spectra. However, a significant shift of absorption towards the visible spectrum ( $>400\text{nm}$ ) for FeN–Au/ $\text{TiO}_2$  in comparison with unmodified  $\text{TiO}_2$  was observed on UV–Vis DRS (Figure S3), and the presence of Fe 2p 3/2 on the surface of the catalyst (confirmed by XPS analysis) also indicates the probable surface incorporation of Fe and Au atoms on  $\text{TiO}_2$ . The aim of introducing the Fe atoms to the sample was to increase the absorption toward the visible light wavelength and thus increase the photocatalytic activity in the visible range [40]. The distribution of Fe atoms observed on TEM connected with UV–Vis DRS and XPS results can testify to the surface incorporation of Fe atoms [41,42].

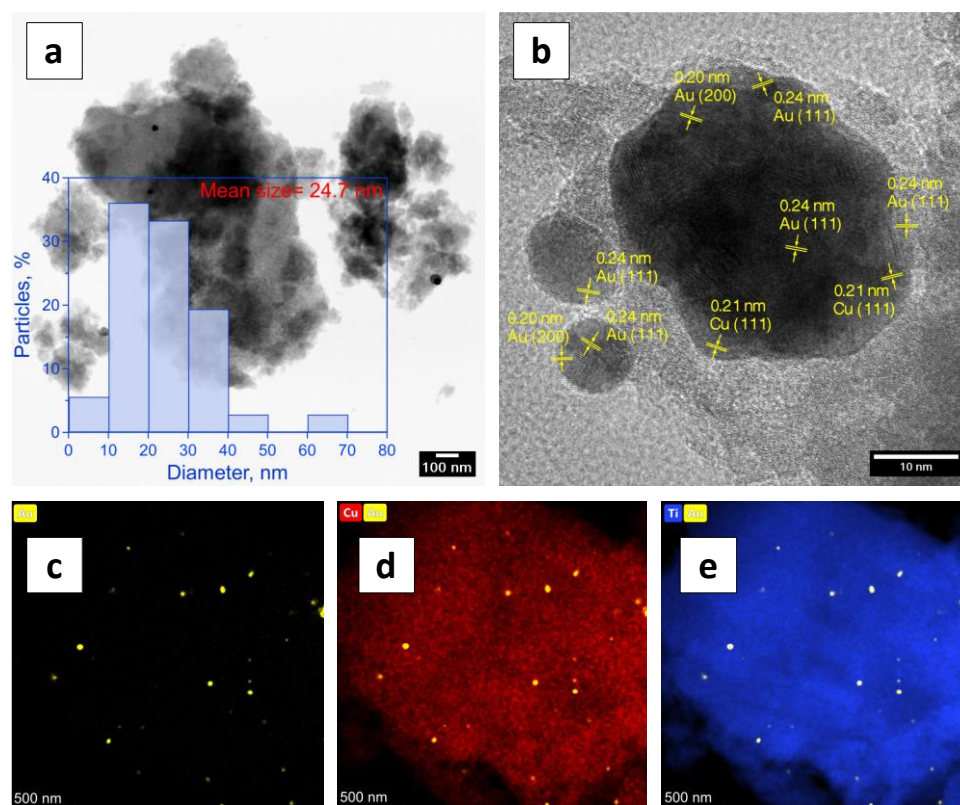


**Figure 4.** TEM images of the obtained CuN–Au/ $\text{TiO}_2$  sample: SE mode with particle size distribution (a), SE mode (b), EDS HAADF analysis of Au (c), EDS HAADF analysis of Cu and Au (d), and EDS HAADF analysis of Ti and Au (e).

In the SEM images of the bimetallic  $\text{TiO}_2$  particles, presented in Figure 6, it was observed that the sample prepared using acetate precursor has a more sponge-like surface, with more cavities in the structure, compared to that obtained with nitrate precursor. CuN–Au/ $\text{TiO}_2$  and FeN–Au/ $\text{TiO}_2$  particles were poorly formed with highly irregular shapes.

The use of sonication improves catalyst deposition in a microreactor aided by enhanced mass deposition, which subsequently improves the overall photocatalytic conversion [43]. We link this activity to the higher availability of the active sites upon the deposition on the wall of the microreactor. On the deposition of these catalysts in the microflow system under the influence of ultrasound, the breakage of the agglomerations into smaller sizes was observed. The big agglomerates (300–500 nm) in the case of CuA–Au/ $\text{TiO}_2$  disturb the flow of the solution inside the microtube, reducing the activity of the catalyst (Figure 1). The small agglomerations (80–250 nm) and good dispersion in the case of CuN–Au/ $\text{TiO}_2$  and FeN–Au/ $\text{TiO}_2$  (Figure 6) can lead to the improved transfer of light and better interaction of the reagent with the surface of the catalyst. The thickness of the deposited catalyst inside

the wall of the microreactor was 5–7  $\mu\text{m}$ , measured with an optical microscope image, hence the better photocatalytic activity in the microflow system for this catalyst.

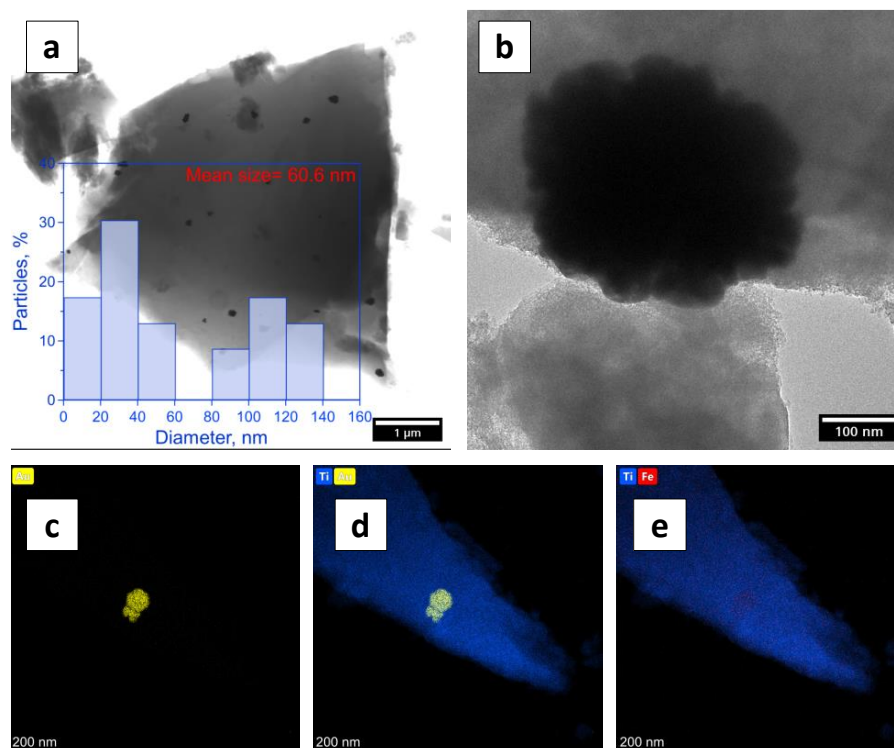


**Figure 5.** TEM images of the obtained FeN-Au/TiO<sub>2</sub> sample: SE mode with particle size distribution (a), SE mode (b), EDS HAADF analysis of Au (c), EDS HAADF analysis of Ti and Au (d), and EDS HAADF analysis of Ti and Fe (e).

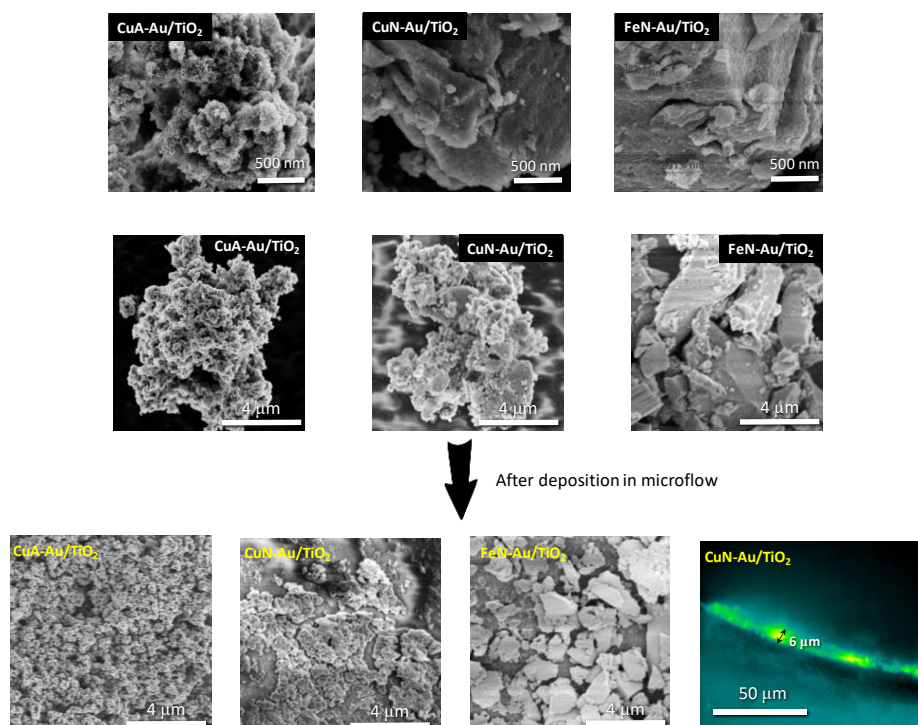


**Figure 6.** SEM and optical microscope image of sol-gel-synthesized bimetallic TiO<sub>2</sub> and after deposition in the PFA microreactor.

The synthesized CuA-Au/TiO<sub>2</sub> catalyst was considered for the oxidation of aromatic alcohols (vanillyl alcohol (VanOH), coniferyl alcohol (ConOH), and cinnamyl alcohol (CinOH)) under UV (375 nm) light, as this catalyst showed better activity under UV light for BnOH oxidation (Figure 1a) in the batch system. Before light experiments, dark adsorption studies were performed to determine the adsorption/reactivity, and the duration to reach adsorption equilibrium was 30 min. Strong adsorption of VanOH (37%) and ConOH (30%) was observed on the surface of bimetallic CuA-Au/TiO<sub>2</sub> in the dark, which might be because of the complex formation between these alcohols with TiO<sub>2</sub>.

After 2 h of the light experiment, BnOH and VanOH conversion were 54% and 95%, respectively (Figure 7b). Comparing the structure of the molecules of BnOH and VanOH (Figure 7a), it can be seen that the main difference between these two alcohols was that VanOH has in its structure an OH group directly connected with the aromatic ring and also a methoxy (OCH<sub>3</sub>) group connected with the next carbon atom of the aromatic ring. In contrast, benzyl alcohol has only an OH group at the end of the alkyl chain, which was not directly connected with the aromatic ring, and no methoxy group. As mentioned above, the OH and OCH<sub>3</sub> groups in the vanillyl alcohol are electron-donating groups which were providing the electrons to the aromatic ring. An excess of electrons causes lower production of aldehyde, which results in low selectivity towards aldehyde in the case of VanOH (25%) in comparison to BnOH (100%) under UV irradiation (Figure 7b) after 2 h of the light experiment. As the selectivity of producing vanillyl aldehyde (VanAld) was strongly reduced, other products of vanillyl alcohol oxidation were achieved (Figures S5–S7). Furthermore, the lower selectivity can also be ascribed to the strong adsorption (37%) of alcohol on the surface of the catalyst, which can lead to partial oxidation, dimerization, or C-O, C-C coupling products.

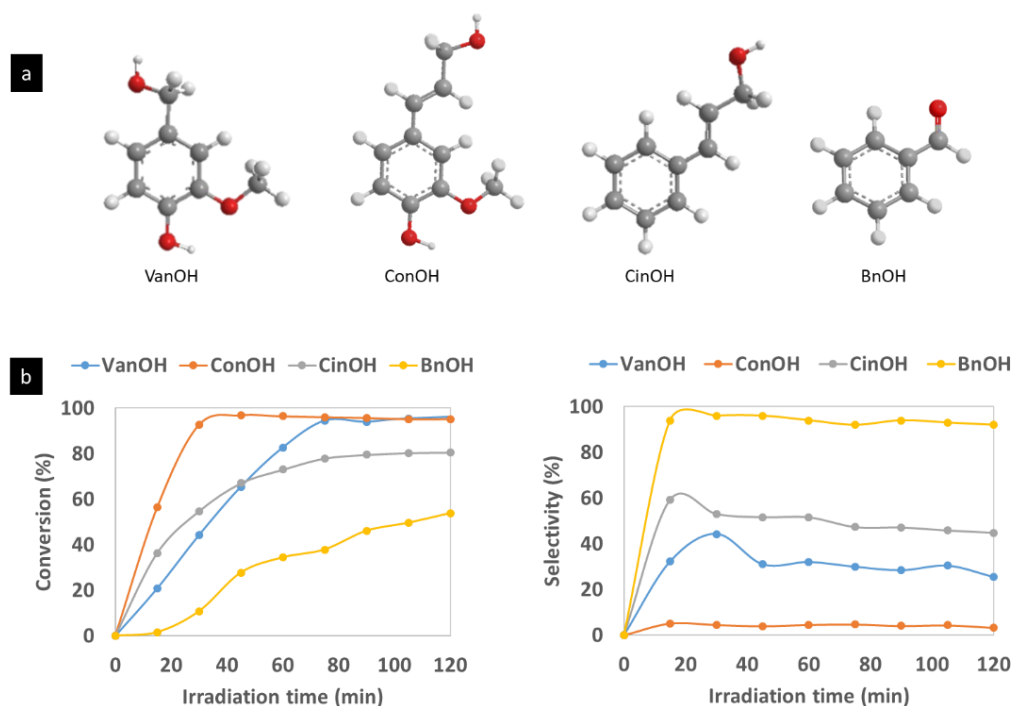


**Figure 7.** Chemical structure of the aromatic alcohols (vanillyl alcohol (VanOH), coniferyl alcohol (ConOH), cinnamyl alcohol (CinOH), and benzyl alcohol (BnOH)) (atomic representation: white—hydrogen, grey—carbon, and red—oxygen) (a) and photocatalytic oxidation with CuA-Au/TiO<sub>2</sub> under UV light with 1 mM of aromatic alcohols in the batch system (b).

Considering ConOH and CinOH alcohols, it can be seen that very high conversions were achieved (95% and 81%, respectively). In the case of ConOH, the selectivity of producing coniferyl aldehyde (ConAld) was very low (5%), with 7% selectivity towards VanAld (Figure 7), with additional products verified by GC-MS analysis (Figures S5–S7). Along with the OCH<sub>3</sub> and OH groups, ConOH has a double bond in its structure, which can potentially also provide

the electrons to the aromatic ring, which causes further reduction, lowering the selectivity. The side products formed are benzaldehyde from CinOH and vanillyl aldehyde from ConOH (partial oxidation) [44], as well as 3-phenoxy benzaldehyde from ConOH (C-O coupling product), which probably was the result of many complex chemical reactions leading to the dimerization of ConOH under the influence of the oxidizing environment (UV radiation) [45]. The conversion of aromatic alcohols and the selectivity to its aldehyde were the main criteria to estimate catalyst performance as the other products were in traces. For CinOH oxidation, the selectivity towards cinnamyl aldehyde (CinAld) was 45%. Furthermore, the catalyst showed highly selective toward BnOH oxidation to BnAld.

After conducting the selective photocatalytic oxidation experiments in UV radiation, the CuA-Au/TiO<sub>2</sub> photocatalyst was selected for experiments also under visible light in the batch system (Figure 8). Under visible irradiation (515 nm), the satisfactory conversion of the alcohols was obtained only for ConOH and VanOH (93% and 52%, respectively), with 8% and 17% selectivity towards their respective aldehydes, with the formation of other side products. Increased photocatalytic conversion in the range of visible radiation for ConOH and VanOH, with a complete lack of activity for BnOH and CinOH, was probably related to the structures of these alcohols. In the case of BnOH and CinOH, there are no groups that could be a direct source of additional electrons for the aromatic ring and no group which can form complexes with TiO<sub>2</sub>. In order to explain this, UV–Vis DRS and FTIR analyses were performed for the aromatic alcohol-adsorbed TiO<sub>2</sub> complexes (Figures 9 and 10) [46,47].

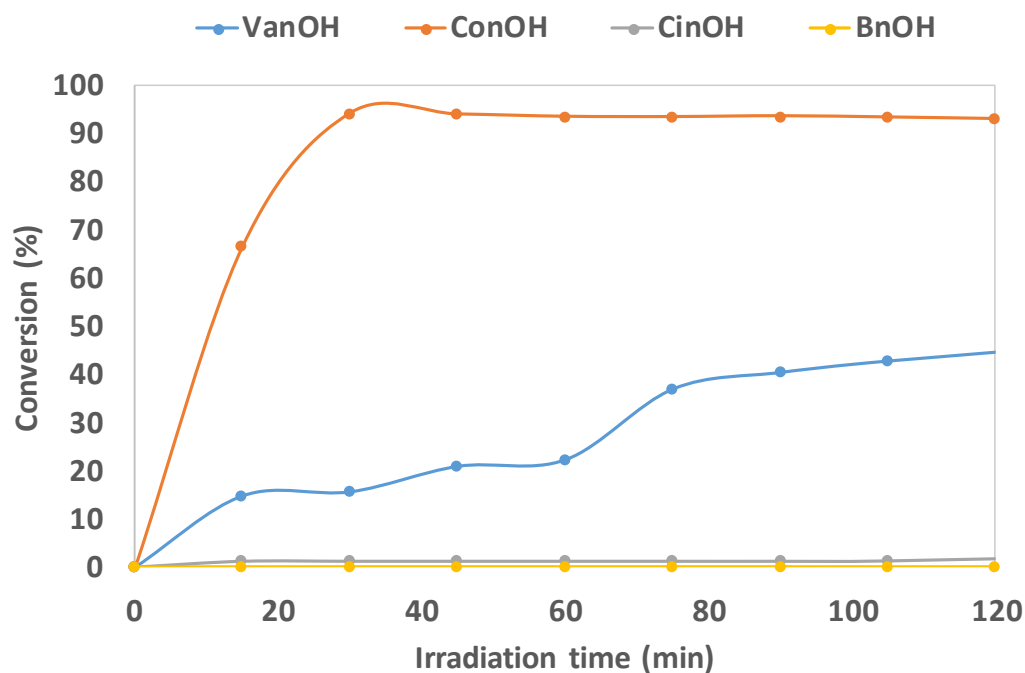


**Figure 8.** Visible light (515 nm) activity of other aromatic alcohols with bimetallic CuA-Au/TiO<sub>2</sub> in the batch system.

As a result of the adsorption of ConOH and VanOH on the TiO<sub>2</sub> catalyst, a significant change in the color of the catalyst from white to yellow can clearly be seen, which resulted in a shift of absorption toward visible radiation (Figure 9). A plausible reason can be complex formation by the ligand-to-metal charge transfer (LMCT) [48,49]. During this process, electrons are transferred from the highest occupied molecular orbital (HOMO) of substrates/adsorbates to the conduction band of TiO<sub>2</sub> upon visible light irradiation. (Scheme 1) [46]. Consequently, the samples forming the colorful complexes exhibited an excellent conversion of aromatic alcohols under visible light (Figure 10).

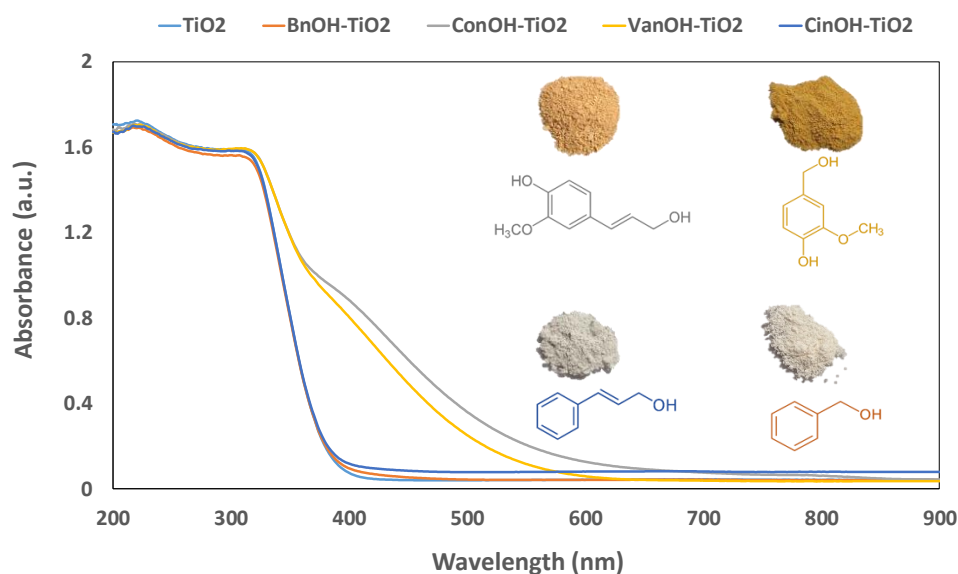


**Figure 9.** UV-visible diffuse reflectance absorption spectra of the  $\text{TiO}_2$  and aromatic alcohol-adsorbed  $\text{TiO}_2$  complex.

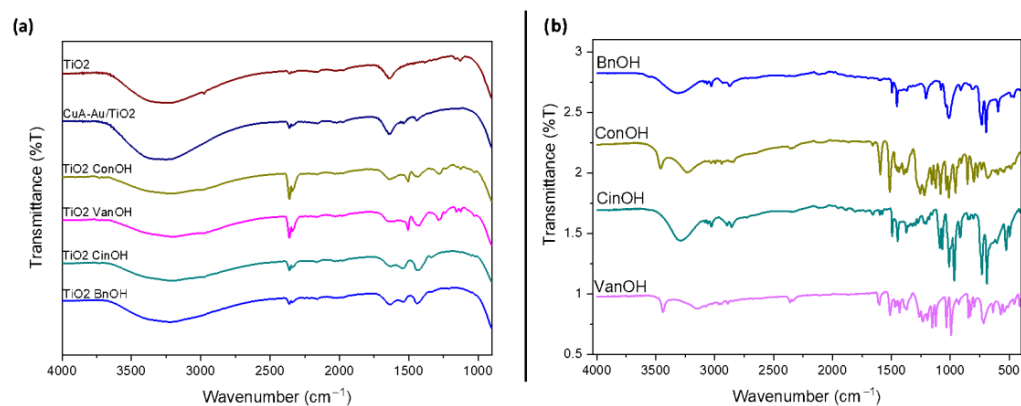
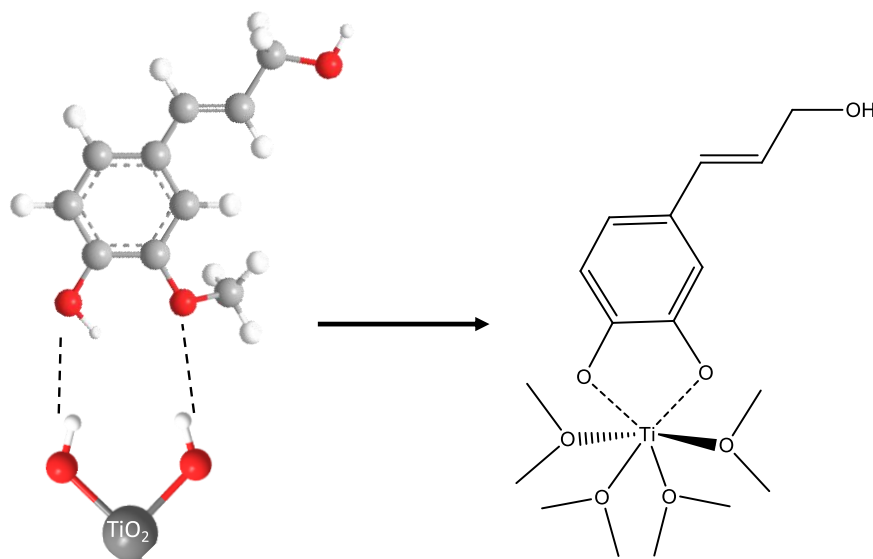


**Figure 10.** Fourier transform infrared spectroscopy (FTIR) of alcohol-adsorbed  $\text{TiO}_2$  (a) and aromatic alcohols (b).



**Scheme 1.** Possible structure of the Ti (IV)-ligand complexes with coniferyl alcohol in the  $\text{TiO}_2$ -based materials with alcohols [48].



The formation of complexes between  $\text{TiO}_2$  and ConOH and  $\text{TiO}_2$  and VanOH was also supported by the FTIR analysis results (Figure 10). Characteristic IR bands for alcohols have also been observed for alcohol-adsorbed titania samples, especially in  $\text{TiO}_2$ -VanOH and  $\text{TiO}_2$ -ConOH (Figure S8). This provided an indication of complex formation via the adsorption of alcohol.

It was mentioned above that the adsorption of alcohols (VanOH and ConOH) on the surface of  $\text{TiO}_2$  occurred by a dissociative mechanism, which means that OH and O-CH<sub>3</sub> groups interacted between titania and aromatic alcohols. In that case, alcohol and  $\text{TiO}_2$  would be linked via the C-O bond. The presence of C-O stretching vibrations was observed at 1000–1200  $\text{cm}^{-1}$  (Figure S8), which can be seen in the case of  $\text{TiO}_2$ -VanOH and  $\text{TiO}_2$ -ConOH; two bands were observed in this region (1118 and 1158  $\text{cm}^{-1}$ ). The bands in the range of 1000–1050  $\text{cm}^{-1}$  were assigned to the presence of =C-H bonds derived from the aromatic ring (Figure 10 and Figure S8). The bands around 1460  $\text{cm}^{-1}$  originated from CH<sub>2</sub> vibrations and around 1640  $\text{cm}^{-1}$  from C=C [46]. Similar spectra were observed for bimetallic CuA-Au/ $\text{TiO}_2$  as well, confirming the formation of the complex with the above aromatic alcohol (Figure S8), which confirms that the metals did not take part in this complex formation. It is worth adding that the oxidation of VanOH and ConOH was successful under visible irradiation due to the formation of the abovementioned complex with  $\text{TiO}_2$ . To further confirm the role of the OH group in LMCT complex formation, the synthesized  $\text{TiO}_2$  was calcined at a high temperature (600 °C) to remove surface OH through condensation (Figure S9). Interestingly, this catalyst was found inactive, suggesting the OH groups are crucial for LMCT complex formation and the visible light activity of the catalyst.

The experiment with the CuN-Au/ $\text{TiO}_2$ -coated microreactor for other aromatic alcohols oxidation was performed under visible light irradiation as (1) CuN-Au/ $\text{TiO}_2$  in the microflow system showed better activity (Figure 1) and (2) the other aromatic alcohols showed better conversion under visible light (Figure 8). Like the batch experiment, BnOH and CinOH did not show any activity in the microflow system under visible light, whereas ConOH and VanOH did. The specific conversion rate of ConOH was higher (198  $\mu\text{mol}/\text{m}^2 \text{ h}$ ) compared to VanOH (46  $\mu\text{mol}/\text{m}^2 \text{ h}$ ), with 11 % and 10 % selectivity towards their respective aldehydes (Figure 11). Other side products, such as batch experiments, were also observed.

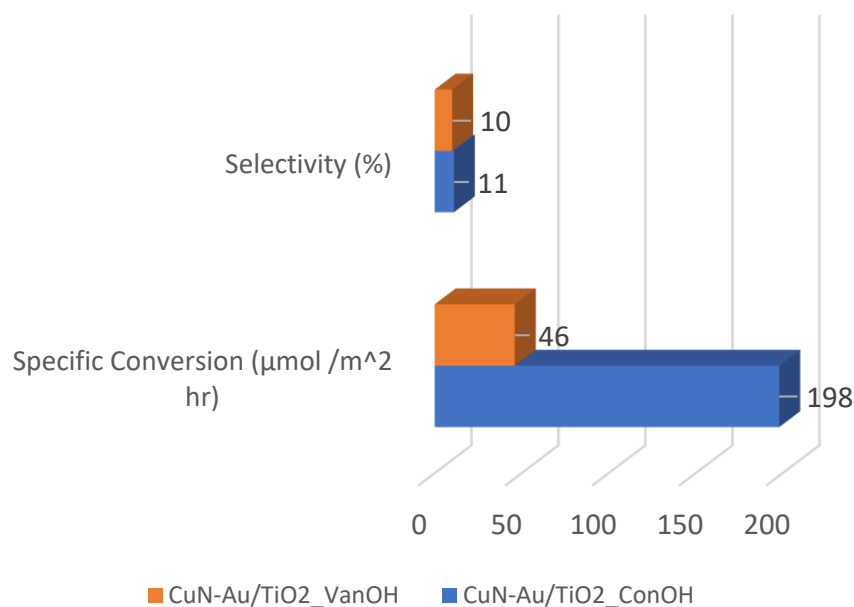


**Figure 11.** Photocatalytic activity of CuN-Au/ $\text{TiO}_2$  under visible light with ConOH and VanOH in the microflow system.

After deposition, the catalyst's surface was more selective towards ConAld for ConOH oxidation than in the batch system (8%). The elevated selectivity in the batch system compared to the microflow system might be because of the higher availability of the catalyst's active sites upon deposition. Additional side products (as discussed above) were confirmed from GC/MS; however, because of the trace amount of some products, it was not easy to calculate the selectivity towards them (Figure S7). The sol-gel-synthesized CuN-Au/TiO<sub>2</sub> catalyst showed promising activity in the batch system as well as in the microflow system for ConOH oxidation. Furthermore, from the catalyst-deposited microtubes, no leaching was confirmed with the ED-XRF analysis after 60 min of the experiment (Figure S10). The recycling test with the best performing catalyst (CuA-Au/TiO<sub>2</sub>) and the one which showed lower activity (TiO<sub>2</sub>) in the batch system were performed by washing the catalyst with acetonitrile and water, and the activity of the catalyst was retained (Figure S11).

### 3. Materials and Methods

#### 3.1. Materials

Titanium (IV) tetraisopropoxide (TTIP, 98%, ACROS ORGANICS, Geel, Belgium), benzyl alcohol (BnOH, 99.5%, CHEMPUR, Piekary Śląskie, Poland), coniferyl alcohol (ConOH, 98%, ABCR, Karlsruhe, Germany), cinnamyl alcohol (CinOH, 98%, ACROS ORGANICS, NJ, USA), vanillyl alcohol (VanOH, 98%, ABCR, Karlsruhe, Germany), ethanol (EtOH, 99.8%, POCH, Gliwice, Poland), acetonitrile (ACN, HPLC grade, POCH, Gliwice, Poland), and propan-2-ol (99.7%, CHEMPUR, Piekary Śląskie, Poland) were used as received. Copper (II) acetate monohydrate (Cu(CH<sub>3</sub>COO)<sub>2</sub>·H<sub>2</sub>O, 98%, ABCR, Karlsruhe, Germany), iron (III) nitrate nonahydrate (Fe(NO<sub>3</sub>)<sub>3</sub>·9H<sub>2</sub>O, 98%, ABCR, Karlsruhe, Germany), copper (II) nitrate trihydrate (Cu(NO<sub>3</sub>)<sub>2</sub>·3H<sub>2</sub>O, pure, CHEMPUR, Piekary Śląskie, Poland), and tetrachloroauric (III) acid trihydrate (HAuCl<sub>4</sub>·3H<sub>2</sub>O, >99.5%, ROTH, Karlsruhe, Germany) were used as received as metal precursors.

#### 3.2. Catalyst Synthesis

The bimetallic Cu-Au/TiO<sub>2</sub> and Fe-Au/TiO<sub>2</sub> nanoparticles were prepared based on the previously established sol-gel method [50]. The required amount of metal precursors (ratio of atomic percent of Au to Cu or Fe was adjusted to 1:4) were added to 15 mL of isopropanol and stirred (magnetic stirrer) at 600 rpm. Under the rotational conditions, 4 mL of TTIP was added dropwise to the mixture. Subsequently, milli-Q water (5 mL) was added to the solution at a rate of 0.167 mL/min using a syringe infusion pump (Programmable Double Syringe Pump (WPI), NE-4000). After 6 h of aging with mixing at 1000 rpm, the resulting solid samples were obtained by centrifugation, washing with deionized water (2 times) and ethanol (1 time), and drying at 80 °C in an oven for 24 h.

#### 3.3. Microreactor Preparation

A visible light transparent perfluoroalkoxy alkane (PFA, 0.8 mm ID, BOLA: S 1811-02) tube was used as a microreactor [50,51]. A 0.5 g/L concentration (previously optimized [50]) of nanoparticles was dispersed in Milli-Q water by ultrasonication for 15 min using an ultrasonic bath (Elma Elmasonic P, 37 kHz, 70% power). Twenty mL of the homogeneous nanoparticle suspension was passed through the cleaned PFA microtube under the influence of ultrasound using a syringe pump. The spiralized fragment (Figure 12b) was the effective length subjected to the ultrasound treatment (Elma Elmasonic P, 37 kHz, 100% power) for 75 min (the flow rate of the suspension was 0.26 mL/min). The tube was placed in the oven for 24 h at 80 °C, and later cleaned by passing Milli-Q water and ethanol, dried with airflow, and then placed in the oven for 1 h at 80 °C. After this procedure, the catalyst-coated PFA tube was used for photocatalytic experiments (Figure 12b).



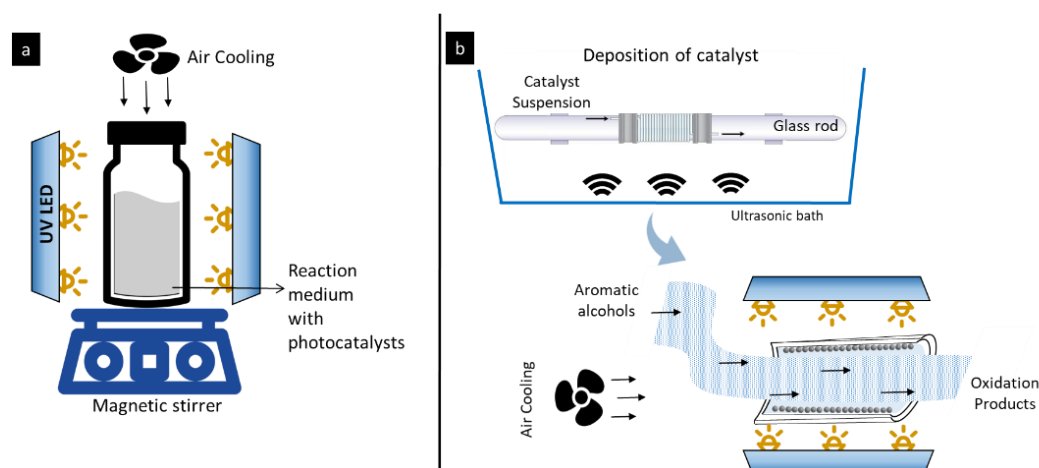


**Figure 12.** Experimental set up of the batch system (a) and microflow (b) photocatalytic system along with preparation of the wall-coated microreactor.

### 3.4. Catalytic Performance Test

The photocatalytic oxidation of the aromatic alcohols over the synthesized catalysts was carried out in batch (Figure 12a) and microflow reactors (Figure 12b, Figure S1). UV-LED and Vis-LED systems were used as light sources (375 nm and 515 nm wavelength, respectively). The flow rate was set at 0.167 mL/min (after optimization) to reproduce enough space–time according to the reactor’s dimensions, and the whole experiment was carried out for 60 min [50]. Experiments in the batch photocatalytic reactor were performed using 20 mL of the reaction solution and 0.5 g/L of catalyst concentration for 60 min under UV light. Alcohol conversion, the specific conversion rate, and selectivity to each product were calculated according to the following equations:

$$\text{Conversion (\%)} = ((\text{Converted moles of aromatic alcohols})/(\text{Initial moles of aromatic alcohols})) \times 100\%$$

$$\text{Selectivity (\%)} = ((\text{Produced moles of aromatic aldehydes})/(\text{Converted moles of aromatic alcohols})) \times 100\%$$

$$\text{Specific Conversion Rate } (\mu\text{mol}/\text{m}^2 \cdot \text{h}) = (C_{\text{OH}_0} - C_{\text{OH}_t}) / (S_C \times \text{time})$$

where  $C_{\text{OH}_0}$  = initial concentration of aromatic alcohols,  $C_{\text{OH}_t}$  = concentration of aromatic alcohols after time,  $t$ , and  $S_C$  is the specific surface area (surface area multiplied by the catalyst concentration) of the catalyst taking part in the photocatalytic conversion.

### 3.5. Characterization

The synthesized samples were characterized using diffuse reflectance spectroscopy (DRS, Shimadzu UV-2600i), and the bandgap was calculated from the Tauc plot. Powder X-ray diffraction (XRD) measurements were performed employing the Bragg–Brentano configuration. This type of arrangement was provided using a PANalytical Empyrean diffraction platform, powered at 40 kV  $\times$  40 mA and equipped with a vertical goniometer, with theta–theta geometry using Ni-filtered  $\text{CuK}\alpha$  ( $\lambda = 1.5418 \text{ \AA}$ ) radiation. The elemental maps of the samples were also obtained by FEI Nova Nanolab 200 scanning electron microscopy (SEM). The textural properties of  $\text{TiO}_2$  were determined by  $\text{N}_2$  physisorption using a micromeritics automated system (Micromeritics Instrument Corporation, Norcross, GA, USA) with the Brunauer–Emmet–Teller (BET) and the Barret–Joyner–Halenda (BJH) methods. Before adsorption, the samples were degassed under vacuum (0.1 Pa) for 12 h at 80 °C. The presence of functional groups on the surface of the catalyst and substrate was determined using a Bruker Tensor II Fourier transform (FT) IR spectrometer.

The samples collected from the outlet of the catalyst-deposited PFA capillary were examined using the energy dispersive X-ray fluorescence (EDXRF) spectrometer (Mini-Pal 4, PANalytical Co., Malvern, UK) with a Rh tube and silicon drift detector to check the titania

residual and other metals. The spectra were collected in an air atmosphere, without a filter, at a tube voltage of 30 kV. To identify and quantify the alcohols, aldehydes, and acids present, the collected samples were analyzed using high-pressure liquid chromatography (HPLC, Waters) with mass spectrometry using a mobile phase containing a mixture of organic solvents and a 0.05% H<sub>3</sub>PO<sub>4</sub> (5M) aqueous solution (CH<sub>3</sub>CN:CH<sub>3</sub>OH: H<sub>2</sub>O = 20:2.5:77.5 *v/v*).

#### 4. Conclusions

In this study, we have made an attempt to promote green chemistry by improving the utilization of lignin—an important waste from the paper and pulp industry, which otherwise would have been disposed of, thus contaminating the environment. To this end, we propose to improve the conversion of the model alcohols by targeting and improving the catalytic activity of TiO<sub>2</sub> doped with bimetals such as Cu-Au, and Fe-Au. In the batch system, as high as 100% benzaldehyde (BnAld) selectivity was obtained for benzyl alcohol (BnOH) conversion of ~60% using CuA-Au/TiO<sub>2</sub> photocatalyst. The high conversion could be explained by the high average pore size (6.8 nm) and better crystallinity of the CuA-Au/TiO<sub>2</sub> catalyst, which were confirmed in subsequent XRD and N<sub>2</sub> physisorption analysis.

Our studies further revealed that the LMCT complex formation of TiO<sub>2</sub> with the methoxy (OCH<sub>3</sub>) and OH groups (directly connected with the aromatic ring) exists in the structure of coniferyl alcohol (ConOH) and vanillyl alcohol (VanOH), which was crucial to activate the catalyst under visible light. This hypothesis has been further corroborated by UV-Vis and FTIR studies. Additionally, the whole process was green/environment-friendly as the catalyst synthesis process did not include any high-temperature calcination steps, unlike commercial P25 TiO<sub>2</sub>, and the photocatalytic selective oxidation route was additive-free (no additional molecular oxygen). We also developed a catalyst-decorated microreactor using ultrasonic irradiation, which helped to increase the turbulence of the liquid phase and to improve the active surface area of our catalyst via the de-agglomeration and fragmentation of the nanoparticles.

In a broader context, we believe that the presented work demonstrates the potential of an ultrasonic-assisted bimetallic TiO<sub>2</sub> wall-coated microreactor for selective oxidation of lignin-based model compounds using solar energy and this will serve as a conceptual blueprint for further developments.

**Supplementary Materials:** The following supporting information can be downloaded at: <https://www.mdpi.com/article/10.3390/molecules27248731/s1>, Figure S1: Experimental set up for photocatalysis in microflow system.; Figure S2: Bandgap calculation of sol-gel synthesized TiO<sub>2</sub> and bimetallic TiO<sub>2</sub> (CuA-Au/TiO<sub>2</sub>, CuN-Au/TiO<sub>2</sub>, FeN-Au/TiO<sub>2</sub>) catalysts; Figure S3: UV-vis diffuse reflectance spectra of synthesized bimetallic TiO<sub>2</sub>; Figure S4: Surface analysis of CuA/Au-TiO<sub>2</sub> by X-ray photoelectron spectroscopy (XPS); Figure S5: Oxidation products from VanOH analyzed with GC-MS and HPLC-MS; Figure S6: Oxidation products from ConOH analyzed with GC-MS; Figure S7: Oxidation products from CinOH analyzed with GC-MS; Figure S8: FT-IR spectra of aromatic alcohols (BnOH, CinOH, VanOH and ConOH) adsorbed TiO<sub>2</sub> and VnOH adsorbed bimetallic CuA-Au-TiO<sub>2</sub>; Figure S9: FT-IR spectra of sol-gel synthesized TiO<sub>2</sub> and calcined (600 °C) TiO<sub>2</sub> confirming removal of OH group; Figure S10: XRF image of CuN-Au/TiO<sub>2</sub>; Figure S11: Photocatalytic experiment with CuA-Au/TiO<sub>2</sub> (left) and sol-gel synthesized TiO<sub>2</sub> (right) (Run 1) and after washing the catalyst with ACN and H<sub>2</sub>O (Run2) under UV irradiation (60 min) in batch system with ConOH.

**Author Contributions:** S.R.P.: writing—original draft preparation, data analysis, catalyst characterization, conceptualization, investigation, and validation. M.P.-G.: writing—review and editing and data curation. D.L.: writing—review and editing and visualization. D.L.: investigation and data processing. J.C.C.: writing—review and editing, resources, conceptualization, supervision, and project administration. All authors have read and agreed to the published version of the manuscript.

**Funding:** This work is supported by the National Science Centre in Poland within Sonata Bis 5 Project No. 2015/18/E/ST5/00306.

**Institutional Review Board Statement:** Not applicable.

**Informed Consent Statement:** Not applicable.

**Data Availability Statement:** Not applicable.

**Acknowledgments:** Swaraj gratefully acknowledges the help from Dorota Staszek and Klara Nestorowicz for the analysis and interpretation of GC/MS. Moreover, the authors acknowledge K. Sobczak (CNBCh University of Warsaw) for the TEM measurement.

**Conflicts of Interest:** The authors declare no conflict of interest.

**Sample Availability:** Samples of the synthesized compounds TiO<sub>2</sub> and bimetallic TiO<sub>2</sub> are available from the authors.

## References

1. Banerjee, S.; Dionysiou, D.D.; Pillai, S.C. Self-cleaning applications of TiO<sub>2</sub> by photo-induced hydrophilicity and photocatalysis. *Appl. Catal. B Environ.* **2015**, *176–177*, 396–428. [[CrossRef](#)]
2. Do, H.H.; Nguyen, D.L.T.; Nguyen, X.C.; Le, T.H.; Nguyen, T.P.; Trinh, Q.T.; Ahn, S.H.; Vo, D.V.N.; Kim, S.Y.; Van Le, Q. Recent progress in TiO<sub>2</sub>-based photocatalysts for hydrogen evolution reaction: A review. *Arab. J. Chem.* **2020**, *13*, 3653–3671. [[CrossRef](#)]
3. Carabin, A.; Drogué, P.; Robert, D. Journal of the Taiwan Institute of Chemical Engineers Photo-degradation of carbamazepine using TiO<sub>2</sub> suspended photocatalysts. *J. Taiwan Inst. Chem. Eng.* **2015**, *54*, 109–117. [[CrossRef](#)]
4. Kashale, A.A.; Rasal, A.S.; Kamble, G.P.; Ingole, V.H.; Dwivedi, P.K.; Rajoba, S.J.; Jadhav, L.D.; Ling, Y.; Chang, J.; Ghule, A.V. Biosynthesized Co-doped TiO<sub>2</sub> nanoparticles based anode for lithium-ion battery application and investigating the influence of dopant concentrations on its performance. *Compos. Part B* **2019**, *167*, 44–50. [[CrossRef](#)]
5. Chen, J.; Qiu, F.; Xu, W.; Cao, S.; Zhu, H. Recent progress in enhancing photocatalytic efficiency of TiO<sub>2</sub>-based materials. *Appl. Catal. A Gen.* **2015**, *495*, 131–140. [[CrossRef](#)]
6. El Mragui, A.; Daou, I.; Zegaoui, O. Influence of the preparation method and ZnO/(ZnO + TiO<sub>2</sub>) weight ratio on the physico-chemical and photocatalytic properties of ZnO-TiO<sub>2</sub> nanomaterials. *Catal. Today* **2019**, *321*, 41–51. [[CrossRef](#)]
7. Gupta, A.K.; Pal, A.; Sahoo, C. Photocatalytic degradation of a mixture of Crystal Violet (Basic Violet 3) and Methyl Red dye in aqueous suspensions using Ag C doped TiO<sub>2</sub>. *Dye Pigment.* **2006**, *69*, 224–232. [[CrossRef](#)]
8. Justyna, Ł.; Paszkiewicz-gawron, M. Visible-Light Photocatalytic Activity of Ionic Liquid TiO<sub>2</sub> Spheres: Effect of the Ionic Liquid's Anion Structure. *ChemCatChem* **2017**, *9*, 4377–4388.
9. Khan, A.; Goepel, M.; Kubas, A.; Łomot, D.; Lisowski, W. Selective Oxidation of 5-Hydroxymethylfurfural to 2,5-Diformylfuran by Visible Light-Driven Photocatalysis over In Situ Substrate-Sensitized Titania. *ChemSusChem* **2021**, *14*, 1351–1362. [[CrossRef](#)]
10. Dozzi, M.V.; Saccomanni, A.; Altomare, M.; Selli, E. Photocatalytic activity of NH<sub>4</sub>F-doped TiO<sub>2</sub> modified by noble metal nanoparticle deposition. *Photochem. Photobiol. Sci.* **2013**, *12*, 595–601. [[CrossRef](#)]
11. Lv, T.; Zhao, J.; Chen, M.; Shen, K.; Zhang, D.; Zhang, J.; Zhang, G.; Liu, Q. Boosted visible-light photodegradation of methylene blue by V and Co co-doped TiO<sub>2</sub>. *Materials* **2018**, *11*, 1946. [[CrossRef](#)] [[PubMed](#)]
12. Pradhan, S.R.; Lisovytskiy, D.; Colmenares, J.C. Flow photomicroreactor coated with monometal containing TiO<sub>2</sub> using sonication: A versatile tool for visible light oxidation. *Catal. Commun.* **2022**, *162*, 106375. [[CrossRef](#)]
13. El Mragui, A.; Logvina, Y.; Luís Pinto da Silva, L.; Zegaoui, O.; da Silva, J.C.G.E. Synthesis of Fe- and Co-doped TiO<sub>2</sub> with improved photocatalytic activity under visible irradiation toward carbamazepine degradation. *Materials* **2019**, *12*, 3874. [[CrossRef](#)] [[PubMed](#)]
14. El Mragui, A.; Zegaoui, O.; Daou, I.; Esteves da Silva, J.C.G. Preparation, characterization, and photocatalytic activity under UV and visible light of Co, Mn, and Ni mono-doped and (P,Mo) and (P,W) co-doped TiO<sub>2</sub> nanoparticles: A comparative study. *Environ. Sci. Pollut. Res.* **2021**, *28*, 25130–25145. [[CrossRef](#)] [[PubMed](#)]
15. Gołębiewska, A.; Lisowski, W.; Jarek, M.; Nowaczyk, G.; Michalska, M.; Jurga, S.; Zaleska-Medynska, A. The effect of metals content on the photocatalytic activity of TiO<sub>2</sub> modified by Pt/Au bimetallic nanoparticles prepared by sol-gel method. *Mol. Catal.* **2017**, *442*, 154–163. [[CrossRef](#)]
16. Liu, H.; Liu, Y.; Li, Y.; Tang, Z.; Jiang, H. Metal–Organic Framework Supported Gold Nanoparticles as a Highly Active Heterogeneous Catalyst for Aerobic Oxidation of Alcohols. *J. Phys. Chem. C* **2010**, *114*, 13362–13369. [[CrossRef](#)]
17. Mullen, G.M.; Zhang, L.; Evans, E.J.; Yan, T.; Henkelman, G.; Mullins, C.B. Oxygen and Hydroxyl Species Induce Multiple Reaction Pathways for the Partial Oxidation of Allyl Alcohol on Gold. *J. Am. Chem. Soc.* **2014**, *136*, 6489–6498. [[CrossRef](#)]
18. Jiang, T.; Jia, C.; Zhang, L.; He, S.; Sang, Y.; Li, H.; Li, Y.; Xu, X.; Liu, H. Gold and gold–palladium alloy nanoparticles on heterostructured TiO<sub>2</sub> nanobelts as plasmonic photocatalysts for benzyl alcohol oxidation. *Nanoscale* **2015**, *7*, 209–217. [[CrossRef](#)]
19. Sankar, M.; Dimitratos, N.; Miedziak, P.J.; Wells, P.P.; Kiely, J.; Hutchings, G.J. Designing bimetallic catalysts for a green and sustainable future. *Chem. Soc. Rev.* **2012**, *41*, 8099–8139. [[CrossRef](#)]

20. Kavitha, R.; Kumar, S.G. Review on bimetallic-deposited TiO<sub>2</sub>: Preparation methods, charge carrier transfer pathways and photocatalytic applications. *Chem. Pap.* **2020**, *74*, 717–756. [[CrossRef](#)]
21. Durndell, L.J.; Parlett, C.M.A.; Hondow, N.S.; Wilsona, K.; Lee, A.F. Tunable Pt nanocatalysts for the aerobic selox of cinnamyl alcohol. *Nanoscale* **2013**, *123*, 5412–5419. [[CrossRef](#)] [[PubMed](#)]
22. Pradhan, S.R.; Colmenares-Quintero, R.F.; Quintero, J.C.C. Designing microflowreactors for photocatalysis using sonochemistry: A systematic review article. *Molecules* **2019**, *24*, 3315. [[CrossRef](#)] [[PubMed](#)]
23. Wan, L.; Jiang, M.; Cheng, D.; Chen, F. Continuous flow technology—a tool for safer oxidation chemistry. *React. Chem. Eng.* **2022**, *7*, 490–550. [[CrossRef](#)]
24. Leofanti, G.; Padovan, M.; Tozzola, G.; Venturelli, B. Surface area and pore texture of catalysts. *Catal. Today* **1998**, *41*, 207–219. [[CrossRef](#)]
25. Sing, K.S.W.; Williams, R.T. Physisorption hysteresis loops and the characterization of nanoporous materials. *Adsorpt. Sci. Technol.* **2004**, *22*, 773–782. [[CrossRef](#)]
26. Yu, X.; Yu, J.; Cheng, B.; Jaroniec, M. Synthesis of Hierarchical Flower-like AlOOH and TiO<sub>2</sub>/AlOOH Superstructures and their Enhanced Photocatalytic Properties. *J. Phys. Chem. C* **2009**, *113*, 17527–17535. [[CrossRef](#)]
27. Olowoyo, J.O.; Kumar, M.; Dash, T.; Saran, S.; Bhandari, S.; Kumar, U. Self-organized copper impregnation and doping in TiO<sub>2</sub> with enhanced photocatalytic conversion of H<sub>2</sub>O and CO<sub>2</sub> to fuel. *Int. J. Hydrogen Energy* **2018**, *43*, 19468–19480. [[CrossRef](#)]
28. Kubiak, A.; Bielan, Z.; Kubacka, M.; Gabała, E.; Zgoła-Grześkowiak, A.; Janczarek, M.; Zalas, M.; Zielińska-Jurek, A.; Siwińska-Ciesielczyk, K.; Jesionowski, T. Microwave-assisted synthesis of a TiO<sub>2</sub>-CuO heterojunction with enhanced photocatalytic activity against tetracycline. *Appl. Surf. Sci.* **2020**, *520*, 146344. [[CrossRef](#)]
29. Chen, Y.; Li, W.; Wang, J.; Gan, Y.; Liu, L.; Ju, M. Environmental Microwave-assisted ionic liquid synthesis of Ti<sup>3+</sup> self-doped TiO<sub>2</sub> hollow nanocrystals with enhanced visible-light photoactivity. *Appl. Catal. B Environ.* **2016**, *191*, 94–105. [[CrossRef](#)]
30. Liu, Z.; Wu, J.; Wang, J.; Wang, R.; Liu, G.; Qi, Y.; Xu, W.; Luo, G.; Xu, M. The effect of different morphology of fluoride-mediated TiO<sub>2</sub> based on Ostwald ripening on photocatalytic activity. *Colloids Surf. A* **2021**, *610*, 125702. [[CrossRef](#)]
31. Nogawa, T.; Isobe, T.; Matsushita, S.; Nakajima, A. Preparation and visible-light photocatalytic activity of Au- and Cu-modified TiO<sub>2</sub> powders. *Mater. Lett.* **2012**, *82*, 174–177. [[CrossRef](#)]
32. Monga, A.; Bathla, A.; Pal, B. A Cu-Au bimetallic co-catalysis for the improved photocatalytic activity of TiO<sub>2</sub> under visible light radiation. *Sol. Energy* **2017**, *155*, 1403–1410. [[CrossRef](#)]
33. Li, N.; Geng, D.; Zhou, J. Ag and Cu Nanoparticles Synergistically Enhance Photocatalytic—CO<sub>2</sub> Reduction Activity of B Phase—TiO<sub>2</sub>. *Catal. Lett.* **2022**, *152*, 124–138. [[CrossRef](#)]
34. Zhang, X.; Chen, Y.L.; Liu, R.; Tsai, D.P. Plasmonic photocatalysis. *Rep. Prog. Phys.* **2013**, *76*, 46401. [[CrossRef](#)] [[PubMed](#)]
35. Go, A.; Zieli, A.; Zaleska, A. Characterization of TiO<sub>2</sub> Modified with Bimetallic Ag/Au Nanoparticles Obtained in Microemulsion System Characterization of TiO<sub>2</sub> Modified with Bimetallic Ag/Au Nanoparticles Obtained in Microemulsion System. *J. Adv. Oxid. Technol.* **2012**, *15*, 71.
36. Liu, S.; Xu, Y. Photo-induced transformation process at gold clusters- semiconductor interface: Implications for the complexity of gold clusters-based photocatalysis. *Sci. Rep.* **2016**, *6*, 1–13. [[CrossRef](#)]
37. Zhuang, Y.; Liu, L.; Wu, X.; Tian, Y.; Zhou, X.; Xu, S.; Xie, Z. Size and Shape Effect of Gold Nanoparticles in “ Far-Field ” Surface Plasmon Resonance. *Part. Part. Syst. Charact.* **2019**, *1800077*, 1–8. [[CrossRef](#)]
38. Goł, A.; Malankowska, A.; Jarek, M.; Lisowski, W.; Nowaczyk, G.; Jurga, S.; Zaleska-medynska, A. Environmental The effect of gold shape and size on the properties and visible. *Appl. Catal. B Environ.* **2016**, *196*, 27–40.
39. Duan, Z.; Huang, Y.; Zhang, D.; Chen, S. Electrospinning Fabricating Au/TiO<sub>2</sub> Network-like Nanofibers as Visible Light Activated Photocatalyst. *Sci. Rep.* **2019**, *6*, 1–8. [[CrossRef](#)]
40. Anwar, D.I.; Mulyadi, D. Synthesis of Fe-TiO<sub>2</sub> Composite as a Photocatalyst for Degradation of Methylene Blue. *Procedia Chem.* **2015**, *17*, 49–54. [[CrossRef](#)]
41. Wang, Z.; De Soto, L.S.; Me, C.; Casale, S.; Delannoy, L. A selective and stable Fe/TiO<sub>2</sub> catalyst for selective hydrogenation of butadiene in alkene-rich stream. *ChemComm* **2021**, *57*, 7031–7034. [[CrossRef](#)]
42. Kruanetr, S.; Wanchanthuek, R. Studies on preparation and characterization of Fe/TiO<sub>2</sub> catalyst in photocatalysis applications Studies on preparation and characterization of Fe/TiO<sub>2</sub> catalyst in photocatalysis applications. *Mater. Res. Express* **2017**, *4*, 76507. [[CrossRef](#)]
43. Bulasara, V.K.; Uppaluri, R.; Purkait, M.K. Effect of Ultrasound on the Performance of Nickel Hydrazine Electroless Plating Baths Effect of Ultrasound on the Performance of Nickel Hydrazine Electroless Plating Baths. *Mater. Manuf. Process.* **2012**, *6914*, 201–206. [[CrossRef](#)]
44. Wu, G.; Brett, G.L.; Cao, E.; Constantinou, A.; Ellis, P.; Kuhn, S.; Hutchings, G.J.; Bethell, D.; Gavrilidis, A. Catalysis Science & Technology Oxidation of cinnamyl alcohol using bimetallic continuous flow packed bed microreactor. *Catal. Sci. Technol.* **2016**, *6*, 4749–4758.
45. Taboada-puig, R.; Moreira, T.; Lema, J.M.; Fagerstedt, K.; Heikkinen, H. Polymerization of Coniferyl Alcohol by Mn<sup>3+</sup>-mediated (Enzymatic) Oxidation: Effects of H<sub>2</sub>O<sub>2</sub> Concentration, Aqueous Organic Solvents, and pH. *Biotechnol. Prog.* **2018**, *34*, 81–90. [[CrossRef](#)] [[PubMed](#)]
46. Zhang, G.; Choi, W. A low-cost sensitizer based on a phenolic resin for charge-transfer type photocatalysts working under visible light w. *ChemComm* **2012**, *48*, 10621–10623. [[CrossRef](#)] [[PubMed](#)]

47. Kim, S.; Choi, W. Visible-Light-Induced Photocatalytic Degradation of 4-Chlorophenol and Phenolic Compounds in Aqueous Suspension of Pure Titania: Demonstrating the Existence of a Surface-Complex-Mediated Path. *J. Phys. Chem. B* **2005**, *109*, 5143–5149. [[CrossRef](#)] [[PubMed](#)]
48. Imparato, C.; D’Errico, G.; Macyk, W.; Kobielski, M.; Vitiello, G.; Antonio, A. Interfacial Charge Transfer Complexes in TiO<sub>2</sub>-Enediol Hybrids Synthesized by Sol-Gel. *Langmuir* **2022**, *38*, 1821–1832. [[CrossRef](#)]
49. Zhang, G.; Kim, G.; Choi, W. Visible light driven photocatalysis mediated via ligand-to-metal charge transfer (LMCT): An alternative approach to solar activation of titania. *Energy Environ. Sci.* **2014**, *7*, 954. [[CrossRef](#)]
50. Pradhan, S.R.; Nair, V.; Giannakoudakis, D.A.; Lisovytskiy, D.; Colmenares, J.C. Design and development of TiO<sub>2</sub> coated microflow reactor for photocatalytic partial oxidation of benzyl alcohol. *Mol. Catal.* **2020**, *486*, 110884. [[CrossRef](#)]
51. Borra, S.; Chandrasekhar, D.; Adhikary, S.; Rasala, S.; Gokulnath, S.; Maurya, R.A. Visible-Light Driven Photocascade Catalysis: Union of N,N-Dimethylanilines and  $\alpha$ -Azidochalcones in Flow Microreactors. *J. Org. Chem.* **2017**, *82*, 2249–2256. [[CrossRef](#)] [[PubMed](#)]

# Bimetallic TiO<sub>2</sub> Nanoparticles for Lignin-Based Model Compounds Valorization by Integrating Photocatalytic Flow-Microreactor

Swaraj rashmi Pradhan <sup>1,\*</sup>, Marta PaszkiewiczGawron <sup>1</sup>, Dariusz Łomot <sup>1</sup>, Dmytro Lisovytskiy <sup>1</sup> and Juan Carlos Colmenares <sup>1,\*</sup>

<sup>1</sup> Institute of Physical Chemistry, Polish Academy of Sciences, Kasprzaka 44/52, 01-224 Warsaw, Poland;

\* Correspondence: jcarloscolmenares@ichf.edu.pl, srpradhan@ichf.edu.pl ; Tel.: +48 22 343 32152

*Supplementary Information*



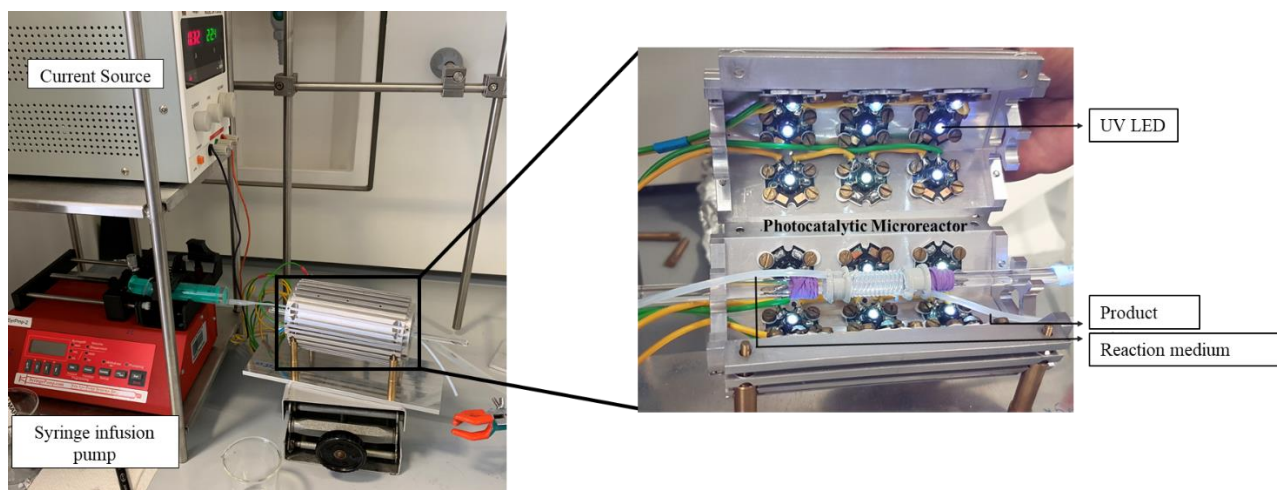
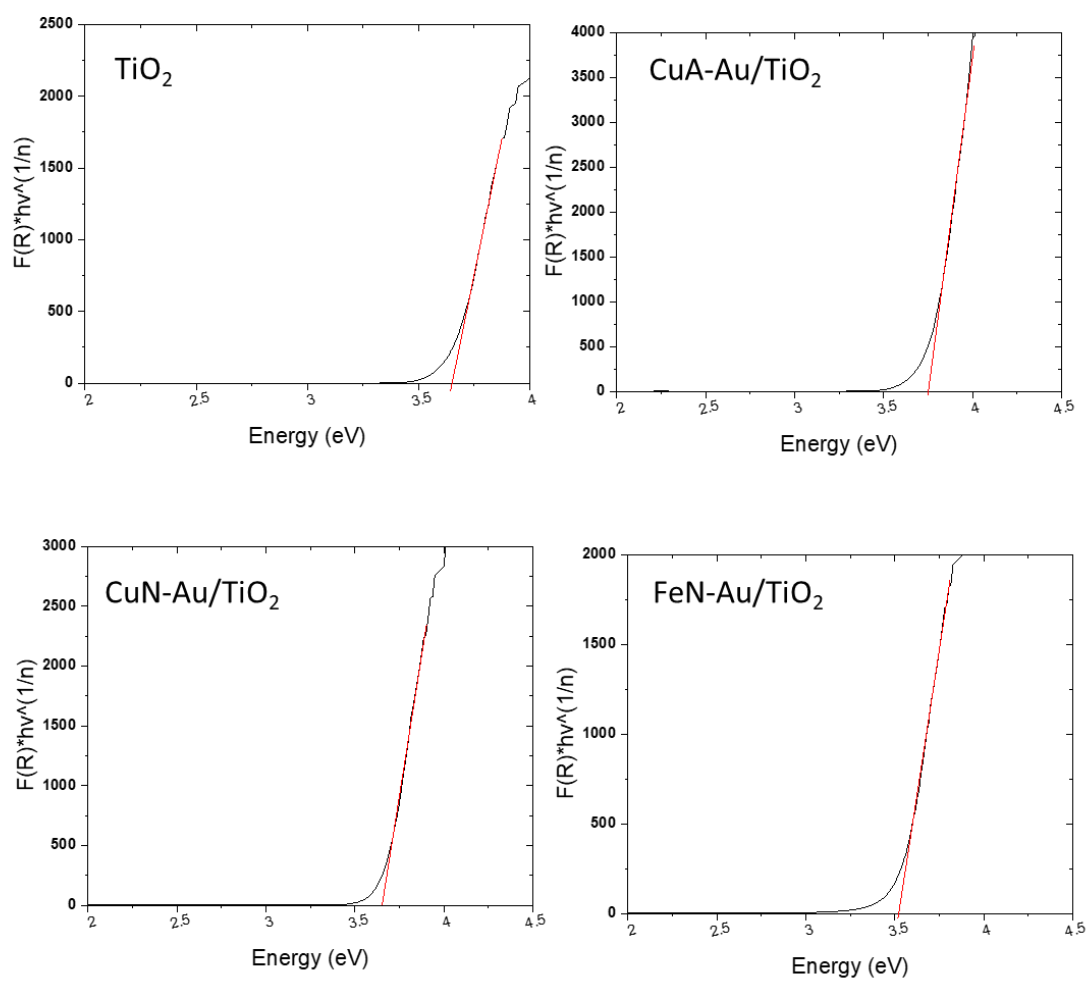
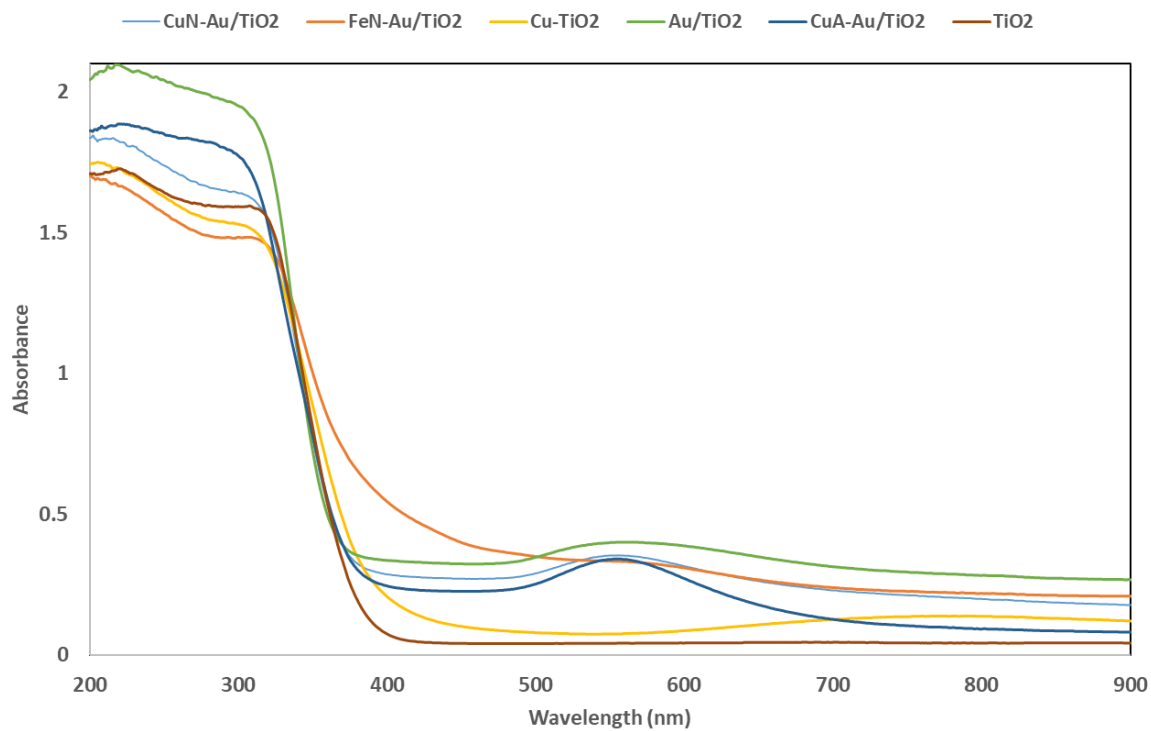


Figure S1. Experimental set up for photocatalysis in microflow system.





**Figure S2.** Bandgap calculation of sol-gel synthesized TiO<sub>2</sub> and bimetallic TiO<sub>2</sub> (CuA-Au/TiO<sub>2</sub>, CuN-Au/TiO<sub>2</sub>, FeN-Au/TiO<sub>2</sub>) catalysts.

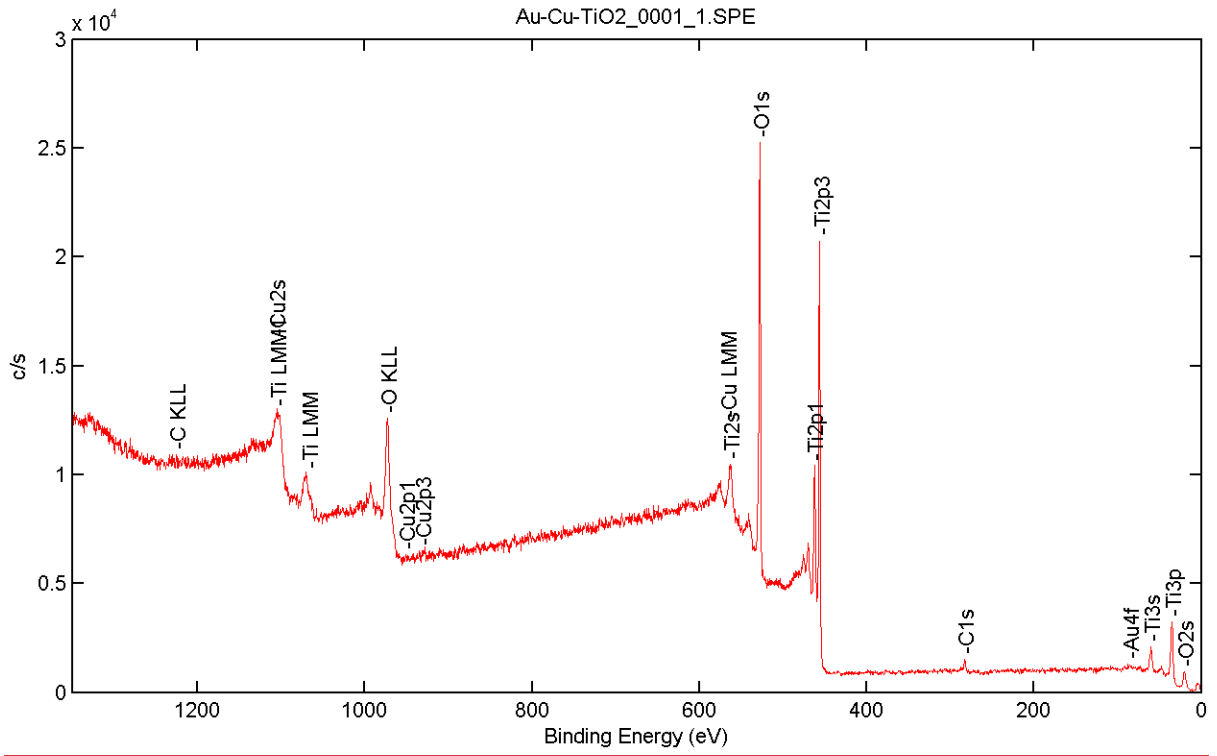


**Figure S3.** UV-vis diffuse reflectance spectra of synthesized bimetallic TiO<sub>2</sub>.

Au-Cu-TiO<sub>2</sub>\_0001\_1.SPE: survey, Al45, 500um2, 100um, 25W,15kV  
2022 Jul 8 Al mono 29.1 W 100.0 μ 45.2° 117.40 eV  
SUR/Area1/1

2.5265e+004 max

Company Name  
14.07 min



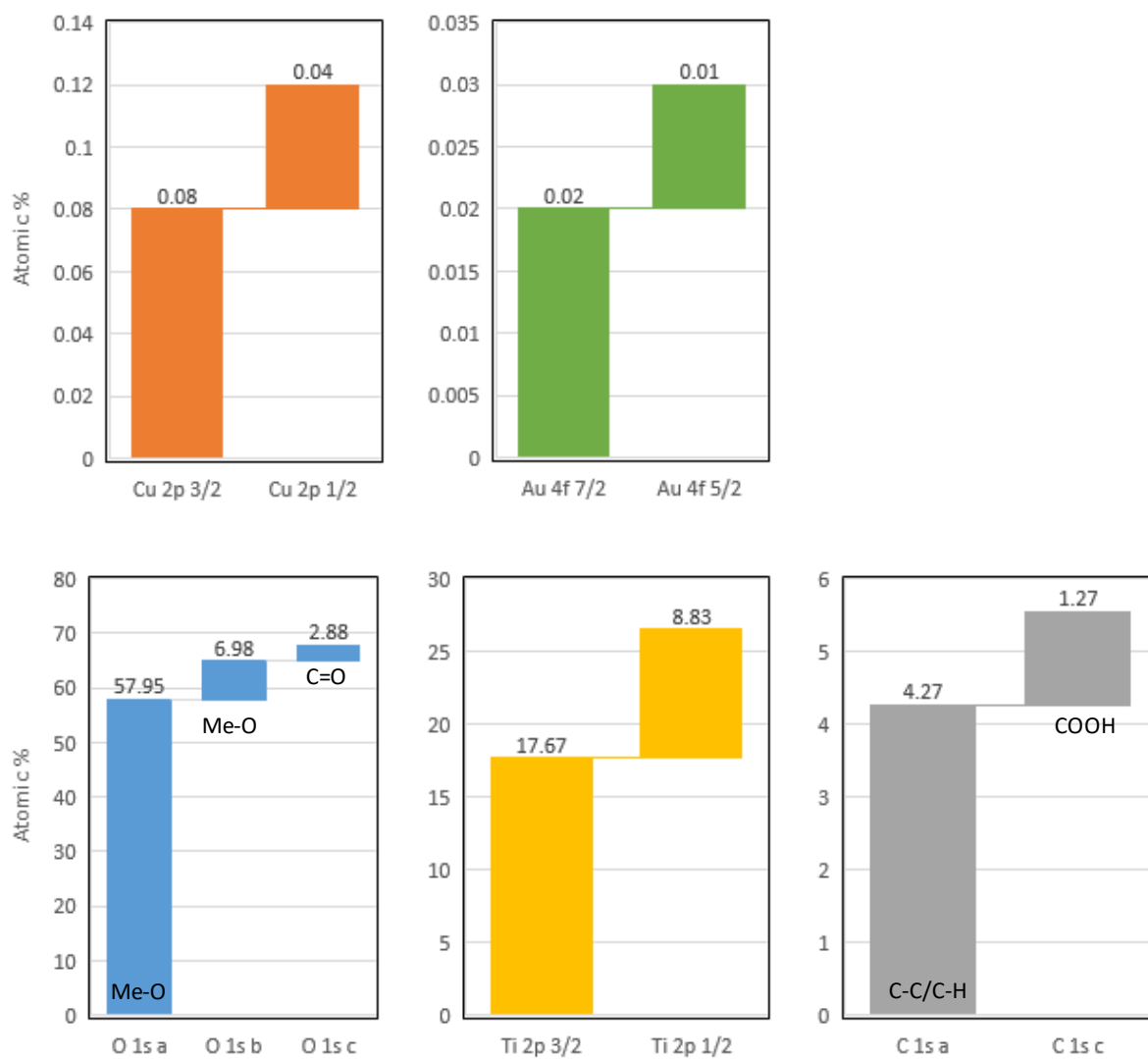


**Figure S4.** Surface analysis of CuA/Au-TiO<sub>2</sub> by X-ray photoelectron spectroscopy (XPS).

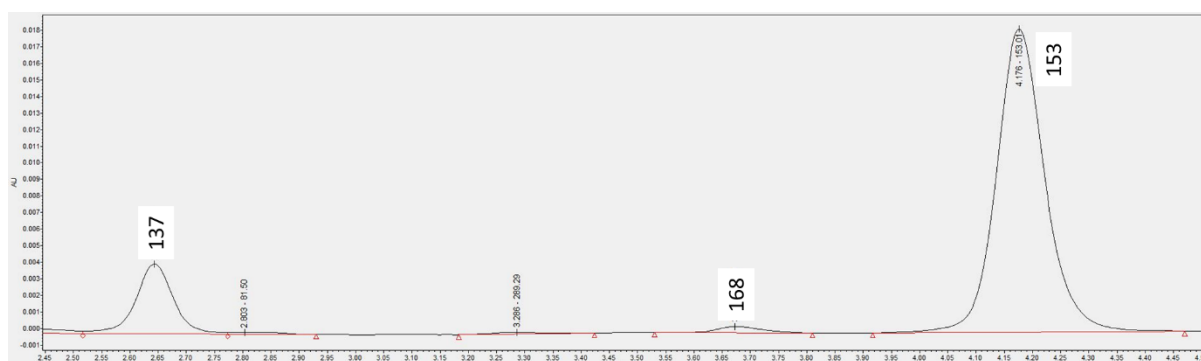
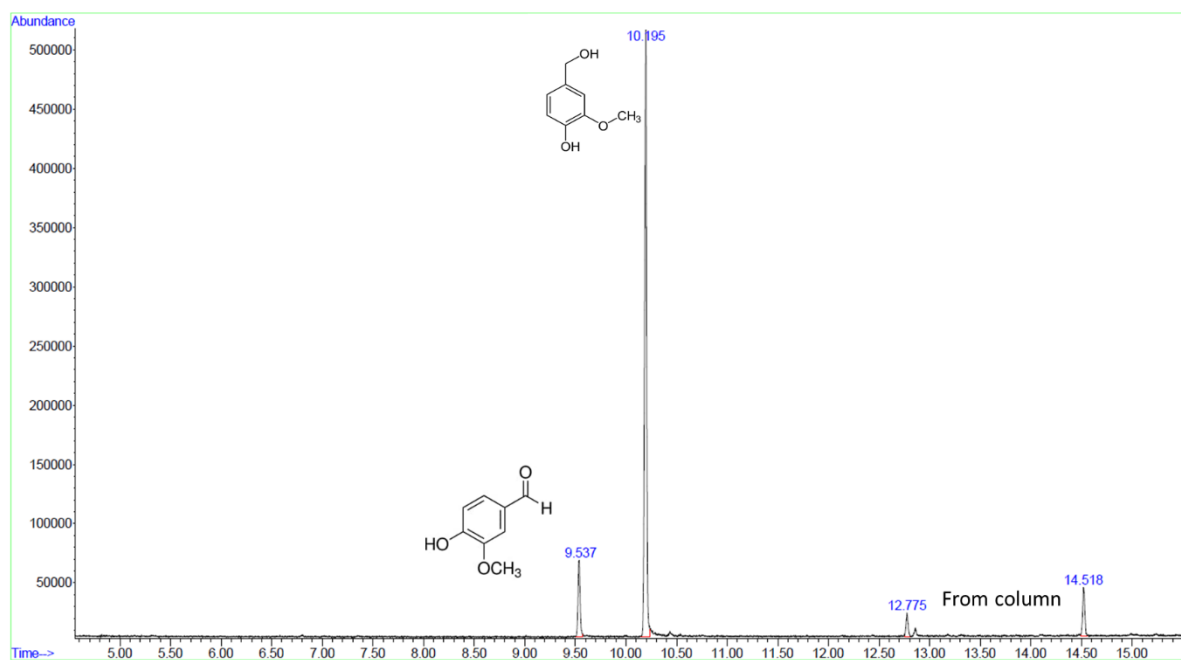


Figure S5. Oxidation products from VanOH analyzed with GC-MS and HPLC-MS.

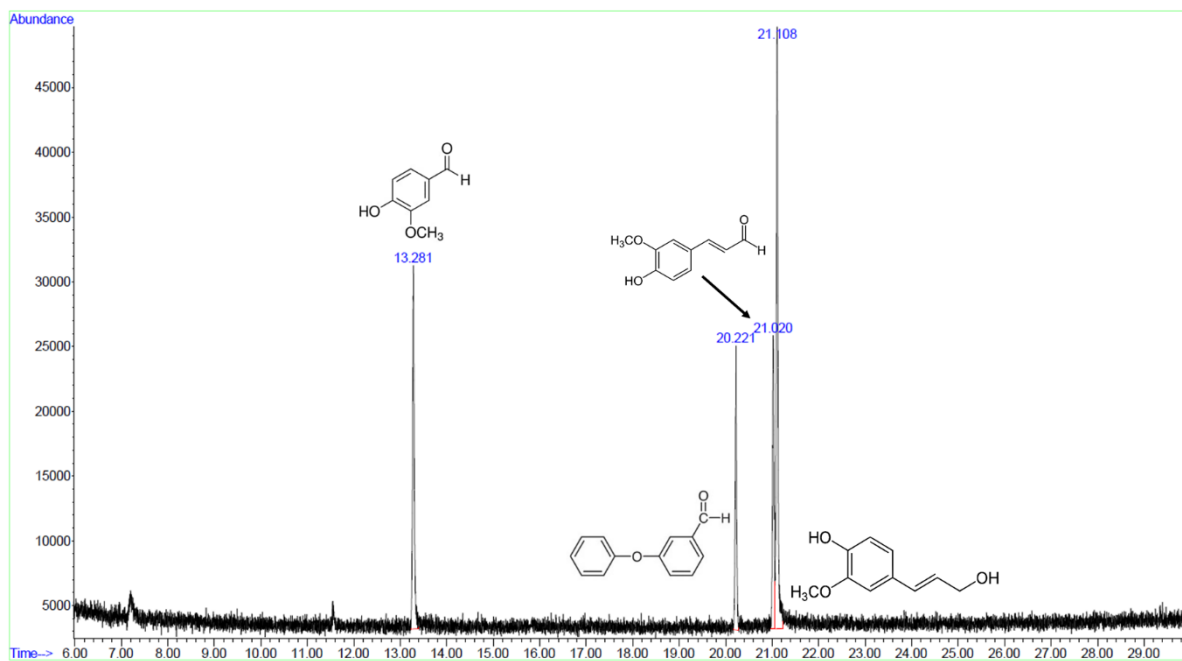


Figure S6. Oxidation products from ConOH analyzed with GC-MS.

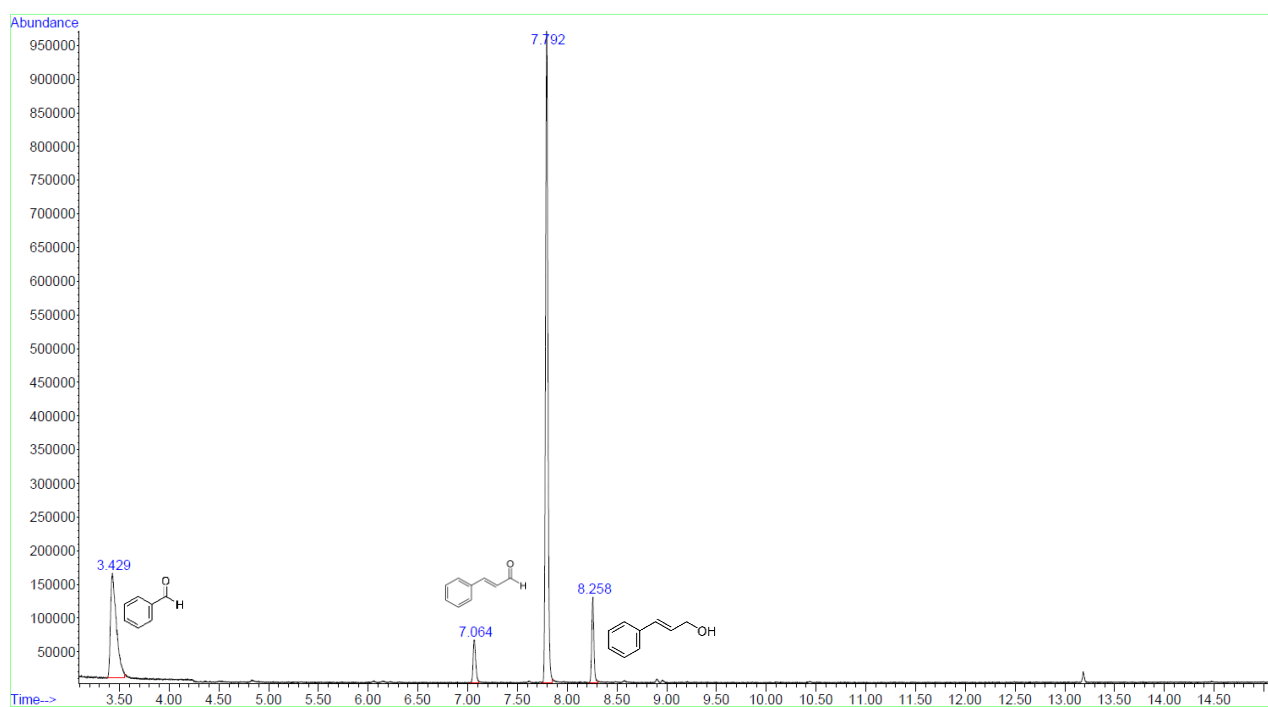
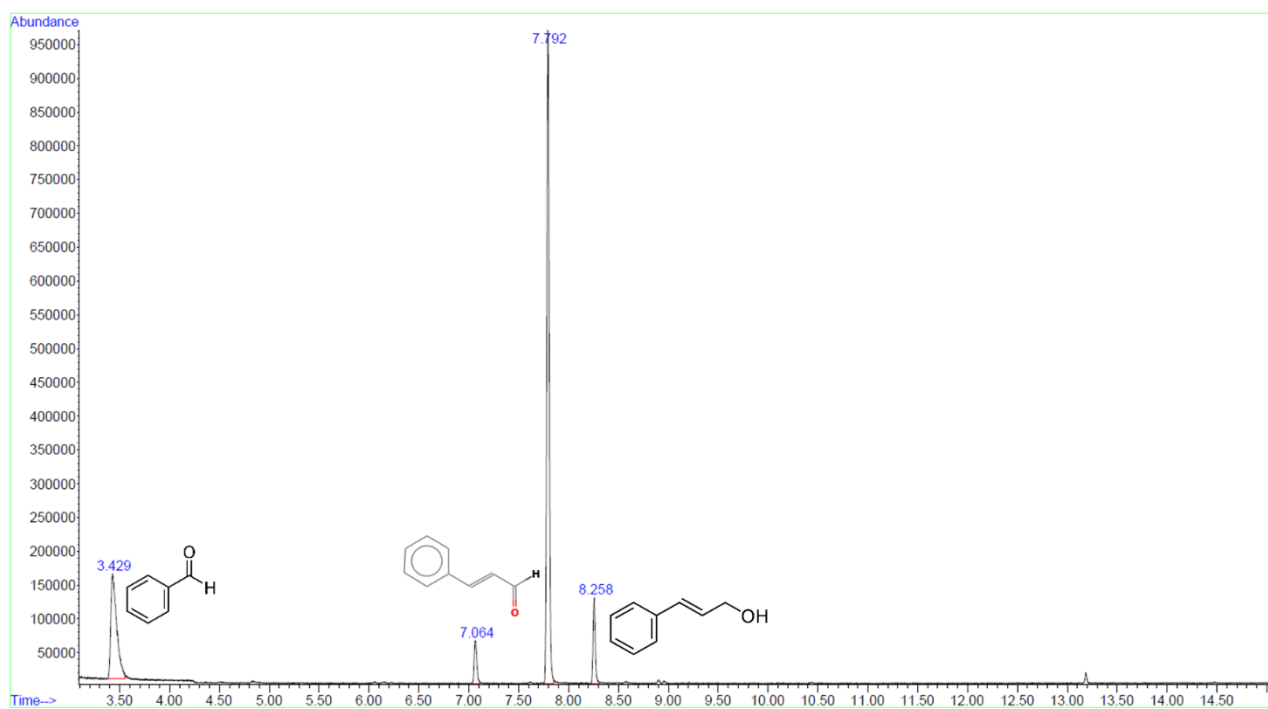
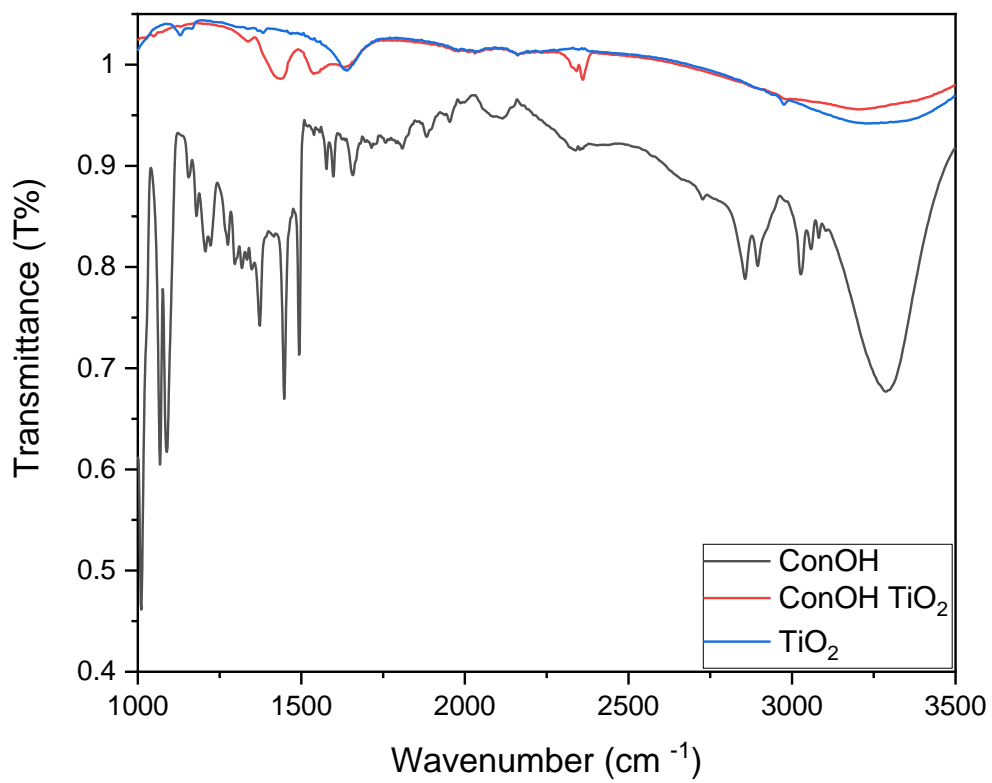
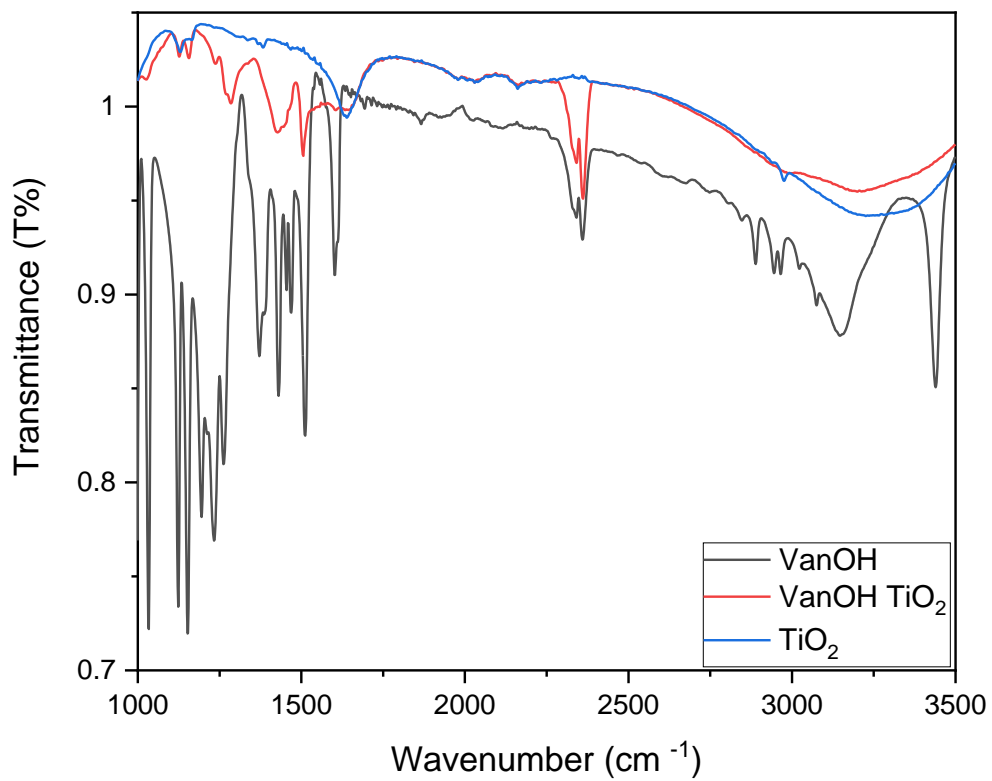


Figure S7. Oxidation products from CinOH analyzed with GC-MS.





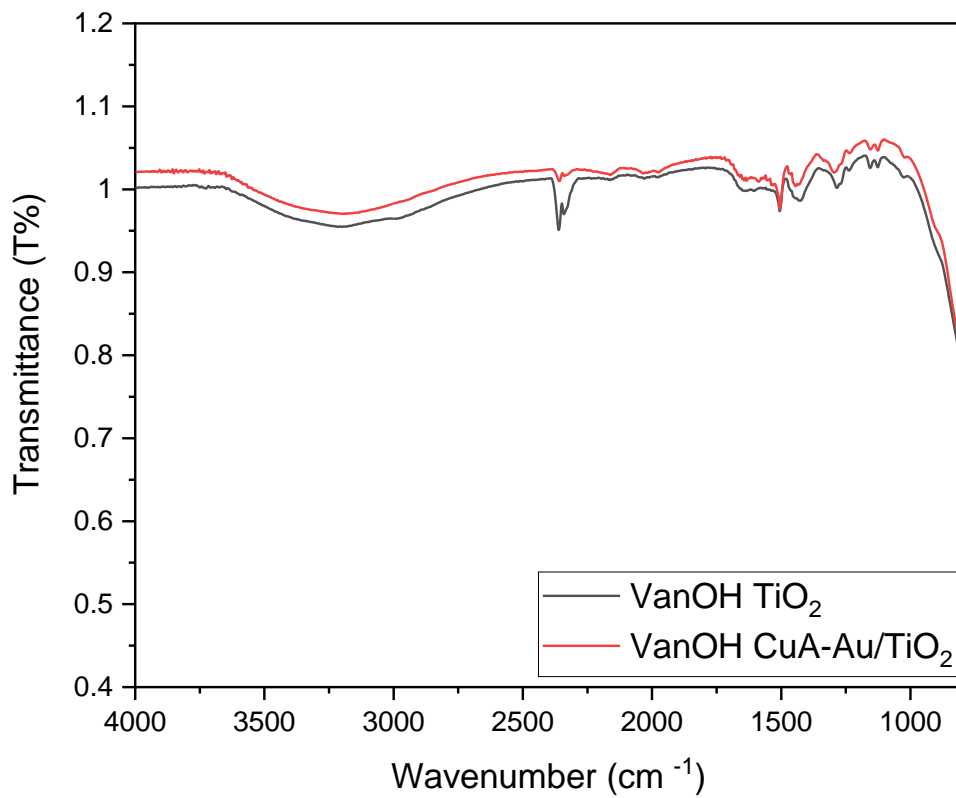
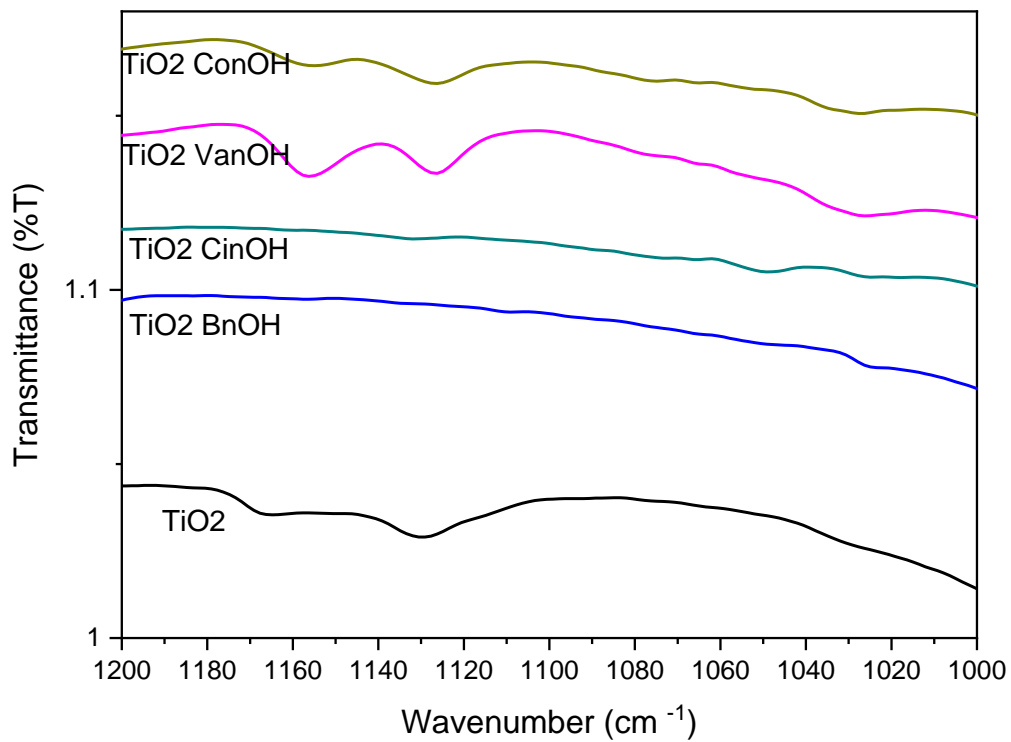


Figure S8. FT-IR spectra of aromatic alcohols (BnOH, CinOH, VanOH and ConOH) adsorbed TiO<sub>2</sub> and VanOH adsorbed bimetallic CuA-Au-TiO<sub>2</sub>.

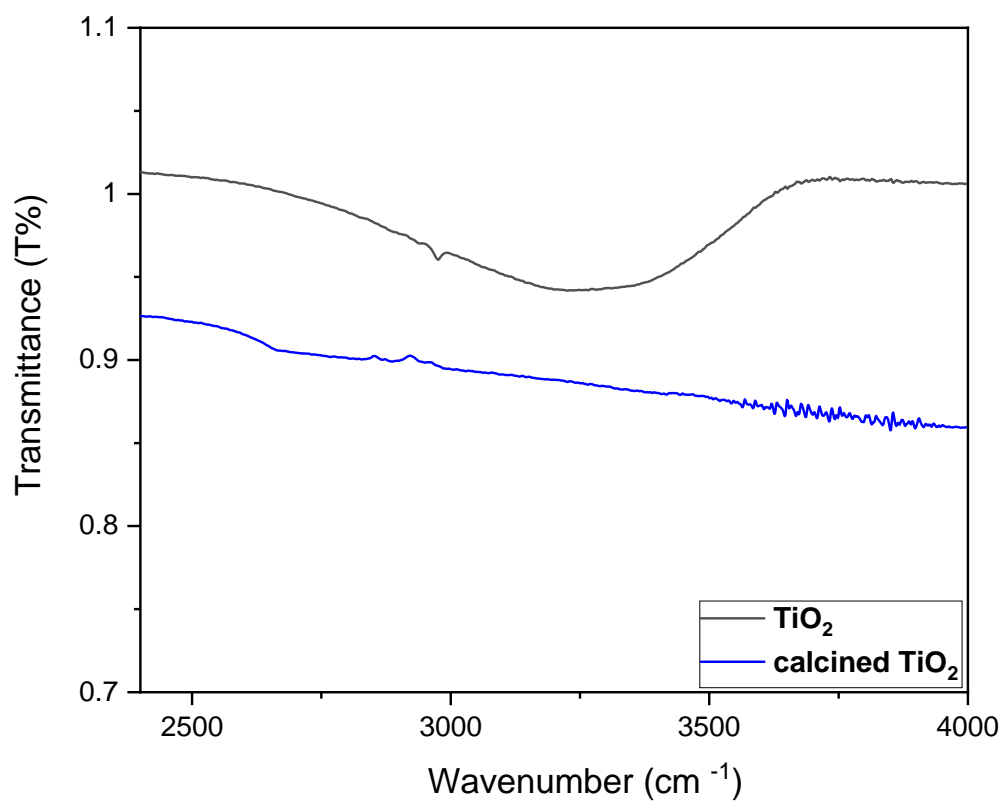
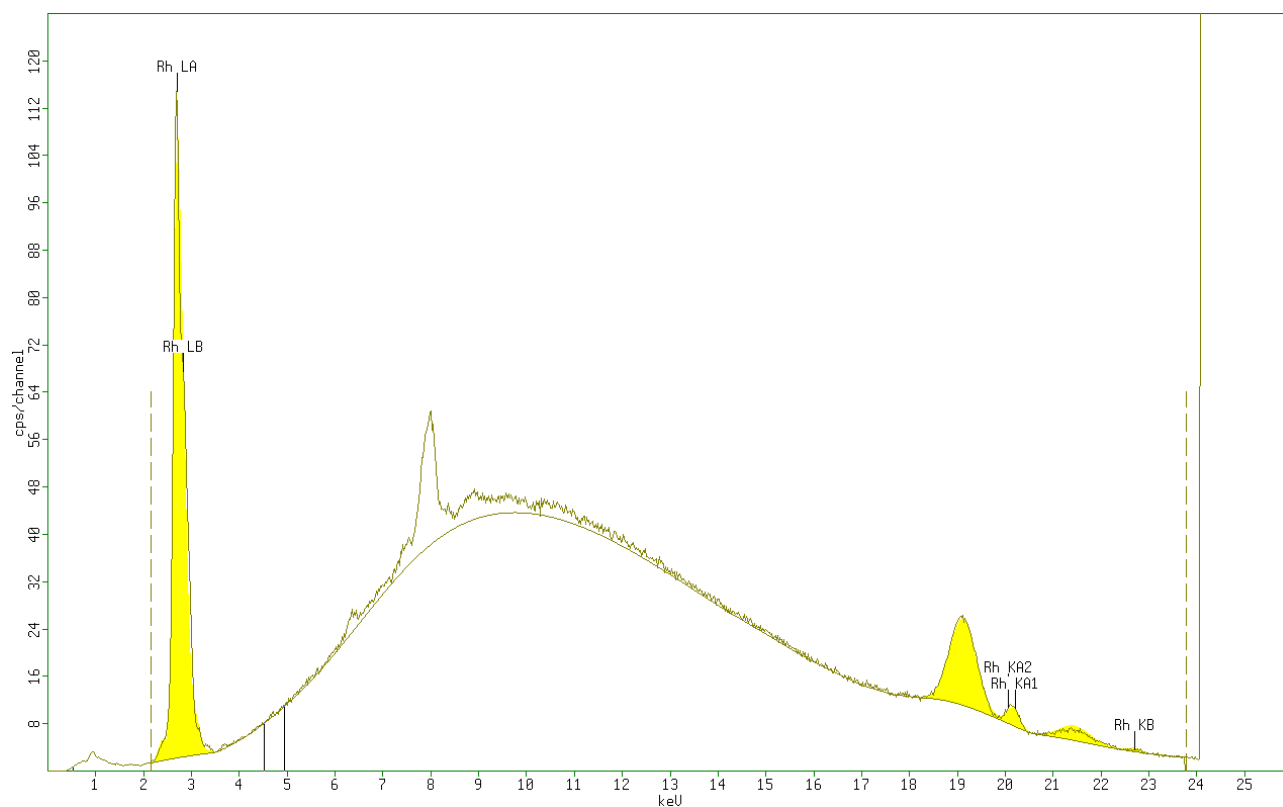


Figure S9. FT-IR spectra of sol-gel synthesized TiO<sub>2</sub> and calcined (600 °C) TiO<sub>2</sub> confirming removal of OH group.



**Figure S10.** XRF image of CuN/Au-TiO<sub>2</sub>.

Good reusability of the catalyst was demonstrated, while no metals were detected in the filtered reaction mixtures. There was no traces of Ti in liquid sample. The other observed peaks are the fingerprint from the instrument.



**Figure S11.** Photocatalytic experiment with CuA-Au/TiO<sub>2</sub> (left) and sol-gel synthesized TiO<sub>2</sub> (right) (Run 1) and after washing the catalyst with ACN and H<sub>2</sub>O (Run2) under UV irradiation (60min) in batch system with ConOH.

## Contributions of Authors:

### My contributions to the articles:

**P 1:** Designing Microflowreactors for Photocatalysis Using Sonochemistry: A Systematic Review Article. co-authors: Swaraj Rashmi Pradhan, Ramón Fernando Colmenares-Quintero, Juan C. Colmenares; *Molecules* 2019, 24, 3315, <https://doi.org/10.3390/molecules24183315>.

I planned the conceptual ideas (based on the idea of Prof. Colmenares) and conceived proof outline. I designed the structure of this publication, did the literature review, prepared some figures and wrote the manuscript. I prepared the replies to the reviewers' comments with help of Prof Colmenares.

**P 2:** Design and development of TiO<sub>2</sub> coated microflow reactor for photocatalytic partial oxidation of benzyl alcohol. co-authors: Swaraj R. Pradhan, Vaishakh Nair, Dimitrios A. Giannakoudakis, Dmytro Lisovytskiy, Juan C. Colmenares; *Molecular Catalysis* 486 (2020) 110884, <https://doi.org/10.1016/j.mcat.2020.110884>.

I synthesized all photocatalysts, performed characterizations and photocatalytic tests. I did data curation, and prepared the original draft. I prepared the replies to the reviewers' comments with help of other co-authors.

**P 3:** Flow photomicroreactor coated with monometal containing TiO<sub>2</sub> using sonication: A versatile tool for visible light oxidation. co-authors: Swaraj R. Pradhan, Dmytro Lisovytskiy, Juan C. Colmenares; *Catalysis Communications* 2022, Volume 162, 106375 <https://doi.org/10.1016/j.catcom.2021.106375>

I analyzed the data, synthesized and characterized the catalyst. I visualized, conceptualized and prepared original draft.

**P 4:** Bimetallic TiO<sub>2</sub> Nanoparticles for Lignin-Based Model Compounds Valorization by Integrating an Optocatalytic Flow-Microreactor co-authors: Swaraj Rashmi Pradhan, Marta Paszkiewicz-Gawron, Dariusz Łomot, Dmytro Lisovytskiy and Juan Carlos Colmenares; *Molecules* 2022, 27, 8731. <https://doi.org/10.3390/molecules27248731>.

I synthesized all photocatalysts studied in this work. I performed all the above photocatalytic test reactions and analyzed the results of HPLC measurements. I performed UV-Vis diffuse-reflectance spectroscopy (DRS), high resolution scanning electron microscopy (HR-SEM), Fourier transform infrared spectroscopy (FTIR) and N<sub>2</sub> physisorption for the synthesized catalysts. I took part in the analysis of all data obtained from other characterization techniques, which were performed by co-authors. I designed the structure of this publication, did the literature review, prepared most of figures, and wrote the manuscript. I discussed the results and prepared the replies to the reviewers' comments with some help of other co-authors.

Contributions of the other authors of these publications are listed on the following pages.



IChF



# Institute of Physical Chemistry Polish Academy of Sciences

Juan Carlos Colmenares Quintero, Ph.D. D.Sc.  
Associate Professor  
Research group leader  
“Catalysis for sustainable energy production and  
environmental protection, CatSEE”

Kasprzaka 44/52, PL-01 224 Warsaw, Poland  
Tel.: +48 22 343 3215  
Fax: +48 22 343 3448  
[jcarloscolmenares@ichf.edu.pl](mailto:jcarloscolmenares@ichf.edu.pl)  
<http://photo-catalysis.org/>

March 23, 2023

## To Whom It May Concern Co-author's Statement

Please, find below my contribution to the publications included in the Ph.D. dissertation of Ms. Swaraj Rashmi Pradhan entitled: “Nanoengineering of Thin Layers Of Semiconductor Photocatalysts In A Microreactor Environment For Lignin-Based Model Compounds Valorization”.

I declare, that the publications listed below was created on the initiative and with the dominant participation of Ms. Swaraj Rashmi Pradhan.

1. **Designing Microflowreactors for Photocatalysis Using Sonochemistry: A Systematic Review Article.** co-authors: Swaraj Rashmi Pradhan, Ramón Fernando Colmenares-Quintero, and Juan Carlos Colmenares **Molecules** 2019, 24, 3315, <https://doi.org/10.3390/molecules24183315>.

*Contribution: conceptualization of ideas, conceived proof outline and revised the manuscript critically for essential intellectual content.*

2. **Design and development of TiO<sub>2</sub> coated microflow reactor for photocatalytic partial oxidation of benzyl alcohol.** co-authors: Swaraj R. Pradhan, Vaishakh Nair, Dimitrios A. Giannakoudakis, Dmytro Lisovytskiy, and Juan C. Colmenares; **Molecular Catalysis** 486 (2020) 110884, <https://doi.org/10.1016/j.mcat.2020.110884>.

*Contribution: Conceptualization, Supervision, Funding acquisition, Writing - review & editing.*

3. **Flow photomicroreactor coated with monometal containing TiO<sub>2</sub> using sonication: A versatile tool for visible light oxidation.** co-authors: Swaraj R. Pradhan, Dmytro Lisovytskiy, and Juan C. Colmenares; **Catalysis Communications** 2022, Volume 162, 106375 <https://doi.org/10.1016/j.catcom.2021.106375>

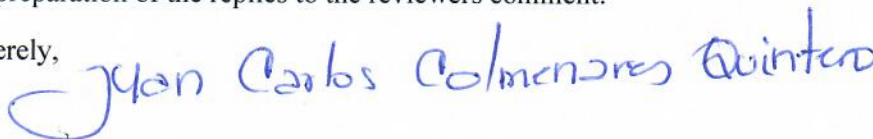
*Contribution: Writing - review & editing, Funding Resources, Conceptualization, Supervision, Project administration.*

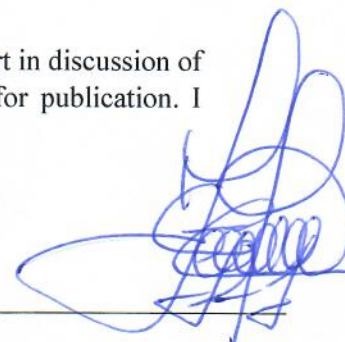
4. **Bimetallic TiO<sub>2</sub> Nanoparticles for Lignin-Based Model Compounds Valorization by Integrating an Optocatalytic Flow-Microreactor** co-authors: Swaraj Rashmi Pradhan, Marta Paszkiewicz-Gawron, Dariusz Łomot, Dmytro Lisovytskiy, and Juan Carlos Colmenares; **Molecules** 2022, 27, 8731. <https://doi.org/10.3390/molecules27248731>.

*Contribution: writing - review and editing, resources, conceptualization, supervision, and project administration.*

I participated in the design and conceptualization of the above publications. I took part in discussion of the results and general comments at the stage of preparation of the manuscripts for publication. I helped in preparation of the replies to the reviewers comment.

Your sincerely,







March 23, 2023

**Engineering Research Institute**  
Universidad Cooperativa de Colombia  
Medellín, COLOMBIA

### CO-AUTHOR'S STATEMENT

To Whom It May Concern,

Please, find below my contribution to the publications included in the Ph.D. dissertation of Ms. Swaraj Rashmi Pradhan entitled: "Nanoengineering of Thin Layers Of Semiconductor Photocatalysts In A Microreactor Environment For Lignin-Based Model Compounds Valorization".

I declare, that the publications listed below was created on the initiative and with the dominant participation of Ms. Swaraj Rashmi Pradhan.

1. **Designing Microflowreactors for Photocatalysis Using Sonochemistry: A Systematic Review Article.** co-authors: Swaraj Rashmi Pradhan, Ramón Fernando Colmenares-Quintero, **Molecules** 2019, 24, 3315, <https://doi.org/10.3390/molecules24183315>.

I conceptualized, and edited the above publications. I also reviewed the manuscript critically for essential intellectual content.

Yours sincerely,



**Ramón Fernando Colmenares Quintero, Prof Dr**  
CEO, Engineering Research Institute  
Email: [ramon.colmenaresq@campusucc.edu.co](mailto:ramon.colmenaresq@campusucc.edu.co)

To whom it may concern

### Co-author's Statement

Please, find below my contribution to the publications included in the Ph.D. dissertation of Ms. Swaraj Rashmi Pradhan entitled: “Nanoengineering of Thin Layers Of Semiconductor Photocatalysts In A Microreactor Environment For Lignin-Based Model Compounds Valorization”.

I declare, that the publications listed below was created on the initiative and with the dominant participation of Ms. Swaraj Rashmi Pradhan.

1. **Design and development of TiO<sub>2</sub> coated microflow reactor for photocatalytic partial oxidation of benzyl alcohol.** co-authors: Swaraj R. Pradhan, Vaishakh Nair, Dimitrios A. Giannakoudakis, Dmytro Lisovytskiy, Juan C. Colmenares; **Molecular Catalysis** 486 (2020) 110884, <https://doi.org/10.1016/j.mcat.2020.110884>.

*Contribution: Supervision, Writing - review & editing*

I took part in intial discussions involving the literatures on the research work. Followed by this discussions of the results and general comments at the stage of preparation of the manuscripts for publication.



Vaishakh Nair

Dr. Vaishakh Nair  
Former Postdoctoral Researcher  
Catalysis for sustainable energy production and environmental protection group  
Institute of Physical Chemistry, Polish Academy of Sciences



Dr. Dimitrios A. Giannakoudakis

Research Associate

e-mail: [dagchem@gmail.com](mailto:dagchem@gmail.com) / [dgiannakoudakis@chem.auth.gr](mailto:dgiannakoudakis@chem.auth.gr)

website: [www.DaGchem.com](http://www.DaGchem.com)

P.O. Box 116, 54124 Thessaloniki, Greece

Mob.: +30 6940 50 95 35

Tel.: +30 2310 99 77 30

<http://ktrianta.webpages.auth.gr/>

March 23, 2023

To whom it may concern

### Co-author's Statement

I hereby present my contribution linked to the publications included in the Ph.D. dissertation of Ms. Swaraj Rashmi Pradhan entitled: "Nanoengineering of Thin Layers of Semiconductor Photocatalysts in a Microreactor Environment for Lignin-Based Model Compounds Valorization".

I declare that the publications listed below was created on the initiative and with Ms. Swaraj Rashmi Pradhan to have the dominant participation.

1. Design and development of TiO<sub>2</sub> coated microflow reactor for photocatalytic partial oxidation of benzyl alcohol. co-authors: Swaraj R. Pradhan, Vaishakh Nair, Dimitrios A. Giannakoudakis, Dmytro Lisovytskiy, Juan C. Colmenares; Molecular Catalysis 486 (2020) 110884, <https://doi.org/10.1016/j.mcat.2020.110884>.

**Contribution:** Writing - Review & Editing.

I took part in reviewing the results and general comments at the stage of preparation of the manuscripts for publication. I helped in preparation of the replies to the reviewer's comment.

Please, do not hesitate to contact me for further details.

Sincerely,

Dr. Dimitrios A. Giannakoudakis  
[www.DaGchem.com](http://www.DaGchem.com)

*Warszawa, 23.03.2023*

To whom it may concern

### AUTHOR CONTRIBUTION

Work title: "Bimetallic TiO<sub>2</sub> Nanoparticles for Lignin-Based Model Compounds Valorization by Integrating an Photocatalytic Flow-Microreactor"

Author name: Dariusz Lomot

The author confirms responsibility for the following: analysis and presentation of results from Transmission Electron Microscopy.

*D. Lomot*

March 23, 2023

to whom it may concern

### **Co-author's Statement**

I declare, that the publications listed below was created on the initiative and with the dominant participation of MSc Swaraj Pradhan.

1. **Design and development of TiO<sub>2</sub> coated microflow reactor for photocatalytic partial oxidation of benzyl alcohol.** co-authors: Swaraj R. Pradhan, Vaishakh Nair, Dimitrios A. Giannakoudakis, Dmytro Lisovytskiy Juan C. Colmenares; **Molecular Catalysis** 486 (2020) 110884, <https://doi.org/10.1016/j.mcat.2020.110884>. *Contribution: Methodology -XRD and XRF measurements were performed.*
2. **Flow photomicroreactor coated with monometal containing TiO<sub>2</sub> using sonication: A versatile tool for visible light oxidation.** co-authors: Swaraj R. Pradhan , Dmytro Lisovytskiy, Juan C. Colmenares; **Catalysis Communications** 2022, Volume 162, 106375 <https://doi.org/10.1016/j.catcom.2021.106375> *Contribution: Investigation, data processing. -XRD measurements and calculation of crystallite size were performed.*
3. **Bimetallic TiO<sub>2</sub> Nanoparticles for Lignin-Based Model Compounds Valorization by Integrating an Optocatalytic Flow-Microreactor** co-authors: Swaraj Rashmi Pradhan, Marta Paszkiewicz-Gawron, Dariusz Łomot, Dmytro Lisovytskiy and Juan Carlos Colmenares; **Molecules** 2022, 27, 8731. <https://doi.org/10.3390/molecules27248731>. *Contribution: Investigation, data processing. XRD and XRF measurements were performed.*

My participation was limited to carrying out measurements and calculations using the XRD and XRF methods, discussion of the results and general comments at the stage of preparation of the manuscripts for publication.

*D. Lisovytskiy*

To whom it may concern

### Co-author's Statement

Please, find below my contribution to the publications included in the Ph.D. dissertation of Ms. Swaraj Rashmi Pradhan entitled: “Nanoengineering of Thin Layers Of Semiconductor Photocatalysts In A Microreactor Environment For Lignin-Based Model Compounds Valorization”.

I declare, that the publications listed below was created on the initiative and with the dominant participation of Ms. Swaraj Rashmi Pradhan.

1. **Bimetallic TiO<sub>2</sub> Nanoparticles for Lignin-Based Model Compounds Valorization by Integrating an Optocatalytic Flow-Microreactor** co-authors: Swaraj Rashmi Pradhan, Marta Paszkiewicz-Gawron, Dariusz Łomot, Dmytro Lisovytskiy and Juan Carlos Colmenares; **Molecules** 2022, 27, 8731. <https://doi.org/10.3390/molecules27248731>.

*Contribution: writing—review and editing, and data curation.*

I took part in writing—review and editing, and data curation at the stage of preparation of the manuscripts for publication.

*Paszkiewicz-Gawron*



# Swaraj Rashmi Pradhan | 28 years old



More than 5 years of experience in **Material Science & Surface Chemistry**, including one year of exposure to **Computational Chemistry** methods. I specialize in heterogeneous catalysis concepts and characterization techniques necessary to understand interfacial interactions in the range of metals and polymers.

## CONTACT

✉ [swaraj.nitr6@gmail.com](mailto:swaraj.nitr6@gmail.com)

☎ +48 579224900

📍 Szczesliwicka 2  
Warsaw, Poland

🌐 [LinkedIn:](#)  
[SwarajPradhan](#)

## SKILLS

### Instruments

HR-SEM XRD

UV-Vis DRS

FT-IR BET AFM

XPS HR-TEM

HPL/MS GC/MS

### Computational Tools

DFT - Gaussian MD

### Other Software/Tools

Design Expert

Chemdraw Origin

MS Office

## PUBLICATIONS

Research Gate



Demonstrated **research, experimental design, & scientific writing skills** via. my 8 peer-reviewed publications with [130+ citations.](#)

## EDUCATION

📍 **Institute of Physical Chemistry, Polish Academy of Sciences (Poland)** **Ph.D** 📅 11/2018 - Now

📍 **National Institute of Technology Rourkela (India)** **Integrated M.Sc. (Chemistry)** 📅 2011 - 2016

## WORK HISTORY

📍 **Institute of Physical Chemistry, Polish Academy of Sciences (Poland)** **Doctoral Researcher** 📅 11/2018 - Now

Doctoral Thesis — *Nanoengineering of Thin Layers of Semiconductor Photocatalysts in a Microreactor Environment for Lignin-Based Model Compounds Valorization.*

- **Synthesized bimetallic TiO<sub>2</sub> catalyst** and studied the structural, optical, and textural properties and surface morphology of the catalysts by various characterization techniques.
- Designed a **novel thin-layered microreactor system** for selective oxidation of lignin-based model compounds using UV (375 nm) and visible (515 nm) irradiation.
- Resulted in a Polish patent application — “A flow microreactor system and the way of conducting photocatalytic processes using it.”

📍 **CSIR-Central Salt And Marine Chemicals Research Institute (India)** **Project Assistant - II** 📅 06/2016 - 08/2017

- Optimized chemical structures using DFT, with B3LYP/6-31+G(d), PM3, and M06-2x/6-311+G\*\* levels, implemented in the GAUSSIAN09 package. Worked on **single point calculation, frequency, and binding energy calculation along with BSSE correction** of the optimized structures.
- Explored flue gas adsorption at a molecular level with the simple cyclohexane system using computational study to enable the development of new separation/storage for these toxic gases.

📍 **National Institute of Technology Rourkela (India)** **Masters Researcher** 📅 05/2015 - 05/2016

Masters Thesis — *Visible light driven efficient photocatalytic degradation of congo red dye catalyzed by hierarchical CuS-Bi<sub>2</sub>Cu<sub>x</sub>W<sub>1-x</sub>O<sub>6-2x</sub> nanocomposite system.*



## PATENTS

[Patent application P.430411 - 30.06.2019 - Poland.](#)

## CONFERENCES

Delivered **7 presentation (as talks & poster)** in international conferences focused on catalysis and green chemistry.

## AWARDS

[2022 Young researchers Award IPC-PAS](#)

[2021 Young researchers Award IPC-PAS](#)

**2018 - 2022** National Science Center - PAS Scholarship

**2015** IITM Summer Fellowship Programme

**2011** TDSQT scholarship by Dharitri (Local Newspaper)

## SUPERVISION

**Masters:** 4 students

**Bachelors:** 1 student

## SOFT SKILLS

Communication

Teamwork

Leadership

## INTEREST

Travel

Badminton

Drawing

Photography

- Synthesized CuS-Bi<sub>2</sub>Cu<sub>x</sub>W<sub>1-x</sub>O<sub>6-2x</sub> nanocomposite and Bi<sub>2</sub>WO<sub>6</sub> nanomaterial and contributed to the characterization studies using XRD, FE-SEM, and FT-IR.
- The findings have been discussed in a peer-reviewed article published in the 'RSC Advances'.

## SELECTED INTERNSHIPS

 **Indian Institute of Technology Guwahati (India)**  05/2014 - 07/2014  
**Summer Internship**

- Investigated ground-state geometries and optical properties of pyridine-pyrrole based donor-acceptor type conjugated polymers using DFT.
- Learned to analyze the band gap approximated from the difference between HOMO and LUMO energies as well as the excitation energies calculated from the time-dependent DFT (TDDFT).

 **National Institute of Technology Rourkela (India)**  05/2013 - 07/2013  
**Summer Internship**

- Synthesized different clay-based nanoporous materials by performing various surface and structural modifications.
- Learned theory of various techniques for characterization of the synthesized materials.

## ADDITIONAL INFORMATION

### Leadership Roles

- Promoted science to school children by designing [interactive experiments on green chemistry](#) for the [2022 Science Picnic](#) at Copernicus Science Centre, Warsaw (Poland).
- Elected among 900 students of C.V.R Hall of Residence, NIT Rourkela to serve as the General Secretary (2013 - 2014).
- Volunteer of [AASRA](#), a student organization working towards imparting primary education to underprivileged children living in slums and villages near our institute campus.

### Selected Publications



[Flow photomicroreactor coated with monometal containing TiO<sub>2</sub> using sonication: A versatile tool for visible light oxidation](#)

 S.R. Pradhan, D. Lisovytskiy, J.C. Colmenares

 2022  Catalysis Communications - Vol. 162, Elsevier

[Exploiting CF Bond of Hexafluorocyclohexane and Decafluoroadamantane Systems to Capture Flue Gases: A Computational Study](#)

 S.R. Pradhan, B. Ganguly

 2017  ChemistrySelect, Wiley